UNIVERSITÀ DEGLI STUDI DI MILANO

PhD Course in Chemistry · XXXII cycle

Department of Chemistry

Kinetic description and process modeling for chemicals and fuels production from renewable sources

CANDIDATE

Antonio Tripodi

CO-SUPERVISORS

Prof. R. Martinazzo
Prof. I. Rossetti

COURSE COORDINATOR

Prof. E. Licandro

A.A. 2018/2019

“Poi diedi l’esame di Chimica Analitica; difficoltà nello studio, scarsa memoria […]

Studiavo e non ricordavo più nulla. L’esame lo diedi con l’aiuto di uno studente molto bravo […]

Senza di lui non me la sarei cavata; longanimità degli assistenti: uno m’aiutò.”

Gadda, C. E. (2008) “Giornale di Guerra e di Prigionia”, in *Saggi Giornali Favole e altri Scritti II*. A cura di D. Isella, Garzanti Editore, Milano, pp. 851-852.

Del mio esame pratico di Chimica Analitica posso ancora ricordare (e sono passati sei anni accademici…): che consistette nella retrotitolazione di vitamina C: e che la gentilissima professoressa Mussini, valutandone l’esito, si contentò di dichiarare: *“… non è indecoroso.”*.

Eppure la suddetta tecnica di analisi mi è tornata più utile, recentemente, di quanto non lo sia stata all’illustre ingegnere: per fortuna sua, forse, e certamente di noi suoi lettori.

The tutors for this phd period, prof. Rocco Martinazzo and prof. Ilenia Rossetti[1] have constantly provided valuable guidance, and greatly helped in valorizing the strongest points of the upcoming projects.

Professor Roberto Piazza and ph.d. Stefano Buzzaccaro[2], have always found some time, over the past ten years, to see each other once again and spare their insight on scientific issues. Many tests, reported in the second part, have been executed after their advice about changing certain conditions of the mixture. I am grateful to both for their lasting friendliness.

The TGA and DSC tests performed within the SmartMatLab have been carried out by ph.d. Serena Cappelli[1], it is also thanks to her carefulness and reliability that the whole body of analysis has been completed. The technical personnel by Mettler Toledo have always been available to spare some time explaining extremely useful details about the machines' working, and to discuss the possible sources of biases. The NMR spectra have been acquired by Americo Costantino[1]. He has also helped during the initial phases of the work, in order to sort out a feasible combination of analyte, solvent and internal standard.

Several other PHD students and post-doc researchers have lent a helpful hand and their valuable advice, in particular Enrico Gandini, Ivan Grigioni, Sebastiano Campisi; Matteo Compagnoni who shared many activities for two years and Elnaz Bahadori who did the same for other two.

Many graduating (and now graduated) students have contributed to different parts of this work.

The latest experiments of ethanol dehydration have been carried out by Igor Fontana; the first version of the bioethylene calculation with Aspen Plus has been put together by dr. Mattia Belotti. and the energy-recovery layout has been unraveled with the help of Martina Frosi.

The steam reforming of ethanol has been tested on many materials, over the past years, by a number of people within this research group: the specific dataset used for this thesis was gathered by dr. Nicola Bagnaresi. The core of the DHCP calculation has been rebuilt on a new basis by dr. Antonio Pizzonia; finally Ing. Andrea Cogliandro has given precise hints on the civil energetic consumptions aspect.

The basis of the Aspen Plus calculation for ammonia, relying on the kinetic data of patented catalysts, has been worked out by ph.d. Matteo Compagnoni (who has done also the basis calculation of the large-scale ethanol reforming project).

The data of the ammoxidation catalysts[3] have been reviewed first by dr. Mattia Belotti. Then the separation of the products' mixture has been studied with the invaluable help of dr. Dario Manzini. Davide Ripamonti has trained the kinetic model for half of the tests, before drawing the first scheme of the staged reactor.

The review on catalysts for the Sabatier reaction has been started by Davide Ceccarelli, while Martina Brazzoli has made the first sketch of the process and the critical review of solubility data.

Marta Di Gangi and Filippo Costantino have carried out drying and separation experiments, respectively; the latter has also worked out full-day backtritration and distillation sessions. The protocol to treat the samples before the NMR analysis has been discussed with dr. Emanuele Agnese, who has also reviewed the aspect of acetonitrile hydrolysis.

Anyway, they're my Faith and my brothers keeping me up.

[1] University of Milan.
[2] Politecnico of Milan.
[3] Courtesy of Prof. F. Cavani, University of Bologna.

Contents

Acronyms & Symbols

AP	Aspen Plus	softwares used
CC	Composite Curve	energy balances
CU	Cold Utility	energy balances
DHPC	Distributed Heat & Power Co-generation	
DMSO	Di-Methyl Sulfoxide	
DSC	Differential Scanning Calorimetry	analysis methods
EoS	Equation of State	thermodynamic models
FC	Fuel Cell	
GCC	Grand Composite Curve	energy balances
HU	Hot Utility	energy balances
LL(E)	Liquid-Liquid (Equilibrium)	
L(N)G	Liquid (Natural) Gas	
MW	Molecular Weight	
NRTL	Non Random Two Liquids	thermodynamic models
PA	Pinch Analysis	energy balances
PSA	pressure-Swing Adsorption	
RKS	Redlich-Soave-Kwong	thermodynamic models
rpm	Rotations per Minute	
SLL(E)	Solid-Liquid-Liquid (Equilibrium)	
SR	Steam reforming	
TGA	Thermo-Gravimetric Analysis	analysis methods
VLE	Vapor-Liquid Equilibrium	
Ea	Activation Energy	kinetic models
$\mathbf{c_p}$	Specific heat	
f	Fugacity	kinetic models
F	Anova test parameter	analysis methods
H, h	Enthalpy, specific	
$\mathbf{k_0}$	Ahrrenius Prefactor	kinetic models
K	equilibrium constant	kinetic models
Q, q	Thermal power, specific	
r	reaction rate	kinetic models
x	liquid molar fraction	
w	weight fraction	
y	vapor molar fraction	
ϵ	void fraction	
λ	Latent heat	
$\mathbf{\Lambda}$	Conductivity	
ρ	density	

Foreword

Primary sources recycle, renewable energy production, and limitation of fossil carbon release as greenhouse gas are deeply connected scientific issues that have been quickly emerging for the last fifty years. Constant improvements of energetic cycles efficiencies and in the atom-economy of chemical reactions are effectively sided by the substitution of carbon and oil with biomass as source of building blocks and power. Sugars or cellulose, in turn, becomes all the more versatile and are exploited more efficiently if converted into methane, syngas or ethanol [1].

This latter liquid has already been established for long as a renewable fuel, its transformation into green plastic is a mature technology thanks first to Alumina- or zeolite-based catalysts for ethylene production; its reforming into hydrogen has been made viable by the skillful use of Ni-based materials (beside more costly noble metals) and further reactions paths are being open on still different catalysts [2, 3].

This work presents three feasibility studies and basic process designs to upgrade ethanol into higher value chemicals: ethylene, ammonia, and acetonitrile. A fourth study is dedicated to the conversion of ethanol into the more versatile hydrogen, that acts also the pivot to feed indirectly a fuel cell and produce electricity, rather than thermal power. A fifth design makes hydrogen follow the reverse power-to-gas route: this key energy-carrier meets then the carbon dioxide released by other processes, and the two are recombined to yield methane. They are graphically shown in figure below.

This thesis consists of two parts. In the first, for each process are reviewed the basic reaction mechanism and the best-performing catalytic formulations, either inherited from the literature or tested directly in the laboratories of this University. The mass and energy balances from the reactor to the separation units are calculated mainly with Aspen Plus[1]; several side-calculations have been performed with other software as specified.

The second part reports the experimental study supporting the calculation of the separative blocks in the ethanol-acetonitrile process. Several experiments of drying, thermal decomposition, miscibility, batch distillation and micro-distillation have been carried out: they show the salting-out of acetonitrile from water in presence of ammonium salts, a phenomenon not always addressed by commonly used thermodynamic calculation packages.

[1] Aspen Technology Inc.

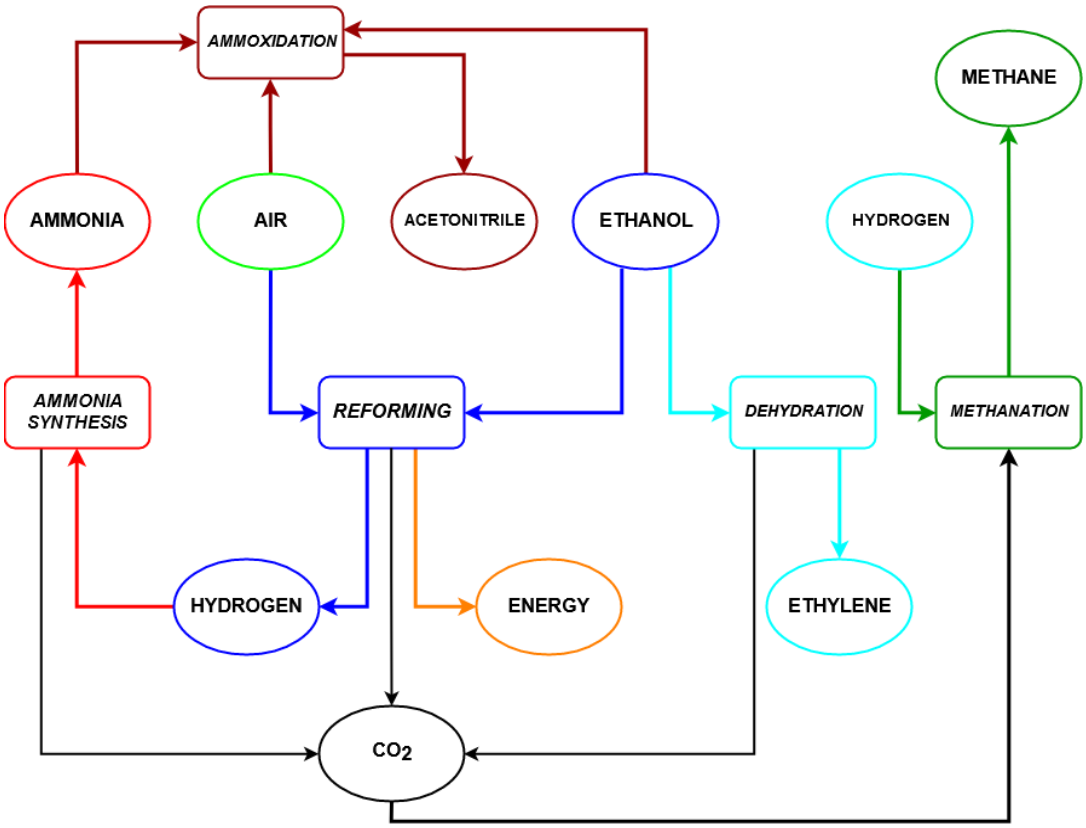

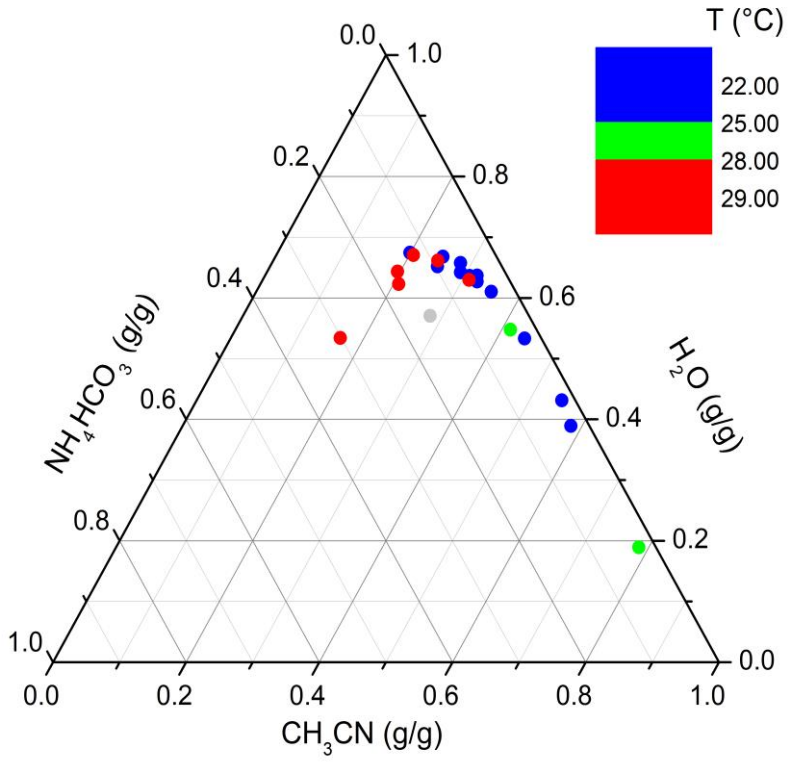

Graphical Asbstract of the work: overall concept of the ethanol and carbon dioxide cycles: critical points of water and acetonitrile in presence of ammonium salt.

Part I

Computer-aided Process Design

Chapter 1

Ethanol Dehydration

Several facilities worldwide provide a fully-integrated process from concentrated bioethanol to polyethylene [4, 5], because most plants are already optimized for fuel-grade alcohol and its on-site conversion into plastic results in a product more practical to handle and sell than gaseous or liquefied ethylene.

In principle, anyway, the green-ethylene process can actually be operated with non-refined ethanol: as a matter of fact, most plants [6] and process studies [7] foresee additional steam injections (in addition to the water generated by the reaction itself) into the reactor to sustain its thermal balances, without detrimental effects on the kinetic. The water content of the reacting mixture is eventually determined by the general stream and energy routing in the overall bio-refinery context [1, 8–10], but diluted ethanol could be used in place of the azeotrope whenever possible: a pre-flash or a straightforward partial distillation of the fermentation beer is sufficient to avoid catalyst fouling [11, 12].

Different plant data have been reviewed as a starting point for process design [13–15]; according to these the byproduct spectrum has been identified [16], and the target yield relevant for further optimization studies fixed to 100 kton/year of ethylene, a scale in line with the up-to-date renewable processes [15]. The work described hereafter has already been partially published [17], its original contribution relies in the study of dehydration starting from a diluted feed, needing less energy input than anhydrous ethanol. This is an improvement from the point of view of process intensification and energy saving.

1.1 Reaction Mechanism

The mechanism of ethanol dehydration has been extensively studied [18]: most catalysts are zeolites [19, 20] or aluminas [21, 22]. The particular nature of the material, however, introduces differences in the mechanism. For example, in several cases the dehydrogenation to acetaldehyde becomes a possibility [23, 24], beside uni or bi-molecular paths to dehydration [25, 26].

Moreover, the plant data available in the literature (either directly or already reveiwed in various simulation works), display a wider spectrum of byproducts [16] with respect to what is obtained in well managed and often isothermal laboratory reactors.

The kinetic model adopted has been therefore built in the following way:

- a set of laboratory data has been taken loading with alumina a tubular reactor (INCOLOY 800, 0.9 cm inner diam., 40 cm length), placed within a cylindrical electric oven connected to a temperature controller (Eurotherm 3204 TIC) and

fluxed with a stream of nitrogen (0.95 mol/mol) carrying a nebulized hydroalcoholic mixture (ethanol:water = 1:3 mol/mol, via a Hitachi L7100 HPLC pump): the exiting gas has been analyzed via gas cromatography (Agilent 7890). Temperature and contact time have been varied around a central experimental point.

- After a review of available microkinetic models [25–31], the one proposed by De Wilde & al. [23, 24] is adopted, because it takes into account specifically the formation of acetaldehyde, that is often observed in the mentioned tests; nevertheless this model is modified in order to account for C_4 byproducts (often observed in real plants as ethylene shows the tendency to polymerize [27], even if only partially, before reaching the polymerization reactor itself), the due reactions are added following the approach of the reviewed material.

- The kinetic constants and the activation energies have been retrofitted in order to have the reaction network (reactions 1.1-1.5) reproduce the laboratory data: their tabulation and the best calculation outputs are presented in section C.1.

- Reactions belonging to the ethanol reforming path (that requires a supported metal, but to a lesser extent is possible also on bare acidic supports) are added to explain the existence of C_1 byproduct (reactions 1.6-1.7); then their kinetic prefactors [32] are adjusted heuristically to achieve a byproduct spectrum in line with those reviewed. The summary of kinetic parameters is in Table 1.1.

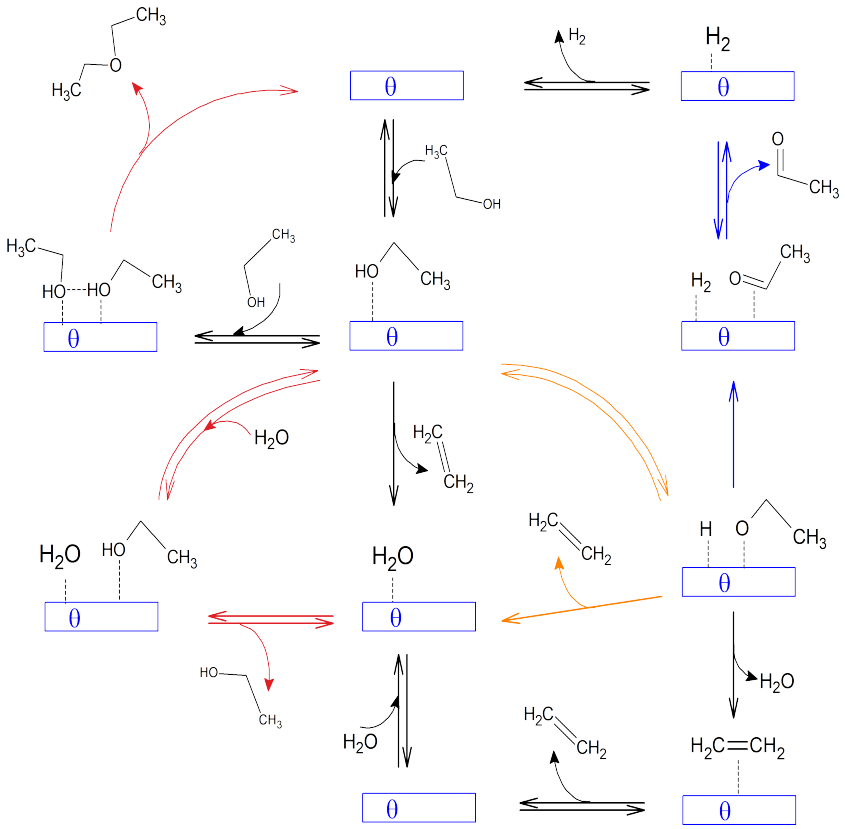

Figure 1.1: Adopted mechanism for ethanol dehydration

$$C_2H_6O \rightleftharpoons C_2H_4 + H_2O \tag{1.1}$$
$$2\,C_2H_6O \rightleftharpoons C_4H_{10}O + H_2O \tag{1.2}$$
$$C_2H_6O \rightleftharpoons C_2H_4O + H_2 \tag{1.3}$$
$$C_4H_{10}O \longrightarrow 2\,C_2H_4 + H_2O \tag{1.4}$$
$$2\,C_2H_4 \longrightarrow C_4H_8 \tag{1.5}$$
$$C_2H_6O \longrightarrow CO + CH_4 + H_2 \tag{1.6}$$
$$C_2H_6O + H_2O \rightleftharpoons CO_2 + 2\,H_2 + CH_4 \tag{1.7}$$

$$r_1 = k_1\, y_{C_2H_6O} \left(1 - \frac{Q_1}{K_{eq,1}}\right) \frac{1}{D^d} \tag{1.8}$$
$$r_2 = k_2\, y^2_{C_2H_6O} \left(1 - \frac{Q_1}{K_{eq,2}}\right) \frac{1}{D^d} \tag{1.9}$$
$$r_3 = k_3\, y_{C_2H_6O} \left(1 - \frac{Q_1}{K_{eq,3}}\right) \frac{1}{D^d} \tag{1.10}$$
$$r_4 = k_4\, y_{C_4H_{10}O} \frac{1}{D^d} \tag{1.11}$$
$$r_5 = k_5\, y_{C_2H_4} \frac{1}{D^d} \tag{1.12}$$
$$r_6 = k_6\, y_{C_2H_6O} \tag{1.13}$$
$$r_7 = k_7\, y_{C_2H_6O} y_{H_2O} \left(1 - \frac{Q_7}{K_{eq,7}}\right) \tag{1.14}$$

where: $k = k^0 \times exp\left(-\frac{E_a}{RT} + \frac{E_a}{RT_0}\right)$ and: $D = 1 + 47\, y_{C_2H_6O} + 17\, y_{H_2O}$.

The reaction quotients and the equilibrium constants are calculated automatically on the basis of the products stoichiometric coefficients and the free energy balance: $K_{eq} = exp\left(-\frac{\Delta^0_r G}{RT}\right)$.

Reaction	k_0 $(\frac{mol}{g_{cat}\,s})$	Ea $(\frac{kJ}{mol})$	T_0 (°C)	d	A
1	6.84×10^{-6}	66.5	300	1	500
2	0.249	63.9	300	2	100
3	3.07×10^{-5}	60.0	300	1	0.025
4	5.57×10^{-4}	107	300	1	5×10^4
5	2.78×10^{-7}	114	300	2	1×10^4
6	1.13×10^{-7}	123	625	0	5×10^5
7	3.06×10^{-7}	195	625	0	1×10^7

Table 1.1: Kinetic parameters for ethanol dehydration. Parameter 'A' modifies the prefactor to obtain data closer to the plant reviews.

1.2 Thermodynamic Description

The chemicals and the thermodynamic models involved in the simulations are listed in Table 1.2.

Specie	**Formula**	**MW**	**Reports ID**
Ethanol	C_2H_6O	46	ETHANOL
Acetaldehyde	C_2H_4O	44	ACETALD
Diethylether	$C_4H_{10}O$	74	ETOET
Butylene	C_4H_8	56	BUTYLEN
Water	H_2O	18	WATER
Carbon Monoxide	CO	28	CO
Carbon Dioxide	CO_2	44	CO2
Methane	CH_4	16	METHANE
Hydrogen	H_2	2	H2
Ethylene	C_2H_4	28	ETHYLENE
Methyl-Diethanolamine	$C_5H_{13}NO_2$	119	MDEA
Hydronium	H_3O^+	19	H3O+
Hydroxide	OH^-	17	OH-
Bicarbonate	$HCO_3{}^-$	61	HCO3-
Carbonate	$CO_{32}{}^-$	60	CO3- -
Methyl-Diethanolammonium	$C_5H_{14}NO_2{}^+$	120	MDEA+
Models	**Parameters**		
NRTL	APV90 VLE-RK		
ELECNRTL	APV90 ENRTL-RK		
RKS	APV90 EOS-LIT		
HENRY	AP90 HENRY-AP		
	AP90 BINARY		
STEAM-TAB	National Bureau of Standards		

Table 1.2: Species involved in the Ethanol dehydration process

In the reaction section, where only superheated vapor is present, the thermodynamic model adopted is the Redlich-Kwong-Soave equation of state. Its modified version Predictive-Soave-Redlich-Kwong performs pretty well also for the foreseen ethylene - butylene mixture (see Figure 1.3). When a liquid phase appears, a check on the systems' capability to reproduce all the involved solubilities is made. As shown in Figures 1.2 to 1.4, the PSRK equation describes correctly all the involved species except diethylether, while the Non-Random Two Liquid model coupled with the Redlich-Kwong equation (NRTL-RK) is always less accurate but never too much wrong (Figures 1.2, 1.3 and 1.4). Moreover, this latter system allows one to describe the vapor phase separately via an empirical Henry's constant. Considering that the liquid-vapor problem of this simulation actually consist in a fair account of solubilities respect to water, and the greater deviations between the two models are seen at high temperatures and pressures, the combination of the NRTL-RK model with the ethylene Henry constant is adopted.

Other adjustments have been operated on the Henry constant of butylene and CO in

Stoichiometry	A	B	C
$2\,H_2O \rightleftharpoons OH^- + H_3O^+$	132.90	-13446	-22.477
$MDEA + H_3O^+ \rightleftharpoons MDEAH^+ + H_2O$	9.416	4235.0	0
$CO_{2(g)} \rightleftharpoons CO_{2(l)}$	Henry constant		
$CO_2 + H_2O \rightleftharpoons HCO_3{}^- + H_3O^+$	231.46	-12092	-36.782
$HCO_3{}^- + H_2O \rightleftharpoons CO_3{}^{2-} + H_3O^+$	216.05	-12432	-35.482

Table 1.3: Equilibrium reactions used to calculate the distribution of charged species formed in the ternary water-MDEA-CO_2 system, with equilibrium constants expressed as: $ln\frac{K}{(1\,mol/mol)} = A + B(K)/T + Cln(T/K)$

water, after reviewing the correlations proposed by Serra & al. [39] and by Sander [40] (Figure 1.5).

Since the carbon dioxide capture is simulated through the basic-wash strategy [41–43, 43], the involved blocks are set to work with a variant of the NRTL model, ELEC-NRTL [44]. In addition, a set of equilibrium reactions taking place in the aqueous solvent are added to the embedded calculation of these blocks, as listed in Table 1.3.

The Vapour-Liquiq Equilibrium (VLE) for the amine-capture system as predicted by the AP database is reviewed in graphics 1.6.

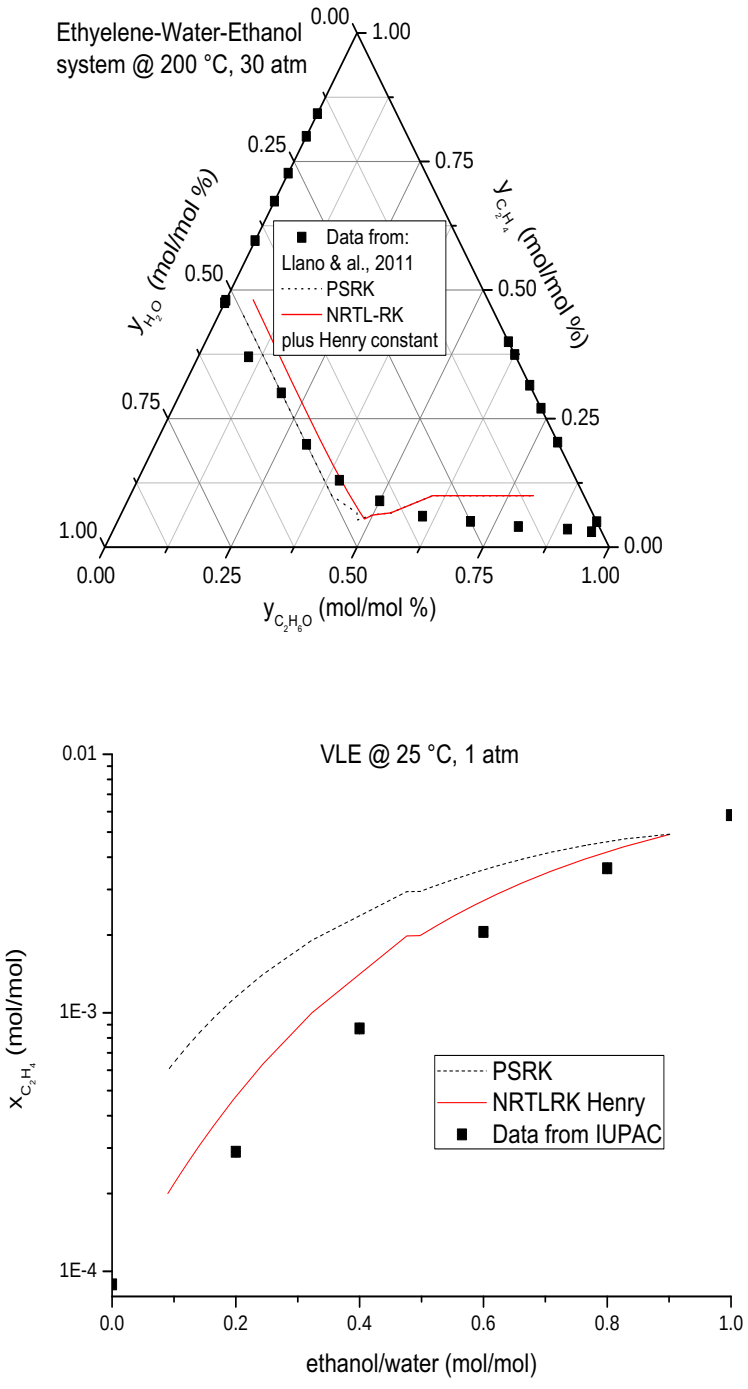

Figure 1.2: Ethylene-water-ethanol and Ethylene-water VLE. Data from [33] and [34].

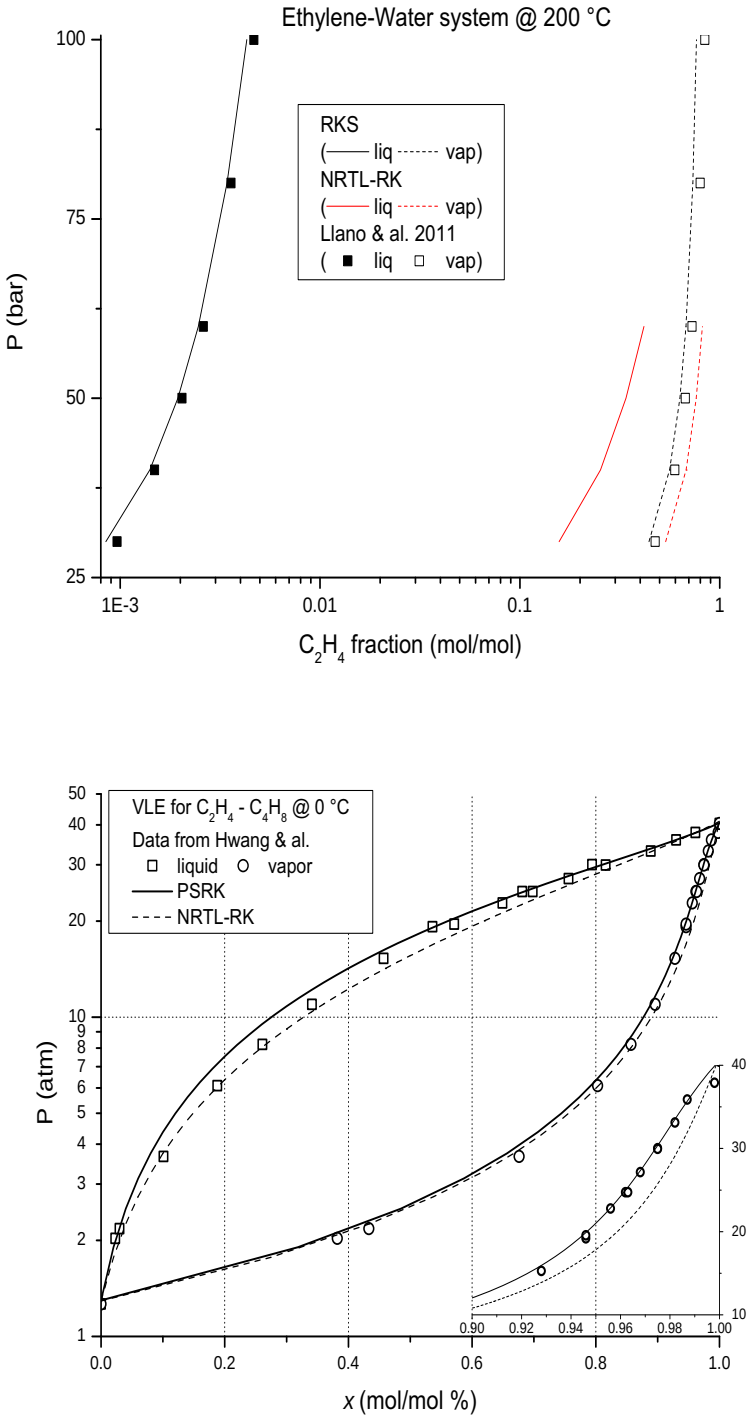

Figure 1.3: Ethylene-water and Ethylene-butylene equilibria. Data from [33,35] and [36].

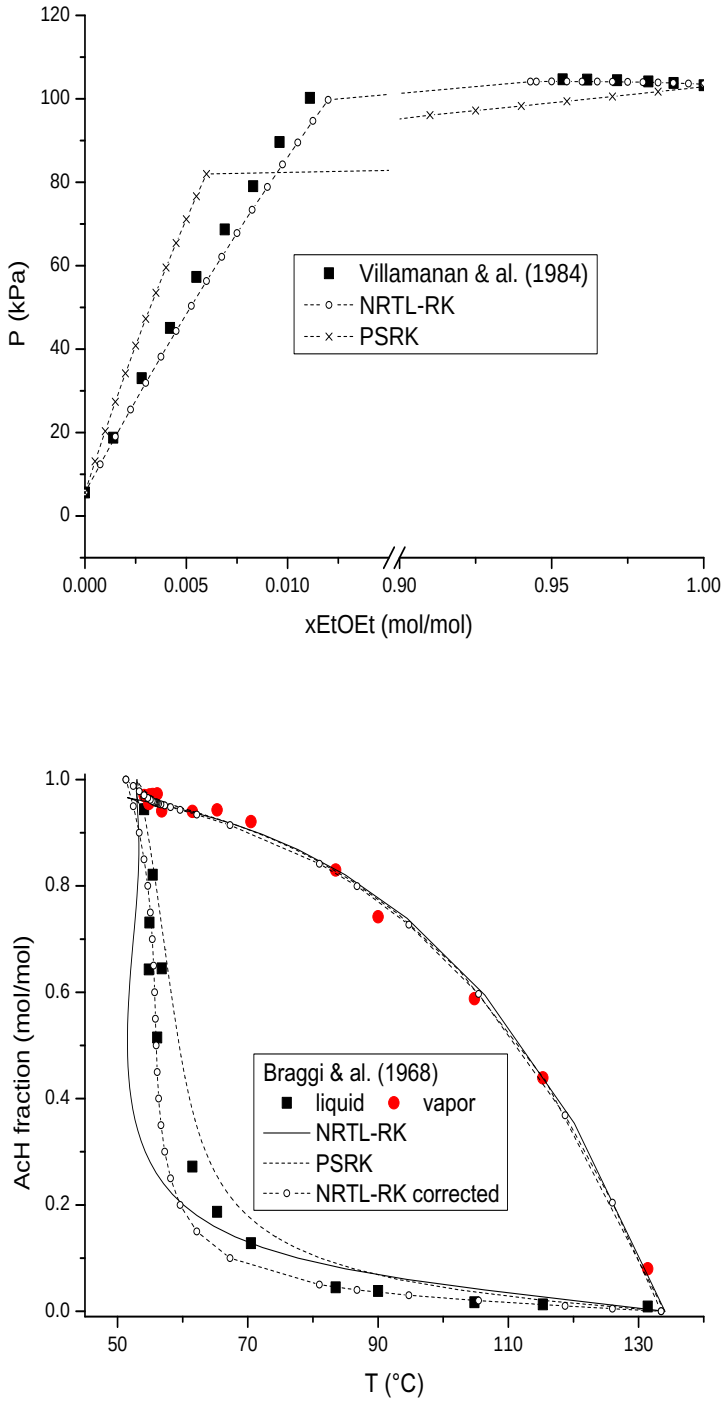

Figure 1.4: Diethylether-water [37] and acetaldehyde-water equilibria [38].

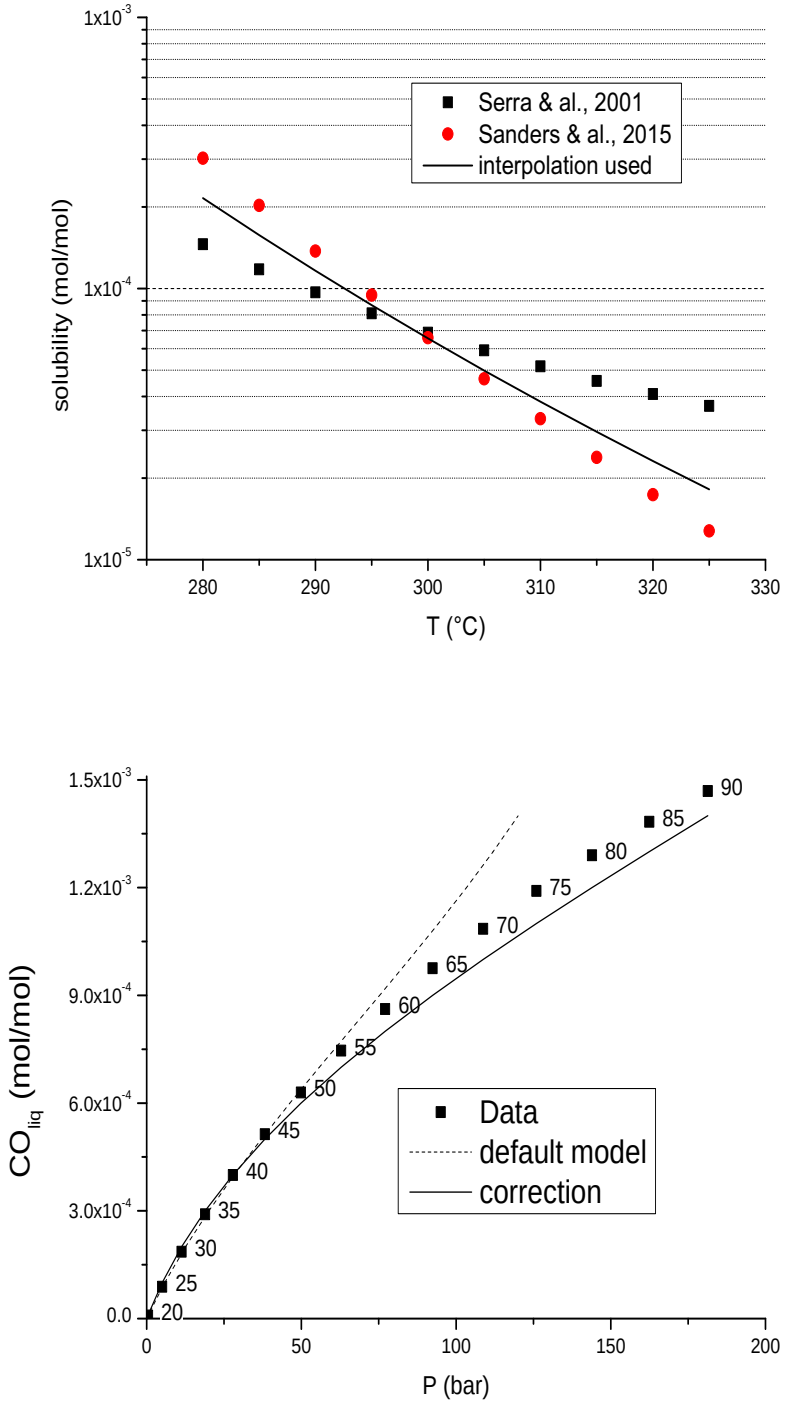

Figure 1.5: Butylene-water solubility and CO solubility (temperature in labels).

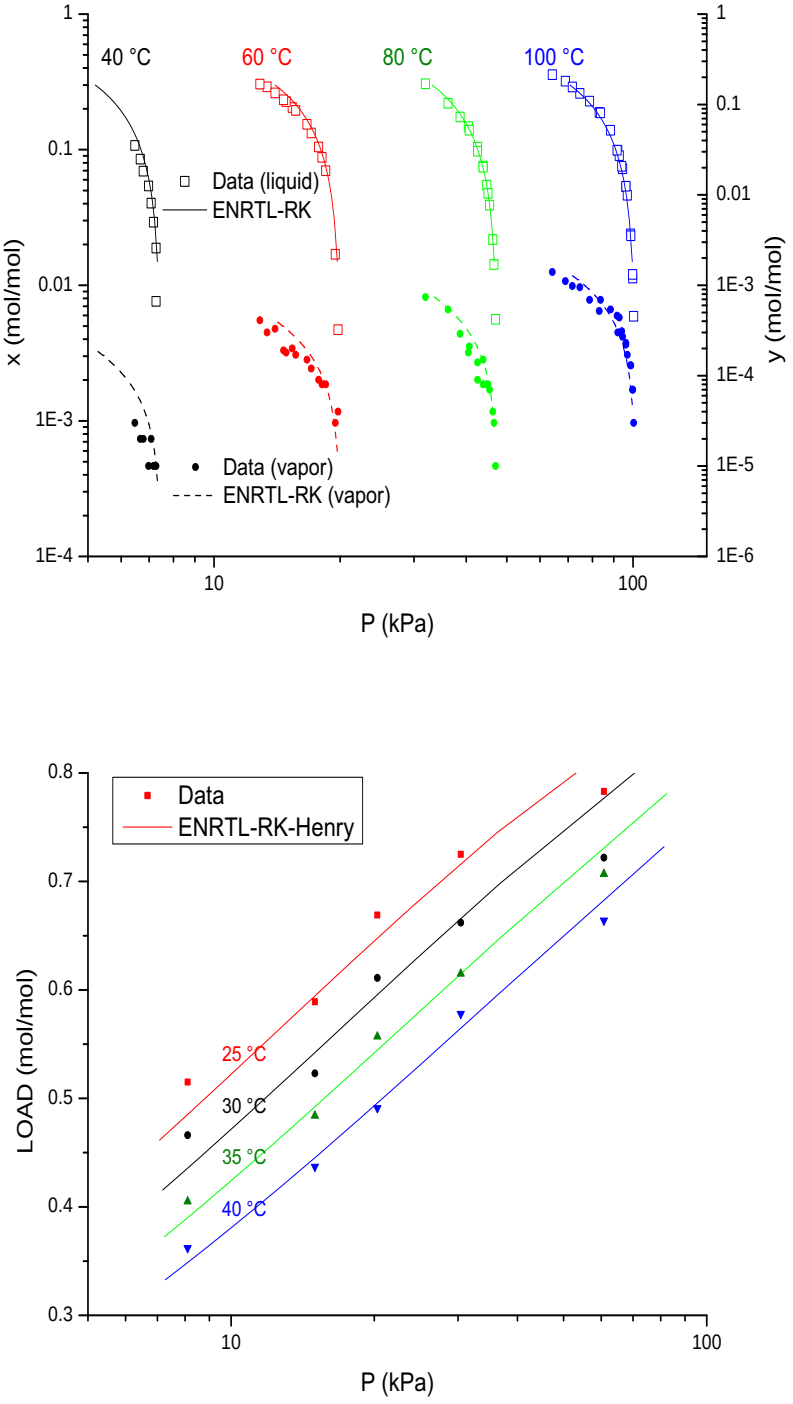

Figure 1.6: MDEA-water VLE (data from [45]); and $CO_{x(l)}$:MDEA molar ratio (i.e. 'Load') vs $CO_{2(g)}$ partial pressure for the MDEA-CO_2-water system [46].

1.3 Process Outline

The bioethylene process is divided into five main sections (see also the other plant reviews [47, 48] and the simulations works [7, 13, 16, 49–53]), as shown in the schemes 1.7-1.8:

1) reaction and first water separation;

2) pressurization, further water discharge and stripping of the process condensate to retrieve ethanol [51];

3) basic wash to capture carbon dioxide;

4) pressure-swing dehydration;

5) cryogenic distillation to separate ethylene from the higher olefines.

The process scale is set to the order of 10^3 t/day of ethylene, fully representative of up-to-date bioethylene plants [15]; while considering bioethanol facilities themselves, the supposed feed consumption of 76 t/h corresponds to a very large plant [54].

The reactor is modeled as three adiabatic catalytic beds placed in series, with a reheating of the process stream between each. The water already present in the feed (and increasing as the main reaction proceeds) makes up for a thermal inertia that, despite the endothermic character of the reaction, prevents the reacting mixture to cool down too quickly. For example, the vaporized and heated feed to the first reaction stage has a calculated heat capacity of 101 kW/°C, while the same quantity of azeotropic ethanol in the same condition had 53 kW/°C, so the same conversion would roughly mean a doubled temperature decrease and the need of more reheating stages. The diameter, void fraction and catalyst pellets size are chosen in order to grant an overall pressure drop $\leq$0.2 bar, though it has to be pointed out that the original fit of the kinetic parameters is done considering the mass of active material only, without inert fillers.

The first separation takes place in a flash block, followed by a multistage compression with staged intercoolings and water separation. The behavior of th first section is outlined in Figure 1.9.

The carbon dioxide removal is developed following the regular layout of an adsorbing column and a stripper, between which is circulated an aqueous solution of Methyldiethanol-amine (MDEA, 19% by weight); this kind of process is often the choice when the processed gas flow is large [55]. The stripping column is equipped with a condenser in order do decrease the quantity of MDEA lost with the vent gas. This section is balanced to leave 122 ppm of CO_2 in the sweet gas circulating 2.5 moles of MDEA for every mole of CO_2 (Figure 1.10). This aspect of the calculation is very sensitive to the liquid-vapour equilibrium for carbon dioxide and water. A comparison of the thermodynamic model behaviour with a set of literature data is showed in Figure 1.6.

The water still present is removed by adsorption on an acidic solid via the pressure-swing technique (chapter B.2), that takes advantage of the pressure increase performed in the water-dump section. A part of the dehydrated gas itself (34% of the produced ethylene) is used to purge the off-duty bed, and is then recycled to the CO_2 absorber (see [56] for a similar approach). Being a dynamic process, the pressure-swing section cannot be calculated directly within a steady-state simulation, so it is solved separately taking the water content and the off-gas flow as design parameters (the results are showed briefly in Figure 1.11).

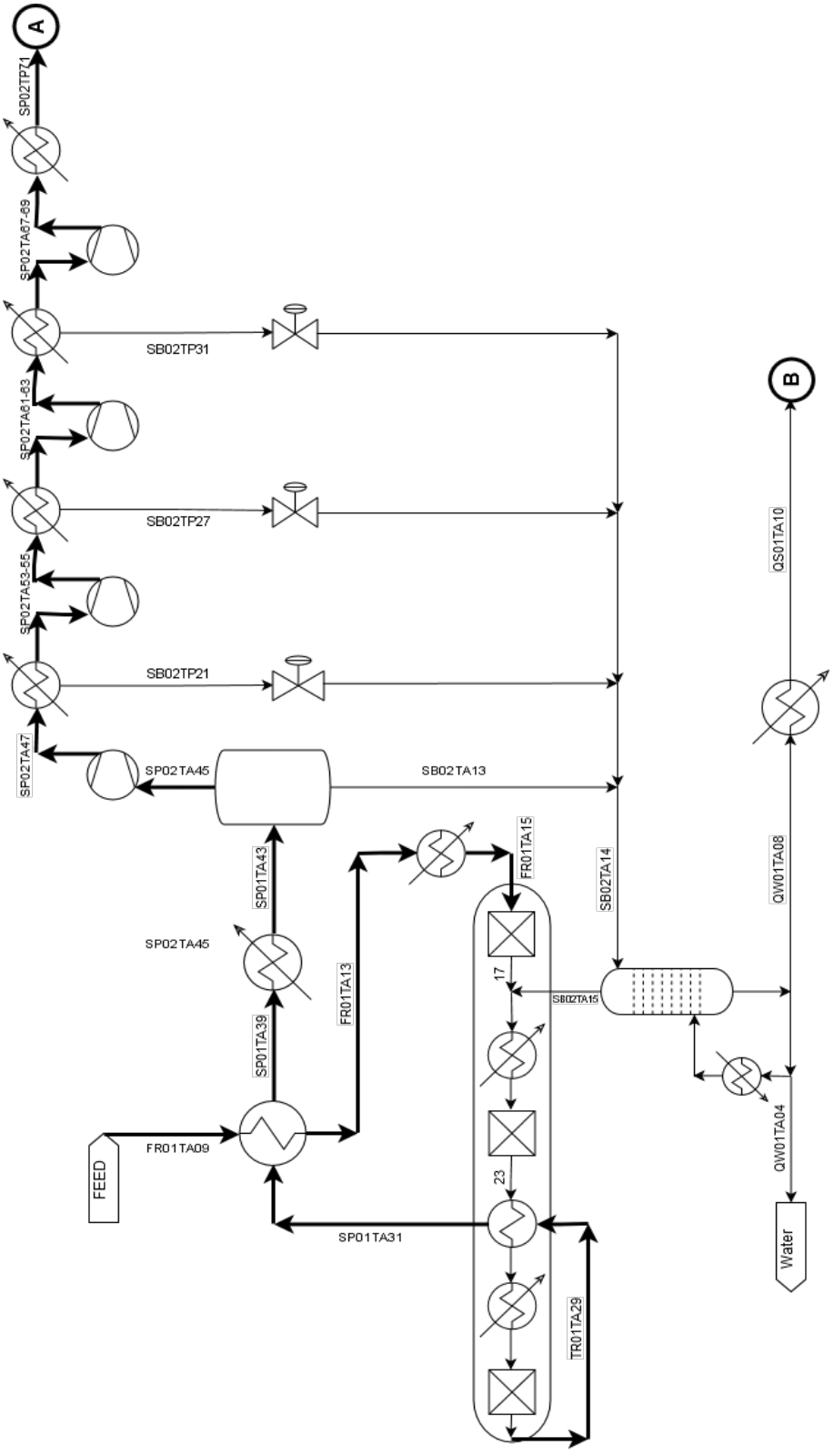

Figure 1.7: Reactive section process layout.

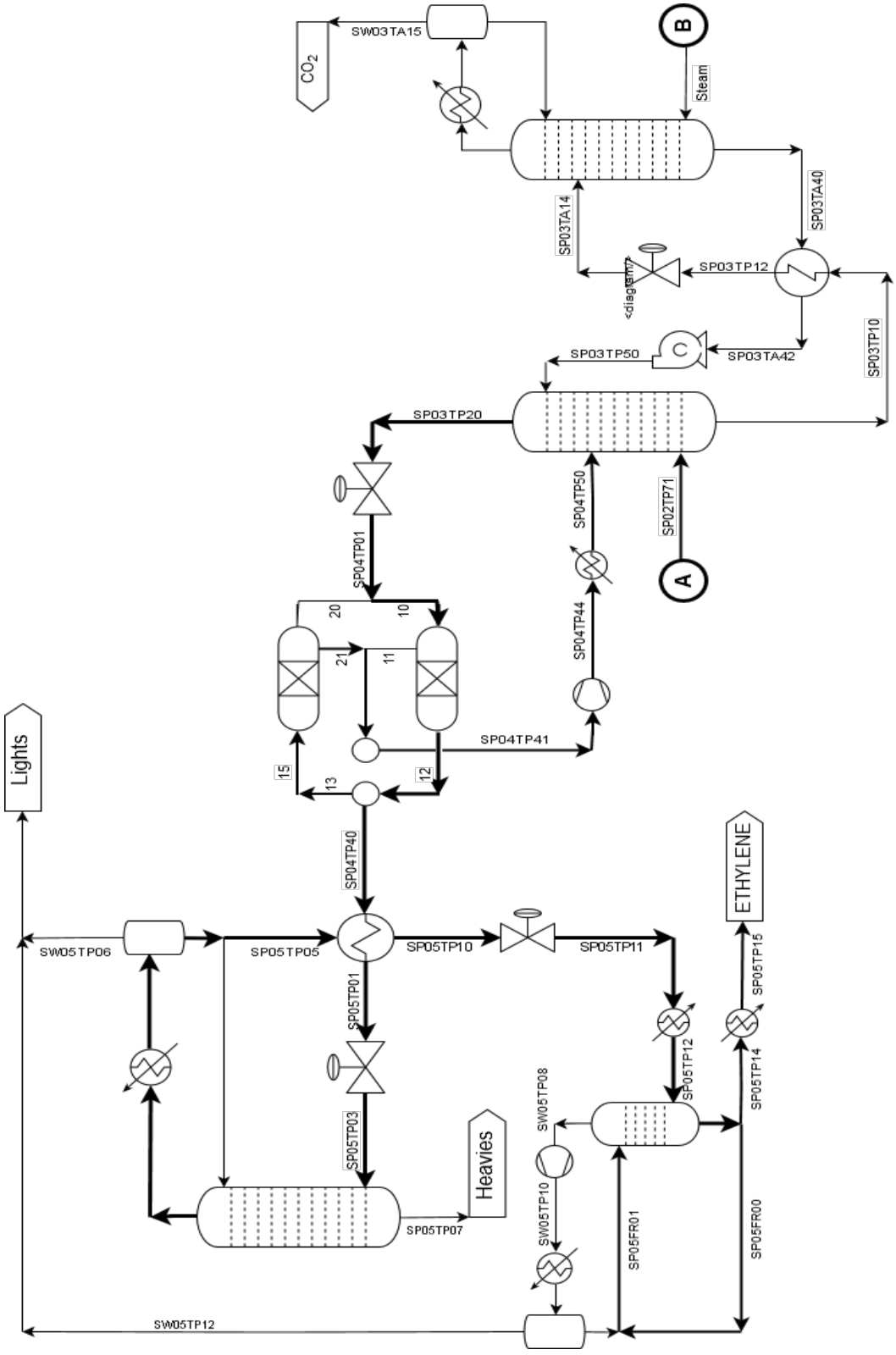

Figure 1.8: Overall process layout.

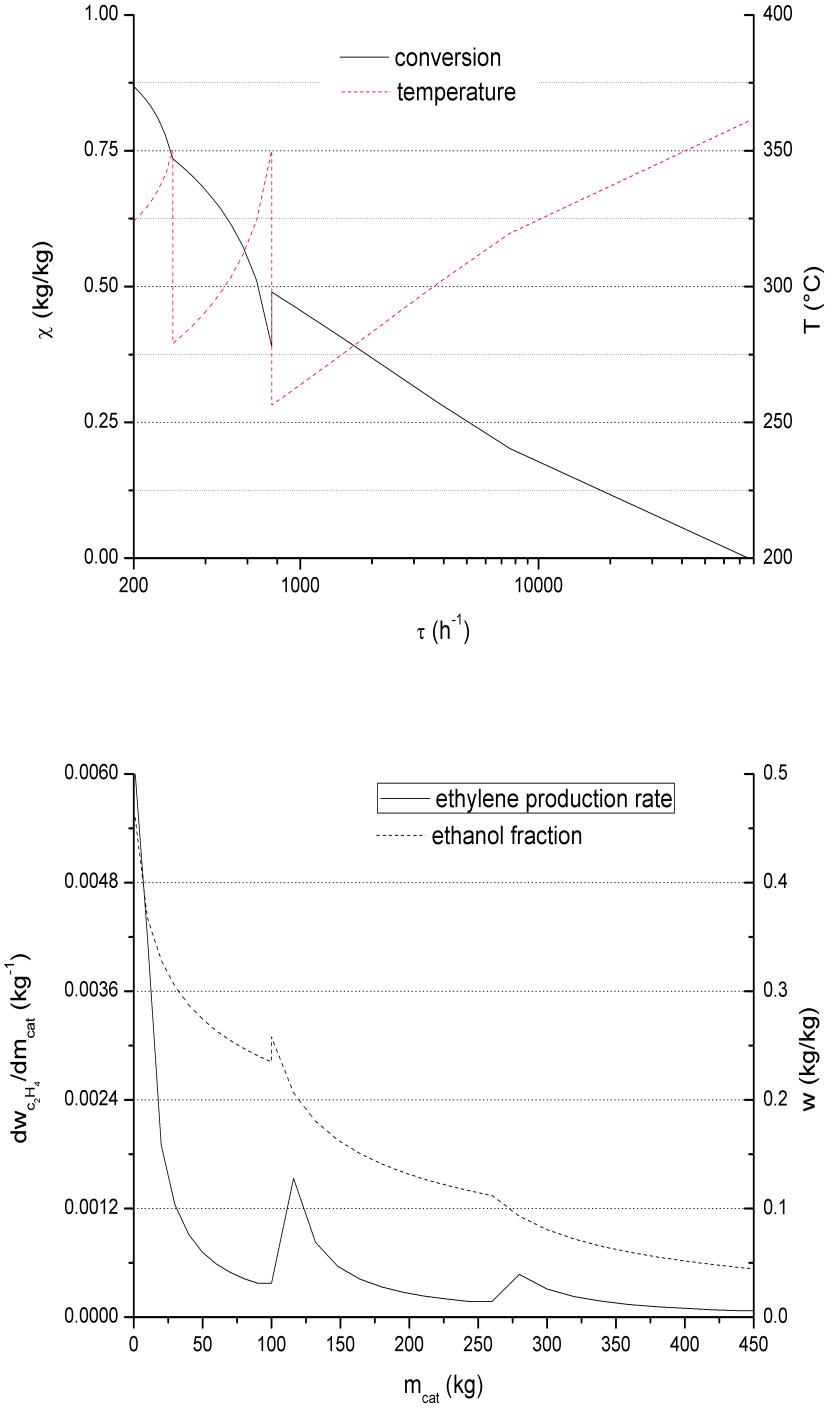

Figure 1.9: Reactor profiles as functions of contact time and catalyst loading.

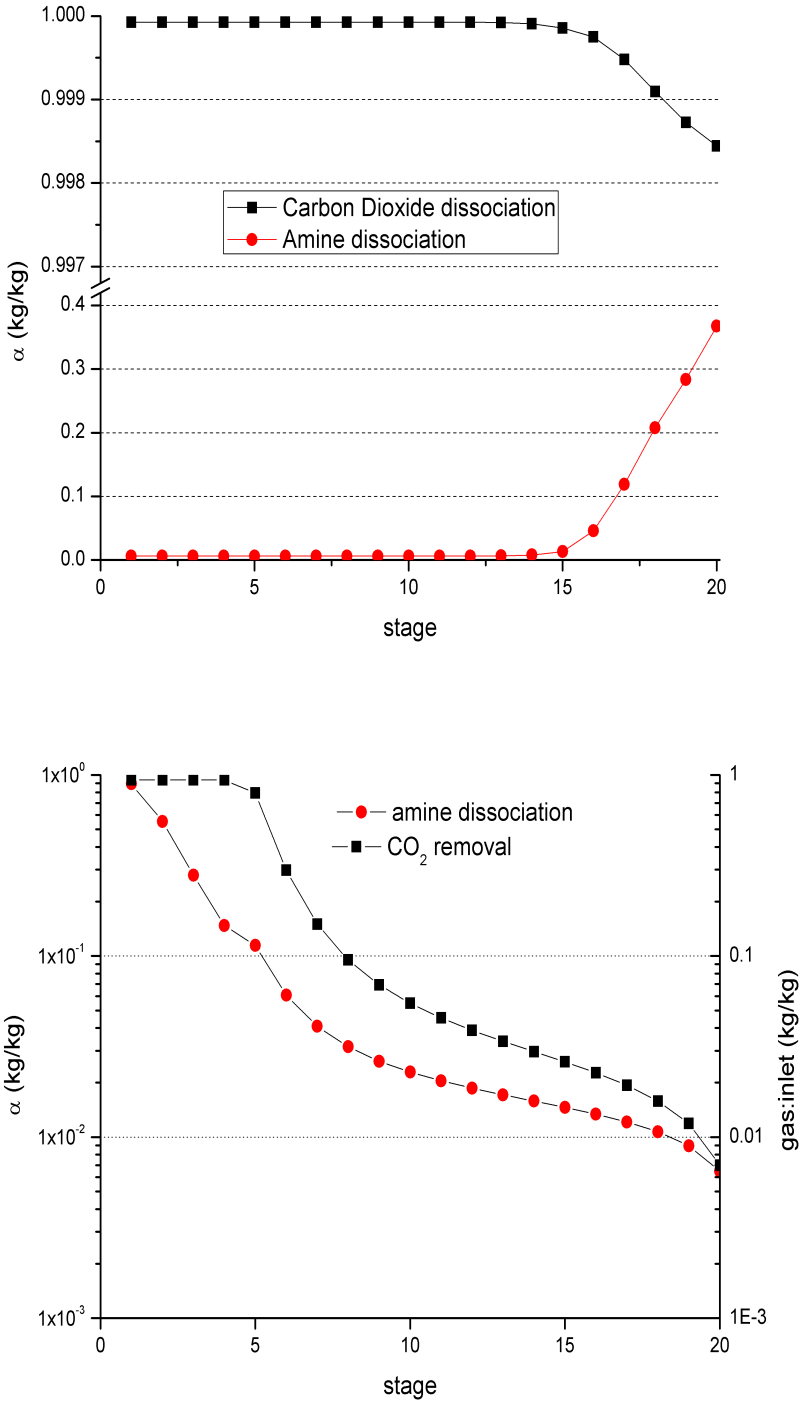

Figure 1.10: Adsorber-Stripper profiles (α: dissociation fraction).

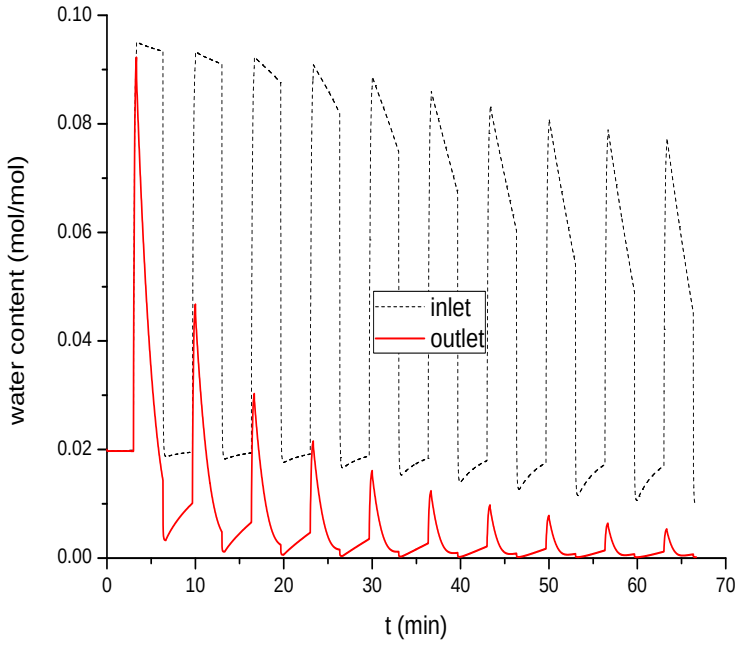

Figure 1.11: Water content at the inlet and exit of the purification beds from the start to the steady-state functioning of PSA.

The final task is the cryogenic separation of ethylene from the heavier olefines (here conventionally represented as butadiene) that may arise from early polymerization in the latest reactor's stages [57]. Since the reaction rates adopted for this test are set to produce an appreciable quantity of light gases (methane, hydrogen and CO, beside CO_2) in order to estimate possible outcomes of real or pilot-scale reactors [50], the ethylene is drawn from the overhead partial condenser as liquid, letting off most of the lights. It has to be noticed, however, that depending on the amount of gas still present, a more complex lights-heavies purification train could be needed. Relying just on a partial condenser with the set-up reaction kinetic yields still 1412 ppm of impurities with a recovery of 99.86% kg/kg. Adding a second series of trays as in the scheme 1.8can reduce the impurities to 250 ppm, but decreasing the ethylene recovery to 83.4% kg/kg.

1.4 Energy Recovery

The overall power balances are displayed synthetically in Figure 1.12 for the process streams only, without including the utilities.

Most of the energy recovery possibilities rely in an effective match between the heat needed to boil-up the feed, and the heat released to condensate and separate the water. The present analysis considers the mixed ethanol-water feed as liquid, because otherwise it would be needed to asses the particular point of integration of the dehydration reaction into a whole biorefinery context.

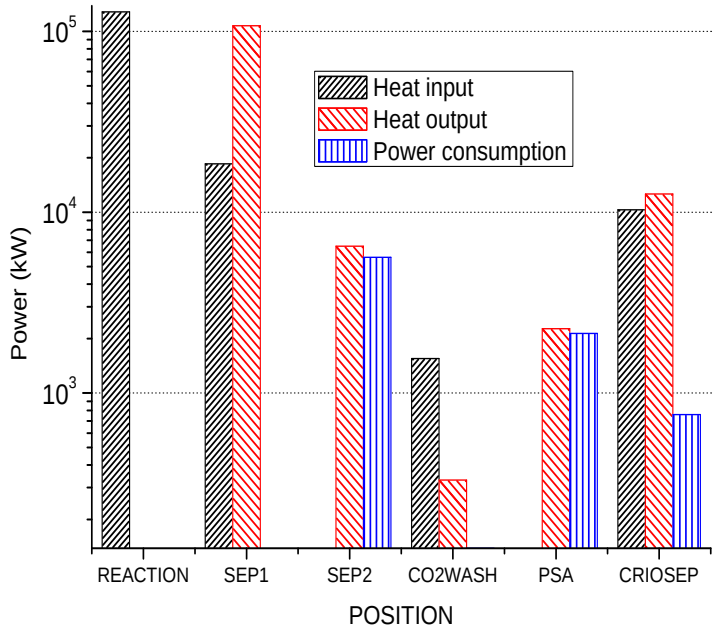

Figure 1.12: Power balances of the main process sections.

The Pinch Analysis [58] of the system (without considering process fluids matches), performed with a custom-made Matlab routine, is shown in Figure 1.14 for a minimum temperature approach of 10 °C.

On this basis, the crucial feed-to-product heat recovery has been designed in order to avoid pinch-crosses in the regenerative exchangers. Actually, to achieve this goal the global requirement has been relaxed to a temperature approach of 5 °C only, since in this point there's a latent heat-exchange taking place, and a local pinch (90.5 °C ca) has been found slightly below the global one, according to a process-sectioning approach [58] - see Figure 1.13.

After the more relevant fluid matches, the process energetic analysis is modified as shown in Fig. 1.15 and reported in Table 1.4.

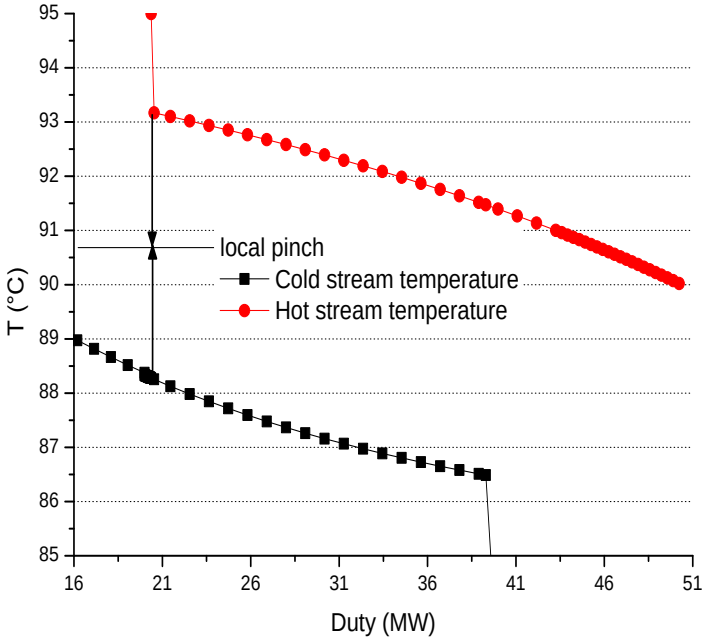

Figure 1.13: Analysis of the regenerative heat-exchange blocks.

Case	ΔT_{min} (°C)	T_{pinch}	H.U. (kW)	C.U. (kW)	Heat in (kW)	Heat out (kW)
no matches	10.0	92.0	1.18×10^5	9.48×10^4	1.53×10^5	1.29×10^5
actual	10.0	92.5	6.87×10^4	7.37×10^4	2.27×10^4	8.21×10^4

Table 1.4: Main energetic parameters (HU: Hot Utility, CU: Cold Utility).

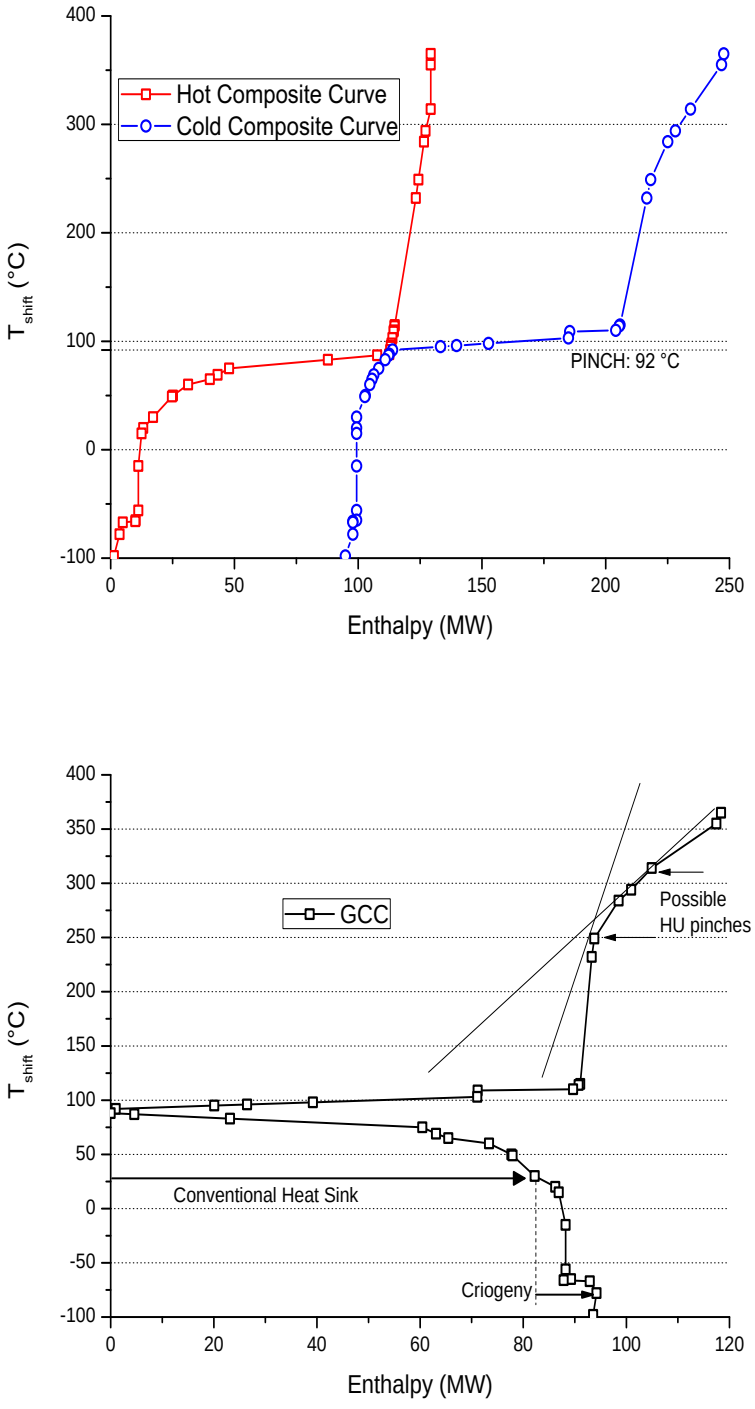

Figure 1.14: Process Composite Curves and Grand Composite Curve, with different possibilities of heat feeding according to the hot utility top temperature and heat capacity.

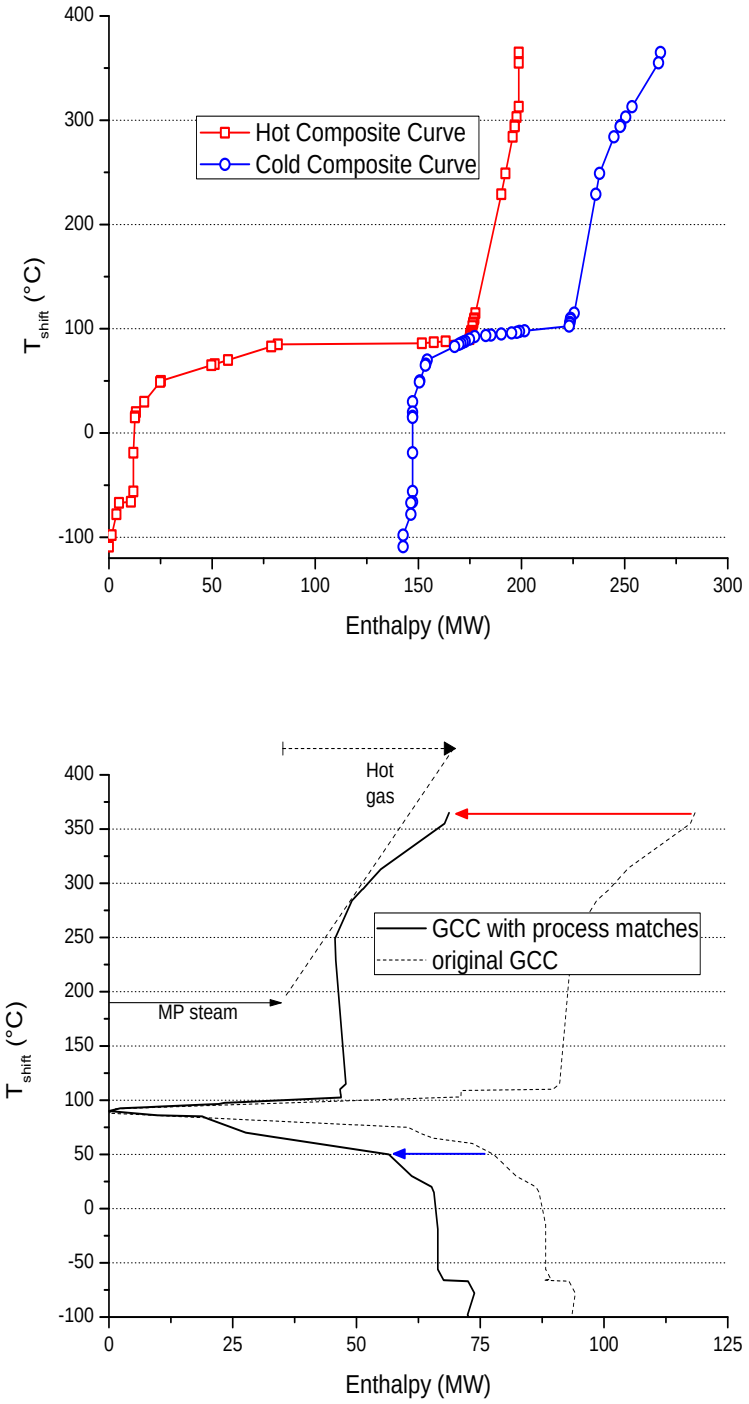

Figure 1.15: Overlapped Composite Curves and modified GCC with main savings and hypothetical T-H profiles for the hot utilities.

Chapter 2

Ethanol Steam Reforming

The production of sustainable hydrogen is considered a promising solution to reduce the CO_2 emissions in the automotive and industrial sectors, because it opens new perspectives for the use of many organic materials: for example, while ethanol itself is a renewable fuel for conventional engines, its conversion into hydrogen makes it available also for fuel cells [59, 60], beside turning it into a much more versatile building block.

A medium to large scale reforming plant can therefore be a solution to exploit bioethanol as a hydrogen source, while the production of electric energy (via a fuel cell) looks more suited to small and micro scale contexts, and in both cases the diluted alcohol could prove a less expensive feedstock than fuel-grade ethanol.

Moving a step further on this route, it is observed that the water condensation (to purify the reformate) and the hydrogen reaction (in the fuel cell) release heat at temperatures below the foreseen pinch-points of the reforming process: one approximately at the boiling point of the hydroalcoholic feed (cold feed - hot products exchange), an the other at the catalyst activation temperature (reacting mixture - combustion gases exchange); yet these sub-pinch heat loads are aligned with the typical sanitary water temperatures in civilian buildings, making it possible to design a Heat & Power cogeneration system suited for micro-scale distributed use.

2.1 Mechanism and Kinetic descriptions

The mechanism of the ethanol steam reforming has been extensively studied for the past years, both theoretically [61,62] and experimentally [63,64]: Nickel (with various dopants) has often been preferred over noble metals because is as active but less expensive [65–70]. Depending on the catalyst support and active material, the adsorbed ethanol can be activated by a first abstraction of the oxygen-bound hydrogen [71]; some ethanol can then be lost by dehydration to ethylene, while the reforming path is generally believed to involve a first partial oxydation to acetaldehyde followed by the C-C bond break and steam-reforming of the resulting methane [72]. The importance of the methane reforming reaction over the $CH_4 \rightleftharpoons CO_2$ and water-gas shift equilibria depends much on the peculiar catalyst's properties and reaction temperature (usually in the range 400-600 °C) [71, 73, 74].

In general, the theoretical output of 6 moles of H_2 per mole of ethanol (at the balanced ratio of 1 mole of ethanol and 3 of water) is not reached due a residual presence of methane [71]. Thermodynamic equilibrium, in fact, allows a substantial conversion of

the carbon monoxide via two water-gas shift stages (usually with catalyst showing redox capabilities [72]), but blocks the methane consumption [75]. Though water molecules may hamper the ethanol absorption on acidic supports (chiefly aluminas) [76], water:alcohol ratios higher than three mol/mol have been successfully tested [77], either for the fact that water undergoes a dissociative absorption turning into the active mojeties $-\mathrm{OH}\cdot$ and $-\mathrm{H}\cdot$ [76], and for its role in reforming and removing the coking (ensuing from ethylene polymerization or by $-\mathrm{CH}\cdot$ aggregation into sooth, depending on the material [69, 78, 79]).

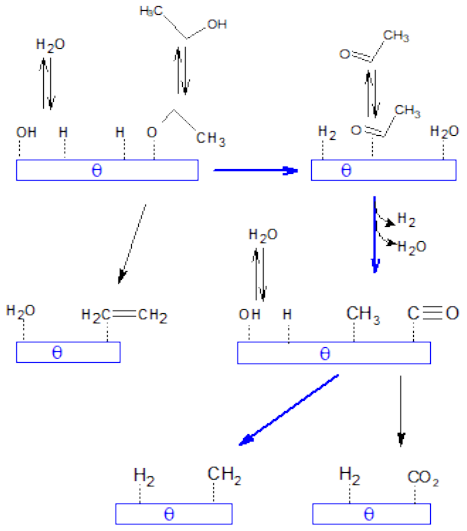

Figure 2.1: Mechanism of ethanol reforming.

A reaction network compliant with the above sketched mechanism (see also Figure 2.1) can be built to different complexity levels [73, 76, 80–84], with a heuristic or microkinetic approach [31]. The latter solution has been worked out successfully [32] and further adapted to a set of proprietary data [69], and can be used to calculate in detail the thermal profile and the material balances rising in a reformer:

$$\mathrm{C_2H_4O} \longrightarrow \mathrm{CH_4} + \mathrm{CO} \tag{2.1}$$

$$\mathrm{C_2H_6O} + \mathrm{H_2O} \longrightarrow \mathrm{CO_2} + \mathrm{CH_4} + 2\,\mathrm{H_2} \tag{2.2}$$

$$\mathrm{CH_4} + 2\,\mathrm{H_2O} \rightleftharpoons 4\,\mathrm{H_2} + \mathrm{CO_2} \tag{2.3}$$

$$\mathrm{CO_2} + \mathrm{H_2} \rightleftharpoons \mathrm{CO} + \mathrm{H_2O} \tag{2.4}$$

$$\mathrm{C_2H_6O} \longrightarrow \mathrm{C_2H_4O} + \mathrm{H_2} \tag{2.5}$$

$$\mathrm{C_2H_6O} \longrightarrow \mathrm{C_2H_4} + \mathrm{H_2O} \tag{2.6}$$

$$\mathrm{C_2H_4} \longrightarrow 2\,\mathrm{C} + 2\,\mathrm{H_2} \tag{2.7}$$

$$r_1 = k_I \frac{y_{H_2}^{1/2}\, y_{CH_4}^{-1}\, y_{AcH}}{(1+D)^2} \tag{2.8}$$

$$r_2 = k_{II} \frac{y_{H_2O}\, y_{CH_4}^{-1}\, y_{AcH}}{(1+D)^2} \tag{2.9}$$

$$r_3 = k_{III} \frac{y_{H_2}^{-5/2}\, y_{CH_4}\, y_{H_2O}^2 - \frac{1}{K_{SRM}}\, y_{CO_2}\, y_{H_2}^{3/2}}{(1+D)^3} \tag{2.10}$$

$$r_4 = k_{IV} \frac{y_{CO_2}\, y_{H_2}^{1/2} - \frac{1}{K_{WGS}}\, y_{CO}\, y_{H_2O}\, y_{H_2}^{-1/2}}{(1+D)^2} \tag{2.11}$$

$$r_5 = k_V \frac{y_{EtOH}\, y_{H_2}^{-1/2}}{(1+D)^2} \tag{2.12}$$

$$r_6 = k_{VI} \frac{y_{EtOH}}{(1+D)^3} \tag{2.13}$$

$$r_7 = k_{VII} \frac{y_{CH_4}\, y_{H_2}^{-1/2}}{(1+D)^2} \tag{2.14}$$

$$D = \sum_{j'} \left[K_{0j'} \times e^{-\frac{\Delta_{ads}H_{j'}}{R}\left(\frac{1}{T}-\frac{1}{T_0}\right)} \times \prod_j y_j^{\alpha_{j'j}} \right] \qquad lnk = lnk_0 - \frac{E_a}{R}\left(\frac{1}{T}-\frac{1}{T_0}\right)$$

$$lnK_{SRM} = 1.007 - \frac{22512}{T_0} + \frac{22512}{T} \qquad lnK_{WGS} = 0.7458 - \frac{4353}{T_0} + \frac{4353}{T}$$

and the other parameters are listed in Table 2.1 and in the original work [32], depending on the dataset on which the retro-fit has been operated (i.e. on the catalyst).

Reaction	**Dataset 1**			**Dataset 2**		
	$ln\, k_0$ $\left(\frac{mol}{mg\, min}\right)$	Ea $\left(\frac{J}{mol}\right)$	T_0 K	k_0 $\left(\frac{mol}{mg\, min}\right)$	Ea $\left(\frac{J}{mol}\right)$	T_0 K
2.8	-10,51	39500	898	-11,04	60000	873
2.9	-9,89	1130	898	-11,68	20	873
2.10	-3,36	1000	898	-8,80	500000	873
2.11	-6,23	302000	898	-10,41	22000	873
2.12	-7,81	191000	898	-8,87	200000	873
2.13	-41,44	189000	898	-7,71	28000	873
2.14	-93,76	580000	898	-12,56	10	873

Table 2.1: kinetic parameters

Nevertheless, it has to be pointed out that this set of rate equations may present some calculation drawbacks, expecially because the presence of many enthalpy-related parameters make the system very sensitive to temperature variations. Therefore, it is here considered the adoption of a simpler system of heuristic equations to model a reformer belonging to relatively complex flow-charts, after the review on available literature models [85]:

$$C_2H_6O \rightleftharpoons C_2H_4O + H_2 \qquad r_1 = k_1 \left(e^{\frac{E_{a1}}{RT}}\right) \frac{y_{EtOH}(1 - e^{A+B/T}\, Q)}{D} \tag{2.15}$$

$$C_2H_4O \rightleftharpoons CO + CH_4 \qquad r_2 = k_2 \left(e^{\frac{E_{a2}}{RT}}\right) \frac{y_{AcH}(1 - e^{A+B/T}\, Q)}{D} \tag{2.16}$$

$$CH_4 + H_2O \rightleftharpoons CO + 3\,H_2 \qquad r_3 = k_3 \left(e^{\frac{E_{a3}}{RT}}\right) \frac{y_{CH_4} y_{H_2O}(1 - e^{A+B/T}\, Q)}{D^2} \tag{2.17}$$

$$CO + H_2O \rightleftharpoons CO_2 + H_2 \qquad r_4 = k_4 \left(e^{\frac{E_{a4}}{RT}}\right) \frac{y_{CO} y_{H_2O}(1 - e^{A+B/T}\, Q)}{D^2} \tag{2.18}$$

$$D = 1 + KA_2\, y_{EtOH} + KA_3\, y_{H_2O} + KA_4\, y_{H_2} + KA_5\, \frac{y_{H_2O}}{y_{H_2}^{0.5}} + KA_6\, \frac{y_{CH_4}}{y_{H_2}^{0.5}} + KA_7\, y_{CO} + KA_8\, y_{H2}^{0.5}$$

where Q are the reaction quotients, and the parameters are as per in Table 2.2.

Reaction	k_0 $\left(\frac{kmol}{kg_{cat}\, s}\right)$	Ea/R (K)	A	B (K)
2.15	11.4	-3825	-14.7	8116
2.16	8.42	-2983	-14.7	-1609
2.17	9.87×10^6	-14313	-53.0	26154
2.18	1.06×10^6	-7264	-4.39	-4657
KA_2	4.1	596.5		
KA_3	5.0×10^{-6}	6845		
KA_4	7.4×10^{-4}	8030		
KA_5	1.2×10^{-6}	6440		
KA_6	$6.8e \times 10^{-9}$	8025		
KA_7	5.6×10^{-9}	3260		
KA_8	1.0×10^{-8}	9565		

Table 2.2: The parameters KA_{2-8} have the same form as the reaction constants k_{1-n}

Notice that some equilibrium constants in the above equations are modified, with respect to the original values reported by the authors, to correct the fugacities at 10 bar (i.e. the supposed pressure for the process described below in par. 2.3) with respect to the atmospheric pressure of the lab tests.

The first formulation (2.8-2.14) is used to simulate a reformer for the process in section 2.5, while the abridged reaction set (2.15-2.18) is used for the more extended diagram of section 2.3. In the first case, the water-gas shift and methanation steps after the reformer are assumed in equilibrium. For the second scheme, instead, the high temperature water-gas shift stage is still in equilibrium being just an intermediate stage of the processes), while the lower temperature reactor downstream (that can actually modify the process balances) is modeled after the reviewed literature [86] as:

$$r = 82.2\, \frac{kmol/s}{kg\, atm^2}\, exp\left(\frac{-5701}{T}\right) P_{CO} P_{H_2O} \left[1 - \frac{Q}{exp(-4.33 + 4579/T)}\right] \tag{2.19}$$

2.2 Thermodynamic Description

The chemicals and the thermodynamic models used are listed in Table 2.3.

Specie	**Formula**	**MW**	**Reports ID**
Ethanol	C_2H_6O	46	ETHANOL
Water	H_2O	18	WATER
Methane	CH_4	16	METHANE
Carbon Dioxide	CO_2	44	CO2
Carbon Monoxide	CO	28	CO
Hydrogen	H_2	2	HYDROGEN
Oxygen	O_2	32	OXYGEN
Nitrogen	N_2	28	NITROGEN
Acetaldehyde	C_2H_4O	44	ACETALD
Methyl-Diethanolammine	$C_5H_{13}NO_2$	119	MDEA
Methyl-Diethanolammonium	$C_5H_{14}NO_2{}^+$	120	MDEA+
Hydronium	H_3O^+	19	H3O+
Hydroxide	OH^-	17	OH-
Bicarbonate	$HCO_3{}^-$	61	HCO3-
Carbonate	$CO_3{}^{2-}$	60	CO3- -
Models	**Parameters**		
NRTL	APV90 VLE		
ELECNRTL	APV90 ENRTL-RK		
HENRY	APV90 BINARY, APV90 HENRY-AP		
STEAM-TAB	National Bureau of Standards		

Table 2.3: Species involved in the Ethanol reforming process

Also in this case the CO_2 treatment is calculated with the coupling of an adsorbing and stripping column, so for this section the thermodynamic model and the automatically solved equilibrium chemistry are treated as explained in paragraph 1.2; the further purification is instead modeled through an expanded pressure-swing section. The gas phase is treated with the RKS equation, while the liquid phase with the NRTL model. Anyway, methane, hydrogen and carbon monoxide solubilities are calculated with the Henry constants. The performance of the original Aspen Plus data in reproducing literature data [40, 87–91] are reviewed through Figures 2.2-2.3-2.4.

The Henry constant for Hydrogen may need a revision in further developments, but in this case the simulated conditions are in a low-temperature range (below 50 °C, chapter 2.5) or in high-pressure one (chapter 2.3), where the default parameters provide a satisfactory description.

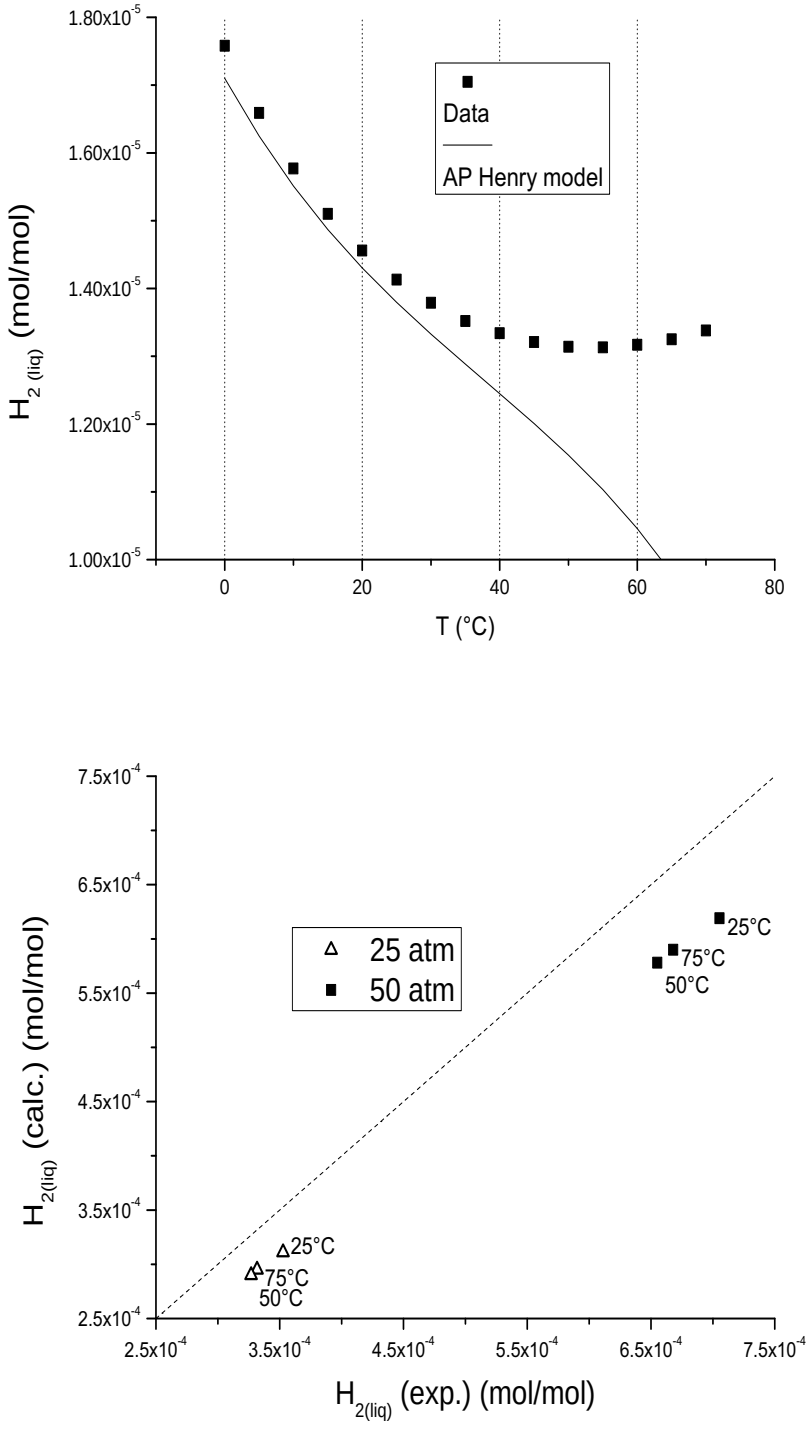

Figure 2.2: Capability of the library models to reproduce the solubility of hydrogen (atmospheric-high pressure) in water.

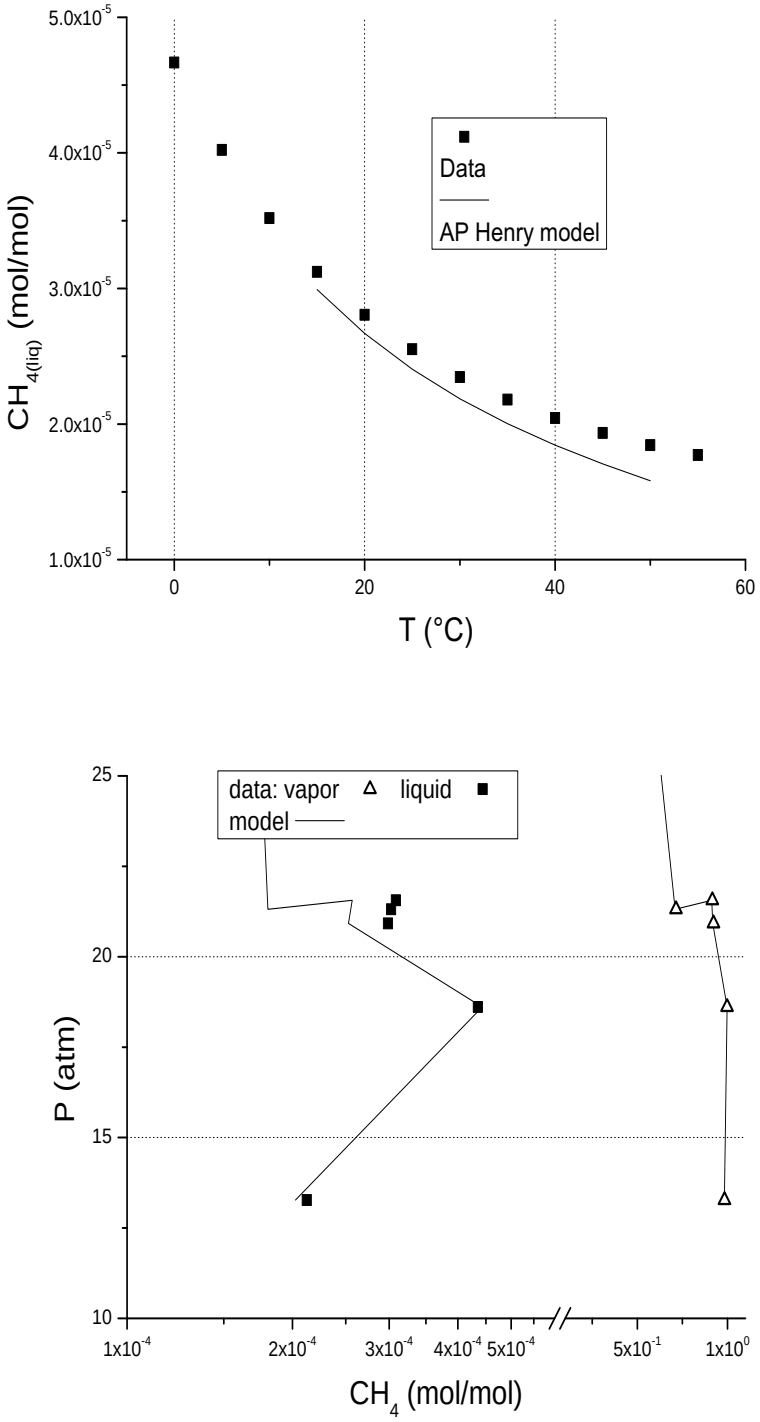

Figure 2.3: Capability of the library models to reproduce the solubility of methane (atmospheric-high pressure) in water.

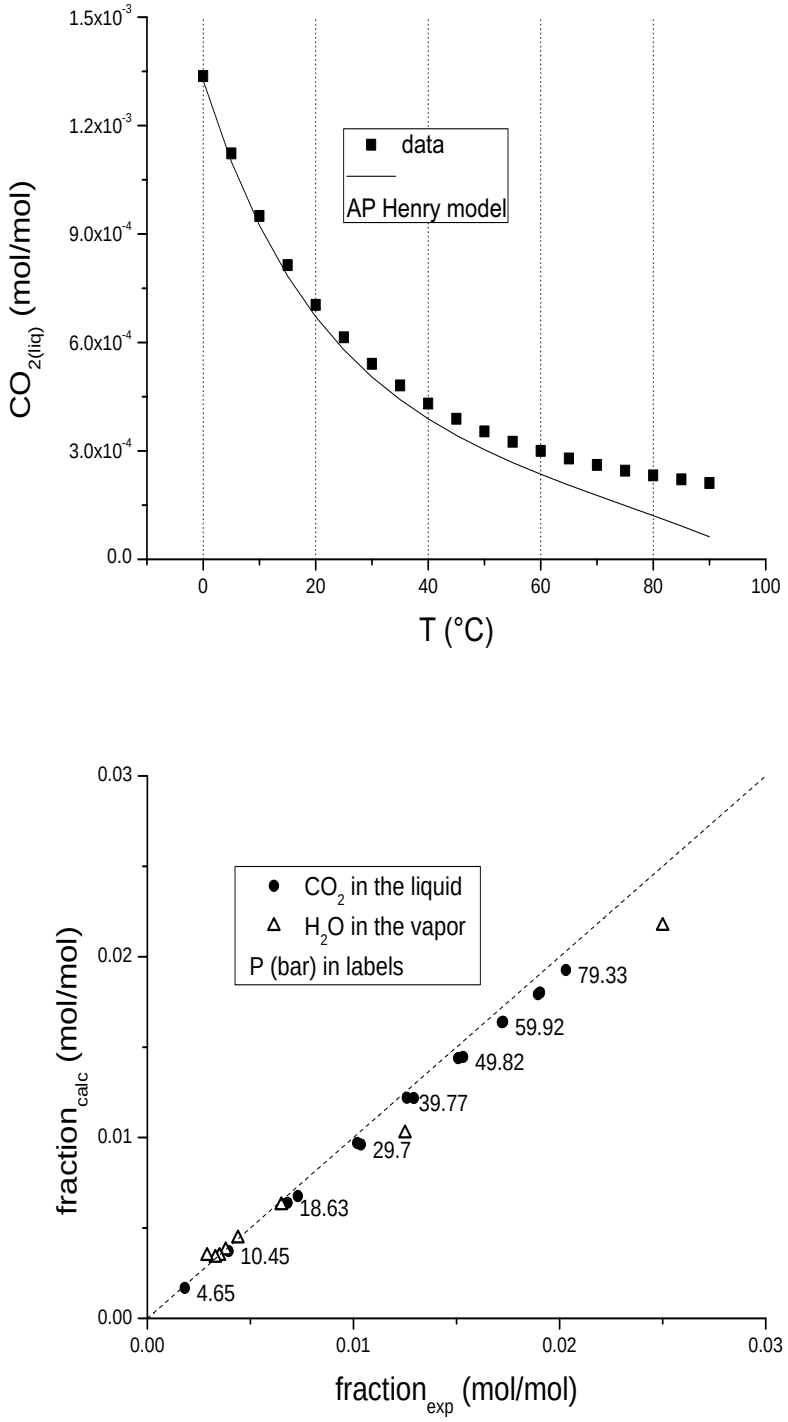

Figure 2.4: Capability of the library models to reproduce the solubility of CO_2 (atmospheric-high pressure) in water.

2.3 Medium-Scale Hydrogen Production

The size chosen for this calculation of a bioethanol-hydrogen production is of 4.6 t/h of ethanol diluted with 3 moles of water per mole of alcohol, i.e. at the stoichiometric ratio. This corresponds to the ethanol produced by a medium-size bio-refinery [54]. Starting by an already diluted mixture, it is implicitly considered that the prior distillation up to azeotropic ethanol is not needed.

The reaction pressure is set to 10 bar, values even higher than this [92, 93] are common in reforming plants in order to limit the piping volume, though unfavorable for thermodynamic reasons. The overall layouts of methane-reforming plants [94, 95] have been reviewed as starting points. The process (see schemes 2.5-2.6) simulates a Reformer conceptually divided into a radiant and convective section via the following criteria:

- part of the heat released by the burned fuel just before the radiant section is actually used to heat the feed, so the combustion is not adiabatic and the higher temperature is fixed to 1000-1100 °C: the resulting heat surplus at the burner is used as an input to the last feed heater;
- the hot flues are split in three, to simulate a parallel cross flow between the hot gases and the process stream in the radiant section: the first part heats up the ethanol before the catalytic bed, the second part constitutes the heating stream of a plug-flow reactor;
- the first catalytic bed is supposed to 'end' where the outlet process and thermal fluid temperatures become closer than 300 °C, so another virtual catalytic bed is added that intercepts the third hot flues crossflow still at 1000 °C - it is deemed that this twofold bed arrangement and threefold flues partition is a reasonable representation of the radiative section: the heat exchange coefficient for this part is conservatively set to 30 $W\,m^{-2}\,°C^{-1}$;
- the convective section is modeled via a single plug-flow-reactor heated by a single flue stream, with a heat exchange coefficient of 15 $W\,m^{-2}\,°C^{-1}$.

The final (and most important) water-gas shift section is designed around 250 °C, resorting to a kinetic expression available in the literature for selective catalysts (see above section 2.1). After this step, the water still in excess can be condensed in one or two steps: the second strategy is convenient if the second separator works at higher pressures, and it is adopted here because pressures of 15 - 20 bar are more effective when CO_2 is to be absorbed in basic aqueous solutions.

The carbon dioxide treatment module is very similar to the one described in the previous chapter, but the quantity of treated gas is smaller while the concentration of carbon dioxide is higher; in this case the quantity of MDEA is calculated as 1.7 moles per mole of CO_2, and a 3% volumetric fraction of carbon dioxide is allowed in the output stream [96], because most adsorption beds as the one foreseen downstream can actually capture also this gas. In both cases, anyway, the equilibrium condition at the stripper condenser makes a non-negligible amount of water to be lost with the carbon dioxide vent (3-4 % kg/kg), and the circuit between the columns is actually calculated with a continuous makeup in the low pressure side just upstream the charging pump.

The pressure-swing purification part is accounted for after the results reported on multi-layer absorption beds capable of trapping different gases [97, 98]. In this case,

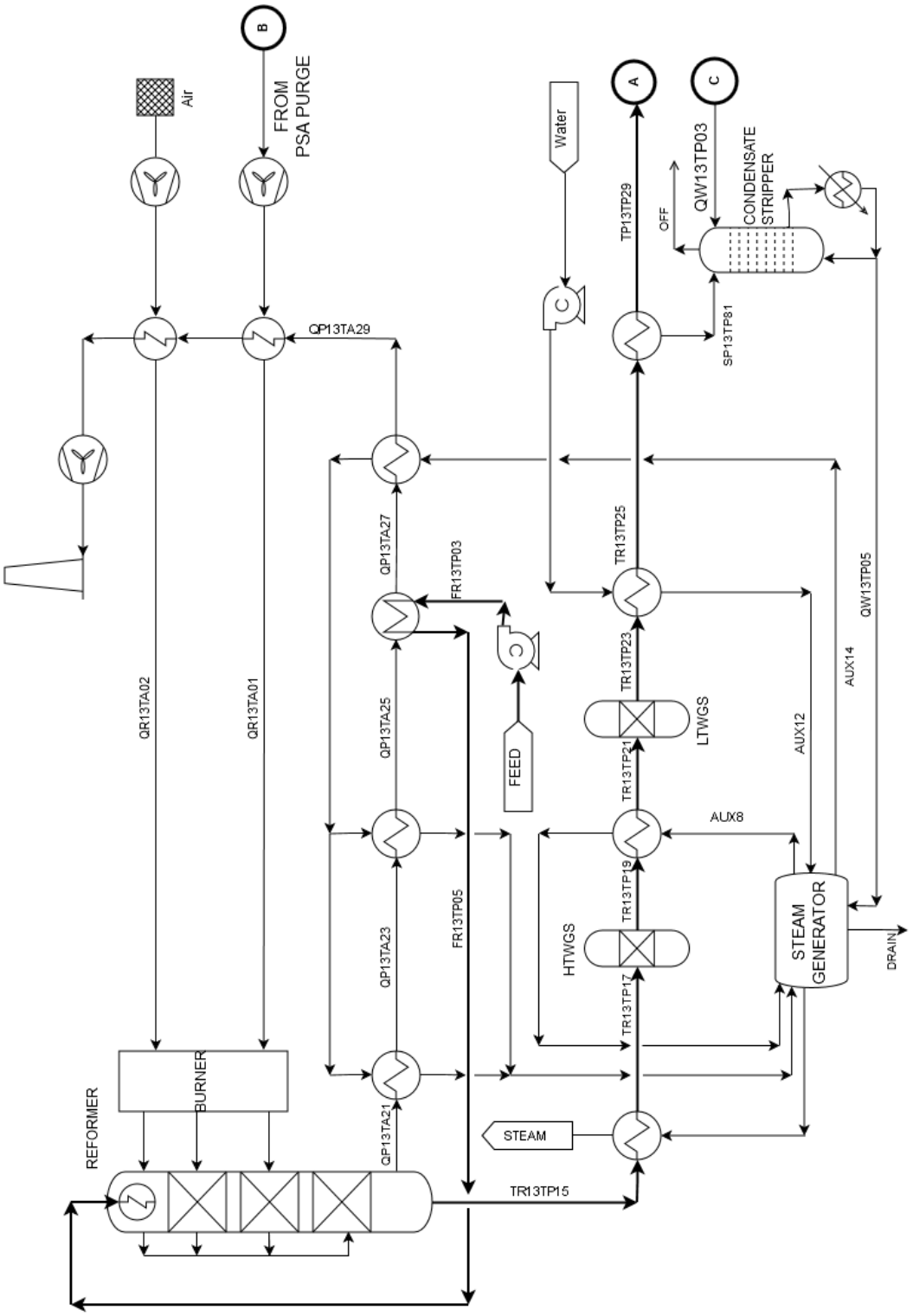

Figure 2.5: PFD of the reforming section

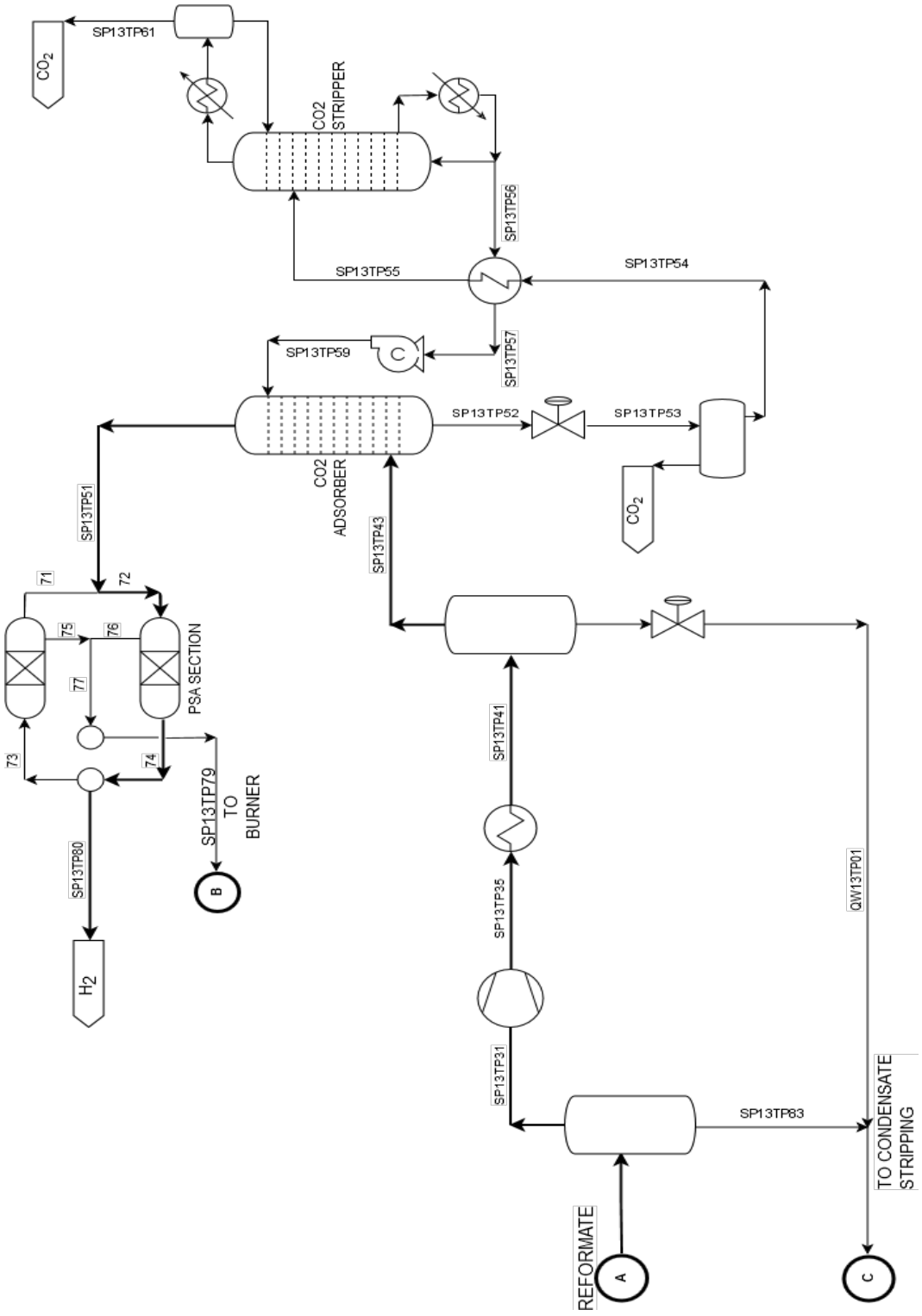

Figure 2.6: PFD of the reformate purification.

unlike in the process diagram of the dehydration, the purge stream is not recycled to recover the hydrogen [95], but routed to the burner. This approach is based on the following considerations:

- though hydrogen is a valuable building block, its use as a fuel is nearly as important, while ethylene is hardly considered as a energy source;
- being the reforming reaction globally endothermic, recycling about the 30% of the produced hydrogen (an already conservative value [99]) as a fuel keeps it within the process balances, and also the appreciable residual quantity of methane is turned into a fuel rather than a byproduct;
- this option lead to the design of a closed process, that don't rely neither on external gas or azeotropic ethanol while it can exploit as desired a diluted inexpensive bioethanol, depending on the context mixture, it is worthwhile to study also a stand-alone version of the process.

Notice that, according to the reviewed references, also large quantities of CO_2 can be treated via a pressure-swing apparatus relying on the same (or very similar) solids that entrap methane and carbon monoxide. The preliminary design has been devised in this way, however considering that:

- for the ethanol dehydration case, purified ethylene is the carrier of the purged specie in the pressure-swing layout, so a neat discharge of CO_2 outside the process would anyway be needed in the residual light gases separation downstream, unless some ethylene be sacrificed;
- for the reforming case, where carbon dioxide flow is much higher, a dedicate and selective purification section makes it available for re-utilization or capture purposes.

The simulation's results are displayed synthetically in Figures 2.7 for the reactive part and 2.8 for the purification part, while the overall process balances are found in the graphs 2.9. The delay in hydrogen production with respect to methane formation (due to the used reaction network) appears clearly in Figure 2.7-right, leaving to the last reformer stage the task to switch the two species' ratio.

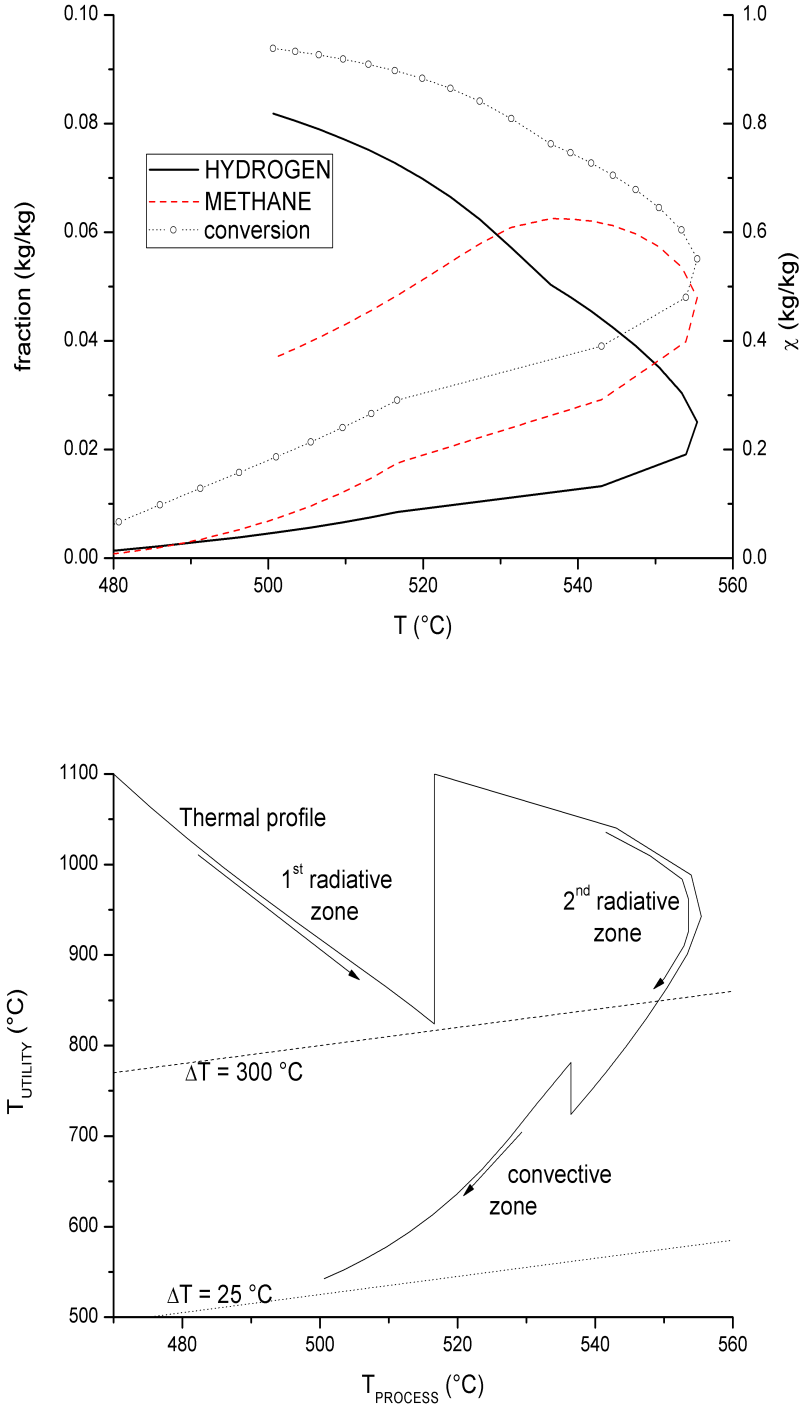

Figure 2.7: Left: profile of the energy-carrying species and conversion in the reformer; right: temperature difference map between the reacting mixtures and the flues.

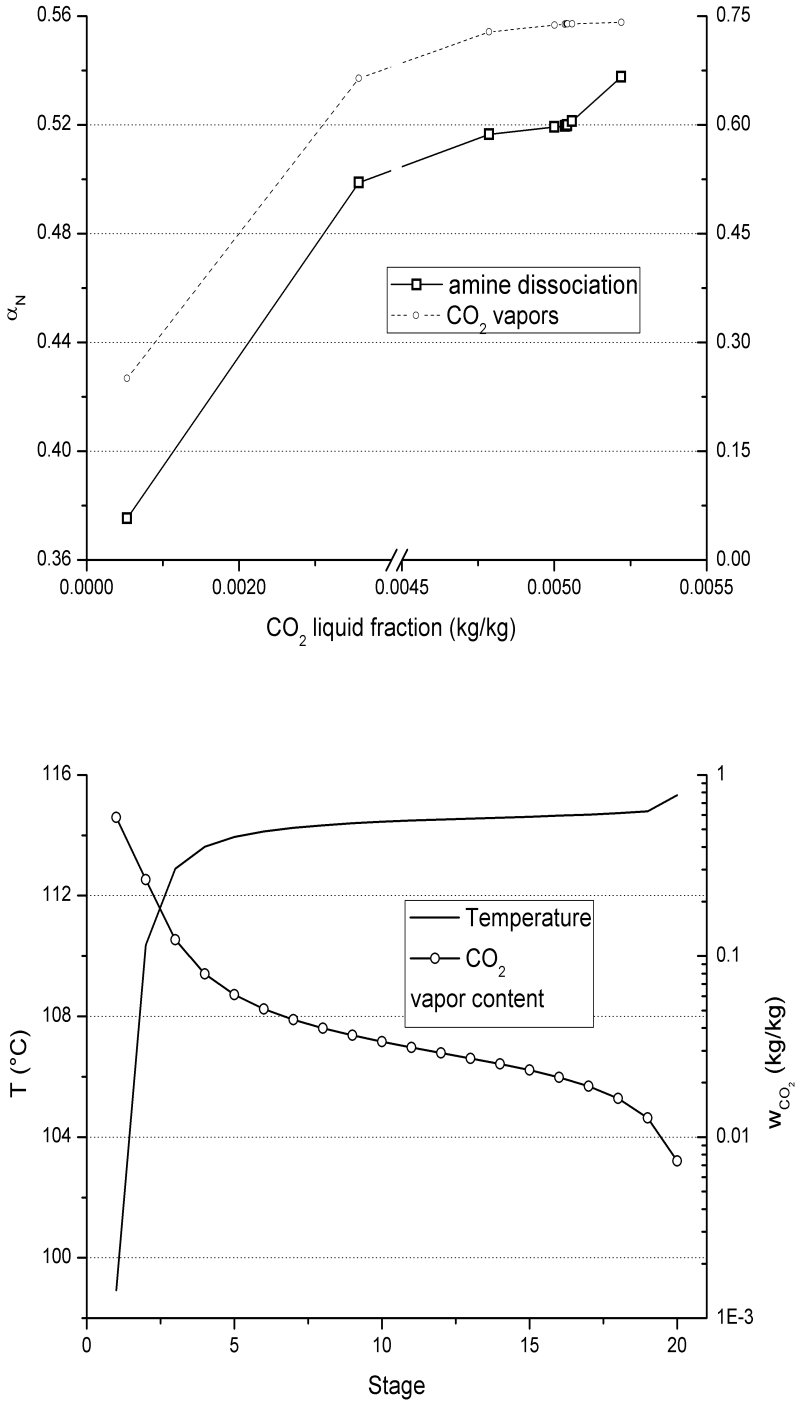

Figure 2.8: Profiles of absorber (left) and stripper (right).

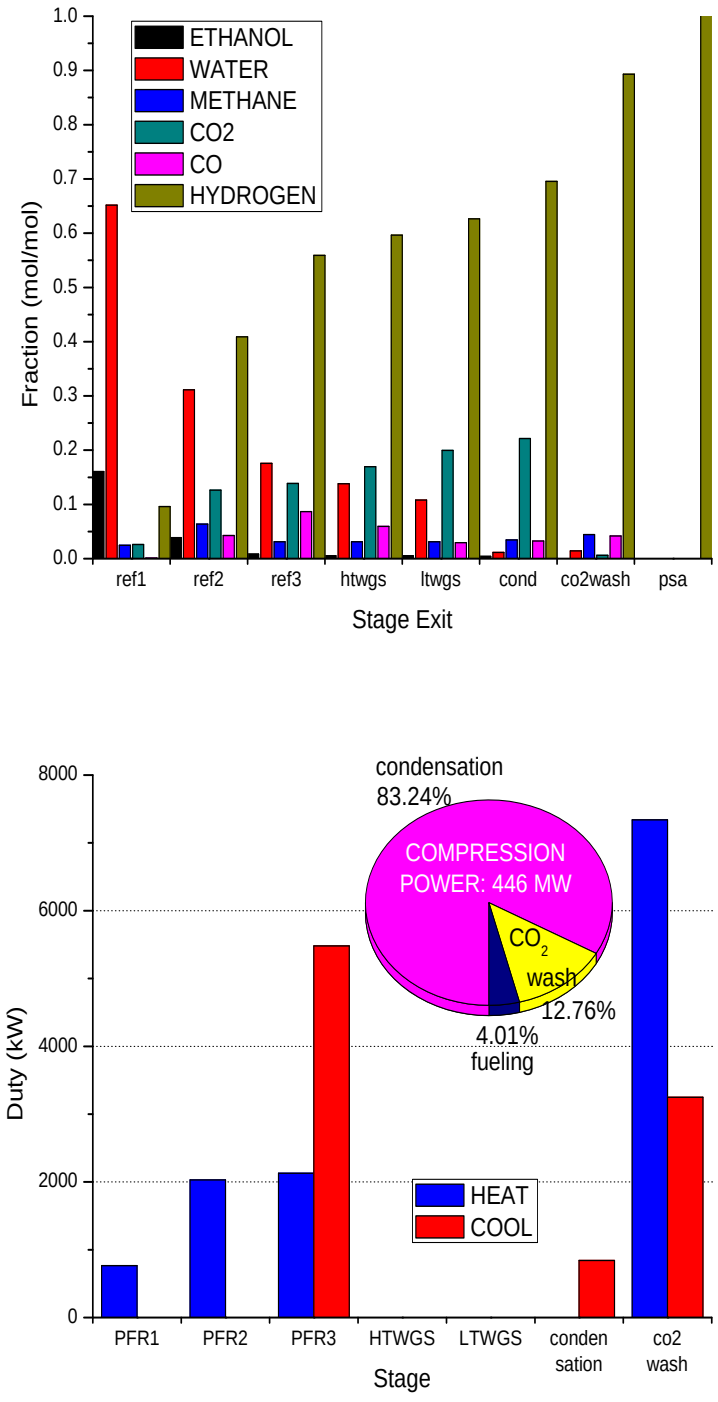

Figure 2.9: Composition of the streams and plant duties.

2.4 Energy Recovery

The reformate that cools down to the condenser temperature (chosen slightly above 80 °C) and the burner flues exiting the reformer still contain some thermal energy that is partly used to pre-heat the feed and partly to rise low pressure steam. In principle, the feed heating stages depends on how the diluted ethanol is actually provided:

1) as base case, it is supposed to start from a mildly preheated (50 °C) hydro-alcoholic mixture at the stoichiometric ratio, charged at the process pressure; this working point can be taken as reference to consider at least other two options [100–102]:

2) reboil a fermentation broth up to the desired ethanol concentration, and route it to the second feed heater;

3) distillate azeotropic ethanol and mix it with the steam produced by the plant.

The water used to raise steam could belong to a closed cycle. If, instead, an open cycle were designed, then there would be at least three different entry-levels for water into the system, according to what described above:

1) as base case, fresh water enters the process and is mixed to the process condensate stripped from the soluted gases;

2) in this case the additional water could come from the bottoms of the wine boiler, but another pre-treatment would be needed;

3) in this case the water could enter the system first in the auxiliary steam section, then be used as process feed to dilute the azeotrope.

The heat-recovering utilities have been designed after reviewing and adapting the already cited process layouts, beside [103, 104].

Save for the ethanol/water feeding sections, subject to further optimization according to the above sketched criteria, the main thermal and power balances for the base case are summarized in the Figure 2.9. The basic Pinch Analysis, restricted to the process streams only, is reported in Figure 2.10. It is possible to see that, even at the process pressure, the dew point of the reformate is below the temperature level requested in the MDEA stripper reboiler, leading to the poor overlap of the HCC and CCC. The choice of burning part of the hydrogen to supply the reaction energy leads naturally to the coupling of a Hot Utility profile (as indicated in the same graph), following the criterion of setting a utility pinch at the top kink of the GCC. The excess heat carried by the hot flues is spent rising steam at 15 bar (195-198 °C) which brings to the convex shape of the composite curve below 430 °C. The analysis let foresee, anyway, at least two options for further energy recoveries: lowering the highest flue temperature (e.g. by adding over-stoichiometric comburent air) and/or rising more steam.

Table 2.4 highlights the main thermal parameters of the process and the process plus utilities. Notice that the final heat sink foreseen is atmospheric air.

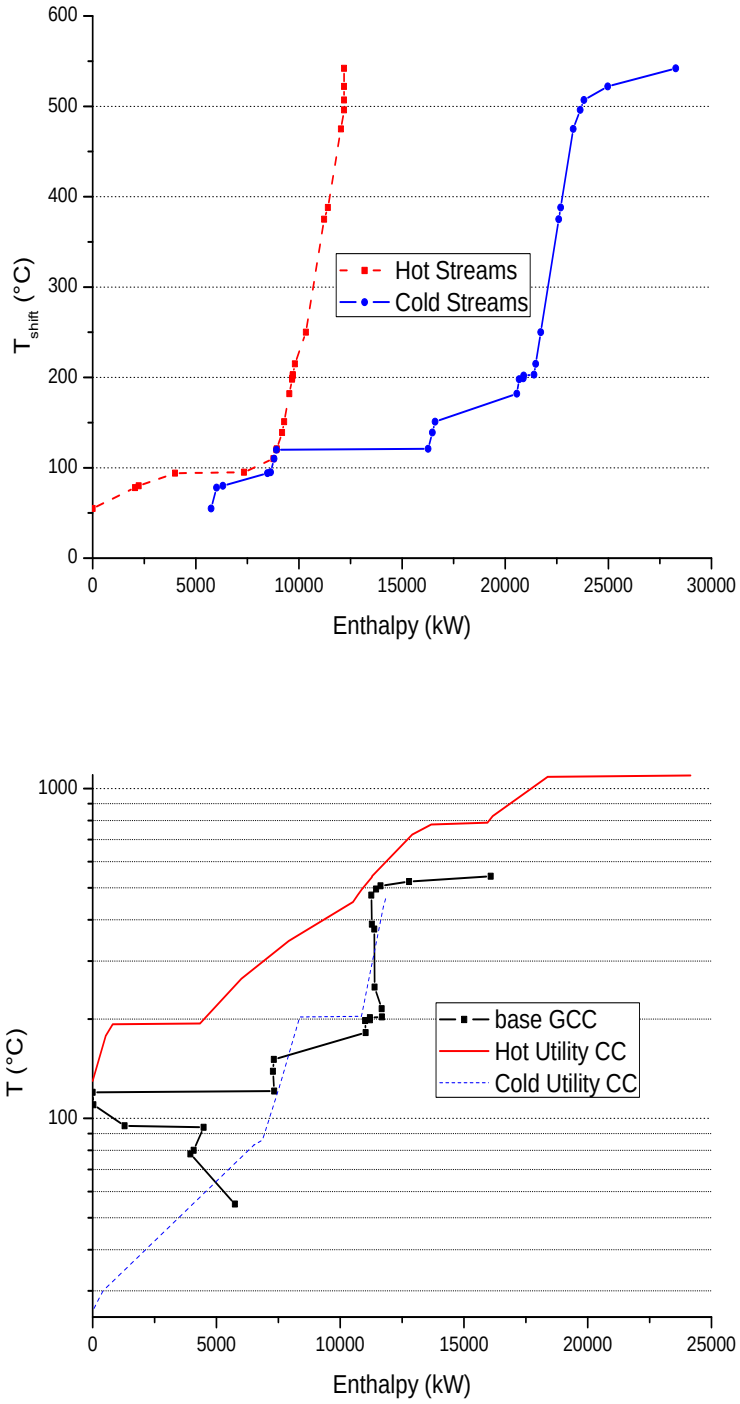

Figure 2.10: Composite curves and Grand-Composite curve for the process. The y-scale reports the shifted temperature.

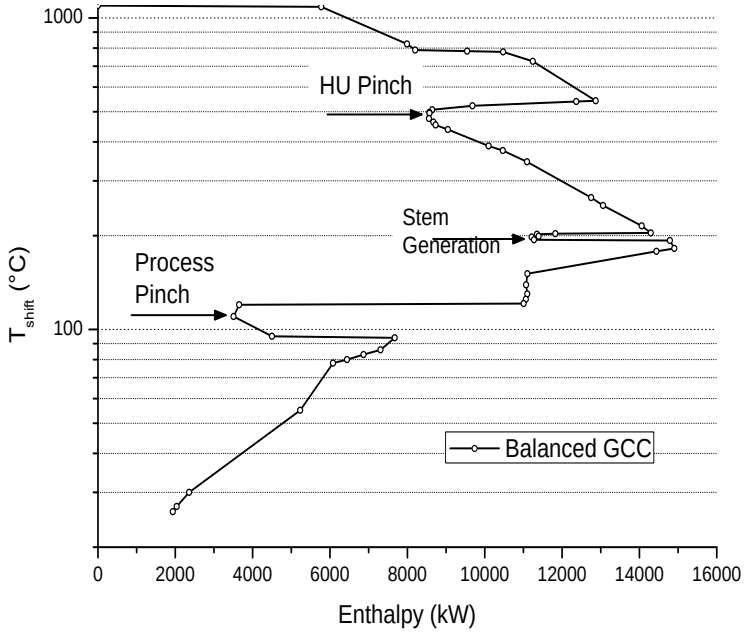

Figure 2.11: Grand-Composite curve for the process plus utilities.

Case	ΔT_{min} (°C)	T_{pinch}	H.U. (kW)	C.U.	Heat in (kW)	Heat out
no matches	10	121	16100	5740	21800	12200
matches & utilities	10	111	0	1940	0	-

Table 2.4: Main energetic parameters of the simulation cases.

2.5 Distributed Heat and Power Cogeneration

The main layout difference between the large-scale reforming and the micro-scale hydrogen production are [105–107]:

- only CO must be removed but not CO_2, then just a methanation bed is foreseen upstream the water condenser (fuel cells could be flooded if excess water is present at their inlet) [60];
- the fuel to heat-up the reformer is extracted *before* the FC, then the system is intrinsically stable (in terms of global power output), bacause the electric power (hydrogen to the cell) and the thermal (hydrogen to the burner) are dependent - this is true, however, as long as the hot utility flows through the reformer [77, 108];
- the residual heat recovery is carried out in a series of blocks that simulate a common household heating system: since the quantity of ethanol needed to provide

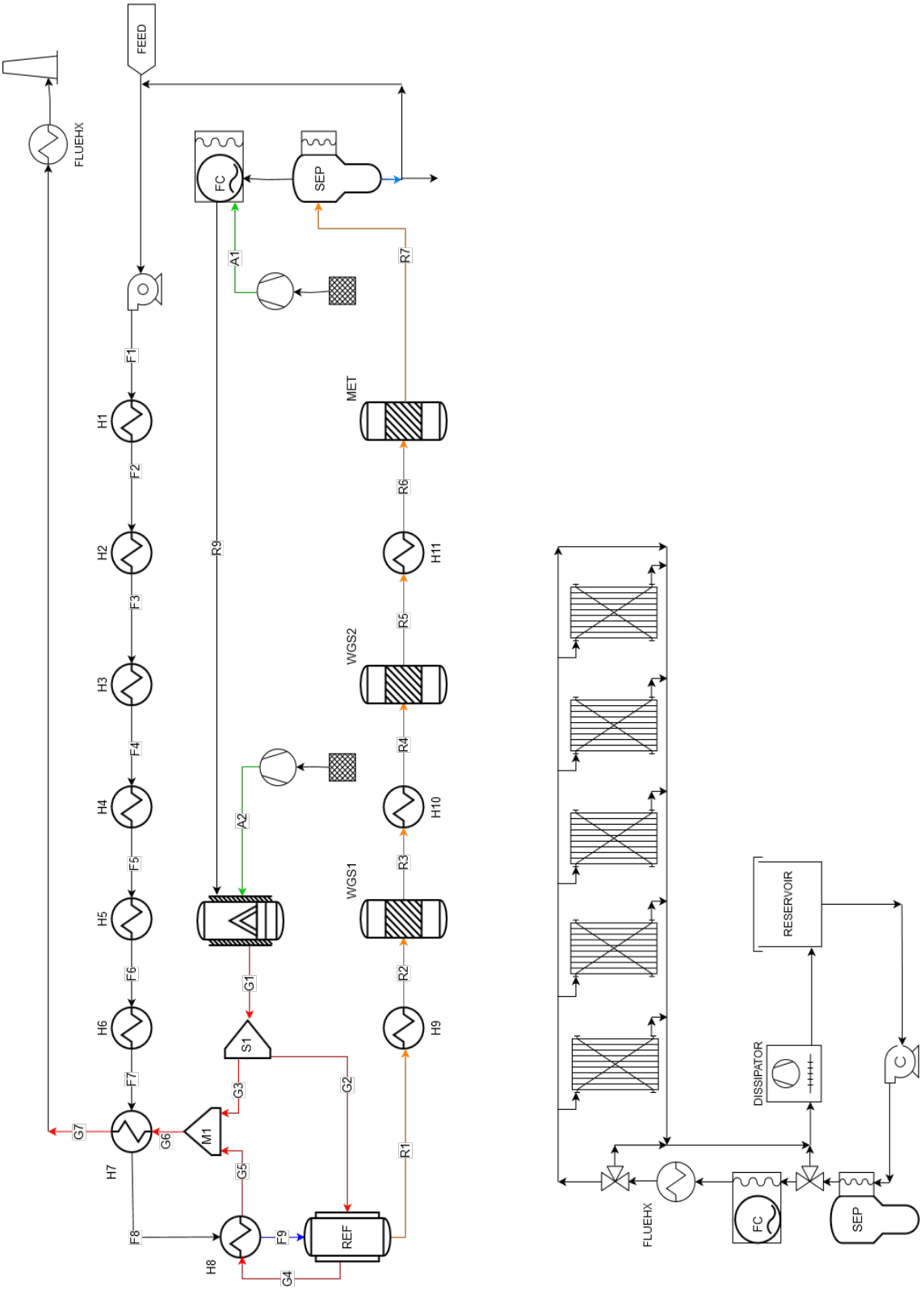

Figure 2.12: Process flow diagram of a small scale Heat & Power Cogeneration.

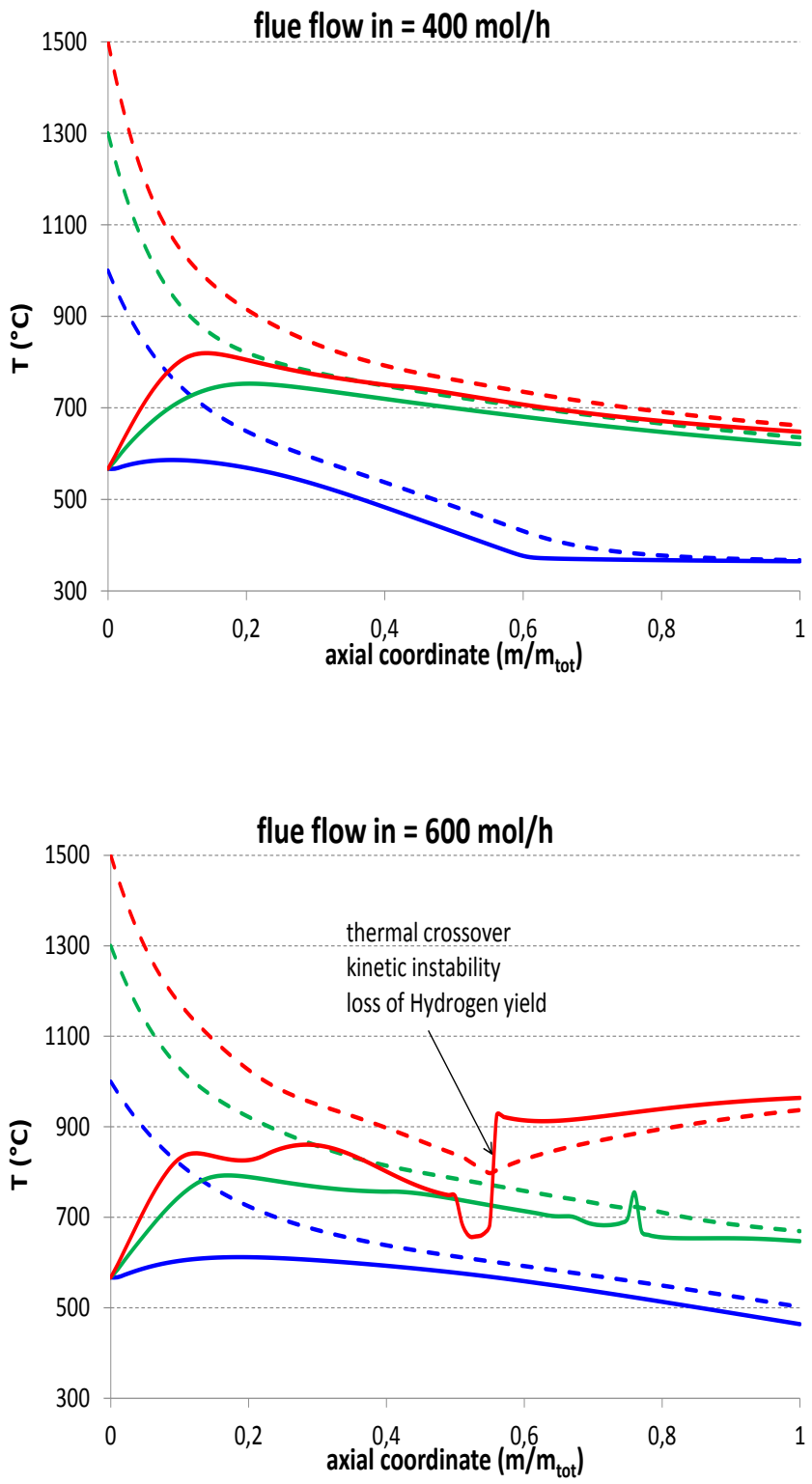

Figure 2.13: Thermal behavior of the reformer at 400 (up) and 600 mol/h (bottom) of hot flues (feed: 420 mol/h). Solid lines: reformate - dashed lines: flues.

the standard electrical supply (i.e. 70 mol/h of alcohol diluted with 350 mol/h of water, that exceed the nominal 5 kW target and leave a margin for fuel cell efficiencies possibly lower than 50%) cannot cover, at the same time, also the installed thermal need (usually up to 20-25 kW for burners with hot convective flue flow), the calculation is solved dynamically exploiting the fact that most of the time the two kind of appliances don't deliver their target power at the same time.

Referring to scheme 2.12, the reforming system is represented in the upper section, while the house-heating system is drawn below, but only for its steady-state functioning part (i.e. the production of hot water to feed the radiators).

The key point of the material and energy recycle is the reformer behavior, as is modeled rigorously via the reaction network presented above. In Figures 2.13 it can be seen that right flowrate and temperature of the burned gas is crucial to avoid an anomalous temperature profile (with the given activation energy), that means in turn loss of the hydrogen output.

2.6 Dynamic Energy Integration

As already mentioned, the supply of sanitary water (up to 12 l/min) cannot be covered with the above mentioned feed, supposing to start from grid water at 5 °C to a high set-point of 50 °C (see [109] and references therein), so a static heat reserve is put in order to store the power continuously discharged and not consumed [110]. Also the steady-state operation, however, can shift from an enhanced electricity production to the delivery of more thermal power.

Schemes in Figure 2.14 clarify the working philosophy:

- the hydrogen usage at the FC determines the electric power, and leaves more or less enthalpy after the burner;
- according to the feed water content, some hot gas has to bypass the burner and/or the feed boiler to keep the reactor at the rated condition (around 500 °C);
- a reduced electricity production leaves then enough heat available, at the cell and flue gas heat exchangers, to meet the 6.5 kW - 70 °C wintertime utility requirement usually considered in most northern Italy houses (ibidem);
- when sanitary water is needed, the line passing though the dissipator is bypassed and all the heat available remains in the system: this set-up, coupled with the reservoir's thermal inertia, keeps a milder sanitary set-point of 47-48 °C for more than 30'.

The main results are reported in Figure 2.17 and Figures 2.15-2.16.

In conclusion, it has been verified the possibility to produce hydrogen through diluted hydroalcoholic solutions. This technology has been applied to the centralized production of hydrogen (big scale plant) and to the distributed co-generation of heat and power by using fuel cells. In this latter case it has been considered dynamically the time-to-time availability of sanitary water during winters, when demanding working conditions are yet present for heating.

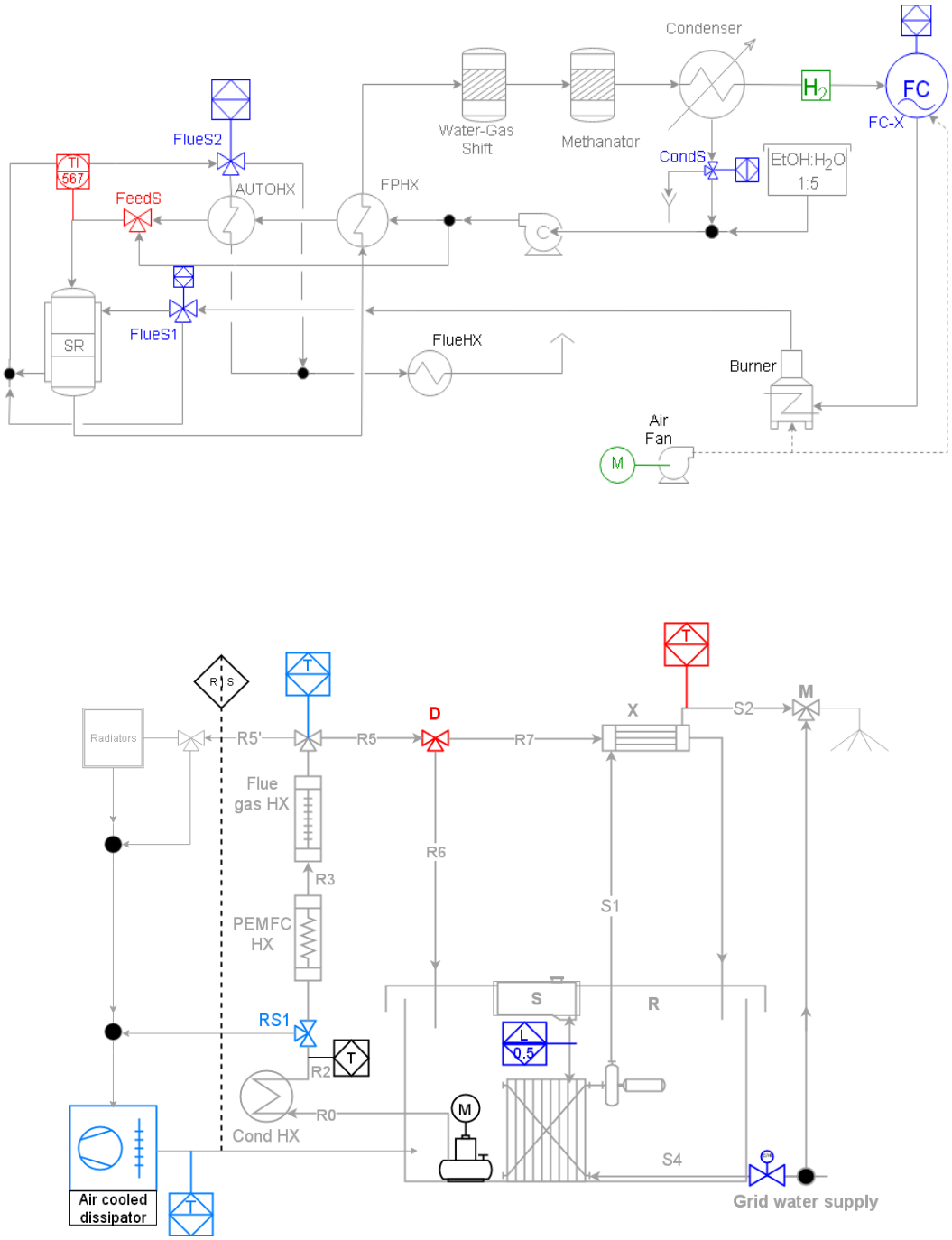

Figure 2.14: Schemes for the dynamic calculation of the sanitary water delivery of the distributed-HPC.

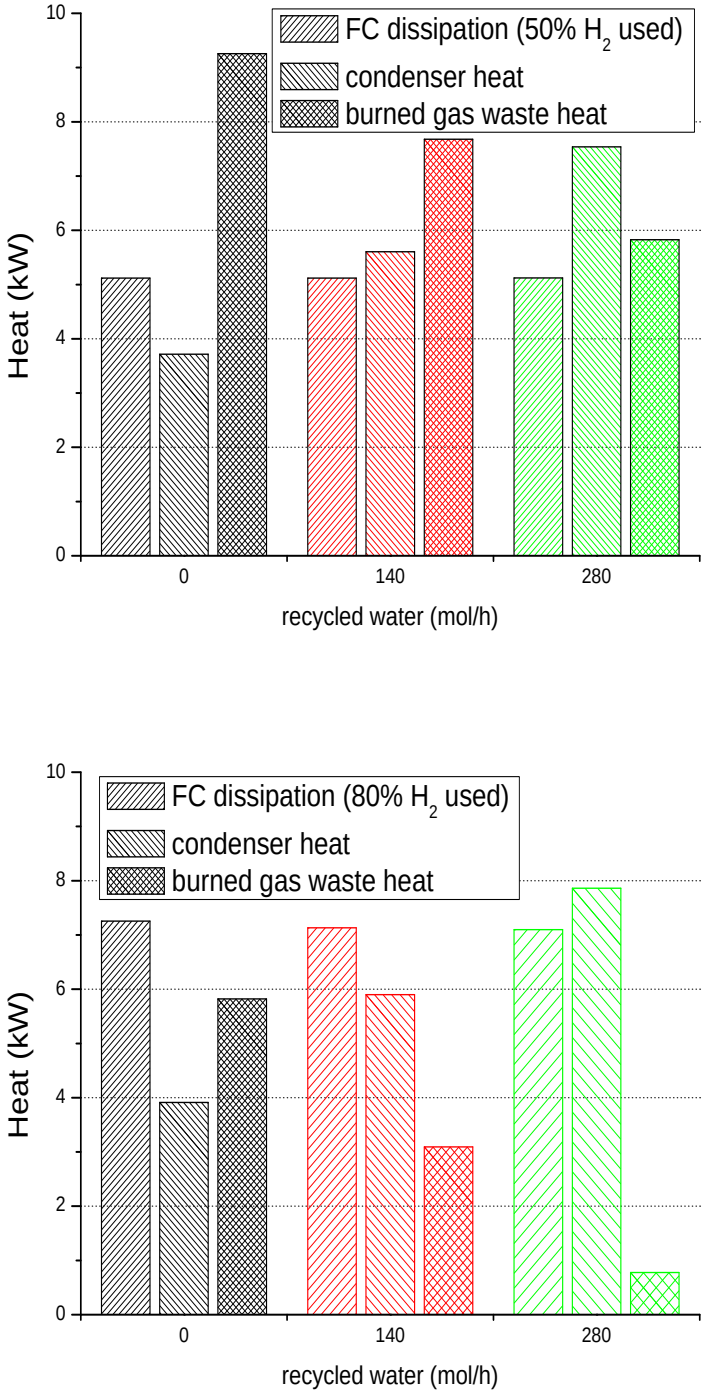

Figure 2.15: Heat released at different ethanol:water ratios (40% of burned gas to the reformer).

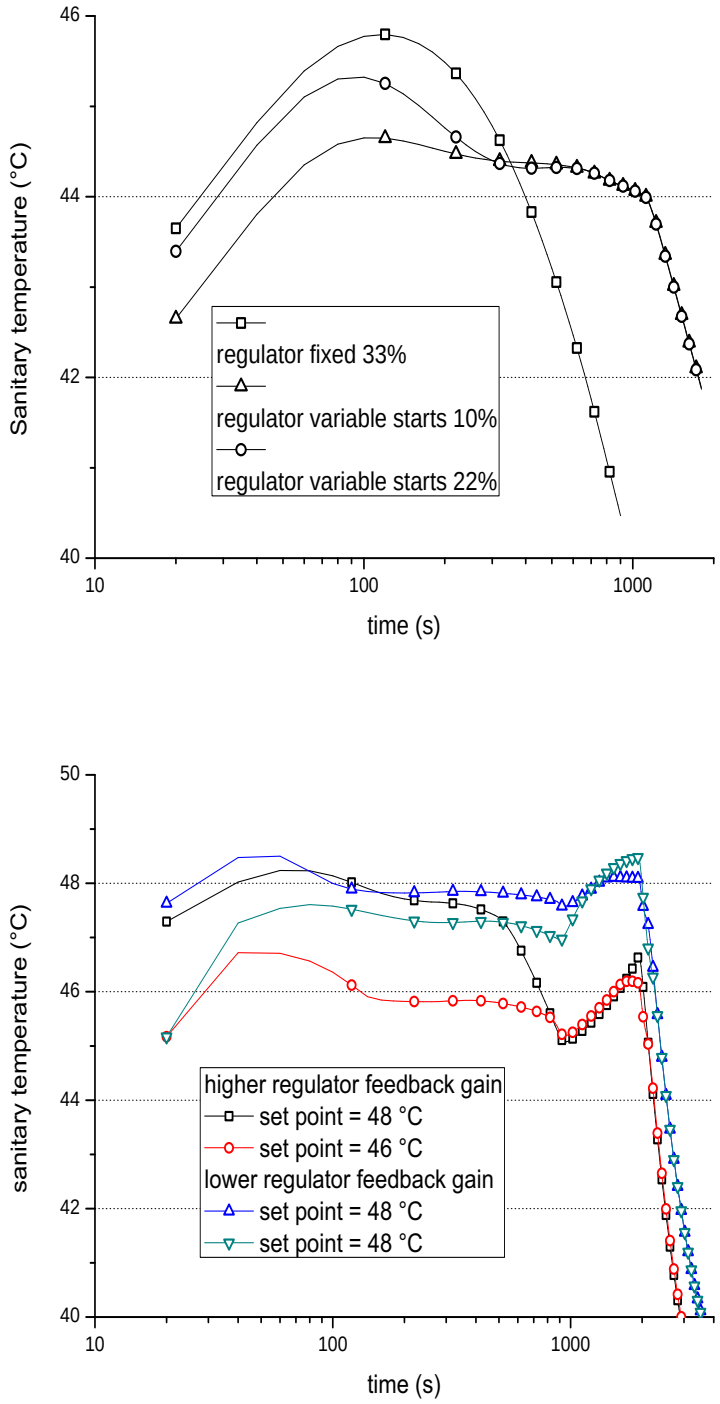

Figure 2.16: Adjustment of sanitary set point via time-dependent water-mixing strategies.

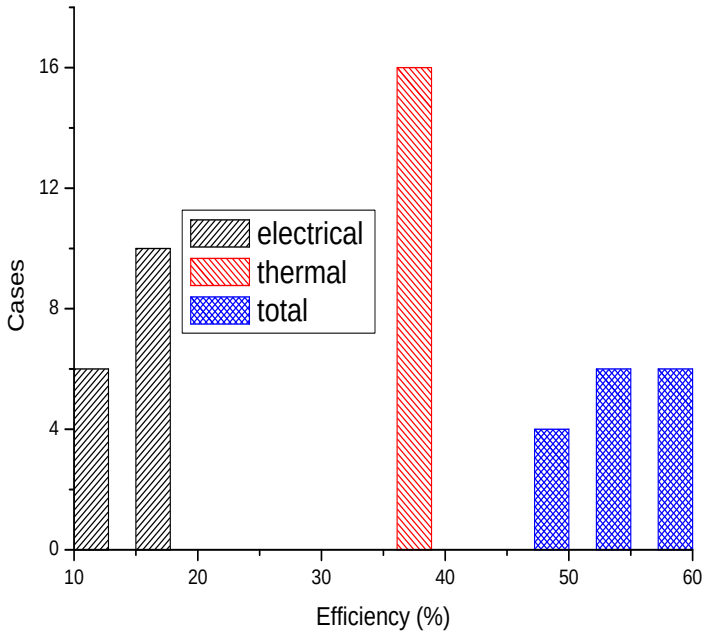

Figure 2.17: Efficiency (%) of all the tested working cases. The enthalpy content of ethanol has been set to 1370 kJ/mol: the heat recovery is such as to maintain a nearly constant thermal efficiency.

Chapter 3

Syngas and Ammonia Production

Ammonia synthesis, a fundamental process for the world industrial and crops-growing system, has been continuously studied in all its aspects: peculiarities of the reaction mechanism [111], in fact, makes different catalytic formulations have an appreciable impact on large size reactors, that benefit of any possible decrease of the operating pressure and temperature [112, 113].

Smaller scale projects, on the other hand (where conditions substantially milder than those regularly adopted are even more necessary), may be yet not attractive from an economic point of view, but retain the intriguing feature of making atmospheric nitrogen chemically available while "trapping" renewable, pure hydrogen into a less reactive molecule [114, 115].

In this framework, is presented a standard ammonia synthesis loop coupled to a bioethanol reforming section, whose net output is then renewable ammonia. The choice between (possibly diluted) ethanol and methane depends on different general considerations (gas on-site availability, local biorefineries size, reforming technology, etc.), but the alcohol-hydrogen route to ammonia is indeed viable. Where pure nitrogen is available, it's also possible to consider a reforming process that produces directly pure hydrogen.

3.1 Catalytic Materials

The reactor model in this work is based on the detailed description of two patented catalyst, one made of Wustite and a newer one made of Ruthenium deposited on Carbon, developed years ago in this University. This latter shows a lower activation energy and is less easily inhibited by the produced ammonia with respect to Iron-based catalysts. The details about the catalysts' preparation and tests are reported in the literature and in the relative patents [116–118]; the kinetic expressions have been revised (mainly to harmonize the units of measure and the equilibrium constant [119]) as [120]:

$$Wustite: \qquad r_{NH_3} = k \left(K_{eq}^2 f_{N_2} \frac{f_{H_2}^{1.5}}{f_{NH_3}} - \frac{f_{NH_3}}{f_{H_2}^{1.5}} \right) \tag{3.1}$$

$$Ru/C: \qquad r_{NH_3} = k \frac{f_{N_2}^{0.5} \frac{f_{H_2}^{0.375}}{f_{NH_3}^{0.25}} - \frac{1}{K_{eq}} \frac{f_{NH_3}^{0.75}}{f_{H_2}^{1.125}}}{1 + K_{H_2} f_{H_2}^{0.3} + K_{NH_3} f_{NH_3}^{0.2}} \tag{3.2}$$

with parameters listed in Table 3.1.

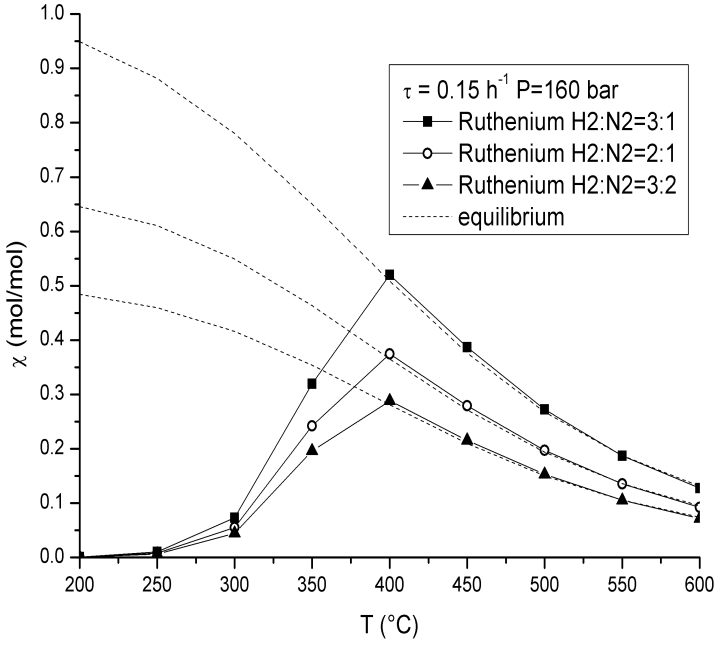

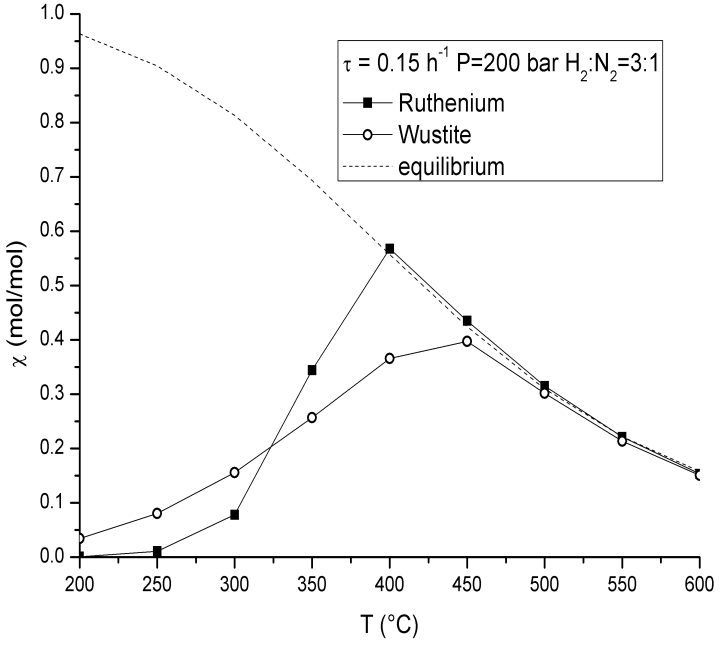

Figure 3.1: Kinetic-equilibrium behavior for the two catalysts: Ruthenium at 200 bars and different feeds (up), and comparison between Ruthenium and Wustite (bottom).

Rate Expression	Ru/C	Wustite
$Ea\ (kcal \times mol^{-1})$	23.0	45
$k_0\ (kmol \times kg_{cat}^{-1} s^{-1})$	426	7.47×10^8
Adsorption Term for Ru/C		
$lnK_{H_2} = -10.3 + 4529/T$		
$lnK_{NH_3} = -6.48 + 3523/T$		

Table 3.1: Kinetic parameters for formulas 3.1 and 3.2.

The performance of the two materials, as calculated from the above expressions, is synthetically reported in the isothermal charts 3.1, relative to the conditions adopted in the process.

3.2 Thermodynamic Description

The chemicals and the thermodynamic models involved in the simulations are listed in Table 3.2.

Specie	**Formula**	**MW**	**Reports ID**
Ethanol	C_2H_6O	46	ETHANOL
Water	H_2O	18	WATER
Methane	CH_4	16	METHANE
Carbon Dioxide	CO_2	44	CO2
Carbon Monoxide	CO	28	CO
Hydrogen	H_2	2	HYDROGEN
Oxygen	O_2	32	OXYGEN
Nitrogen	N_2	28	NITROGEN
Acetaldehyde	C_2H_4O	44	ACETALD
Methyl-diethanolammine	$C_5H_{13}NO_2$	119	MDEA
Methyl-diethanolammonium	$C_5H_{14}NO_2{}^+$	120	MDEA+
Hydronium	H_3O^+	19	H3O+
Hydroxide	OH^-	17	OH-
Bicarbonate	$HCO_3{}^-$	61	HCO3-
Carbonate	$CO_3{}^{2-}$	60	CO3- -
Ammonia	NH_3	17	AMMONIA
Models	**Databases**		
NRTL-RK	APV90 VLE		
	APV90 EOS-LIT		
ENRTL-RK	APV90 ENRTL-RK		
HENRY	APV90 HENRY-AP		
	APV90 BINARY		

Table 3.2: Species involved in the Ethanol Reforming and ammonia synthesis process.

The adoption of the more suitable thermodynamic model depends, also in this case,

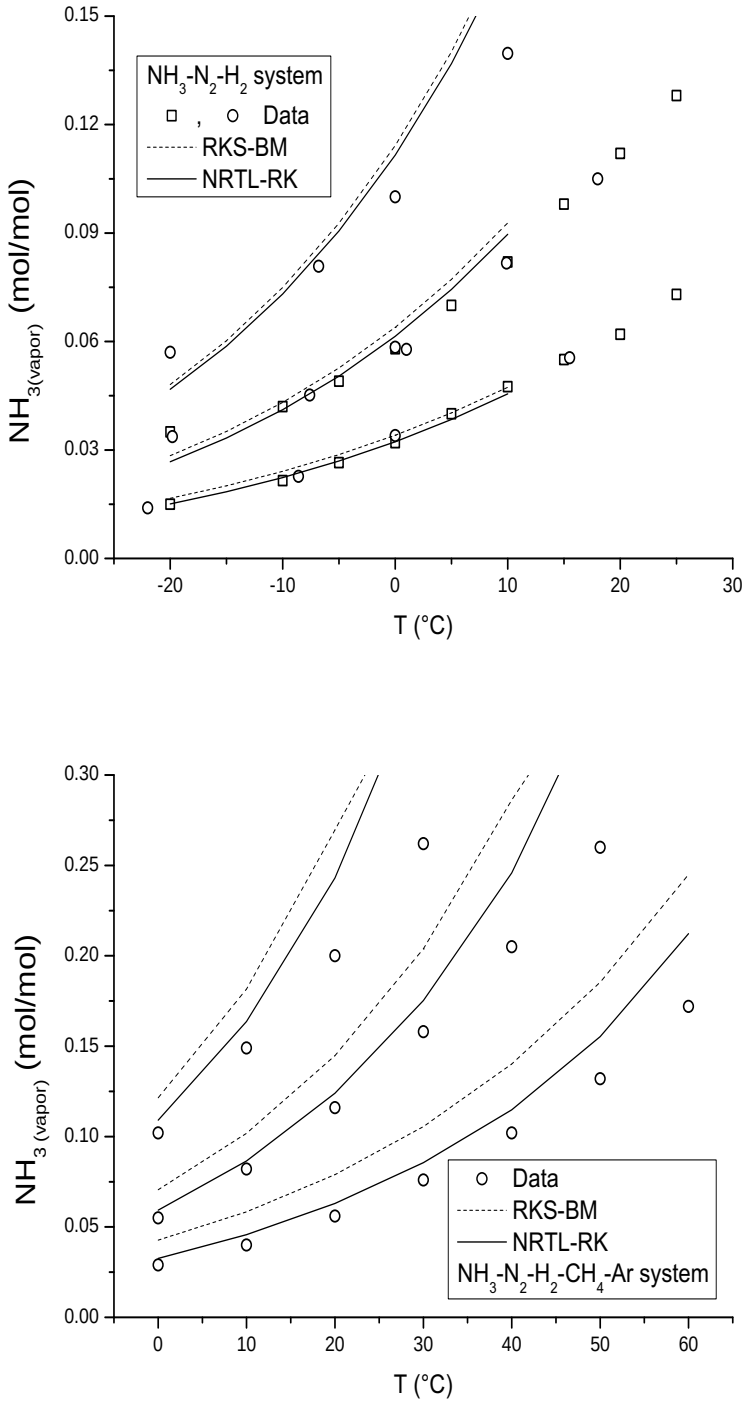

Figure 3.2: Calculated and experimental equilibria for typical mixtures and conditions of ammonia cycles.

mainly on the vapor-liquid equilibrium treatment. The description of the reacting gas is achieved via the Soave-Redlich-Kwong equation of state or a purposely modified version (Redlich-Kwong-Soave-Boston-Mathias [121]). This system seems also best suited for the calculation of hydrogen an nitrogen solubility into liquid ammonia, while the vapor-liquid partition for ammonia itself looks still better described by the NRTL-RKS couple (see Figures 3.2), especially in presence of methane (the main residual component in the syntheses loop [122]). The simulation is not insensitive to the adoption of one or another model, yet the overall mass balances can be leveled adjusting the separation temperature. The experimental data on the NH_3-N_2-N_2 system are from various sources [123–129].

3.3 Reforming for Ammonia Synthesis

The ammonia synthesis calculated is coupled to an ethanol reforming process that consumes 4.6 t/h of ethanol mixed with water in a ratio of 3:1 moles of water per mole of alcohol. Ammonia processes display different arrangements for the reacting gas cooling and the recycles reheating and mixing. In this case, the reactor is calculated as a series of three adiabatic catalytic beds with distributed recycle mixing and product-feed thermal exchange (see schemes 3.3-3.4). Two calculations are run, to estimate the different catalyst load and thermal profile when the third bed is constituted of Ru/C instead of Wustite. Other possible configurations will be tested in further extensions of this work. The reforming section has been adapted from the one already described, with the following main modifications:

- before the water-gas shift section is added the secondary reformer, modeled with two equilibrium reactors representing the different zones of this kind of units;
- the carbon dioxide capture and the CO removal are performed as in the established ammonia processes, i.e. via an amine scrubbing followed by a catalytic conversion of carbon monoxide into methane at the expenses of some hydrogen;
- without a purge stream containing burnable species (as is the case when hydrogen is purified via a pressure-swing apparatus), the heat input to the primary reformer is provided by a separate supply of ethanol.

The secondary reformer implements the stoichiometry reviewed in [130], but without a kinetic model because in this case we are less interested in calculating the contact time. In the combustion zone one has the reactions:

$$CH_4 + O_2 \longrightarrow CO + H_2O + H_2 \tag{3.3}$$

$$2\,H_2 + O_2 \longrightarrow 2\,H_2O \tag{3.4}$$

$$CH_4 + 2\,O_2 \longrightarrow CO_2 + 2\,H_2O \tag{3.5}$$

$$C_2H_6O + 3\,O_2 \longrightarrow 2\,CO_2 + 3\,H_2O \tag{3.6}$$

while in the catalytic zone the partial methane reforming and water-gas shift take place:

$$CH_4 + H_2O \rightleftharpoons CO + 3\,H_2 \tag{3.7}$$

$$CO + H_2O \rightleftharpoons CO_2 + H_2 \tag{3.8}$$

In both cases the reactions reach their equilibrium according to the set temperature and the gas fugacities calculated automatically by the thermodynamic model used in the

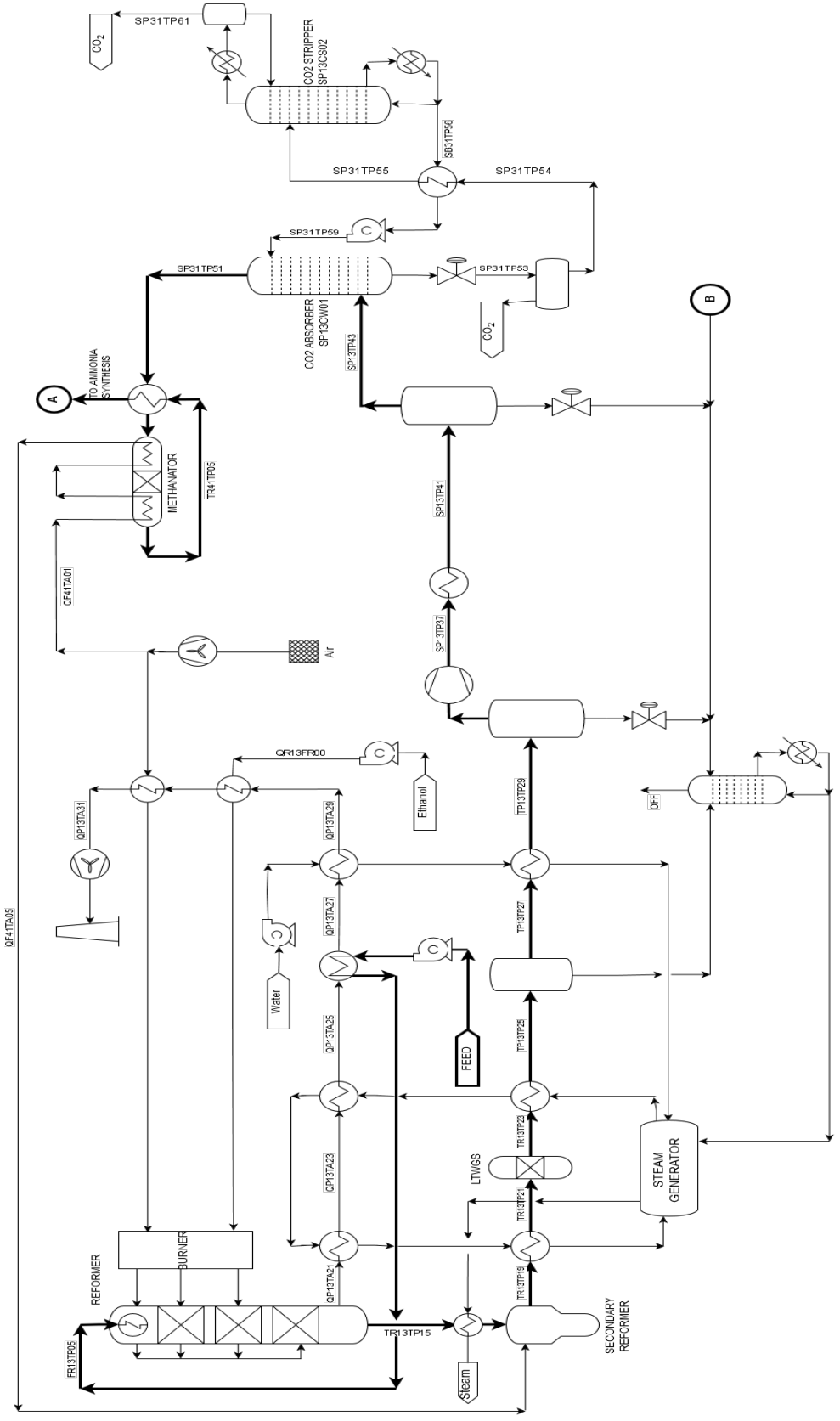

Figure 3.3: Reforming section to feed the ammonia reactor.

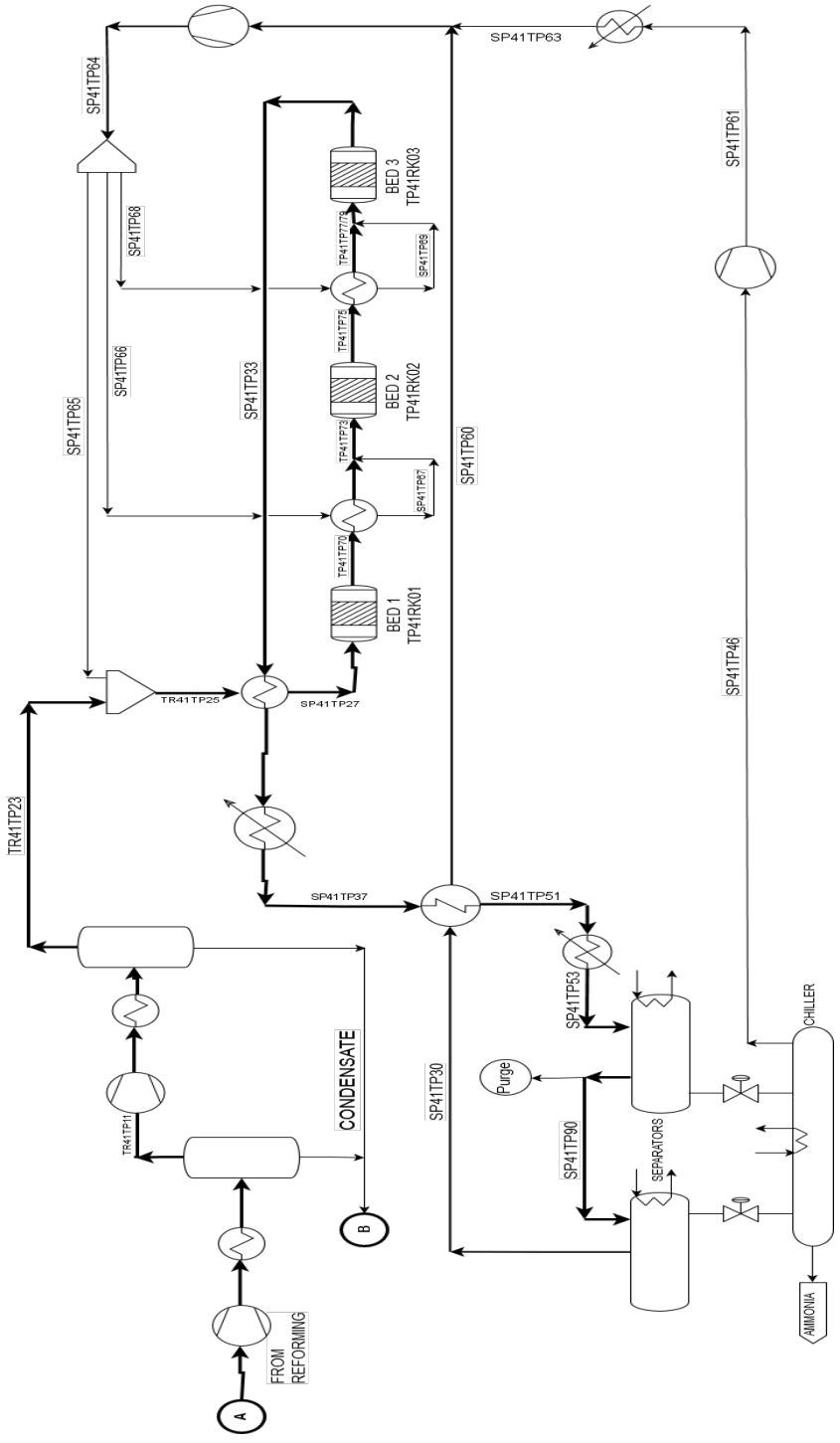

Figure 3.4: Ammonia synthesis loop.

blocks (RKS EoS). The air flow to the first combustion section (that is adiabatic) and the temperature of the second one (supposed isothermal to fix the exiting condition, and actually characterized by a very low heat duty which makes the assumption reasonable) are adjusted heuristically to keep the gas in the 800 - 900 °C range while burning more methane than hydrogen. As a result, the Nitrogen:Hydrogen ratio is about 2.7 after the shift section and 2.2 after the methanator.

The water-gas shift section is treated as already described in chapter 2.3. The methanation reactor is described according to the kinetic formulation presented in [131], suitable for pressurized gases:

$$r_{CO} = \frac{712.7 \, \frac{kmol}{kg_{cat} \, h \, bar^{1.5}} \times exp\left(\frac{-29 \, kJ/mol}{RT}\right) P_{CO}^{0.5} P_{H_2}}{1 + 5.8 \times 10^{-4} (e^{5050/T}) \, P_{CO}^{0.5} + 0.016 \, (e^{1920/T}) P_{H_2}^{0.5}} \tag{3.9}$$

with partial pressures in bar.

The separation and synthesis loop are modeled at the relatively low pressure of 160 bar, after reviewing several process simulations (see [132–135] for a brief selection): the separation is divided into two steps, first at a relatively high temperature (15 °C), and then at 0 °C, the liquid product is further degassed from methane at a lower temperature and pressure. Both the separators are cooled deviating a part of the liquid output to a cryiogenic heat exchanger: the ratio of this flow has been adjusted manually to maximize the net outflow to the product stream. The overall process is represented in the scheme 3.4.

The ammonia reactor behavior has been first recalculated two times, with the last reacting stage (Figure 3.4) specified in turn with the wustite or ruthenium reaction kinetic, as represented in Figure 3.5. It can be appreciated that less Ru/C than Wustite is needed to reach similar performances.

With an input of 10 t/h of ethanol and water (1:3 mol/mol) and 5.8 t/h of air, the ammonia production is 5 t/h and the feed loss (mostly as unreacted gas) is 0.3 t/h, the separation conditions calculated so far grant a purity of 98%. The carbon atom balance through the different blocks, showing the Hydrogen:Nitrogen ratio, and the heating and cooling duties are represented in Figure 3.6.

3.3.1 Energy Recoveries

In this case, the detailed energy recovery to rise LP steam (see previous chapter 2.4) has not been implemented in the flowsheet. In any case, it is here reported the Stream Chart 3.7, with the more straightforward couplings above the pinch.

Concluding this section, an ethanol steam reformer has been coupled to one of the most important processes in industrial chemistry, i. e. ammonia synthesis, considering this time hydrogen as a building block instead of an energy carrier. The approach is feasible, and its economical analysis will be realized as next step.

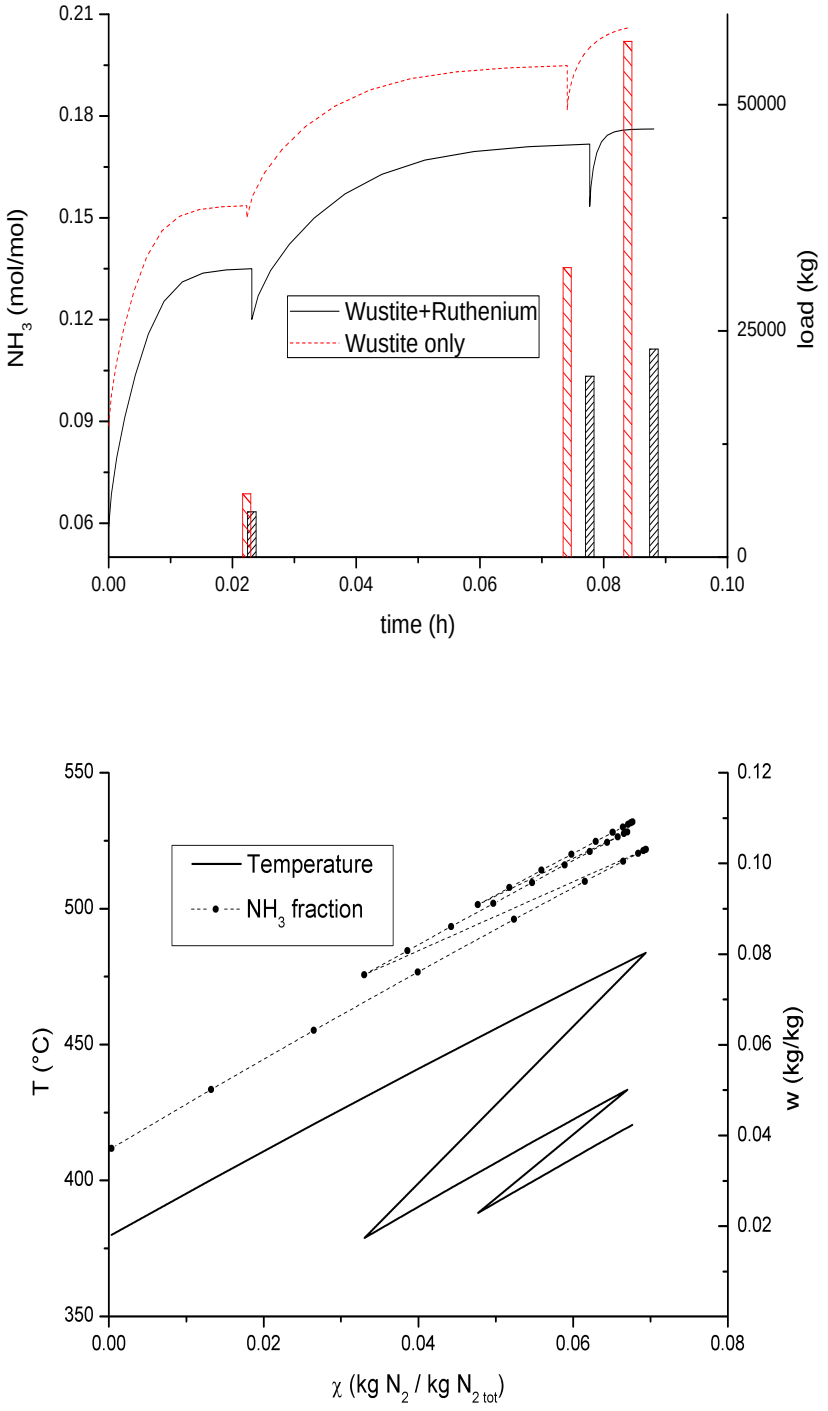

Figure 3.5: Comparison of the reactive stages of an ammonia loop (ammonia yield of 5 t/h, catalyst loads are shown by the columns) with different materials; temperature and ammonia fraction profile of the final adopted configuration, calculated with respect to the overall gas flow through the stages (spikes ar caused by recycles injection).

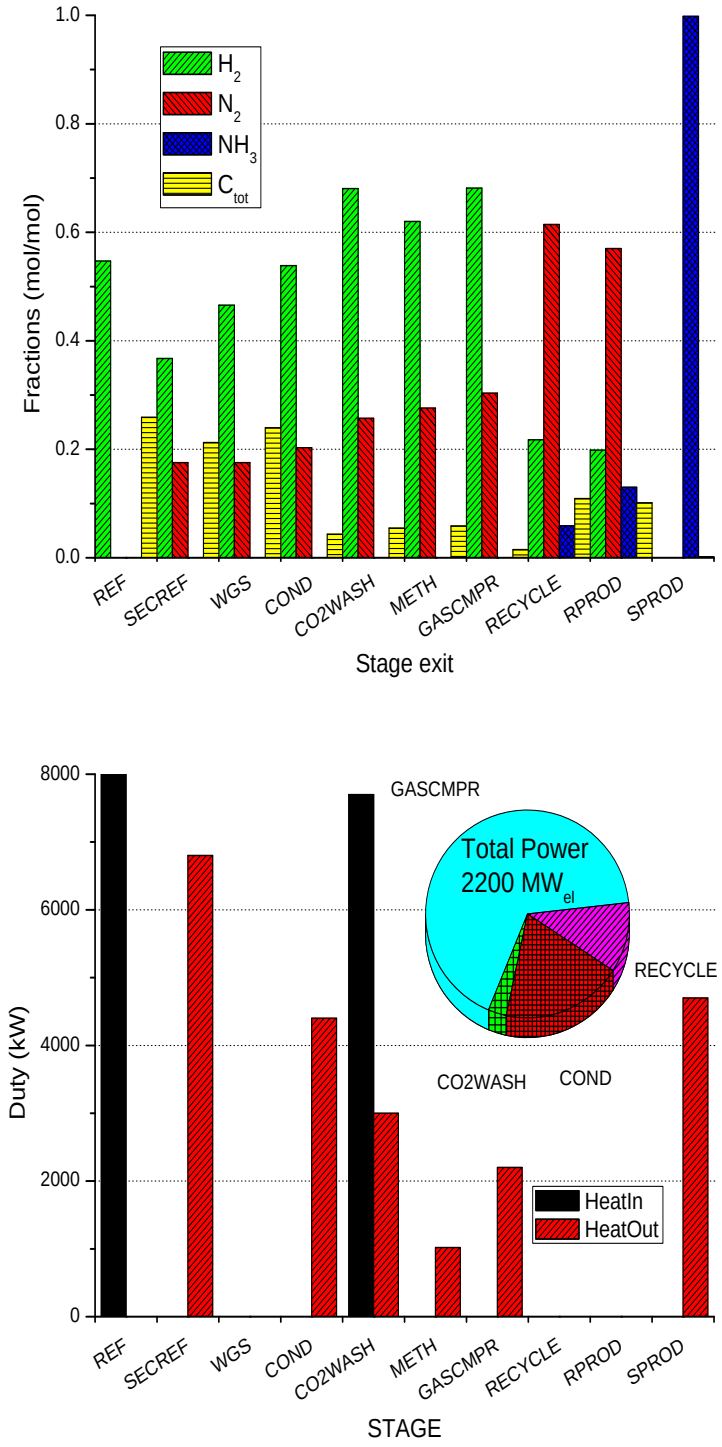

Figure 3.6: Atoms and energy distribution along the stages of the ammonia process (ammonia yield of 5 t/h).

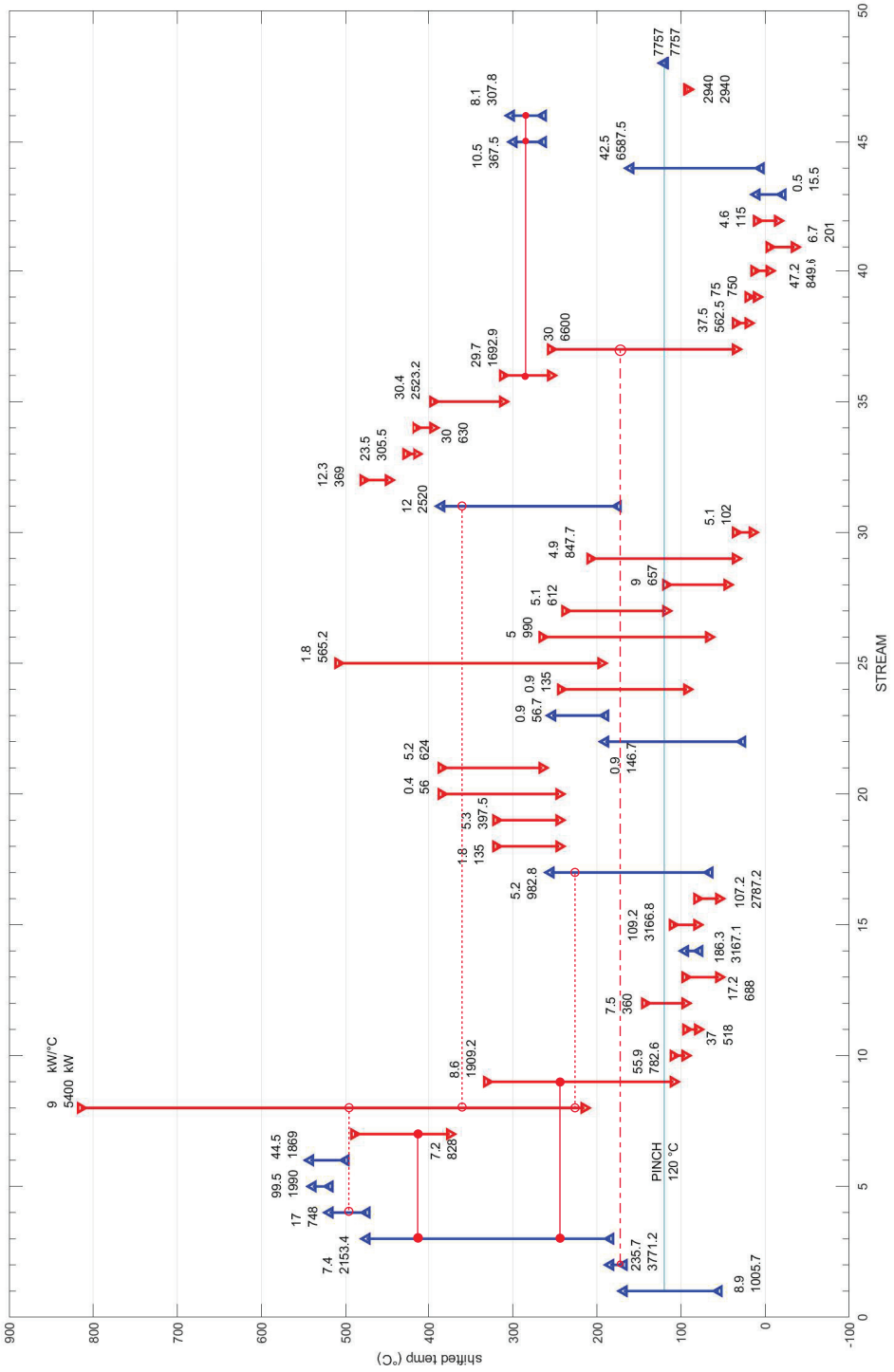

Figure 3.7: Stream chart for the simulated process.

Chapter 4

Ethanol Ammoxidation

The use of ethanol as a base for fine chemicals is mostly indirect [136], as ethylene is generally used. The adoption of bioethanol as a source for acetonitrile would establish a renewable, material-saving (from C_2+N_1 substrates to a C_2N_1 product) and autonomous production process (where acetonitrile is not a byproduct of the acrylonitrile production [137], thus depending on a potentially conflicting and however non-dedicated plant management).

Several studies for an alternative route to acetonitrile have started out in this way, soon matched by works proposing ethanol as substrate in virtue of the reduced environmental burdens (with respect to oil-based ethylene).

This chapter presents: the kinetic description of ethanol ammoxidation starting from the data collected on different catalysts by the team of Prof. F. Cavani[1], who has kindly agreed to share them with our group: therefore, a comprehensive process is designed from the grass roots where attention focuses on the separation stages.

As when undergoing steam reforming, ethanol is the limiting reactant (in this case more for kinetic rather than thermodynamic reasons), therefore the excess ammonia can be recovered, together with the carbon dioxide and a part of the water resulting from unavoidable parasite combustion, as solid ammonium bicarbonate. This allows the full conversion of the reactants into marketable products, the reuse of additional CO_2, and defines a multi-phase separation method.

4.1 Reaction Kinetics

The ammoxidation of C_2 substrates has been studied, up to now, more to find out active and selectivie catalyst than to describe precisely the role of specific reaction conditions [138]. Furthermore, no attempt at all has been established to design a possible process from bioethanol to acetonitrile. Therefore, this reaction has been investigated also in view of several details of the process: a separation process has been built ex novo, accounting for interesting issues of non-ideality. To retrieve the needed equilibrium data an experimental investigation with multiphase and multicomponent systems has been carried out, as detailed in Part II.

Both ethylene [139, 140] and ethanol [141–143] can react with ammonia to yield acetonitrile, nevertheless ethylene is not necessarily a reaction intermediate when the

[1] Università degli Studi di Bologna.

reagent is ethanol, depending on the catalyst. Conversion and selectivity vary appreciably also on the basis of the C_2:O_2 and C_2:NH_3 ratios.

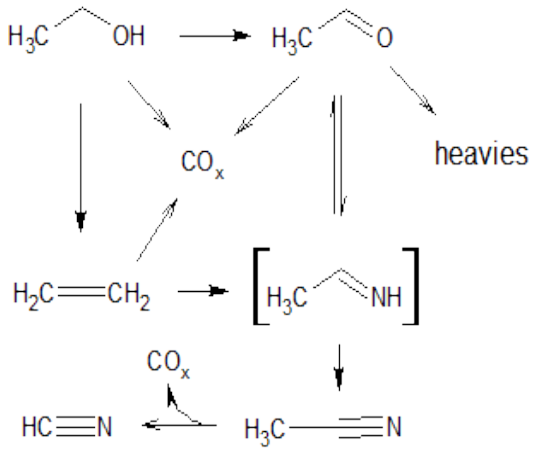

Figure 4.1: Simplified mechanism of ethanol ammoxidation.

An extensive set of experimental data on ethanol ammoxidation has been recently published by Folco et al. [144, 145] and reviewed in light of the accepted mechanisms (Figure 4.1) [146]. This collection contains tests on different materials, that are taken as separate data groups and treated with the same approach already described in sections 1.1 and 2.1.

The results of the kinetic parametrization for each catalyst of the above mentioned work are listed in the already published works [145,146], while here are presented just the main outcomes and formulas used to describe the chosen catalyst V/ZrO_2; the acidity of the support plays an essential role in the selectivity, as rationalized in the mechanisms of Figure 4.2.

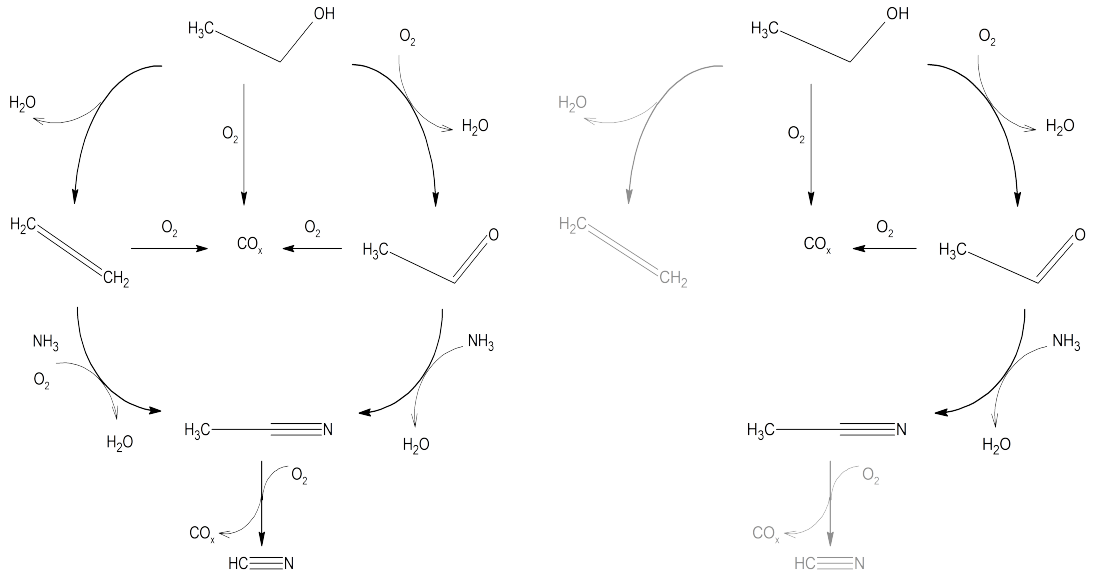

Figure 4.2: Proposed mechanism on a more acidic (left) catalyst, or for one able to suppress ethylene and HCN formation (right).

$$C_2H_6O + \frac{1}{2}\,O_2 \longrightarrow C_2H_4O + H_2O \tag{4.1}$$
$$C_2H_4O + \frac{1}{2}\,O_2 + NH_3 \longrightarrow C_2H_3N + 2\,H_2O \tag{4.2}$$
$$C_2H_6O \longrightarrow C_2H_4 + H_2O \tag{4.3}$$
$$C_2H_3N + \frac{5}{4}\,O_2 \longrightarrow HCN + \frac{1}{2}\,CO + \frac{1}{2}\,CO_2 + H_2O \tag{4.4}$$
$$C_2H_4O + 2\,O_2 \longrightarrow CO + CO_2 + 2\,H_2O \tag{4.5}$$
$$2\,NH_3 + \frac{3}{2}\,O_2 \longrightarrow N_2 + 3\,H_2O \tag{4.6}$$
$$2\,HCN + 2\,O_2 \longrightarrow CO + CO_2 + N_2 + H_2O \tag{4.7}$$
$$C_2H_6O + \frac{5}{2}\,O_2 \longrightarrow CO + CO_2 + 3\,H_2O \tag{4.8}$$

$$r_1 = k_1 \times y_{C_2H_6O}\; y_{O_2}^{0.5} \times \frac{1}{D^d} \tag{4.9}$$
$$r_2 = k_2 \times y_{C_2H_4O}\; y_{NH_3}\; \frac{y_{O_2}^{0.5}}{y_{H_2O}} \times \frac{1}{D^d} \tag{4.10}$$
$$r_3 = k_3 \times y_{C_2H_6O} \times \frac{1}{D^d} \tag{4.11}$$
$$r_4 = k_4 \times y_{C_2H_3N} y_{O_2} \times \frac{1}{D^d} \tag{4.12}$$
$$r_5 = k_5 \times y_{C_2H_4O} y_{O_2}^{1.5} \times \frac{1}{D^d} \tag{4.13}$$
$$r_6 = k_6 \times y_{NH_3}^2 y_{O_2}^{1.5} \times \frac{1}{D^d} \tag{4.14}$$
$$r_7 = k_7 \times y_{HCN} y_{O_2} \times \frac{1}{D^d} \tag{4.15}$$
$$r_8 = k_8 \times y_{C_2H_6O} y_{O_2} \times \frac{1}{D^d} \tag{4.16}$$

$k = k^0 \times exp\left(-\frac{E_a}{RT} + \frac{E_a}{RT_0}\right)$, $D = 1 + 20\,y_{C_2H_6O} + 0.13\,y_{H_2O} + 7.4\,y_{NH_3} + 0.13\,y_{O_2}$ other numerical parameters are reported in Table 4.1.

Reaction	$ln\,k_0$ $(\frac{mol}{mg_{cat}\,s})$	Ea/R (1/K)	T_0 (°C)	d
1	-10.8	18000	300	2
2	-9.32	12400	300	2
3	-16.5	21700	300	1
4	-10.8	12600	300	3
5	-7.13	12000	300	5
6	-13.8	15000	300	5
7	-7.82	18600	300	3
8	-13.1	14400	300	2

Table 4.1: Kinetic parameters for ethanol ammoxidation on V/Zr.

4.2 Thermodynamic Description

The chemicals and the thermodynamic models involved in the simulations are listed in Table 4.2.

Specie	**Formula**	**MW**	**Report ID**
Ethanol	C_2H_6O	46	ETHANOL
Water	H_2O	18	WATER
Ammonia	NH_3	17	AMMONIA
Oxygen	O_2	32	OXYGEN
Acetonitrile	C_2H_5N	41	MECN
Acetaldehyde	C_2H_4O	44	ACH
Ethylene	C_2H_4	28	ETHYLENE
Carbon Monoxide	CO	28	CO
Carbon Dioxide	CO_2	44	CO2
Cyanidric Acid	CHN	27	HCN
Nitrogen	N_2	28	NITROGEN
Hydronium	H_3O^+	19	H3O+
Hydroxide	OH^-	17	OH-
Ammonium	$NH_4{}^+$	18	NH4+
Bicarbonate	$HCO_3{}^-$	61	HCO3-
Carbonate	$CO_3{}^{2-}$	60	CO3- -
Ammonium Bicarbonate	CH_5O_3N	79	AMMON(S)
Models	**Databases**		
NRTL-RK	APV90 VLE-RK		
ENRTL-RK	APV90 ENRTL-RK		
HENRY	APV90 BINARY		
	APV90 HENRY-AP		

Table 4.2: Species involved in the Ethanol ammoxidation process

Also in this case, the thermodynamic description is relatively less important for the reaction block (that deals only with a super-heated vapor phase), but more for the downstream separation. The ammoxidation can be carried out with air or oxygen, but the first option seems more convenient because doesn't require an additional feed-purification section and provides an inert gas (Nitrogen) that limits the temperature rise due to the strong exothermal character of the overall oxidative reactions; this means that the primary separation is between condensing species and gases (N_2, CO, ethylene).

Then the following issues already present:

- ethanol forms a ternary azeotrope with water and acetonitrile, and binary azeotropes with each of other two [147], then it is instrumental to operate the reactor at nearly 100% conversion (as the catalytic tests do indeed let foresee) because any reactant-product separation would be hard to accomplish;

- as the mixture is below its dew point, some ammonia (excess reactant) and carbon dioxide (minor byproduct) are solubilized in water (major byproduct and bulk of

the liquid phase), resulting in a potentially three-phase system according to the simultaneous equilibria in the liquid phase of Table 4.3 (where other salts beside ammonium bicarbonate are not considered [148]).

Stoichiometry	A	B	C
$2\,H_2O \rightleftharpoons OH^- + H_2O^+$	132.90	-13446	-22.477
$NH_{3(g)} \rightleftharpoons NH_{3(l)}$	Henry constant		
$NH_3 + H_2O \rightleftharpoons NH_4^+ + OH^-$	-1.2566	-3335.7	1.4971
$CO_{2g} \rightleftharpoons CO_{2l}$	Henry constant		
$CO_2 + H_2O \rightleftharpoons HCO_3^- + H_3O^+$	231.46	-12092	-36.782
$HCO_3^- + H_2O \rightleftharpoons CO_3^{2-} + H_3O^+$	216.05	-12432	-35.482
$HCO_3^- + NH_4^+ \overset{K_{exp}}{\rightleftharpoons} H_5CO_3N_{(s)}$			

Table 4.3: Equilibrium reactions used to calculate the distribution of charged species formed in the ternary water-NH_3-CO_2 system, with equilibrium constants expressed as: $ln\frac{K}{(mol/mol)} = A + B(K)/T + ClnT$

The binary azeotrope between acetonitrile and water doesn't present particular modeling problems with well-established packages such as NRTL-RK [149], and also the $NH_3-CO_2-H_2O$ system has been studied and parameterized extensively [150]; in this case both ammonia and carbon dioxide solubility is calculated via the Henry constant.The graphics in Figures 4.3-4.4 give a visual evaluation of the NRTL-RK model to reproduce the VLE of water and acetonitrile at different pressures. The shift of the azeotropic composition towards richer water mixture at increasing pressures is needed to choose the proper pressure-swing parameters in the process [151, 152].

This figure is complicated, anyway by the following considerations:

- ethanol is a known antisolvent for ammonium bicarbonate [154], thus it shifts equilibrium 4.2 to the right: also if it is completely converted, this problem subsists since also acetonitrile acts much in the same way (see section 7);
- the description of the electrolytes provided by the standard simulation packages assumes water as the only solvent, this means that the salt precipitation in ethanol and acetonitrile is not foreseen;
- if water is present, all the interacting pairs ion-water and water-acetonitrile contribute to the overall mixture's free energy, but the salt solubility is calculated with respect to water only, then neglecting this correction, which would be a good approximation only at very low ionic strengths and acetonitrile:water ratios.

To overcome possible issues, a bench-scale analysis of the four-species system NH_3-CO_2-H_2O-C_2H_3N has been performed, dissolving ammonia and carbon dioxide in water (or in a mixed solvent) at the same time, in equimolar amounts, starting from solid ammonium bicarbonate. The description and findings of these experiments are explained in chapter 7 and 8 below; here are reported just the two more relevant observations:

- ammonium bicarbonate solubility can be corrected to keep into account acetonitrile presence up to 0.3 grams per gram of solvent;

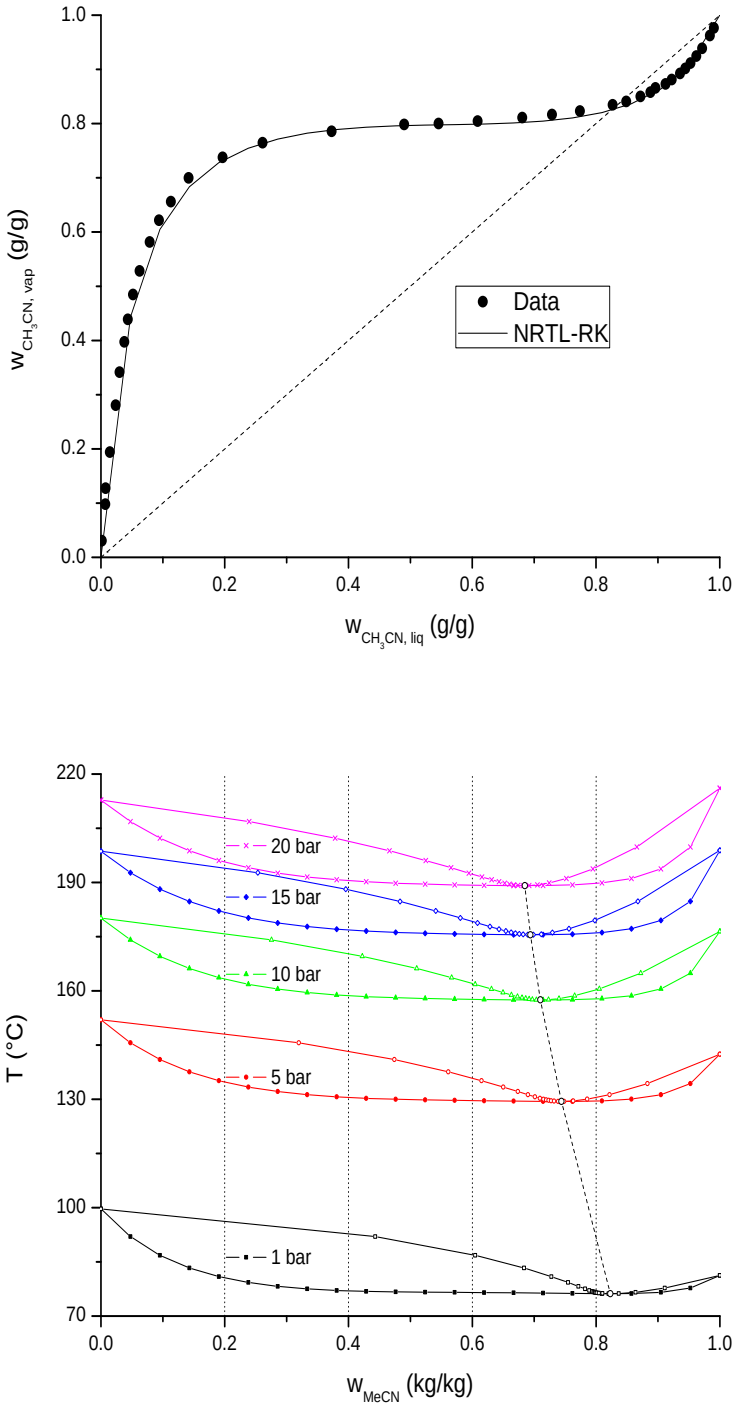

Figure 4.3: Up: xy diagram for water and acetonitrile at 1 atm (model and data), bottom: Txy diagrams at higher pressures (model only).

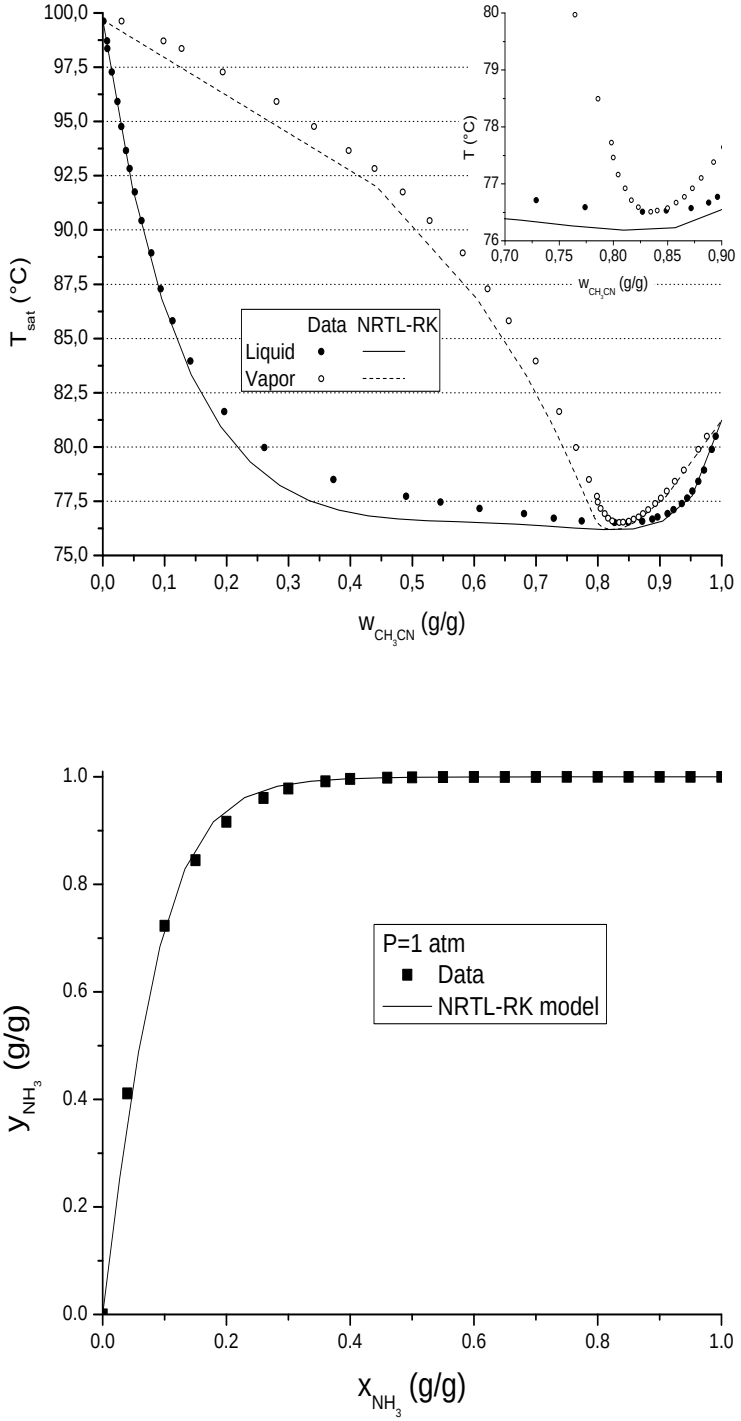

Figure 4.4: Use of the NRTL-RK model to reproduce the equilibrium temperature of the acetonitrile-water system, and the same for water and ammonia (data from [153]).

- above this threshold, the solvated ions induce a liquid-liquid separation in the solvent: one phase is lighter and contains (on average) 0.75-0.80 grams of acetonitrile per gram, the other is heavier and contains circa 0.25 grams of acetonitrile (on the total weight) and all the salt and ionic species.

The mass balances of these ensuing equilibria are studied with enough accuracy to describe reliably the separation process, but the energetic aspects could not have been investigated. The heat balances are still usable supposing that the salt solvation enthalpy is greater than the phase-split enthalpy of mixing. These phase separation data are further used to refine the products separation section of the flowsheet.

4.3 Process Layouts

In principle, the product separation must in any case consider three steps represented below (see also the scheme 4.5):

- absorbing of the condensing species cooling the vapors downstream the reactor;
- precipitation and separation of part of NH_3 and CO_2 as ammonium bicarbonate;
- stripping of residual NH_3 and CO_2, separation of acetonitrile from water.

the third step poses two criticalities: first, below the bubble point of the mixture, the removal of NH_3 and CO_2 is not effective because they are in equilibrium with charged species; second, above the bubble point the acetonitrile released and lost with the vapors is not negligible. Since some acetonitrile is lost together with the volatiles, then a recycle, downstream the stripping section back to the precipitation block, is mandatory. The precipitation of part of ammonia and CO_2 as ammonium bicarbonate (second step) opens up a solution to avoid the build-up of these recycled species and leaving the removal of the gaseous ammonia to the first washing stage.

The facts that: i) ammonium bicarbonate is marketable [155], ii) it is formed starting from the compounds already leaving the reactor and, depending on the excess of ammonia and parasite oxidations, iii) additional CO_2 can be needed (according to a strategy already foreseen as a greenhouse gases control strategy [156–158]), make this configuration even more appealing respect to a material-wasting, once-through setup.

Homogenoeus Mixture Purification

The basic development of this solution (block-scheme 4.5) has been at first carried out [159] supposing that:

- the liquid-liquid equilibrium between an acetonitrile-rich phase and a water-rich one in presence of the ammonium is not established: this is the case when the acetonitrile:water ratio exiting the reactor is not above the critical point (see section 8), so the already worked out mass balances for *the whole process* keep valid; the detailed arrangement of the stripping, light venting and refining columns are influenced by this choice [160, 161].
- The particular catalyst' selectivity towards byproducts [144] leaves an appreciable quantity of HCN (a common byproduct in ammoxidation contexts) to be washed

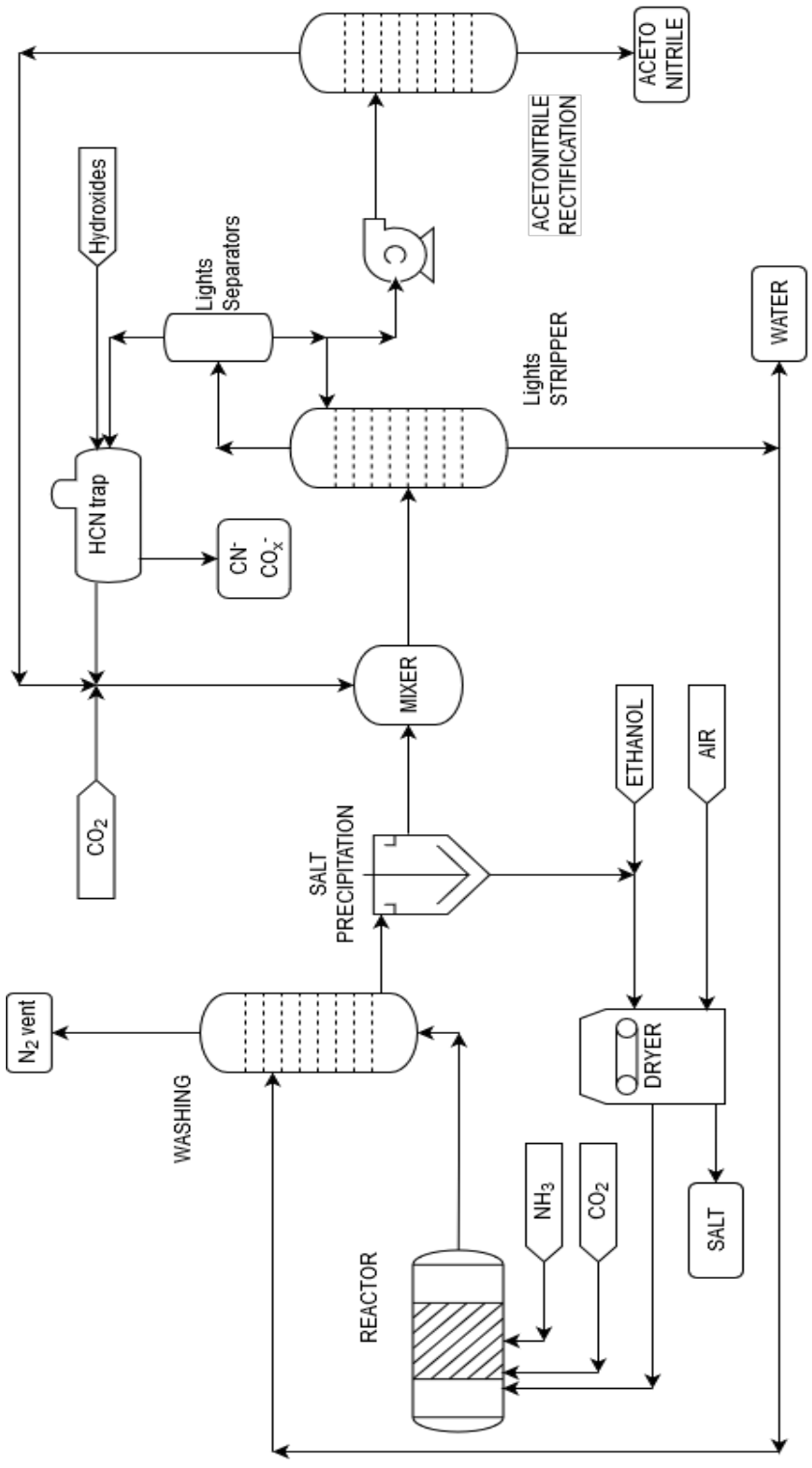

Figure 4.5: Conceptual scheme of the separation, where acetonitrile and water are separated together with the NHx-COx stripping: if HCN is present, the carbonates may be lost and continously reintegrated.

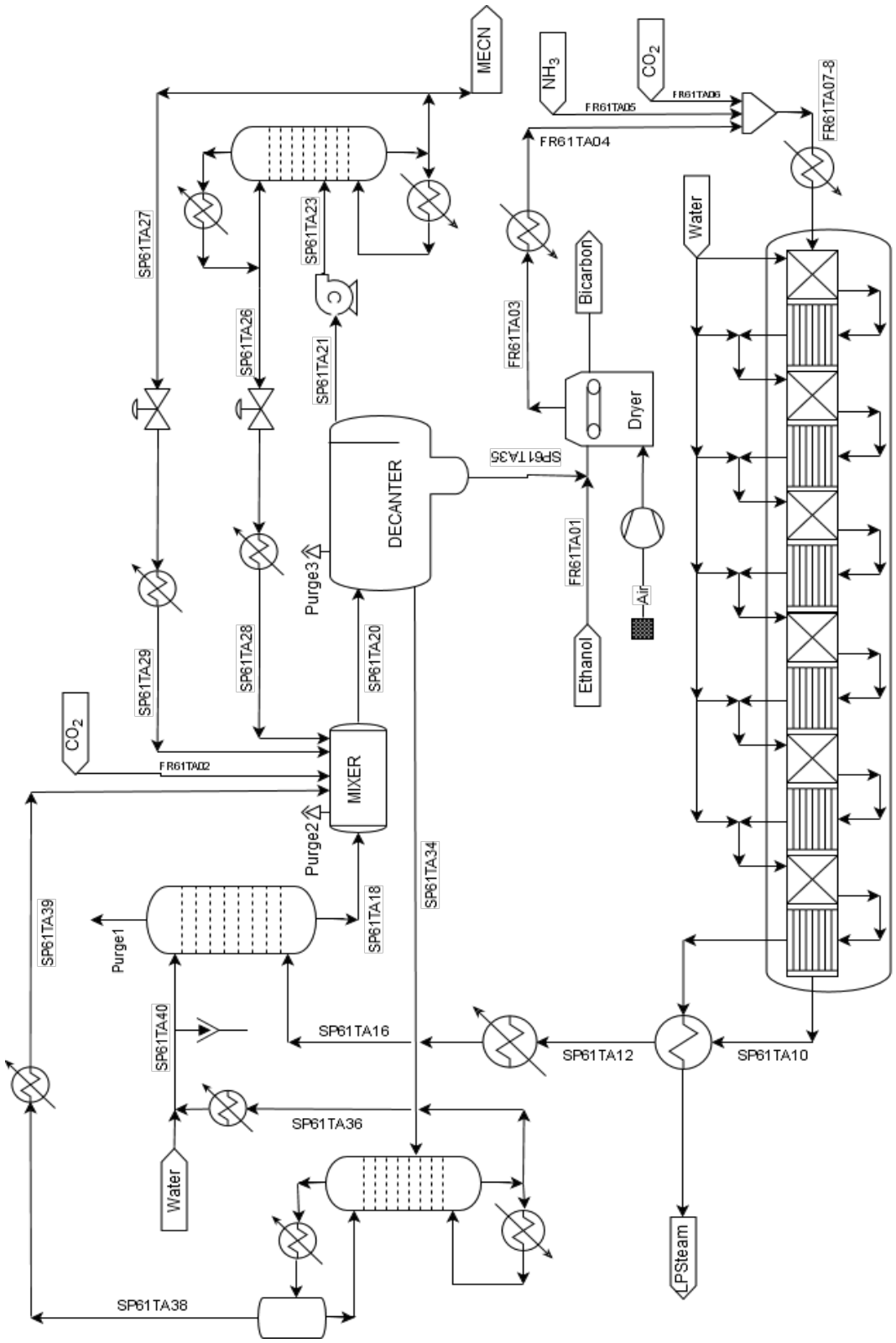

Figure 4.6: PFD for an ethanol-acetonitrile process where the acetonitrile-water-NH_4HCO_3 separation relies on the salting-out.

out with disposable soda or potash, leading to a neat discharge of carbonates and a larger resupply of fresh CO_2 [159]; if this purification takes place between the light separation and recycles, it must be done at moderate temperatures and within short times to prevent acetonitrile hydrolysis.

- the moisture dragged by ammonium bicarbonate is recovered because it contains acetonitrile, so the air needed to dry the salt is also used as oxygen feed to the reactor.

Phase-split Purification

The findings of lab scale separations can otherwise be used to design an alternative purification solution (Fig. 4.6):

- the salting-out of acetonitrile from water in presence of ammonium and bicarbonate ions is taken into account, leading to two rectifying and stripping columns that work in parallel rather than in serie;

- choosing a catalyst that leaves only traces of HCN [146], additional basic washings can be avoided: the traces of acid left in the gases are released through the main vent, while the residual in the liquid is recycled in the loop between the decanter, the dryer and the reactor (see scheme 4.6) up to the equilibrium concentration.

The main separation unit, i.e. the three-phase decanter, has been modeled via a customized block that performs the following step-wise calculation:

- fixing a pH value at 25 °C, all the nitrogen and carbon atoms in the mixtures are assigned to the species in the equilibria of Table 4.3 according to their constants, the oxygen balance yields the free water;

- the partition of acetonitrile between the liquids is adjusted in order to fix its concentration at 0.25 g/g in the heavier, the partition of water to have it at 0.25 g/g in the lighter and the partition of salt and ions to segregate them in the heavier;

- the salt is removed to a separate stream dragging with it 0.30 grams of heavy liquid per gram of solid (see 8.6): this changes the lever-rule adjustment between the liquid phases, so the calculation is repeated until all the design parameters are contemporary satisfied.

The recycle loop must retain a quantity of acetonitrile necessary to achieve a good phase-phase separation ($\geq$ 40% by weight, see section 8), which is correlated also on the water quantity recycled with the strippers' overhead: this quantity is, in turn, not entirely adjustable, because it depends on the equilibrium composition of a NH_3-CO_2-H_2O-CH_3CN vapor carrying all the recycled flow of ammonia and carbon dioxide.

The actual behavior of the stripper has two correlated problems: a) to meet the target on the bottoms purity (exit point for *pure* water outside the process) leaving some degree of freedom on the overhead flow, a condenser should be added to manipulate the reflux ratio, and so b) if the acetonitrile fraction in the reflux is high enough, phase-splits and salt precipitation can still occur. This issue doesn't need to be addressed in detail supposing again that nor the condenser nor the top trays allow a hydraulic regime where the separate phases can settle, so the charged species NH_4^+ and CO^{x-} of the watery

phase can always be converted into neutral NH_3 and CO_2 at a steady rate. If the stripper is operated to achieve an azeotropic acetonitrile concentration in the distillate, then there could be present only one liquid phase where the salt is not soluble (paragraph 7), so the stripping of ammonia and carbon dioxide as gases could be more problematic.

The experimental results gathered up to now (section 8) let one think that however, when ammonia and carbon dioxide are expelled from the water-rich liquid *at or just below* the bubble point, the salt complete re-precipitation can be avoided thanks to the continuous mixing of the species in the liquid droplets dragged alongside with the vapors. In summary, beside foreseeing a condenser working with a non-subcooled reflux, the vapor top-tray (conventionally the second in the Aspen-Plus interface) composition is conservatively set below the acetonitrile:water azeotropic ratio.

Another important aspect must always be kept in mind: all the separation layouts studied so far rely on the complete conversion of ethanol in the reactor, because:

- ethanol is anti-solvent for ammonium bicarbonate but is completely miscible with both water and acetonitrile, so it actually quenches the phase split lowering the ionic strength;
- the VLE of the ternary mixture of acetonitrile-water-ethanol presents three binary and one ternary azeotrope, the ensuing purification would then be made severely more complex (see also chapter 9.5 for further information on this topic).

The reactor layout is quite complex due to the exothermic reactions that tend to a temperature runaway. In this cases, provisions as: a) using air instead of pure oxygen, b) adding a quench gas (here carbon dioxide, according to the general process' philosophy) and c) continuously removing heat by means of saturated water are successful in practice [162]; in the computer simulation, anyway, it is heuristically found out that it's also necessary to split the reaction's coordinate into many stages in serie to maintain the calculated temperature within the model validation limits.

The last graph in Figure 4.9 represents the composite curves and GCC for the process. Despite the strong exothermic character of the reaction, a neat heat input is needed at relatively low temperatures, because the steam raised cooling the reactor doesn't carry enough energy to supply the reboiler of the acetonitrile rectifier. Nevertheless, the pressure-swing strategy for the final purification makes it possible to use the waste heat of this column to boil the water in the lights stripper.

In this part of the activity, it has been studied a reliable layout for a dedicate acetonitrile production as a viable replacement of its obtainment as an acrylonitrile byproduct [137]. This process is based on a fully renewable feedstock and has a much higher sustainability through Life-Cycle Assessment than rival routes from fossil ethane or ethylene [159]. Two different process layouts have been developed, based on different purification strategies; in each case an almost full commercialization of the products is envisaged.

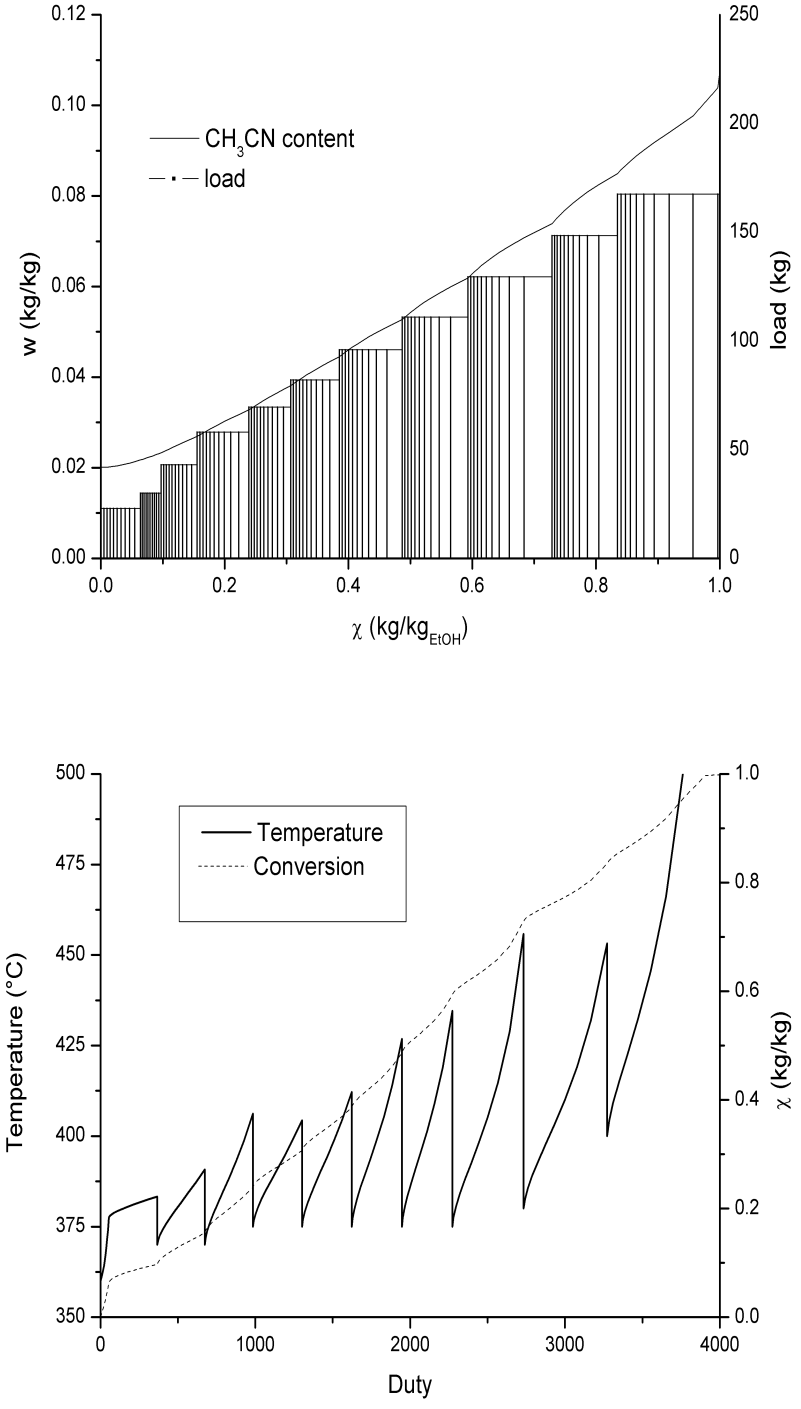

Figure 4.7: Reactor working.

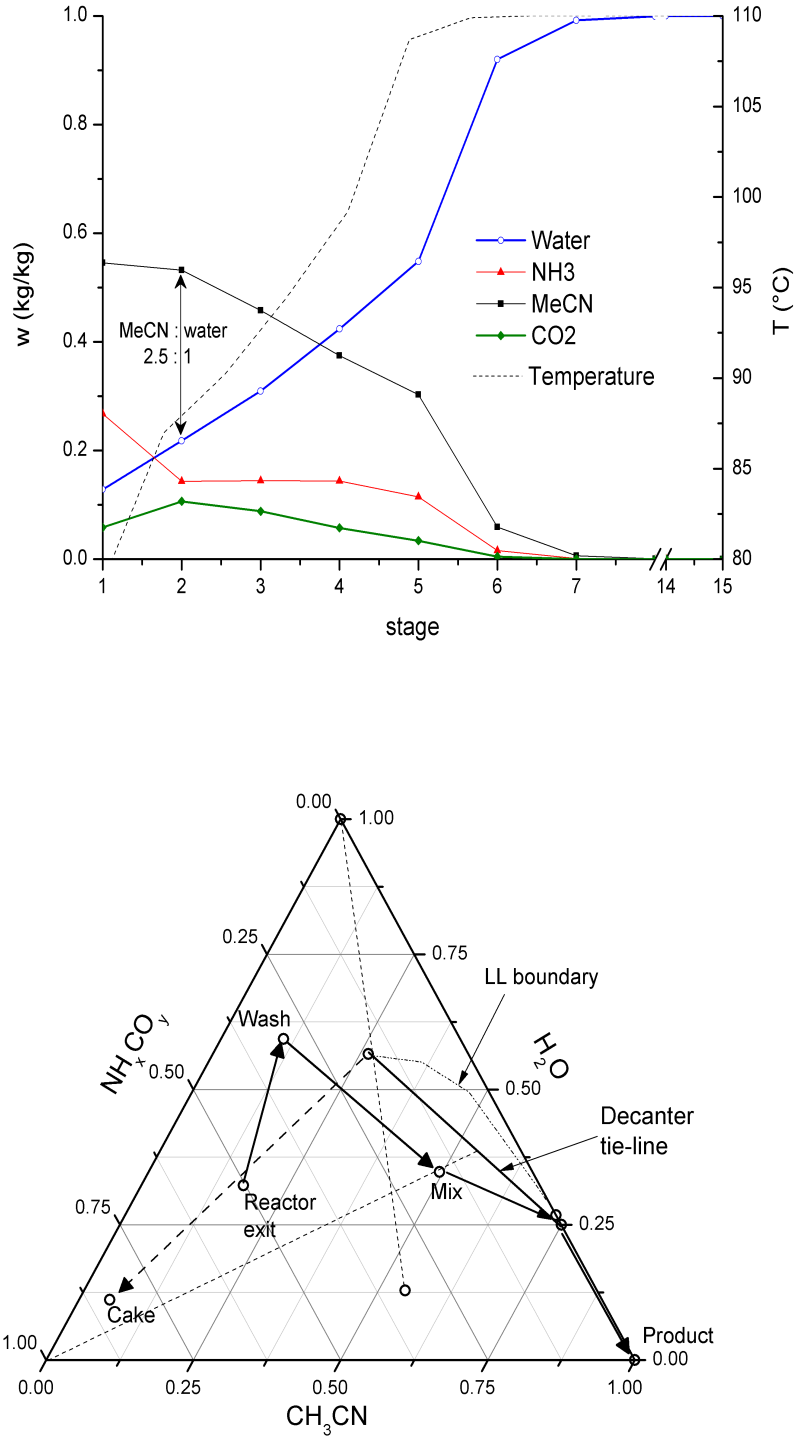

Figure 4.8: Stripper working and mass process balances.

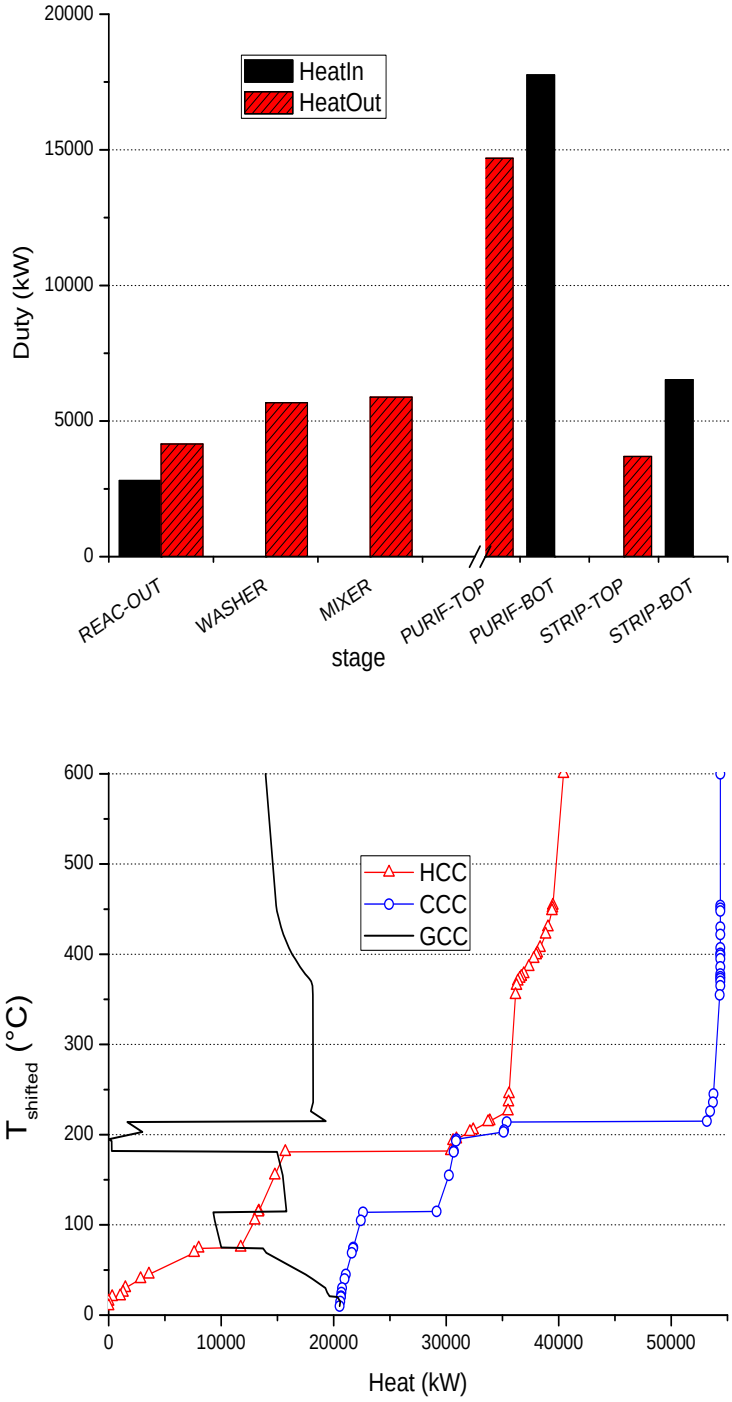

Figure 4.9: Overall energetic balance.

Chapter 5

Carbon Dioxide Methanation

As methane has been establishing itself as the primary energy source with respect to coal, though not without reserves [163], to obtain it from renewable carbon feedstock rather than to extract it as natural gas is even more appealing: biomass-generated methane would be the first option to have an efficient power generation with a virtually closed CO_2 cycle [164].

When renewable hydrogen is available, on the other hand, its conversion into methane would turn it into a gas easier to handle, with an already existing distribution network (a still serious bottleneck when hydrogen is considered), and this option is all the more promising as it implies the reuse of carbon dioxide [164–166]. That's to say that a "power-to-gas" framework could help to overcome the drawbacks of hydrogen as an energy storage medium [167–169]. Research has been developing on new, selective catalysts [170] capable to convert carbon dioxide without releasing CO.

5.1 Reaction Modeling

The direct and indirect conversion of CO_2 into methane:

$$\mathrm{CO_2 + 4\,H_2 \rightleftharpoons CH_4 + 2\,H_2O} \qquad \Delta_r^0 H = -165\,\frac{kJ}{mol} \tag{5.1}$$

$$\mathrm{CO_2 + H_2 \rightleftharpoons CO + H_2O} \qquad \Delta_r^0 H = 41\,\frac{kJ}{mol} \tag{5.2}$$

$$\mathrm{CO + 3\,H_2 \rightleftharpoons CH_4 + H_2O} \qquad \Delta_r^0 H = -206\,\frac{kJ}{mol} \tag{5.3}$$

relies on the ability of catalysts (based mainly on Ruthenium or Nickel), to split the CO_2 and shift the $CO \longrightarrow CH_4$ conversion to completion, in a temperature range from 250 to 450 °C [171–173]. Most side products are poisonous carbon deposits coming from CO reduction rather than alkanes coming from its polymerization [174]. The reaction enthalpy makes the equilibrium conversion nearly complete under 200 °C (at atmospheric pressure), but poses also a problem for the practical temperature control, given the strong exothermicity of the reactions..

In this case, two kinetic models have been adopted between the several reviewed. The first formula [171] has been derived for low conversions and is used to describe the first part of the reactor, while the second [172] covers a wide range of temperature and conversion values. Several adjustments have been made to harmonize the measure units

(in particular, the second formula is originally based on the volumetric contact time, so some assumptions on the catalysts density and void fraction have been made):

$$r_{\chi<0.1} = 3.55 \frac{kmol/s}{kg_{cat}\, kPa^{0.88}} \times exp\left(-\frac{7950\,K}{T}\right) \frac{P_{CO_2}^{0.34} P_{H_2}^{0.88}}{P_{CH_4}^{0.11} P_{H_2O}^{0.23}} \tag{5.4}$$

$$r_{\chi>0.1} = 11.2 \frac{mol/s}{kg_{cat}\, bar^{1.5}} \times exp\left(-\frac{1.29\,K}{T}\right) \times \left(P_{CO_2}^{0.3} P_{H_2}^{1.2} - \frac{1}{K_{eq}} P_{CH_4}^{0.3} P_{H_2O}^{0.6}\right) \tag{5.5}$$

where χ is the conversion and $ln\left(\frac{K_{eq}}{bar^{-0.6}}\right) = 10.47 + 5218/T - 2.55\, ln(T) + 0.000837 \times T$

5.2 Thermodynamic Description

The chemicals and the thermodynamic models involved in the simulations are listed in Table 5.1.

Specie	**Formula**	**MW**	**Report ID**
Carbon Dioxide	CO_2	44	CARBO-01
Hydrogen	H_2	2	HYDRO-01
Methane	CH_4	16	METHA-01
Water	H_2O	18	WATER
Potassium Carbonate	K_2CO_3	138	POTAS-01
Hydronium	H_3O^+	19	H3O+
Hydroxide	OH^-	17	OH-
Potassium Cation	K^+	39	K+
Potassium Carbonate salt	K_2CO_3	138	K2CO3(S)
Potassium Bicarbonate salt	$KHCO_3$	100	KHCO3(S)
Bicarbonate	$HCO_3{}^-$	61	HCO3-
Carbonate	$CO_3{}^{2-}$	60	CO3- -
Models	**Databases**		
PSRK	APV90 EOS-LIT		
NRTL-RK	APV90 ENRTL-RK		
ENRTL-RK	APV90 ENRTL-RK		
HENRY	APV90 BINARY		
	APV90 ENRTL-RK		

Table 5.1: Species involved in the Carbon Dioxide-Methane process. Potassium Carbonate is present two times, because one identifier (POTAS-01) represent the substance in general, whether in solid or solvated form, and is used to provide an input to the mass balances.

The considerations already made for the description of the gas and liquid phases for the main species in the other sections still apply: it is deemed more reliable to describe interaction in the gas via an equation of state, but solubility in water (the bulk constituent of any liquid considered in this process) via Henry constants. A check on the PSRK model for the Hydrogen-Methane couple has yielded the appreciable result summarized in graph 5.1.

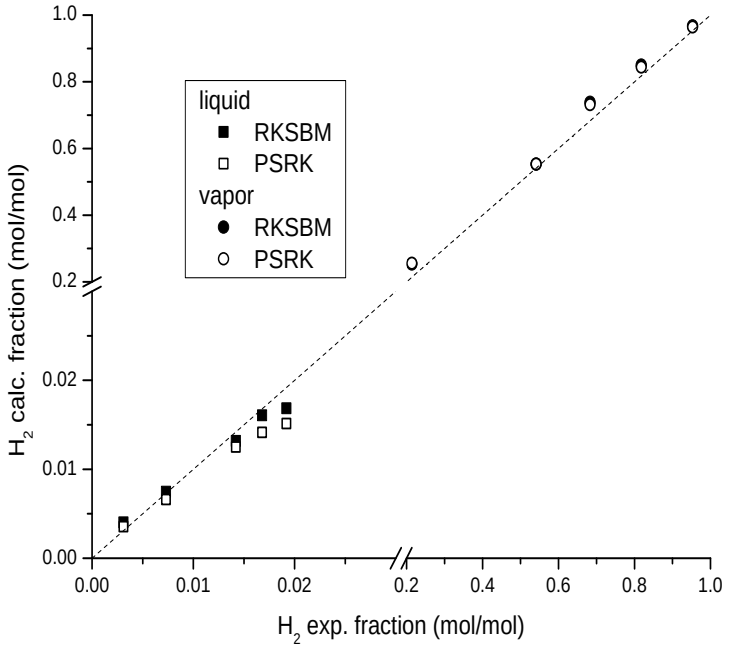

Figure 5.1: Parity plots between literature data [175] and models prediction regarding the liquid-vapor equilibrium of hydrogen dissolved into liquid methane.

In this case, Potassium Carbonate is added as CO_2-scrubber, instead of MDEA, with the associated equilibrium chemistry:

$$K_2CO_3 \longrightarrow 2\,K^+ + {CO_3}^{2-} \tag{5.6}$$

$${CO_3}^{2-} + H_3O^+ \rightleftharpoons {HCO_3}^- + H_2O \tag{5.7}$$

$${HCO_3}^- + H_3O^+ \rightleftharpoons CO_2 + H_2O \tag{5.8}$$

this choice is made to simulate also the mature Bensfield process (still in operation worldwide [176–179]), and then get a more general idea and a firmer background on CO_2-washing purification strategies. In addition to the already listed reviews of thermodynamic parameters, here are presented also the evaluations for the ternary system CO_2 – K^+ – H_2O and for methane in presence of this electrolyte (Figures 5.2 and 5.3, with additional data from [180, 181]).

The estimation obtained using the original AP database are conservative for the methane and for carbon dioxide at pressures lower than 20 bar. For simplicity, the first correction of the Henry constant is proposed with a heuristic approach - nevertheless, the reviewed literature offers many other correlations with a developed theoretical background.

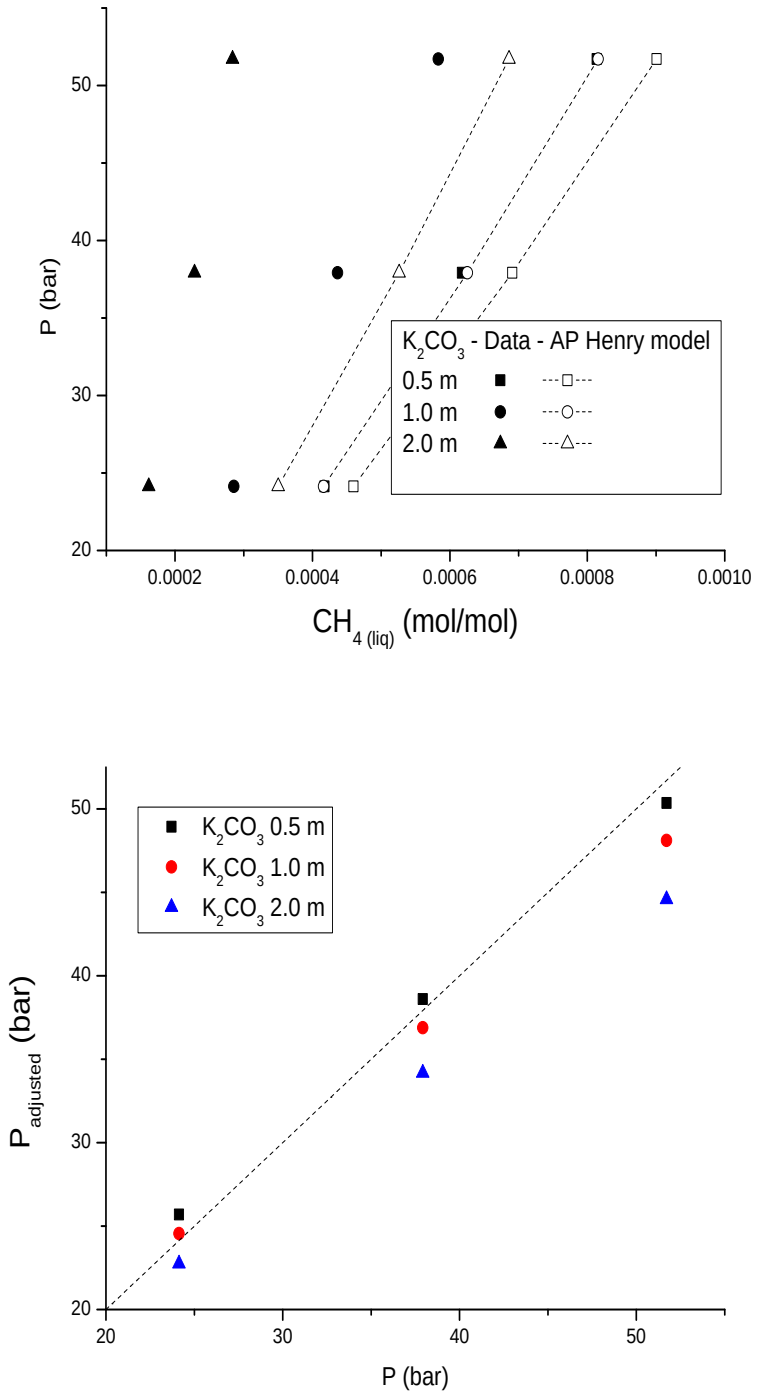

Figure 5.2: High pressure methane solubility in aqueous potassium carbonate (upper) and proposed adjustment for its Henry constant (lower).

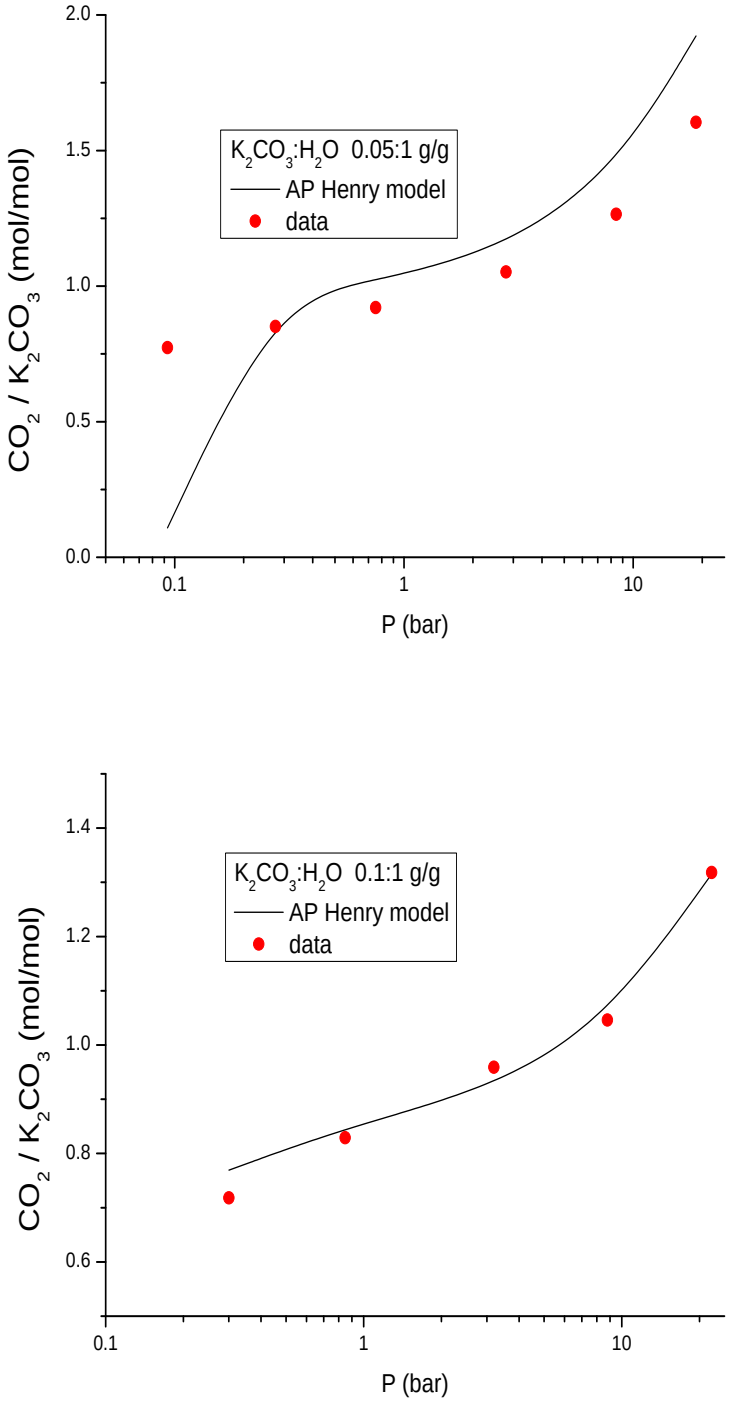

Figure 5.3: Evaluation of the thermodynamic libraries in use for the CO_2-K_2CO_3-H_2O mixture.

5.3 Recycle and Separation Outline

To cope with the esothermal reaction behavior, that leads to a potential temperature runaway, it is necessary to foresee a multi-stage reactor, both in an adiabatic-beds or cooled-beds configuration. In addition, other two design concepts are adopted (see the process scheme 5.5 and also an essential literature review [182–184]):

- the per-pass conversion through the whole reactor is limited at 75% of the CO_2 total flow: in this way the released heat is rescaled by the same ratio, and the equilibrium temperature corresponding to this value is still high enough to grant some catalyst's activity;

- additional water is fed into the reactor to increase the thermal inertia of the reaction mixture: this has a negative effect on the maximum conversion achievable at equilibrium, but a positive effect on the temperature-conversion behavior of the catalyst (see also Fig. 5.4).

The first reactor stage treats only the fresh feed and lets the stream temperature increase adiabatically, then recycled CO_2 and water are injected into the second stage. An adiabatic reactor is designed to have at least five stages in total - if the catalytic beds are cooled (for example, with the cold fresh feed) this number may be reduced, but in this case the beds are kept fixed so to make a comparison on the temperature profile (see Figure 5.4).

The correlation between the maximum conversion and temperature reached in the reactor tail is then considered on the basis of the actual composition of the reacting mixture after the recycle, not on the basis of reaction stoichiometry.

Two condensers, operated at relatively high temperature ($\geq$80 °C) with a 4-stage pressure increase between them, dump the water produced by the reaction. The following basic scrubbing section (an absorption and a stripping column) has not only the task of purifying the produced methane, but also of recycling the unreacted CO_2 to the reactor; the last dehydration stage is instead modeled as a two-bed PSA. In principle, there are several options for the purification section:

- absorb water and CO_2 in a single section (e.g. an array of PSA beds loaded with a suitable material [97]) and use the purge gas as fuel, this option would imply to waste some carbon dioxide, or has to be implemented after a 100% conversion reactor;

- recycle the above mentioned purge vapours into a limited-conversion reactor;

- separate the carbon dioxide and water in different steps; the two resulting purge streams could be disposed of or recycled into the reactor;

- having purified CO_2 and water separately, they can be recycled in different points of the process.

In this work, is chosen the last option, for these reasons:

- discharge or burn the purge streams is not the best option when the reactor is not designed to achieve nearly complete conversion, so the recycle is more appropriate;

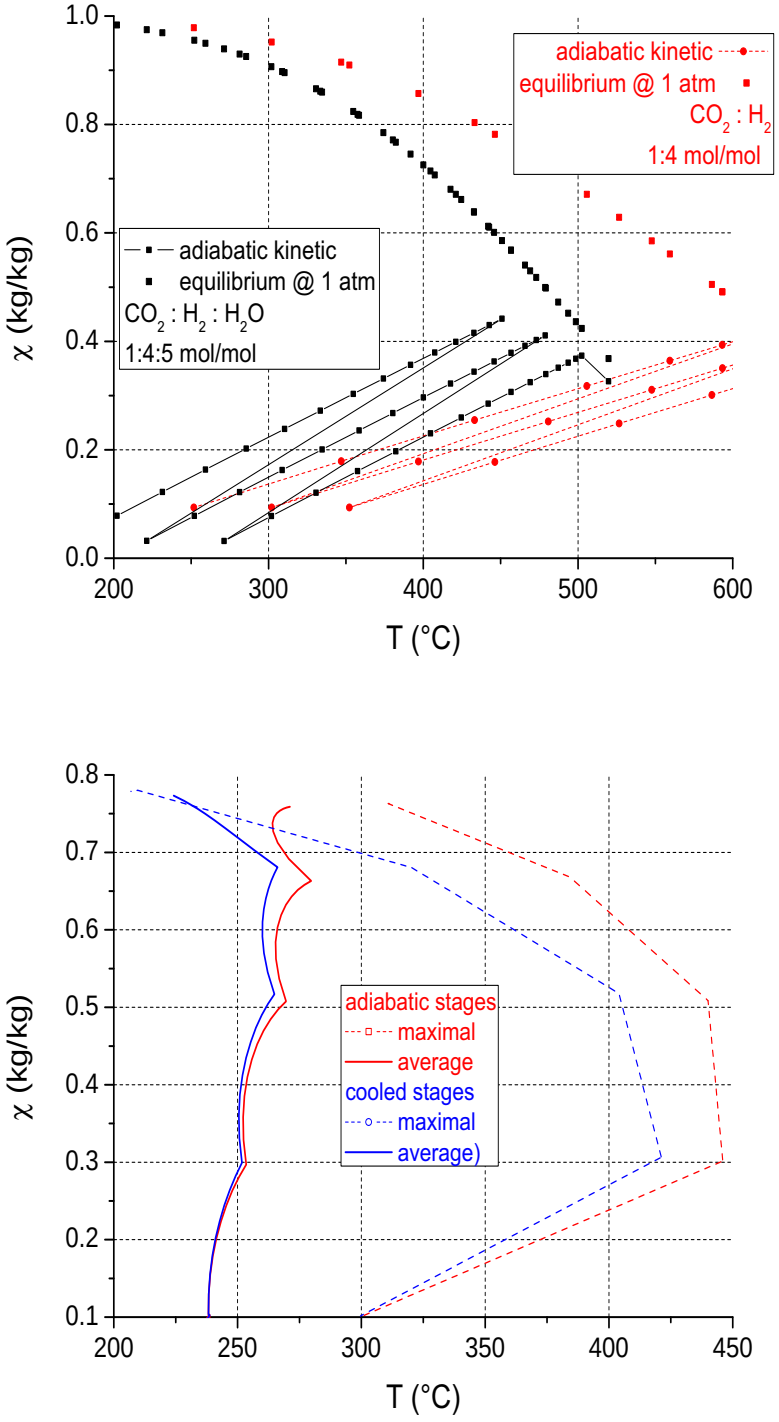

Figure 5.4: Adiabatic boundaries for the reactor behavior with a stoichiometric mixture of with an excess of water; and: temperature profile for 5 adiabatic catalytic beds with intercooling, compared with a continuously cooled reactor.

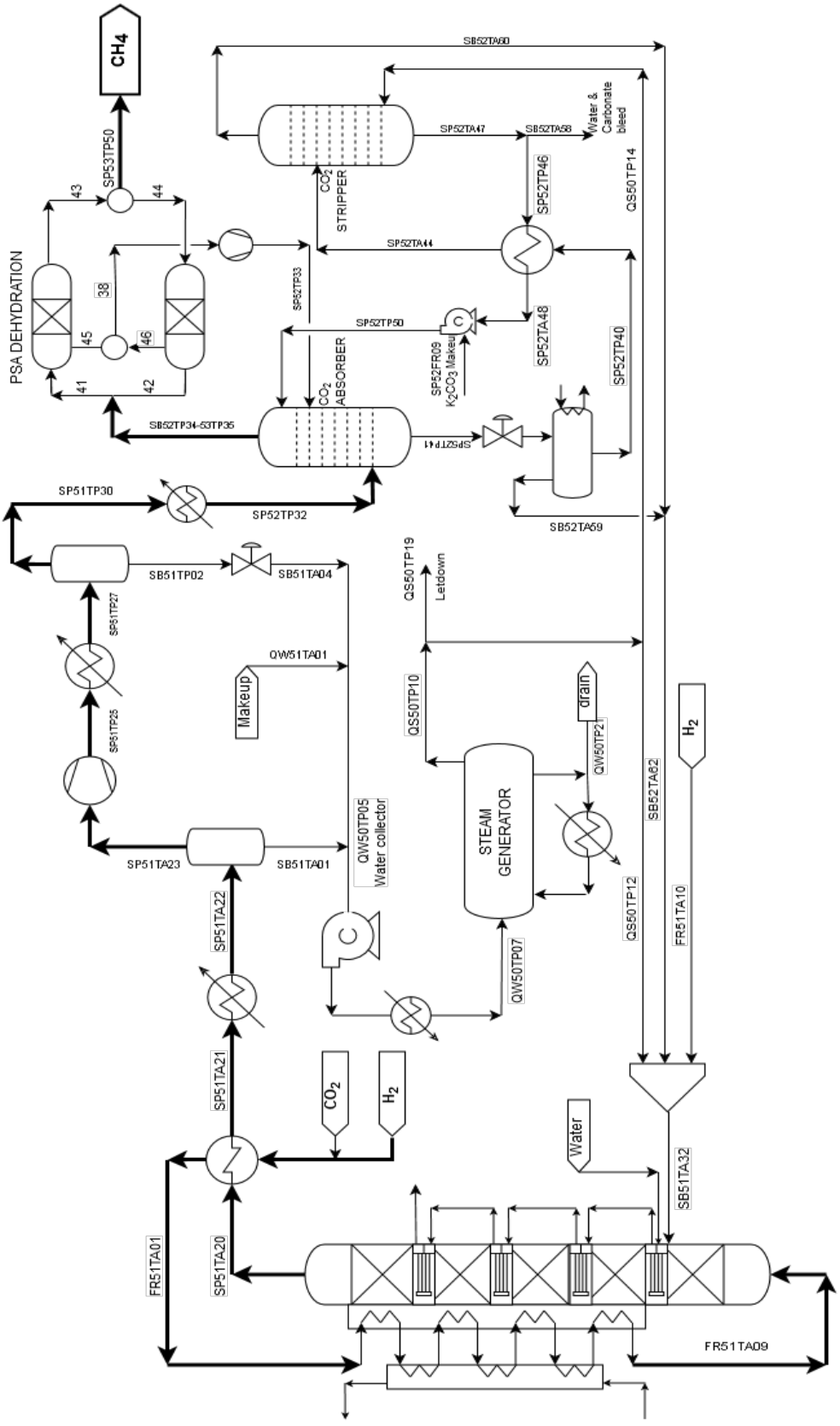

Figure 5.5: PFD of methanation process.

- a single separation block with a return loop would lead to a single large recycle stream encompassing *all* the process units (much as in the case of the ammonia synthesis), moreover this current would contain all the involved chemicals in proportions possibly different from the ratio foreseen for the reactor;

- the last mentioned issue could be dealt with adding small separate feed streams for the reactants, but if water and methane are recycled together, then the hampering effect on the equilibrium is worse than when recycling just water.

According to these criteria, the methane used to carry the last water residuals out of the product is not recycled into the reactor, but into a - perforce separated - purification section that removes only CO_2. At this point, the carbon dioxide removal cannot rely on a PSA arrangement as the one proposed in section 1.3 (and also here for the dehydration task), least having recycled methane coming to the reactor from this point or purging some methane as fuel, as in scheme 2.3.

In this section, it is explored the solution of a nearly completely closed scheme, so the gross separation of reaction water, of CO_2 and of residual water are kept separated; the PSA dehydration is the last and, while all the streams are recycled within the process, only the first two purges are recycled into the reactor. Following the same philosophy of multiple closed circuits, it is observed that the carbonate stripper has to be flowed with steam and potassium cations cannot be lost in the vapors (as could be, instead, the neutral amine of the other processes), so this block can be operated without a condenser and its reboiler is replaced with a centralized steam generator that feeds also the second reactor' stage after having vaporized the water discharged from the product. The concept of *recycling* steam into the reactor as a quencher has been considered also for plant concepts foreseeing complete conversion and no reactants' loops [182]. A single separate feed stream helps to control the reactor's behavior injecting the right quantity of hydrogen that compensate a slightly under-stoichiometric feed.

The process balances foresee an appreciable hydrogen fraction (3% mol/mol) in the outflowing methane, anyway it is not mandatory to design further separations before considering the characteristic of the distribution network downstream [185]. The first calculation is set up to yield 2×10^5 kmol/h of methane, corresponding to 40 millions normal-cubic meter per year (about the natural gas consumption for an italian town with 50000-80000 inhabitants in the 2010s). The total power input is about 2100 kW.

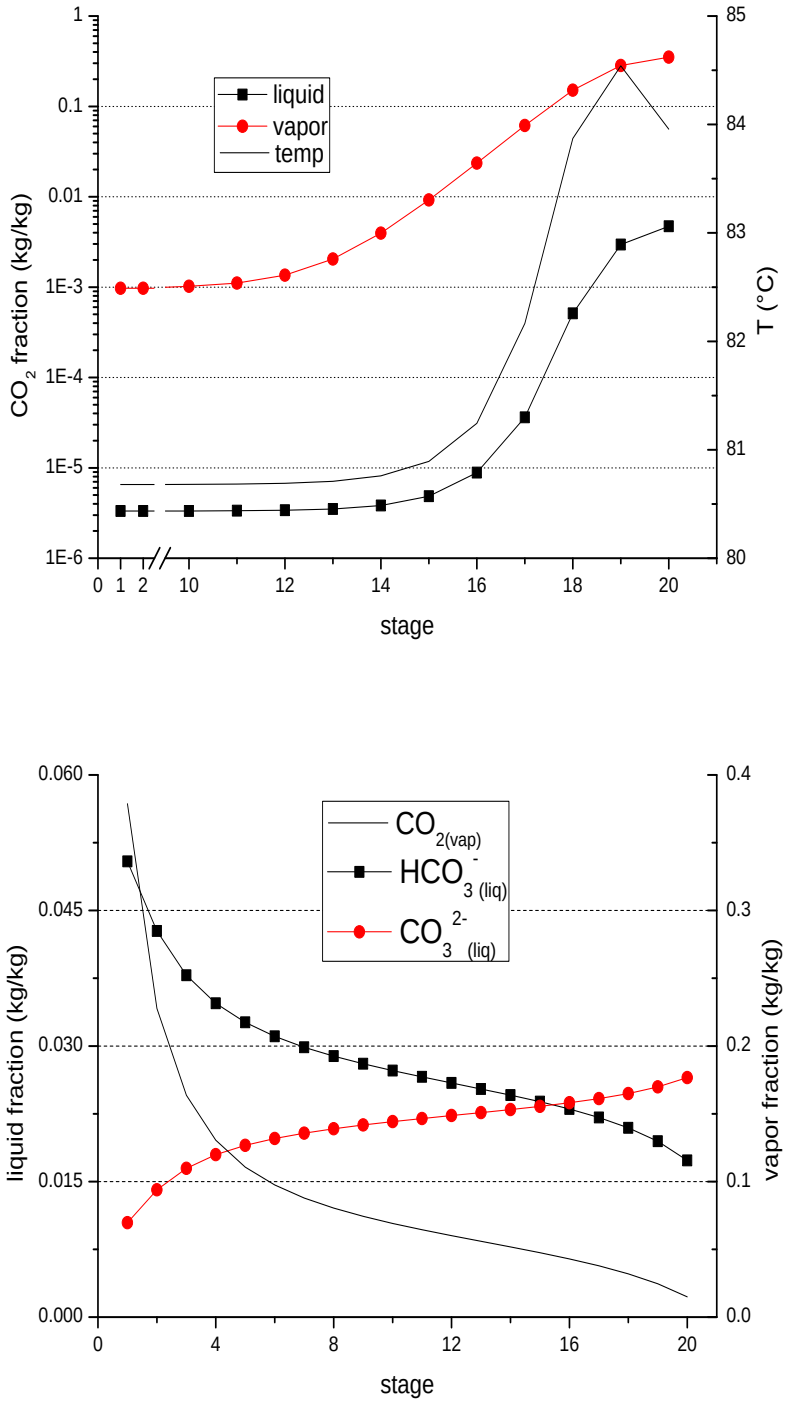

Figure 5.6: Absorber and stripper profiles.

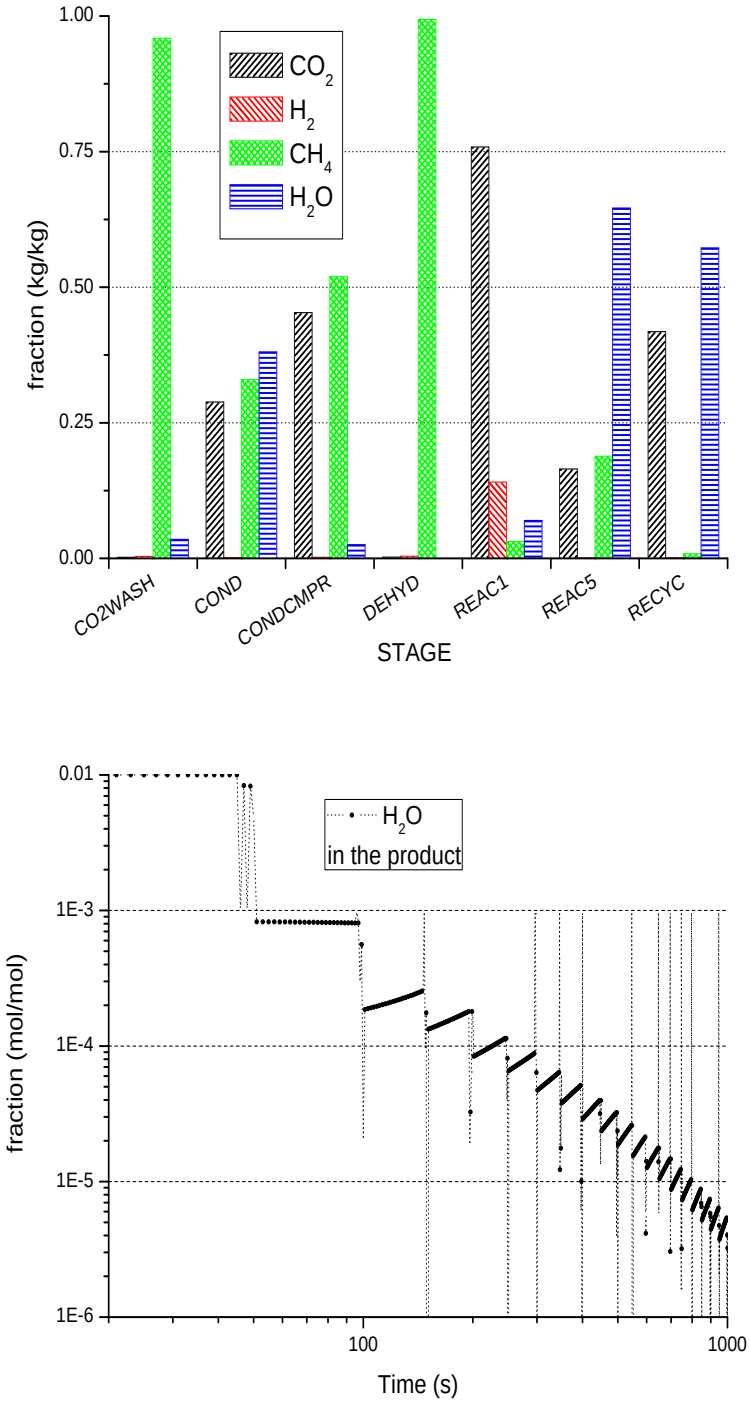

Figure 5.7: Overall mass balances and PSA purification first transient.

5.4 Energy Recovery

In this case, the strongly exothermic reaction and the feed preheating through the reactor jacket make necessary cold utilities only. The left panel of Figure 5.8 shows the possible cold curve corresponding to 8000 kg/h of LP steam (15 bar) being raised with the residual heat. This would result in a gross cold utility saving of about 6900 kW (left panel in Figure 5.8), while 2500 kW would still be available at temperatures high enough for co-generation purposes.

Though LP steam is not the preferred choice to generate electricity (at least when it has to be produced for that specific task, and is not available as waste-heat carrier), supposing to convert it at a 30% efficiency would yield 2300 kW of power with an equivalent neat C.U. saving.

Consider that the energy balances of the system have been calculated taking into account a possible plant extension, i.e. the conversion of gaseous methane into liquid gas. This option would made this case study applicable also for production plants very far from the re-gasification facilities and utilization places, as would be the case if the renewable hydrogen needed were produced at sites chosen according to different criteria.

The LG production simulated here follows the Conoco-Philips process flow diagram [186] (scheme reported in Figure 5.9). This concept is relatively easier to simulate because it employs a cascade of pure refrigerants (propylene, ethylene and methane itself [187]) readily described by the Nist-REFPROP thermodynamic package, instead of proprietary blends with often undisclosed phase diagrams. The main calculation outcomes are in graphs 5.10.

Since the gas enters the liquefaction still pressurized after a PSA, if it's expanded after its temperature has been already lowered then a further separation of the hydrogen still present is achieved, so the LG train is considered also as a final purification tool. The purged hydrogen-rich gas could be recycled to the reactor, or otherwise used as a fuel. This latter option looks somehow more appealing in the context of a power-demanding plant section, so a simple combined cycle [188] has been sketched and calculated (marked-up scheme 5.11). With the foreseen plant outputs, the electrical power available is estimated in 3800 kW.

This study considers the conversion of waste-CO_2 into methane of particular interest when renewable hydrogen is available. In this way, in fact, the difficulties in storage and transport that limit the use of hydrogen as a fuel are overcame, since a capillary network for the distribution of methane is already present worldwide. With this process, renewable hydrogen and/or energy can be effectively stored and made broadly available, with contemporary reuse of a greenhouse gas.

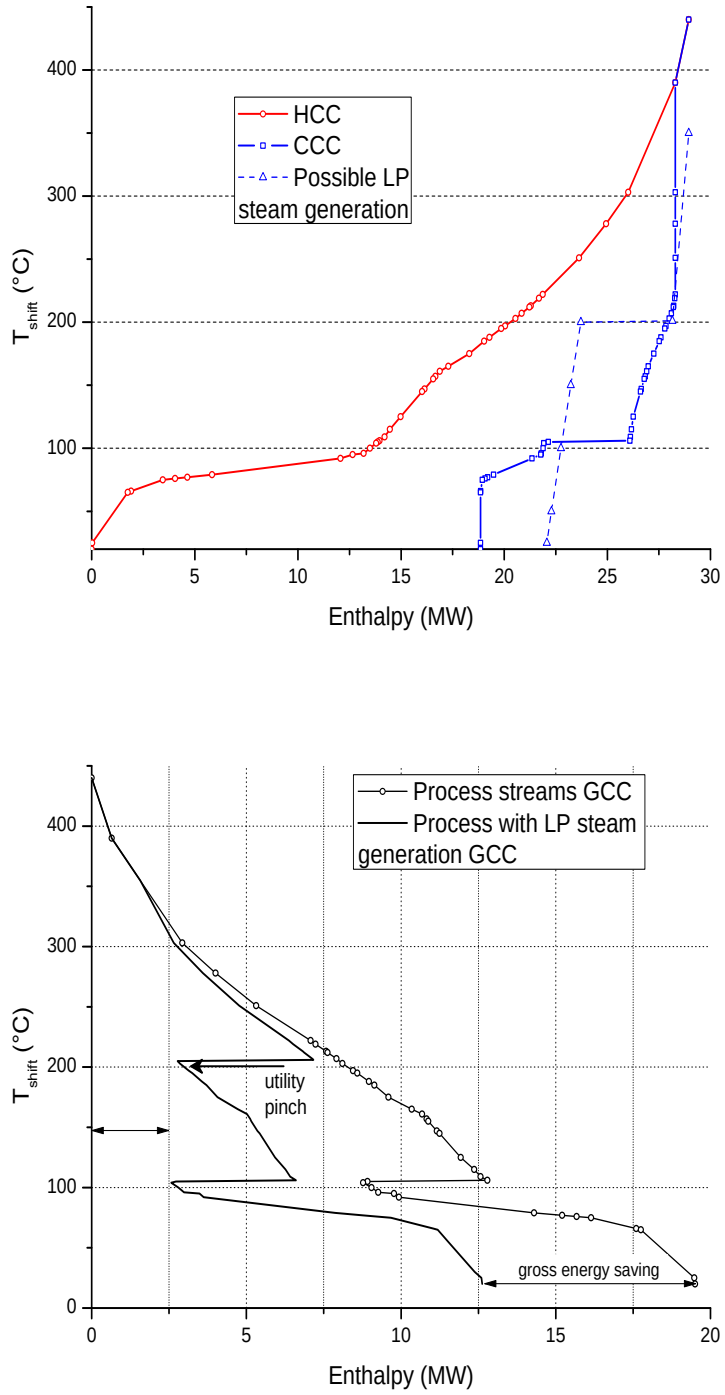

Figure 5.8: Composite Curves and Grand Composite Curve for the process, plus a possible steam-rising.

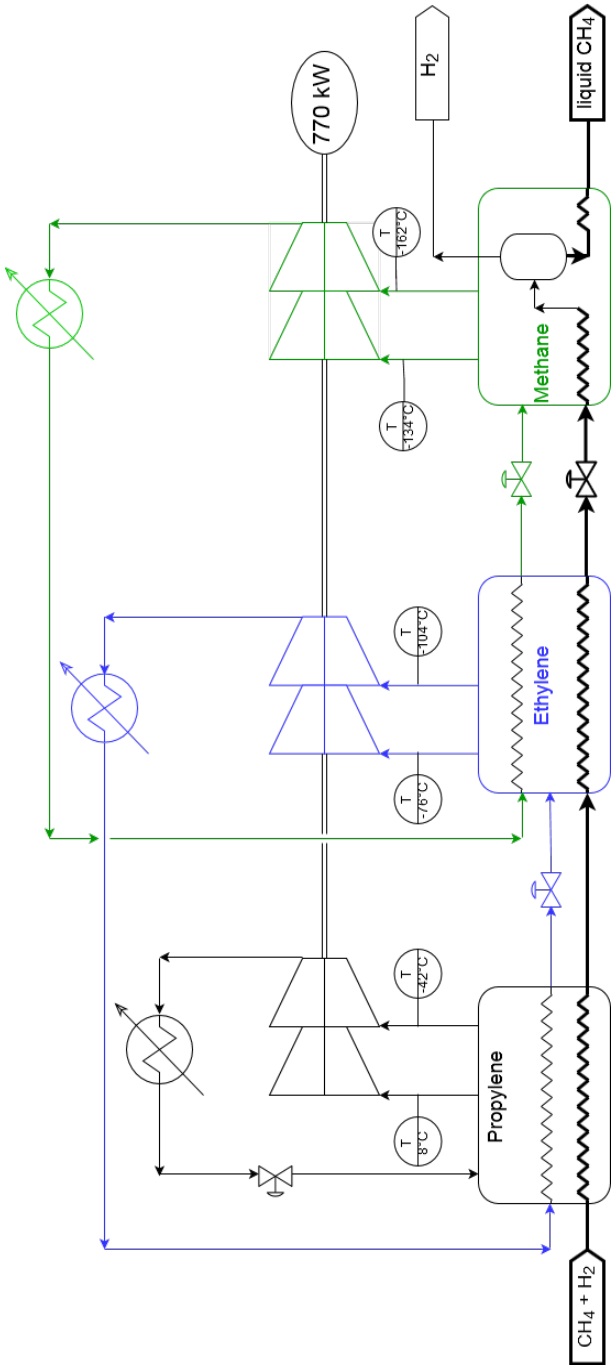

Figure 5.9: Simplified scheme of the Conoco-Philips LNG production process with the needed adaptations. Each section is actually a double-stage cycle (details not shown).

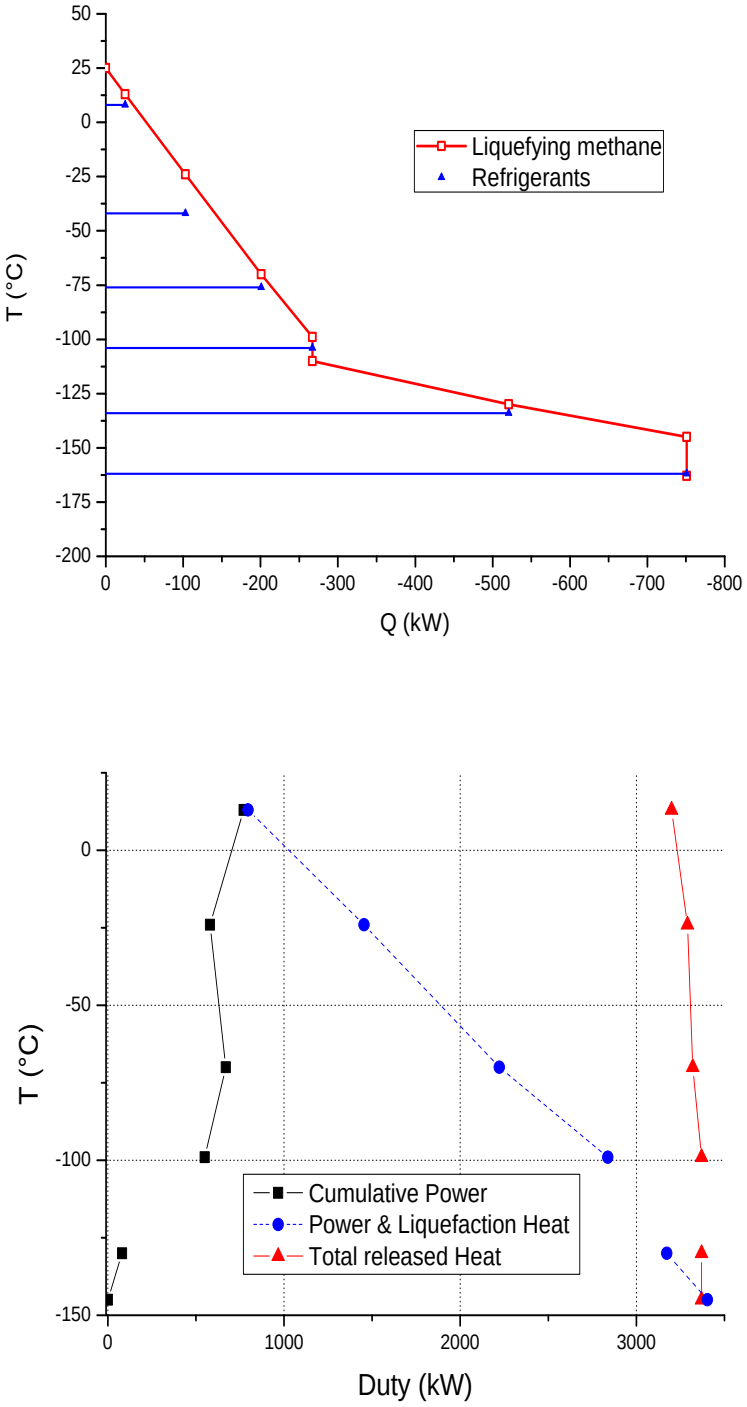

Figure 5.10: Thermal and power-consumption profiles for the liquefaction of Fig. 5.9.

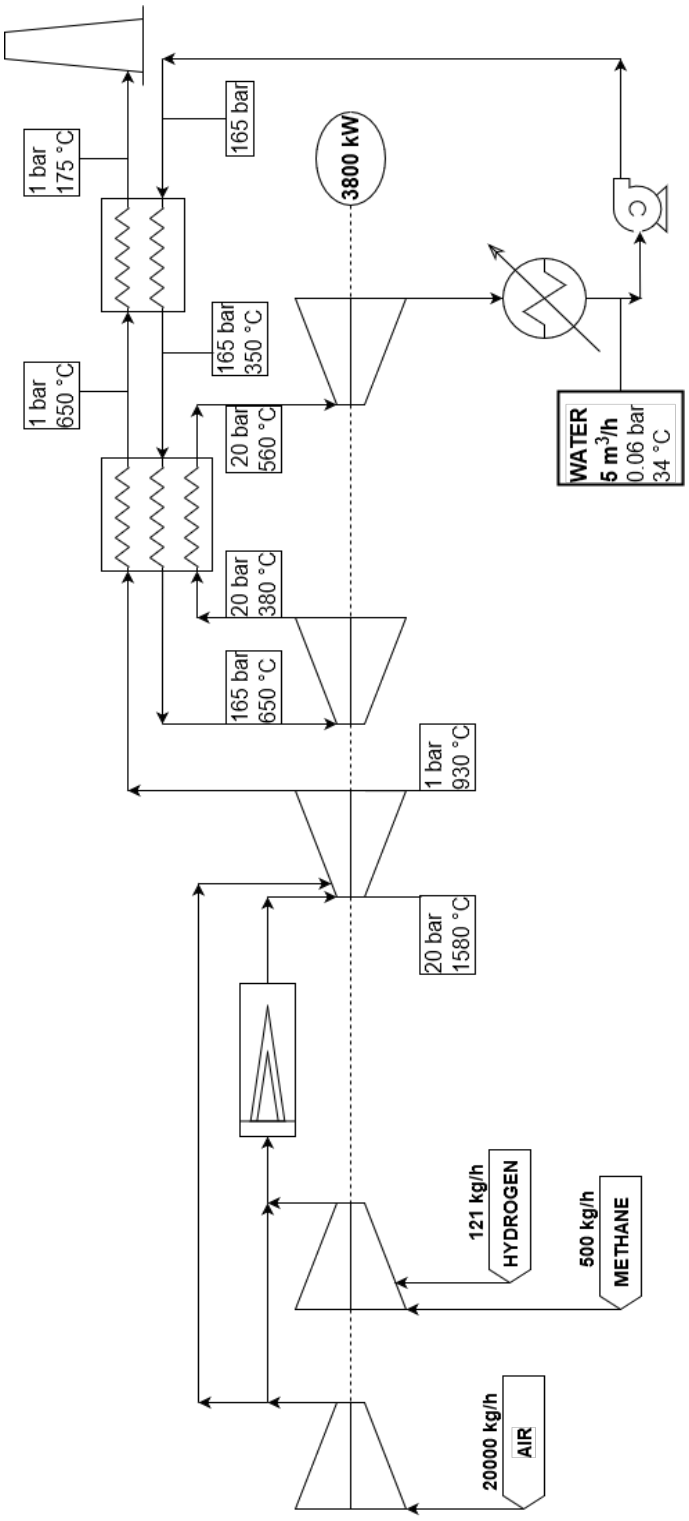

Figure 5.11: Calculation scheme of a combined cycle based on the purged hydrogen and residual methane of the LNG train.

Chapter 6

Process Integration

The processes as described are in parallel, and are connected at their ends as they share the same feed material (ethanol) and one major byproduct (i.e. CO_2). It is observed that air is employed in the ammonia synthesis as a source of nitrogen, and in the ammoxidation reactor as a source of oxygen. There are several possibility to foresee an integration between ethanol reforming and the production of N-containing molecules:

- an air-separation unit could supply pure nitrogen to produce ammonia, and pure oxygen to produce acetonitrile: this option is not considered, for now, because in the acetonitrile reactor nitrogen helps to control the temperature, and its elimination implies the injection of another quencher and the reworking of the whole section;
- all the air is fed to the acetonitrile process, then the nitrogen exiting from the first separator is routed to the ammonia synthesis: the gas has to be purified, and then can be mixed with the reformate downstream a pure-hydrogen production scheme (section 2.3) or downstream the methanator (scheme of section 3.3);
- without adding purification blocks, the nitrogen from the acetonitrile process can be fed into the ammonia plant just upstream the shift reactor, after a simple burner (that substitutes the secondary reformer) has eliminated the residues of ethylene and hydrogen cyanide - this option is the one presently considered.

6.1 Material Balance

The scheme in Figure 6.1 reports the above mentioned integration referred to the balances of a 1000 kg/h acetonitrile production: this scale needs 1330 kg/h of ammonia and gives back 6300 kg/h of nitrogen. Considering then a shift stage, a CO_2-scrubbing section (fresh MDEA in water: 32% by weight, MDEA:CO_2 loading of 2.3 mol/mol) and an equilibrium methanator, one has to consider roughly 9000 kg/h of reformate (with the same composition of scheme 2.3 upstream the water-gas shift) to have a N:H ratio of 1:2 (1:2.4 before the methanator), still viable for most ammonia catalysts.

This figure sets a lower threshold for the reformate flow, because the ammonia produced is already thrice the needed acetonitrile feed.

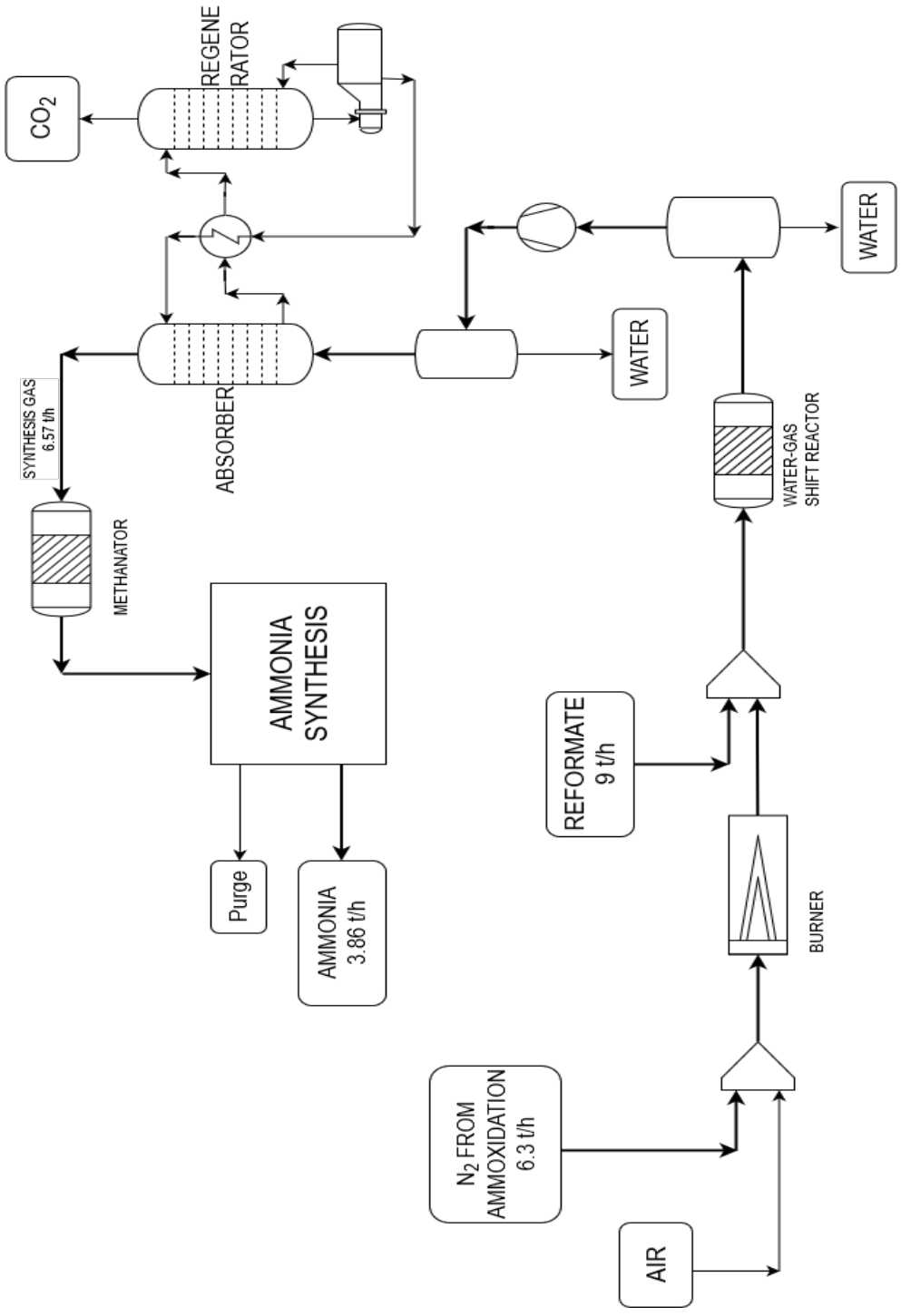

Figure 6.1: Simple scheme showing how impure nitrogen can be routed in the post-reforming section of an ammonia process: the last water discharge is omitted.

Part II

Behavior of Mixtures of Water and Acetonitrile in Presence of Ammonium Bicarbonate

Chapter 7

Phenomenology

As already mentioned (chapter 4), the direct production of acetonitrile results in a product mixture where ammonia and water are the other most abundant species, and additional water is introduced in the foreseen washing block. Carbon Dioxide is already generated by the parasite combustion at a rate depending on the catalyst: then, further additions as quenching-gas and ammonia-capturing agent don't alter the qualitative composition of the system, but are an advantage from the sustainability perspective since the process can convert a net amount of CO_2.

On the other hand, the water-ammonia-carbon dioxide mixture has been studied, both experimentally and theoretically [189], as a carbon-trapping system [156]. When a solid phase appears, ammonium bicarbonate is more abundant than carbamates in a selected pH range [148]. This salt is not soluble in alcohols. Its solubility in nitriles has hardly been considered, though the quaternary mixture obtained by adding acetonitrile to ammonium bicarbonate aqueous solutions is commonly employed in several HPLC and protein-treatment protocols [190–194]: in these cases, however, the salt is kept well within the solubility limit and additional compounds are present in similar (or higher) concentration

In the framework of the devised ammoxidation process, the solubility of ammonium bicarbonate in presence of acetonitrile must be considered to foresee the behavior of the precipitation and the drying blocks (also the moisture content of the solid phase depends on its affinity to the solvent).

Acetonitrile behaves as an anti-solvent towards ammonium bicarbonate, much in the same way as ethanol. When mixing the pure salt with pure acetonitrile in any proportion, the solid is always detected as a separate body. When pure acetonitrile is dropped on the salt (placed upon a filter), there's no appreciable weight loss of the powder to be attributed to its solvation in the liquor.

When water is present, the behavior of the mixture changes in several ways. When the liquids are mixed first, and acetonitrile doesn't exceed the 30% by weight, the salt remains apparently soluble, but the measured ionic strength in the solution shows an appreciable increase when the acetonitrile weight (in the starting mother) is decreased to the 10%. It is noticed that salt concentrations higher than 0.5 mol/L require vigorous stirring and/or a due delay time before solid residues disappear. Liquids composed by more than 80% g/g of acetontrile, on the other hand, behaves as pure acetontrile. If the solid, the acetonitrile and then the water are mixed (in this order), the same behavior is observed.

If pure acetonitrile is added dropwise to a concentrated aqueous solution of ammonium bicarbonate, nothing is observed until further additions make a meniscus appear short below the liquid surface: in some cases, also solid salt particles are seen to form and precipitate, but not always.

If a concentrated solution of water and ammmonium bicarbonate is prepared beforehand and added drop-wise into a vial containing pure acetonitrile, nothing is again observed until a separate liquid droplet settles down at the vial bottom; solid residues are sometimes seen within the droplet. In these cases, however, the liquid body eventually disappears leaving solid residues in its place.

These observations lead to the qualitative conclusion that: mixing acetonitrile with water the solubility of ammonium bicarbonate is decreased, and acetonitrile itself is not fully miscible in ammonium bicarbonate aqueous solutions.

This is an important conclusion of this work. At first, it is a first hand evidence of a phase equilibrium that can find application in other fields and is not predicted, to the author's knowledge, by most thermodynamic models (see also [195], for a similar notice) or experimental solubility reviews. In the context of the newly designed acetonitrile production process, this phenomenon lead to a different approach to the resolution of the water/acetonitrile azeotrope, with consistent simplifications and relying only on already present species.

Chapter 8

Experiments

8.1 Initial survey

The first survey of the ternary mixture is an evaluation of the density change at low salt concentrations. First, the densities of pure liquids binary mixtures are evaluated filling calibrated flasks (to a volume of 10 ml or 25 ml) with weighted amounts of acetonitrile (Sigma Aldrich) and milliq water (see results in Figure 8.1). Weighted quantities of the mother liquids are then added to the powdered salt of ammonium bicarbonate (Carlo Erba) in 10 ml vials; 4 to 10 samples (0.25 ml each) are extracted from the vials and the total weight loss after each sampling is recorded and interpolated linearly (minimum square residuals) to yield the ratio $\rho = \frac{\Delta m}{\Delta V}$.

In this way it is found that, within the uncertainty, the density of under-saturated solutions does not depart from that of pure liquids with the same water:acetonitrile ratio (Figure 8.2). Note that liquid mothers with more than 0.8 g/g of acetonitrile behaves, on the other hand, as anti-solvents, while at salt weight fractions not above 5% the solvent exhibits a single phase. Extrapolating this behavior, it can be assumed at first instance that the upper phases observed have a higher acetonitrile content than the lower ones.

The second set of preliminary trials regards the mutual proportions of pure components that lead to the coexistence of different phases. To this aim, the pure species are weighted and mixed into 10 ml vials belonging to 4 different batches: **a)** a group placed in an ice bath, **b)** a group immersed in a thermostatic bath at 25 °C, **c)** one series prepared at room temperature during the winter (20 °C, afternoon) or **d)** the summer (27-29 °C, early morning). The qualitative outcomes of these experiments are reported in Figures 8.3-8.4. Unfortunately, in several samples belonging the 0°-series the solvent has turned to ice just above and within the solid salt phase (grayed-out points).

Already on this ground it is possible to estimate that the minimum salt content to get acetonitrile to salt-out is no less than 5% g/g, with water fractions between 0.2 and 0.7 g/g ca. Higher temperatures do not only limit the solid-phase region, but favor also the liquid-liquid split, because it is the ionic strength to act as driving force for the separation.

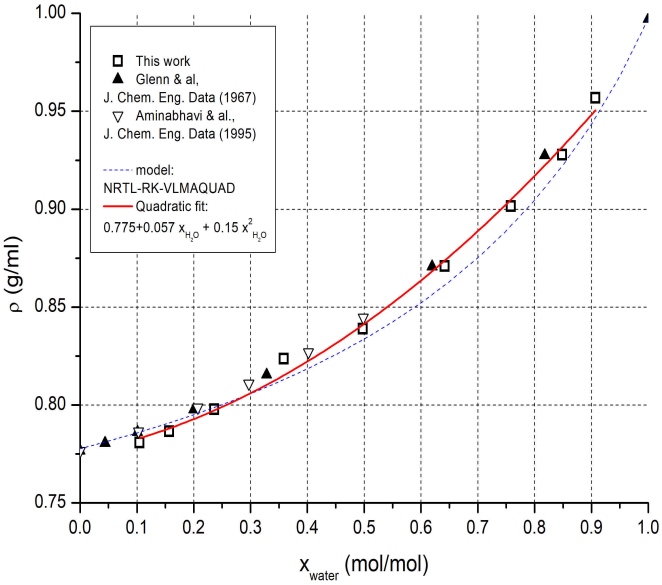

Figure 8.1: Density of water-acetonitrile mixtures at 20 °C

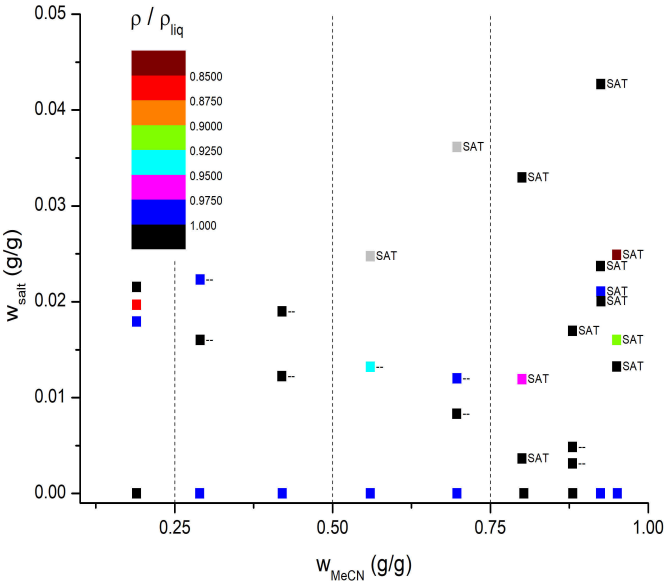

Figure 8.2: Map of the density deviation of water-acetonitrile-salt mixtures (at 20 °C) from the solvent - grayed out squares stand for discarded tests.

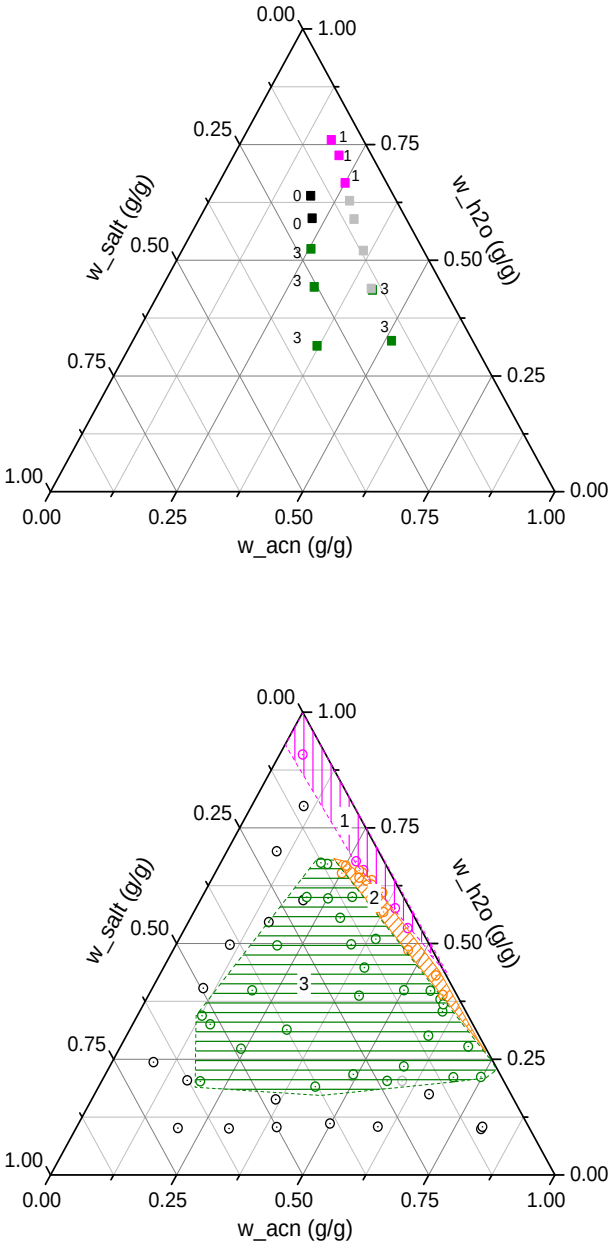

Figure 8.3: Ternary Maps for the preliminary survey of the phase diagram at 0-22 °C. Codes: **(0)** Solid-Liquid: **(1)** Liquid Only: **(2)** Liquid-Liquid: **(3)** Solid-Liquid-Liquid.

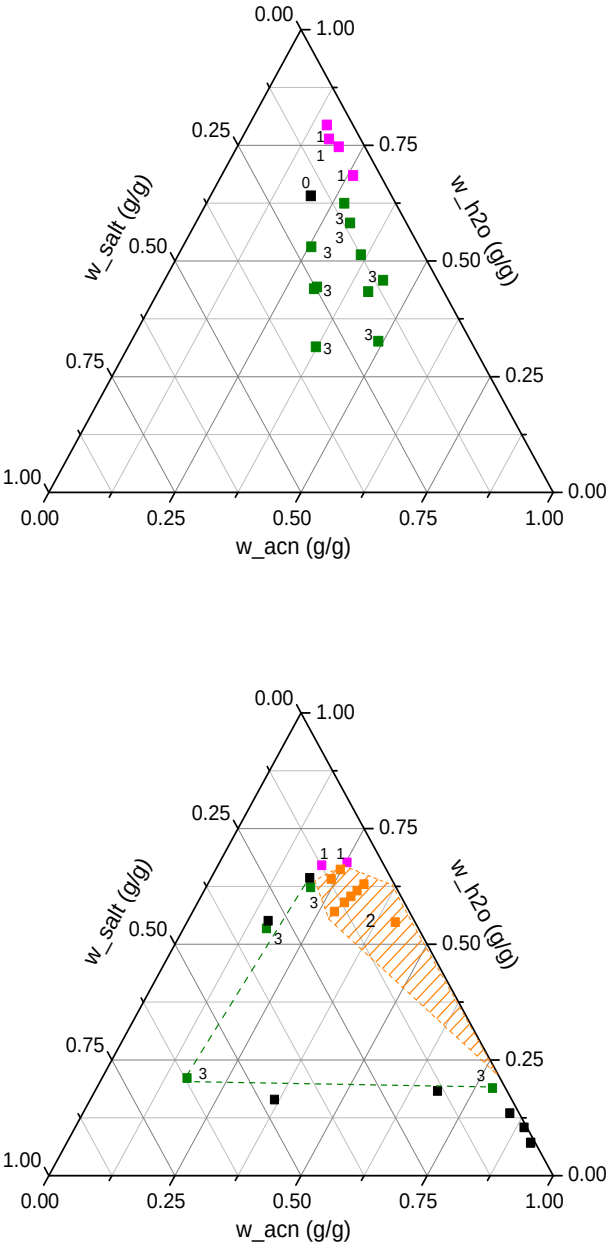

Figure 8.4: Ternary Maps for the preliminary survey of the phase diagram at 25 and up to 30 °C. At higher temperatures the salt solubility increases, and so the LL region at the expenses of SLL zone. Codes as in Figure 8.3.

8.2 Phase splitting

As more systematic tests are planned, the different phases resulting after each mixing (when present) are analyzed quantitatively. An operative procedure has been outlined as follows.

1: some salt is weighted in a vial[1], then acetonitrile, finally water; the vial is screwed and shaken.

2: some samples are placed in fridge or immersed in a thermostatic bath, while other are kept at room temperature (which is anyway registered), then after some time (minutes or hours, depending on the permanence of solid residues and the onset of the liquid-liquid separation) the height of the different liquid levels is measured with a ruler.

3: the vial is opened and fixed volumes of the upper phase are extracted with a micropipette: the samplings are divided into two or three aliquotes for further analysis, while weighting the vial after every sampling the density can be calculated; sometimes a 1-2 mm layer of the upper phase is left in place, in order to prevent evaporation losses from the bottoms at temperatures above 25 °C.

4: the procedure is repeated for the bottom phase, plunging the tip below the light liquid residue (if any), then also the layer is removed. It can be noticed that, at this point, the surface tension creates distortions in the meniscus shape. For samples at 4 °C or above room temperature, the vial is opened after being immersed in a glass flask full of water at the same temperature. An upward drift of the weightings is anyway observed for samples starting at 35-40 °C, due to the unavoidable cooldown.

5: in some cases, the vial workup is concluded with the solid filtration and recording of its weight loss over some days.

Analysis for the light liquids

a: backtritration of ammonium ions, to quantify the salt present in the upper phase;

b: basic hydrolysis followed by backtritration of the formed acetic acid, to have a first estimate of the acetonitrile content;

c: evaporation of a small quantity in a thermo-gravimetry machine and/or in a differential-scanning one;

d: nuclear magnetic resonance to quantify with higher precision the $-CH_3$ groups bore by acetonitrile.

The ammonium backtritrations have been performed on a dozen of samples and then suspended, as they've been yielding a concentrations always lower than the detection limit (0.05 mmol with the adopted protocol - see paragraph 9.1).

The basic hydrolysis work-up has not been performed on every sample because it requires long times and has a low sensitivity: it has been replaced by NMR analysis whenever possible; still several samples have been tested with both methods in order clarify the receipt reliability and to perform cross-checks.

[1] Plastic vials let the phase-phase meniscus be clearly visible, while glass or pirex containers somehow blur it; acrilic cuvettes absorb acetonitrile, soften and leaks within hours.

Analysis for the heavy liquids

e: ammonium and bicarbonate backtritration;

f: thermo-gravimetric or differental scanning calorimetric analysis;

g: proton magnetic resonance, after having devised a treatment procedure slightly different than those employed to prepare the light liquids (chapter 9.3).

The details on these analysis are reported in sections 9, while a general graphical account is given just below (Figure 8.6 and 8.7). Whenever possible, the acetonitrile content in both liquid has been evaluated independently, save for some points that belong actually to duplicated trials and whose consistency has been checked using the lever rule.

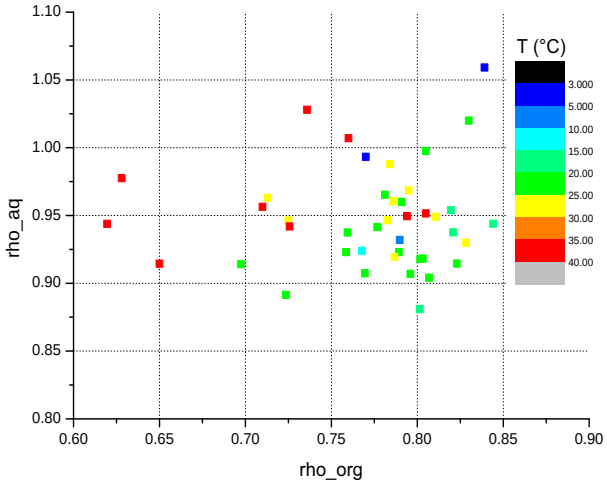

Figure 8.5: Density of the upper ('org') and lower ('aq') liquids, resulting from the linear interpolation of the weights of 4 to 10 samplings (0.100 - 0.250 ml each).

The lighter liquid simply contains more acetonitrile than the lower one, because their densities are not modified by the salt (that is never found in the upper phase). It can be noticed that under-saturated aqueous phases (with less than 0.1 g/g of salt) are in equilibrium with light liquids containing 0.65 - 0.70 g/g of acetonitrile (0.75 at most), while when the saturation limit is crossed then the acetonitrile weight fraction is never less than 0.80: some analysis yields values up to 0.85 for very high initial ionic strengths. It is worthwhile remembering that, at atmospheric pressure, the acetonitrile-water azeotrope composition is 0.82 g/g [147, 149].

After getting a general idea of the phase diagram, the critical points have been searched with dedicate trials. The first series of samples is prepared following the approach of Nagosa [196], adding little amounts of acetonitrile to under-saturated aqueous solutions of ammonium bicarbonate and checking the appearance of the phase-split. This procedure can introduce an error by excess (due to the micropipette tips lower capacity and the short resting time between two consecutive additions), yet its results (Figure 8.8) are fully coeherent (and overally more precise) with the above described tests.

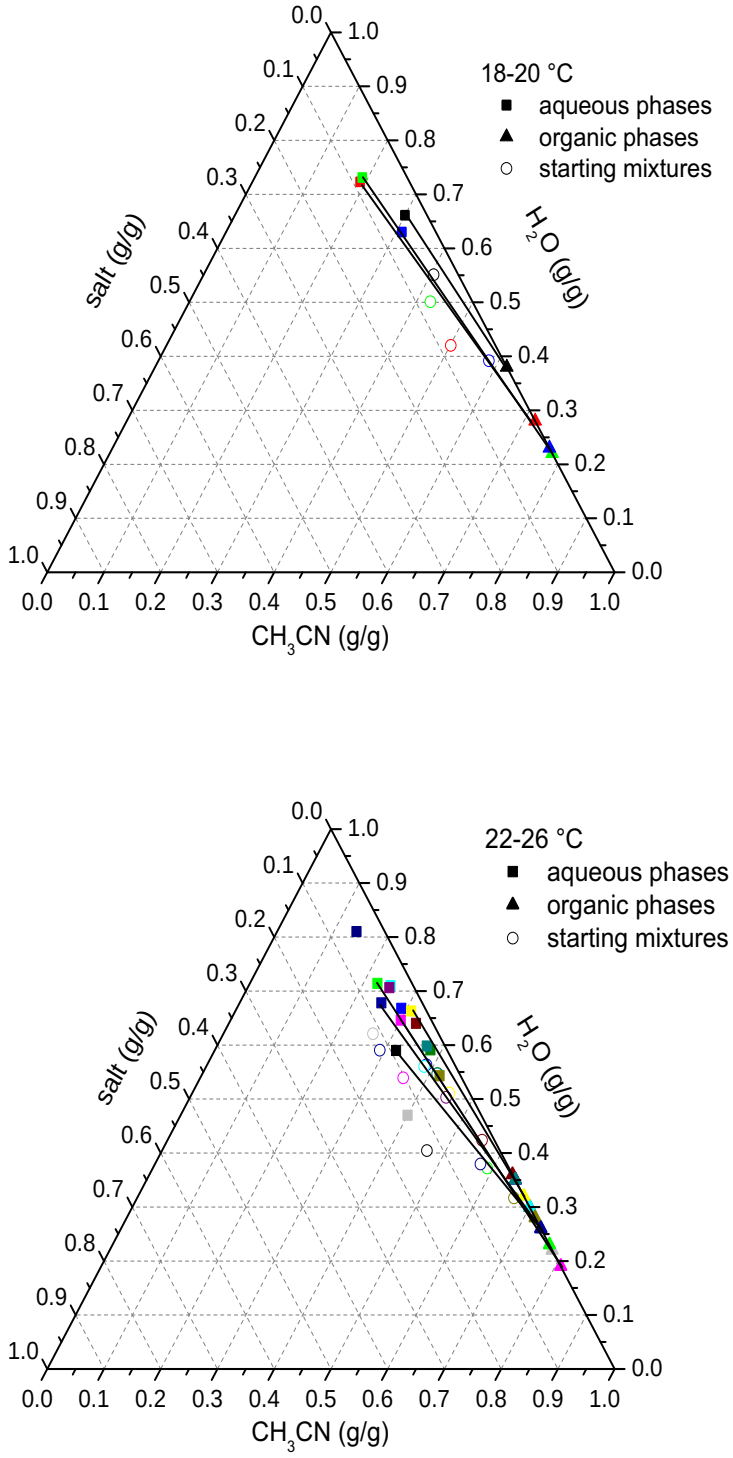

Figure 8.6: Ternary Maps for the liquid phases resulting when a mixture is in the conditions to split (region 2-3 of the charts above), below 30 °C.

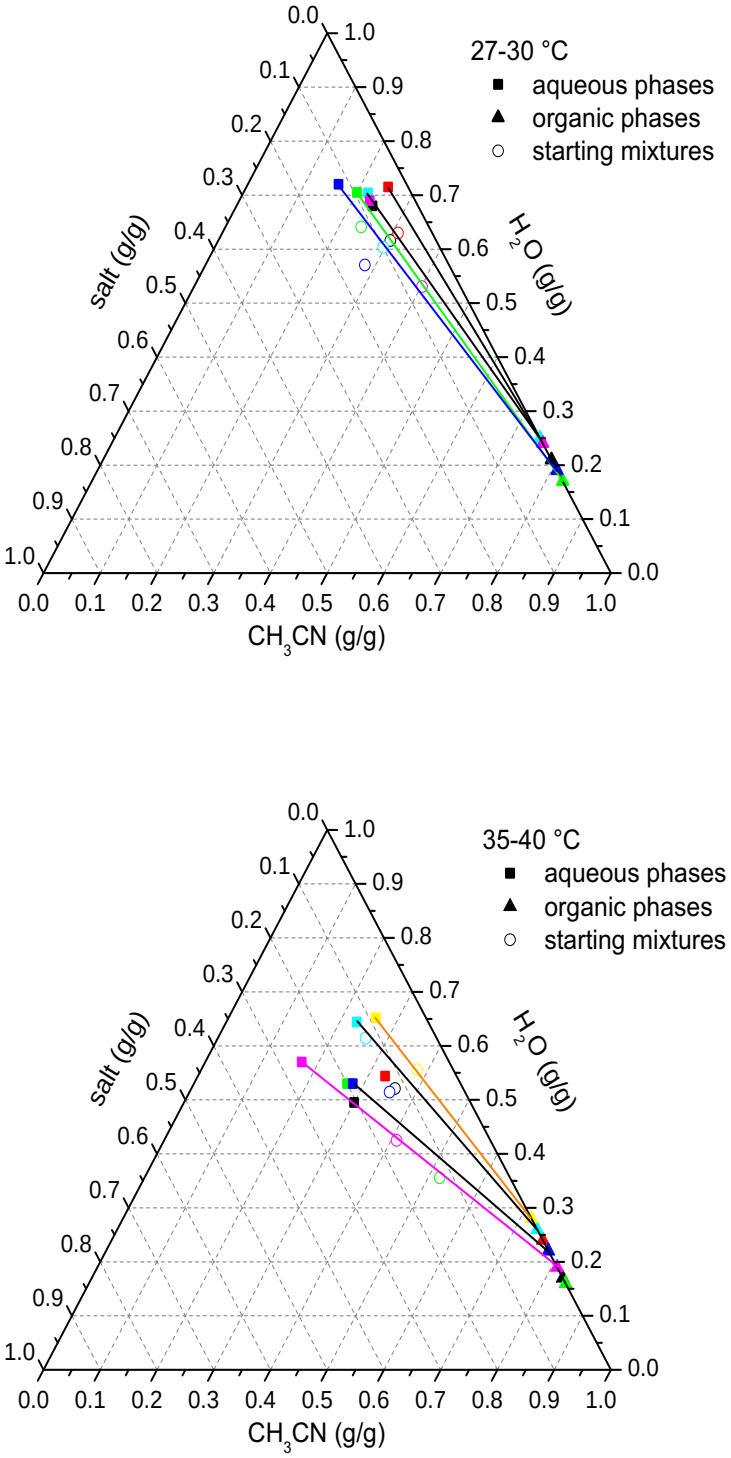

Figure 8.7: Ternary Maps above 30 °C. At higher temperatures the salt solubility increases, and so the driving force of the separation.

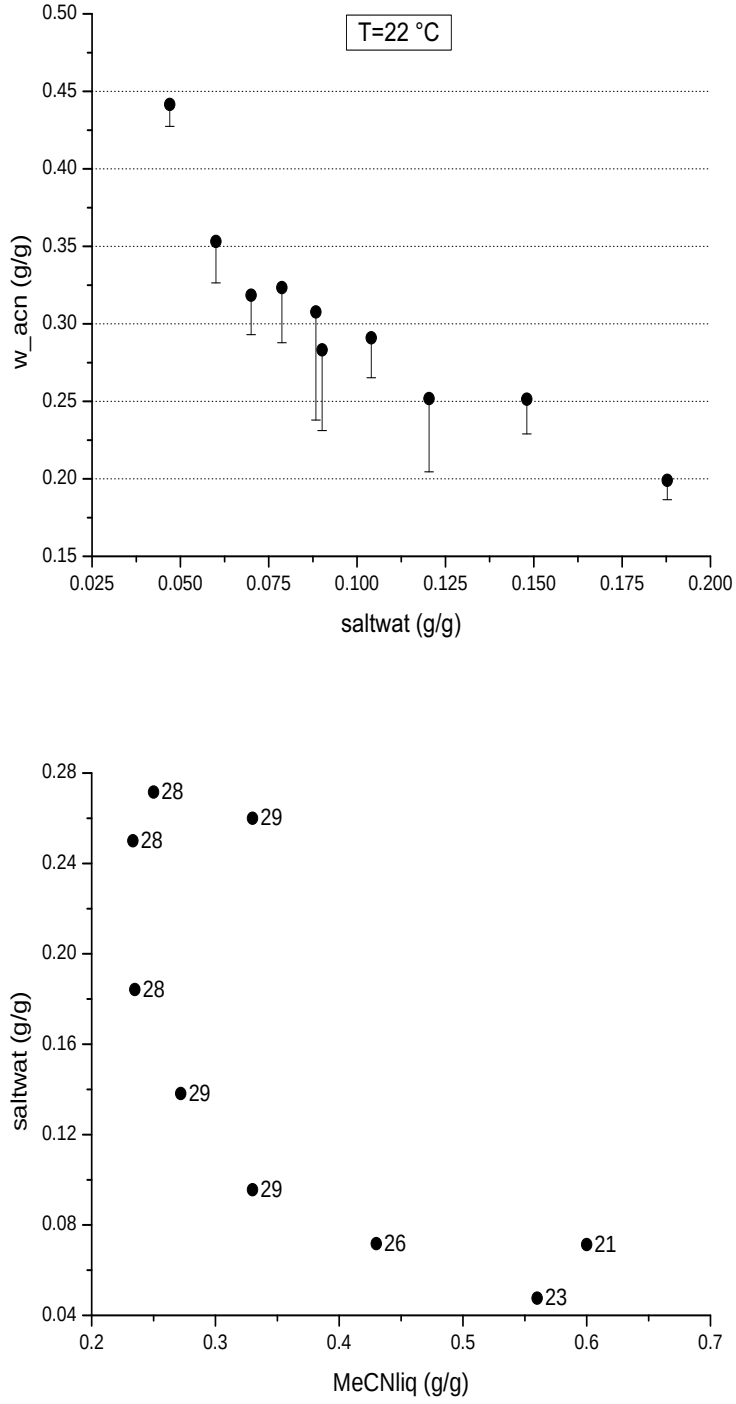

Figure 8.8: **Up:** upper threshold for the solubility of acetonitrile (weight fraction on the total) in aqueous solutions of ammonium bicarbonate at room temperature, as a function of the salt concentration in the initial binary mixture. **Bottom:** salt concentrations (with respect to water) needed to make a given water-acetonitrile mixture split (the numbers indicate the temperature).

Another set of similar trials has been made adding aliquotes of salt to liquid mixtures of water and acetonitrile (Figure 8.8), and the measured trends are coherent with what expected from the more qualitative trials (except for one outliers in the salt vs acetonitrile bottom graph). Making also the quantity of water explicit, it is obtained the diagram 8.9: the points represent with a fair approximation the critical curve.

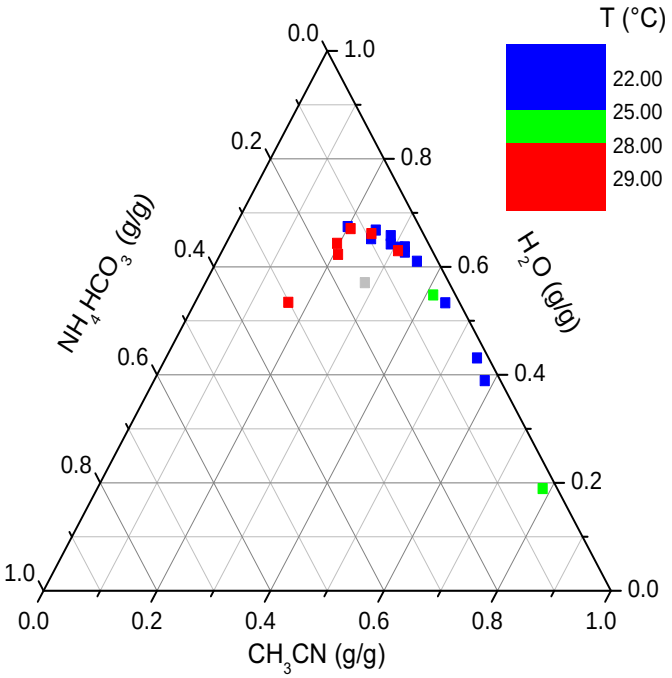

Figure 8.9: Composition of the samples achieving a split condition; that practically represents the position of the resulting aqueous (or total) phases.

8.3 Salt solubility and conductivity

The salt solubility in the mixed water-acetonitrile solvent is studied as follows: known quantities of the liquids are mixed into calibrated flasks, then the pure salt is weighted in a vial and the solvent is added, the vial is screwed and sealed and stored in fridge overnight. The next day, a sample is extracted from the vial (after checking the presence of a solid body) and backtritrated, then the vial is placed in a thermal bath at room temperature. After thermalization, the vial is stirred and replaced in the bath for another hour, then the sampling is repeated. If there is solid salt still governing the equilibrium, the temperature in the bath is raised step-wise. The procedure stops when the salt is entirely solubilized - in some cases the sample has been lost due to overpressure in the vial at temperatures higher than 60 °C. Figure 8.10 represents synthetically the outcome of these experiments, heuristically interpolated by the formula:

$$ln\left[\frac{x^2}{(mol/mol)^2}\right] = a + b \times \frac{m_{C_2H_3N}(g)}{m_{solv}(g)} - \frac{H}{T\,(K)} \tag{8.1}$$

Parameter		Value		Error
a		5.325		2.278
H		3534		681.9
b		-4.335		1.021
Anova:	DF	Σres^2	$\Sigma res^2 \,/\, DF$	F Value
Model	2	16.69	8.347	23.47
Error	34	12.09	0.3556	
Total	36	28.78		

Table 8.1: Fit for the parameters for eq. 8.1.

where the fraction x refers to the moles of ammonium and bicarbonate in the solution, that are equal to the moles of solubilized salt because in these experiments the C:N ratio is fixed to 1 mol/mol. The typical density of these systems is 0.96-0.97 g/ml.

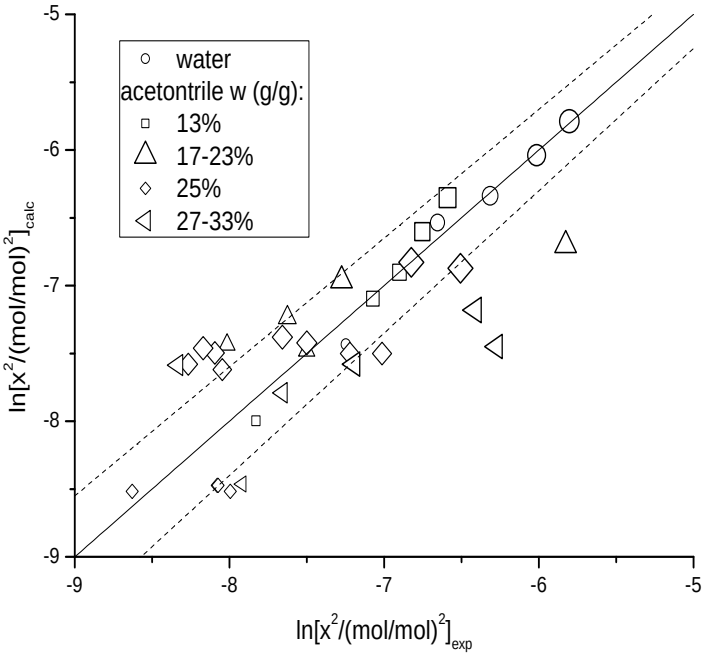

Figure 8.10: Calculated vs experimental ammonium bicarbonate solubility in water-acetonitrile mixtures (the markers' size is proportional to the samples' temperature).

A further trial has consisted in an evaluation of the salt conductivity in the water-acetonitrile mixed solvent. A saturated solution of salt in two different water-acetonitrile mixtures has been repeatedly sampled and diluted with a mother liquor of the same composition, then the saline mother has been backtritrated to fix the reference concentration.

The whole procedure has been carried out at room temperature by volumetric method (but with a density calibration of the liquors), and the dilutions have been performed directly into 10 ml vials that fit the pH and conductimeter electrodes used. The conductimeter response range has been manually rescaled when needed.

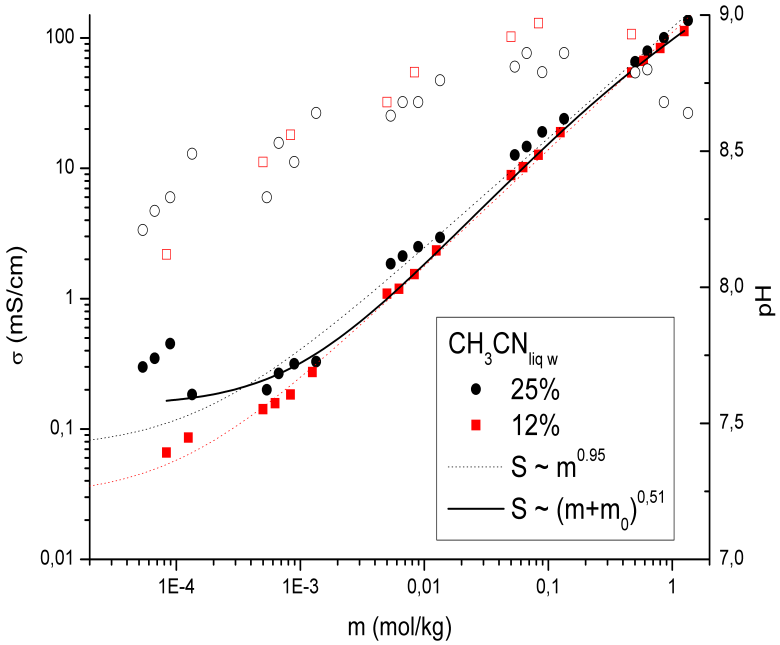

Figure 8.11: Measured conductivity (filled markers) and pH (empty markers) of ammonium bicarbonate in water-acetonitrile mixtures.

The measures are not so precise as to lead to an evaluation of the activity coefficient, nevertheless some features can be highlighted (graph 8.11):

a: changing the acetontrile content of the solvent does not affect the measure, but with just these data is not possible to say if it is sensitivity problem, or an actual interplay between different solvent-ion interactions;

b: the pH is 0.5-0.7 units higher than what expected (see also calibration in Fig. 9.1): this is a systematic error due either to acetonitrile's presence or to the fact of having calibrated the electrode at the pK of acetic acid, i.e. 4 pH units below;

c: the Kohlrausch's Law: $\Lambda = \Lambda_0 - a \times c^{0.5}$ applies only supposing to correct the concentration values as: $c' = c - c_{bias}$, which could be the result of a systematic error during the dilution operations (moreover, distilled instead of ultra-pure water has been used) - otherwise a linear trend seems recognizable.

8.4 Evaporation

The purification process outlined in the first part (chapter 4) takes advantage of the nearly-azeotropic composition of the light liquid, so several bench-scale vapor-liquid separations have been put in order to evaluate their actual outcome. In fact, there are at least two phenomena that should be considered:

- both the salt anion and cation are in equilibrium with volatile species, so any stripping or distillation procedure is meant to drive it out the mixture along with the vapors;
- both the light and the heavy liquid are composed of pure species with different boiling points, so increasing the temperature of the multi-phase mixture (or of one of the phases) at fixed pressure there's a neat loss of acetonitrile;

The evaporation tests are performed without any condensation or reflux of the evaporated phase, placing open vials inside a thermal bath and sampling the liquid at constant temperature - one final test is made with a larger quantity of liquid inside a round flask, heated up to the boiling point.

Figure 8.12 let assume that, when the mixture evaporates below the saturation point, the salt content decreases rapidly below the saturation value at any temperature: afterwards, higher temperatures increase the salt loss rate, but at low salt concentrations there are little NH_3 and CO_2 in equilibrium with the ions, and the process is very slow.

When the temperature rises up to the boiling point (Figure 8.13) the geseous species are effectively stripped. Considering the effect of these experiments on acetonitrile, its rate of evaporation looks even more sensitive on the increasing temperature, and when the mixture is heated to the boiling point it is eventually lost just like ammonium bicarbonate.

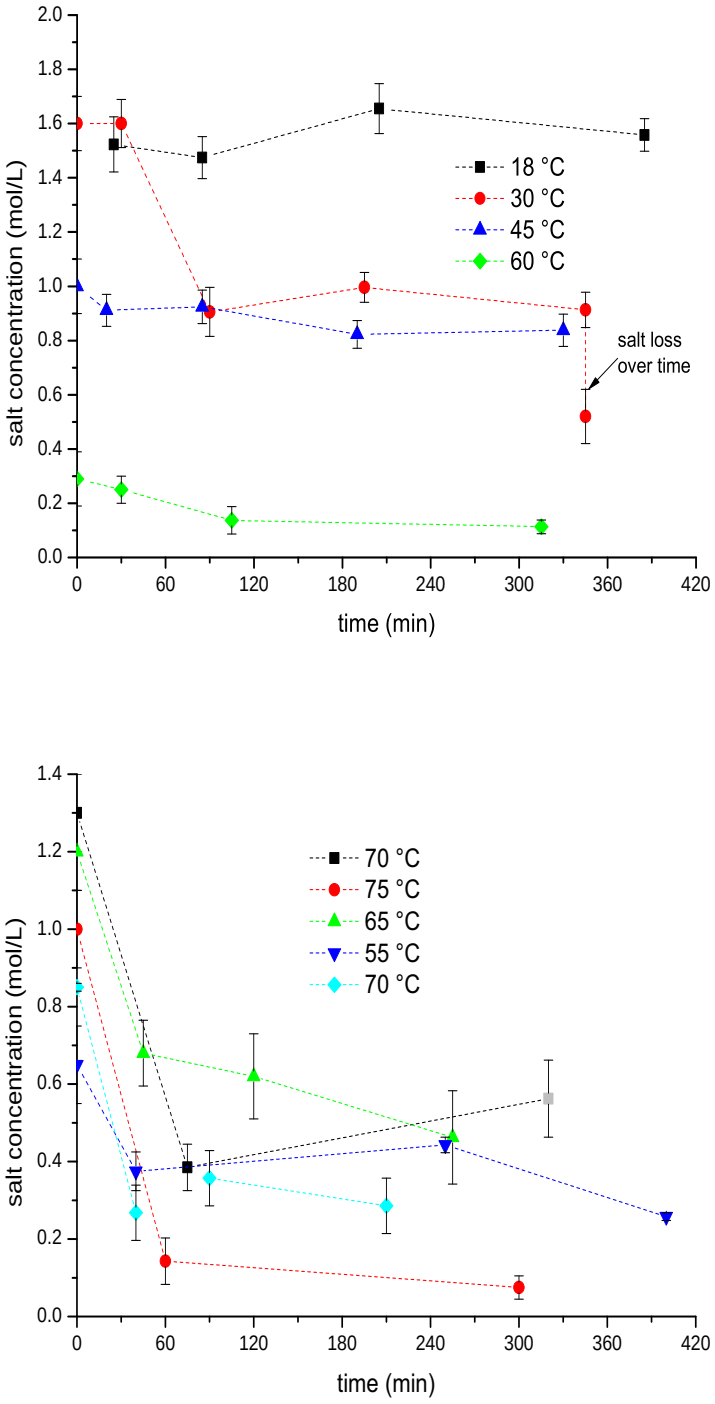

Figure 8.12: Salt concentration over time for samples evaporating at constant temperature (method: backtritration).

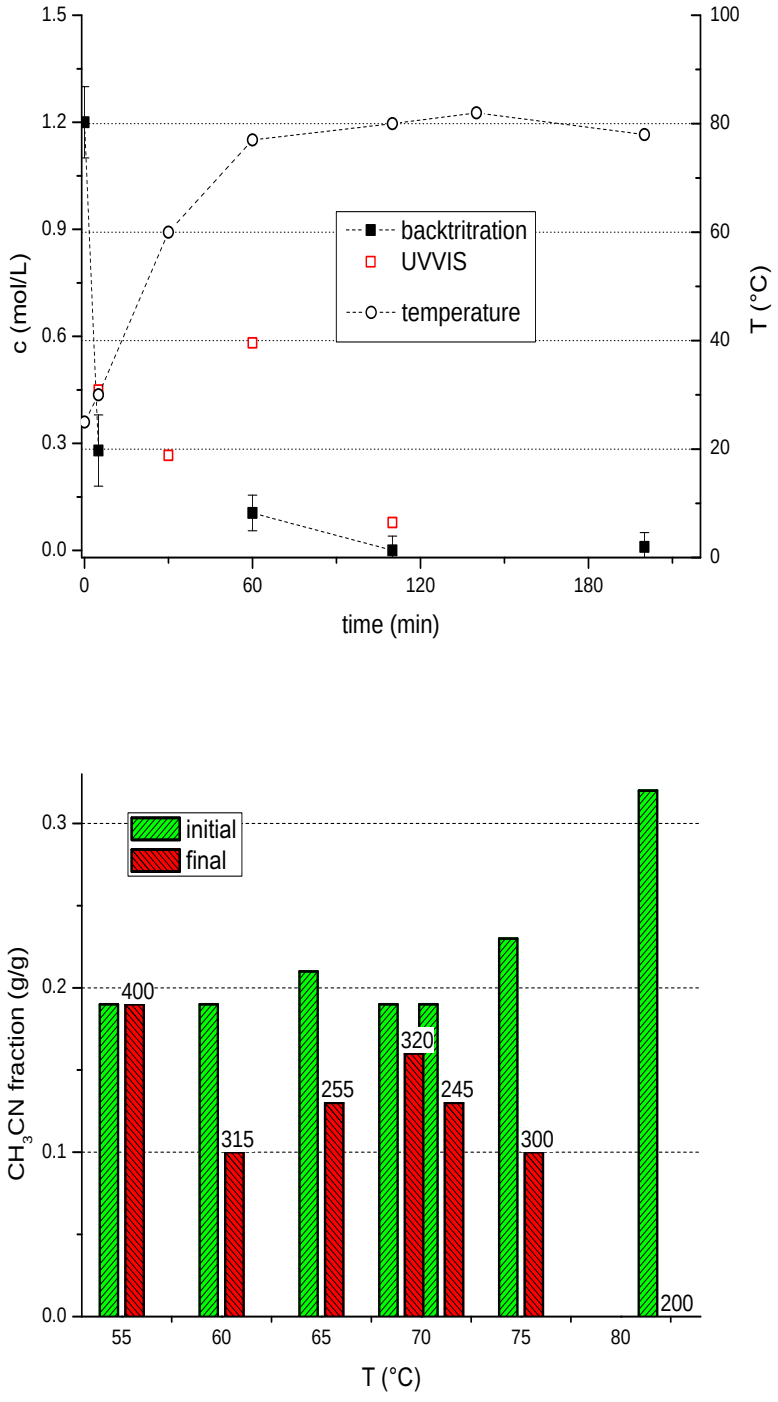

Figure 8.13: Left: salt concentration over time for a boiling sample (method: backtritration - UVVIS); right: acetonitrile mass fraction (on total) at the beginning and end of each experiment (minutes in labels, method: NMR-TGA).

8.5 Distillations

The batch distillations or re-boiling tests help to clarify the saturation temperatures that have to be reached and, moreover, how the acetonitrile and the NH_3-CO_2 couple influence the separation of each other from water. Some of the distilled liquids are not mixed using fresh acetonitrile, but are obtained reusing the solutions the phase-split tests.

Boiling Tests

These trials are made placing the liquid mixture into a 100 ml or 250 ml round flask with a vertical condenser and a thermometer plunging into the liquid. The flask is either heated directly with a thermo-mantle or indirectly with a heat plate and a water bath. When the mixture used has the composition typical of a heavy phase, then at saturation the little amount of ammonia present (in equilibrium with the ammonium) is evaporated, as eventually is carbon-dioxide following the shift in the acid-base condition. Nevertheless, as the vapors are also relatively rich in acetonitrile, the liquid formed in the condenser is a poor solvent for the re-absorbed ammonia and CO_2, which results in salt deposits in the lower section of the condenser.

The graphs (Figure 8.14-8.15) of the temperature as a function of time show that the liquid reaches a boiling point appreciably lower than that of pure water. The fraction of acetonitrile is roughly constant or slightly decreasing, as the simple vertical condenser might not be able to grant a total reflux. The tests n° 4 and 5 has been made with some ammonium bicarbonate present in the liquid: in these cases it has been observed that, once the liquid starts boiling, solid residues form in the lower part of the condenser. This fact could be explained thinking that:

- at first, the ammonium and carbonate are effectively stripped as NH_3 and CO_2;
- these gases are then partially absorbed within the liquid droplets in the condenser;
- as the vapors are rich in acetonitrile, the liquid film wetting the condenser is a poor solvent for ammonium bicarbonate, which then solidifies at the condenser's walls.

Part of the salt comes back into the boiling solution along with the reflux, and a smaller part is slowly decomposed and dispersed through the condenser: as shown in the last graph above (Figure 8.15), there is still some ammonium bicarbonate within the residues at the end of the tests (unlike in the trial at zero reflux described in section 8.4), while most of it is trapped in the condenser and is washed away cleaning the glassware

Batch Distillations

The batch distillations are performed with a round flask, a still and a horizontal condenser. The salt stripping and re-precipitation described above takes place all along the condenser, and influences the composition of the collected liquid, as some salt is dragged along with the distillate; eventually, the boiling of nearly pure water from the flask bottom dissolves the solid still present within the glassware.

The graphics in group 8.16-8.17 represent the outcome of the batch distillations of the organic (test 1) and aqueous (test 2) liquids resulting after a phase split. The starting mixture has been obtained recollecting all the vials used to explore the ternary map (paragraph 8.2). The temperature registered during the second test shows an upward

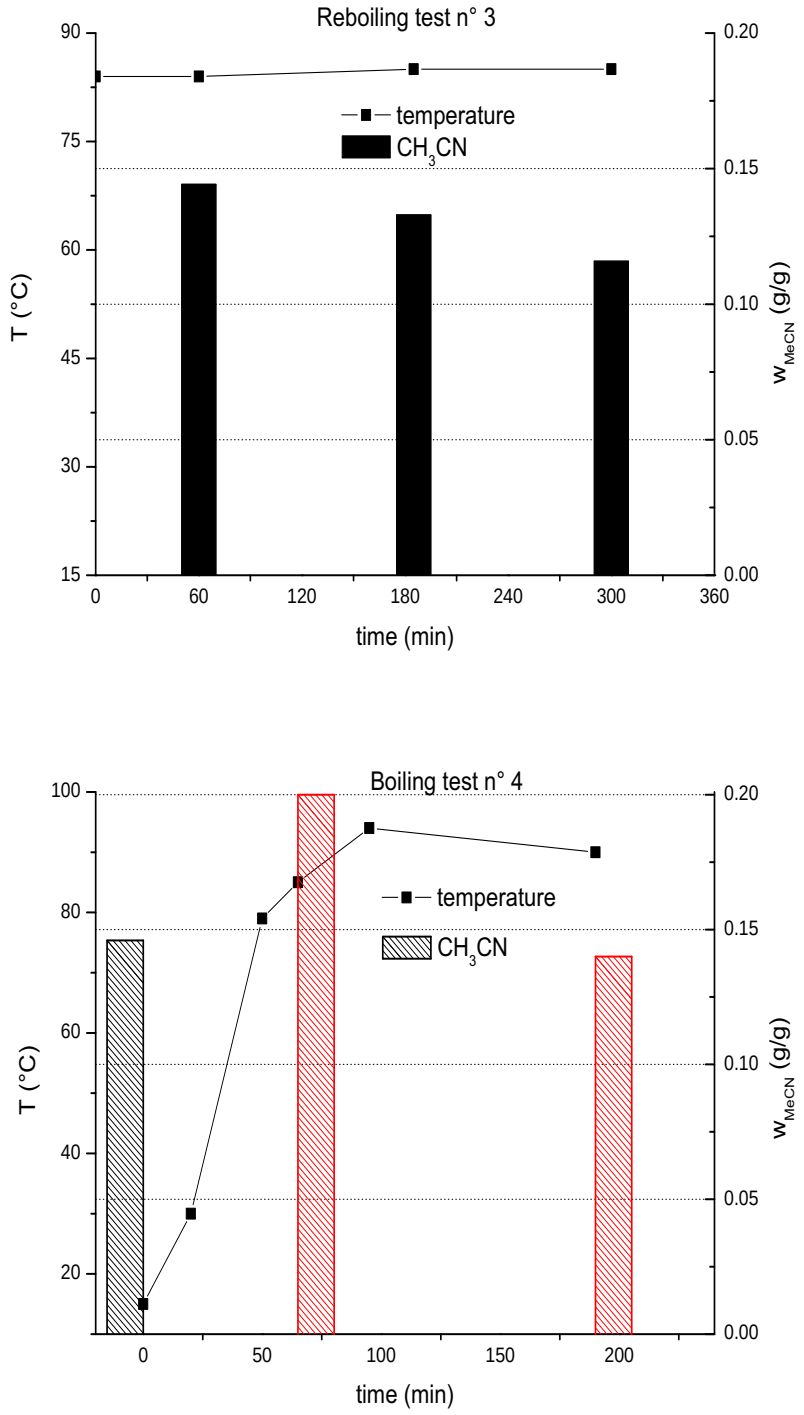

Figure 8.14: Steady states for water-acetonitrile mixtures boiling under total reflux (method); when ammonium bicarbonate is present, it is stripped and blocked in the condenser (method: backtritration).

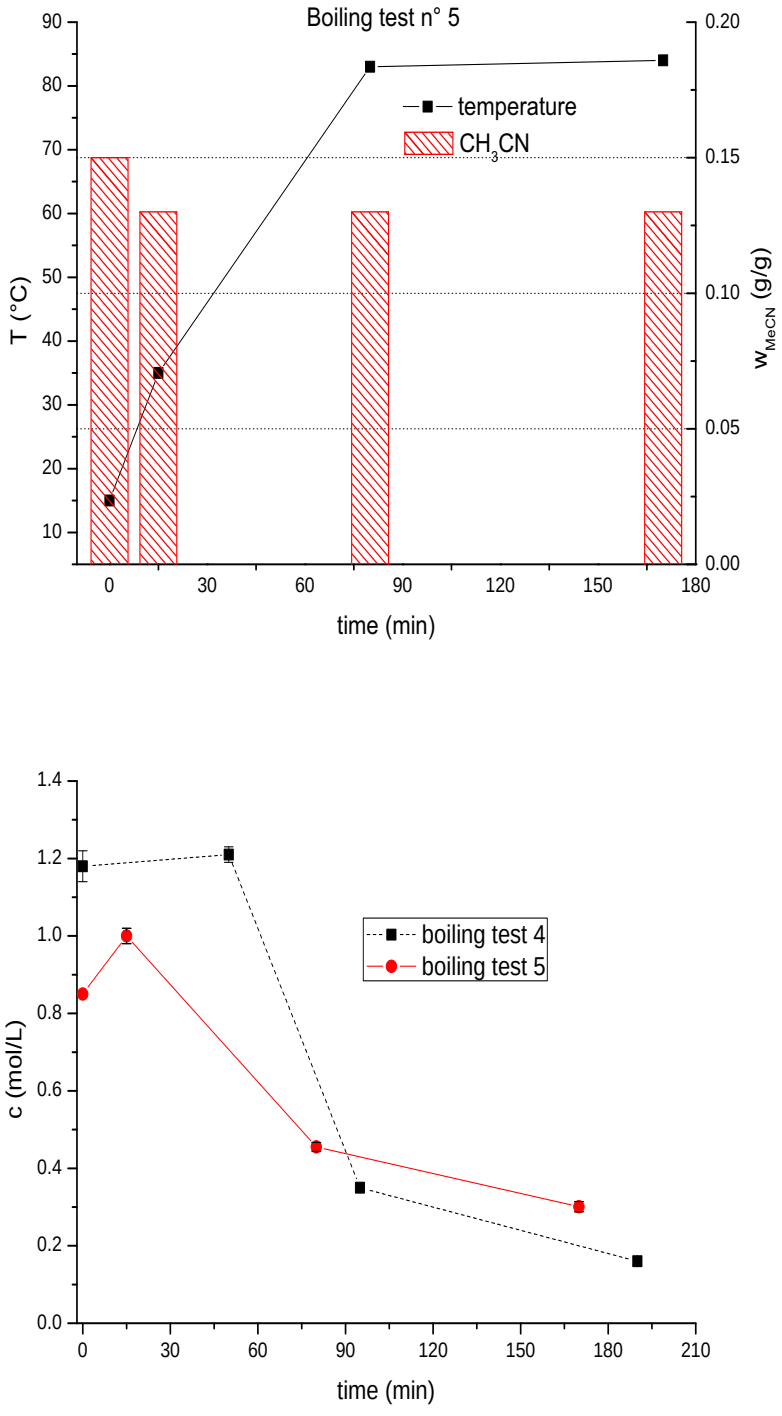

Figure 8.15: Steady states for water-acetonitrile mixtures boiling under total reflux (method: NMR for test 4, TGA for test 5).

drift when the liquid level drops below the thermometer bulb, because the radiative heat transfer from the surrounding thermo-mantle inner surface becomes appreciable: this effect has been avoided, in the first test, supplying the heat indirectly via immersion in boiling water. These different heating procedures, together with the appreciable difference in the boiling points, shows clearly that the light phase is rich in acetonitrile (n.b.p. 87 °C) but probably nearer to the azeotrope (n.b.p. 76 °C [147]).

The distillate fractions collected during test '1' show a constant, high tenor of acetonitrile, except for the last sample, while pure acetonitrile has never been found: these three observation suggest that the organic phase resulting from the split has a sub-azeotropic composition. Unfortunately, the sum of all the collected fractions (either distillate or residues) doesn't match the weight initially loaded in the flask, meaning that some liquid has been lost as vapors leaking from the glassware fittings, so the acetonitrile initial content calculated in this way (i.e. 54% by weight) is surely in defect, and the measured initial residue content (80 %) is likely a more reliable value.

In principle, the whole batch distillation experiment can be reproduced on much smaller scale by a single thermo-gravimetric analysis (TGA) of the liquid, save for the fact that the very small quantities involved in this case (typically from 30 to 60 mg), together with the carrier gas forced flow, determine an early evaporation under the boiling point, thus reducing the overall capability of the technique to discriminate between different mixture's compositions. Both these concepts are exemplified with the trends of Figure 8.18. Though the starting sample is slightly sub-azeotropic, its complete evaporation takes place within the azeotrope b.p.: the maximum weight loss-rate temperature and the final temperature are 66 and 71 °C respectively, that's to say that the *absolute* quantity of free water is too little to yield a distinguishable signal, even with the very slow temperature ramp (5 °C/min) employed. In summary, an acetonitrile-water mixture made of 0.79 grams of acetonitrile per gram (NMR analysis) still behaves as an azeotropic system (0.83 grams of acetonitrile per gram [147]) in the micro-scale automated analysis.

When the water quantity is larger, as in the final residue, then the micro-distillation becomes much more robust from a qualitative point of view, and two evaporation regimes become clearly visible: the end temperature is 101 °C (i.e. pure water) and two maximum-rate values appear (62 and 96 °C, though the first peak is very shallow), the quantitative error being slightly larger than at high acetonitrile contents.

The sensitivity of the technique can be enhanced coupling the information of the weight loss rate to the heat flux (second graph of panel 8.18): the initial organic phase displays one constant latent for all the time, while the aqueous final residue yields back low latent heat values during a first weight decrease range (20-25% of the total mass, when acetonitrile is distilled as azeotrope), and eventually ends with a high single latent heat, when pure water is rectified; in this case the regime change is much clearer than in the weight vs temperature trend. The use of a thermo-gravimetric apparatus to perform and interpreter micro-distillations experiments is described in sections 9.5 and 9.6.

The graphs of groups 8.19-8.20 present other batch distillations made on organic phases (number 6) and on aqueous phases containing salt (13 - 14). Also in this case no salt is detected within the organic phase, because the distillates of the sixth test never splits. Moreover, multiplying the acetonitrile estimated weight in the distilled fractions (source: TGA analysis) by the collected amounts, the overall mass turns out to be the 75% of the starting batch (a value in full agreement with those already estimated), which gives a confirmation of the predictive capability of these experiments, when the apparatus

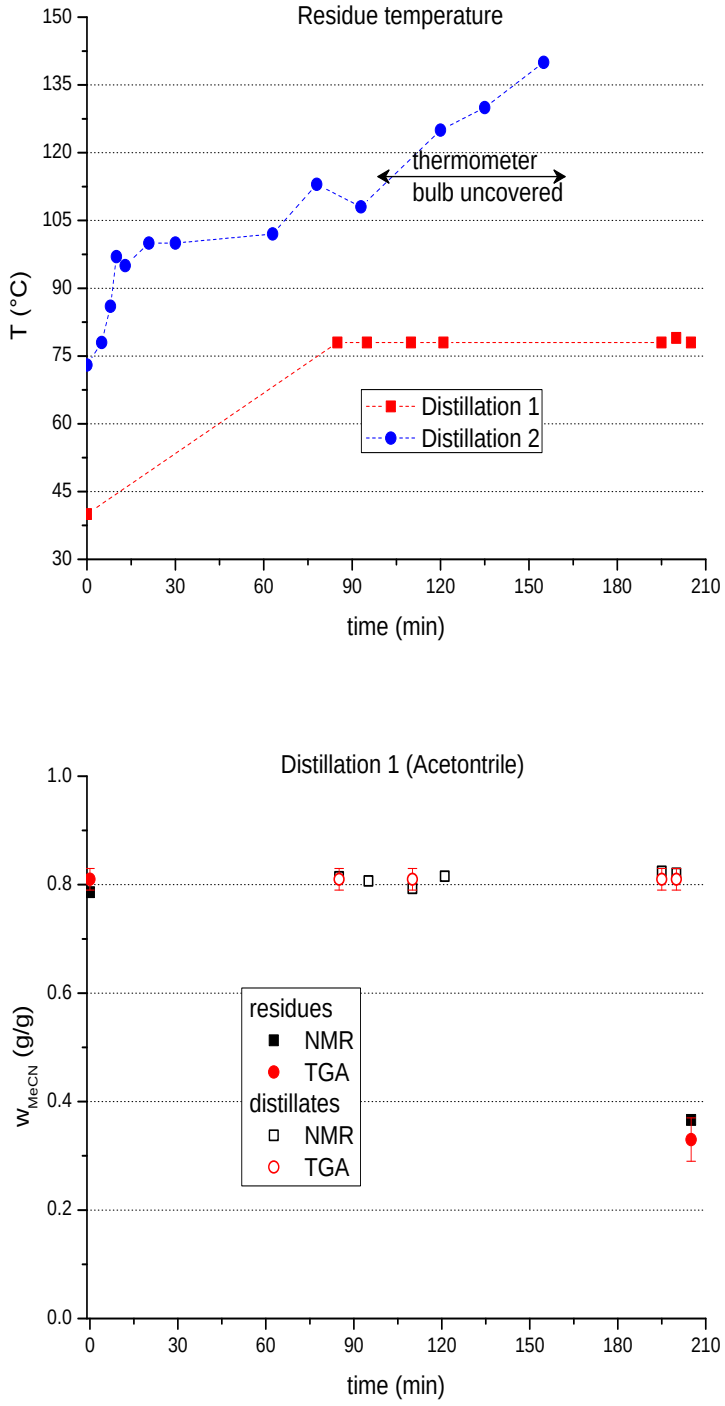

Figure 8.16: Up: temperature registered during the distillations; bottom: acetonitrile content of the test 1 distillates taken over time. Methods: NMR-TGA (CH_3CN)

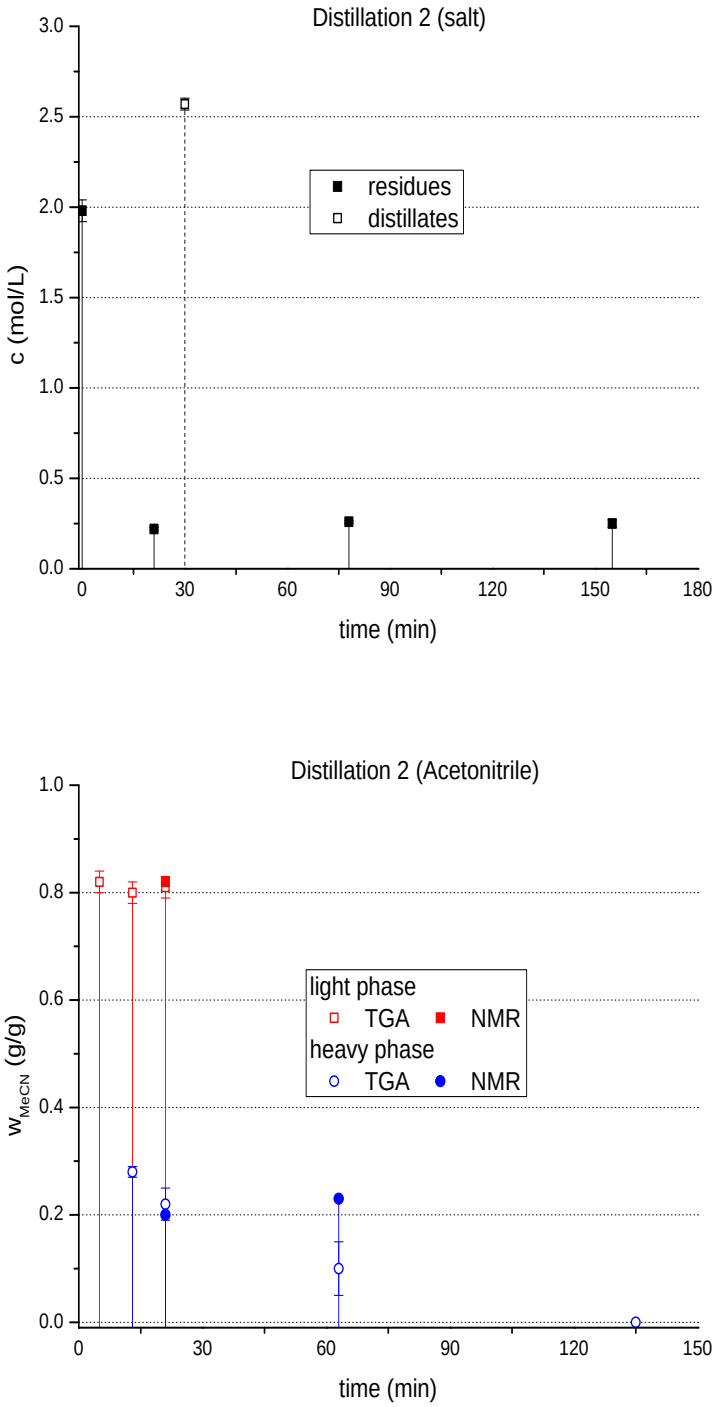

Figure 8.17: Acetontrile and ammonium bicarbonate contents of the samples for test 2 taken over time. Methods: backtritration (salt), NMR-TGA (CH_3CN)

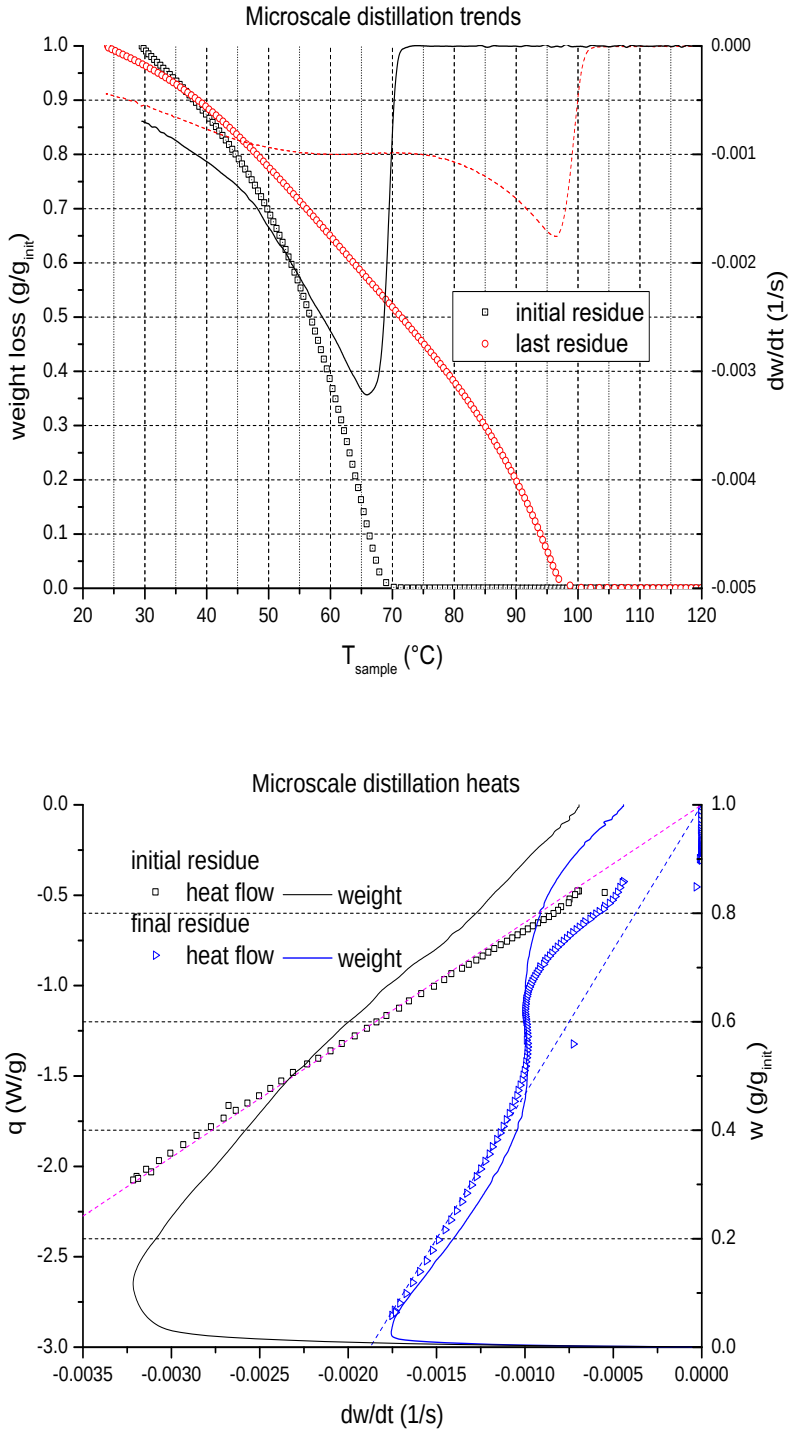

Figure 8.18: Micro-scale batch distillation results (i.e. TGA analysis) for the liquid residue of test 1 at the start and at the end of the bench-scale test.

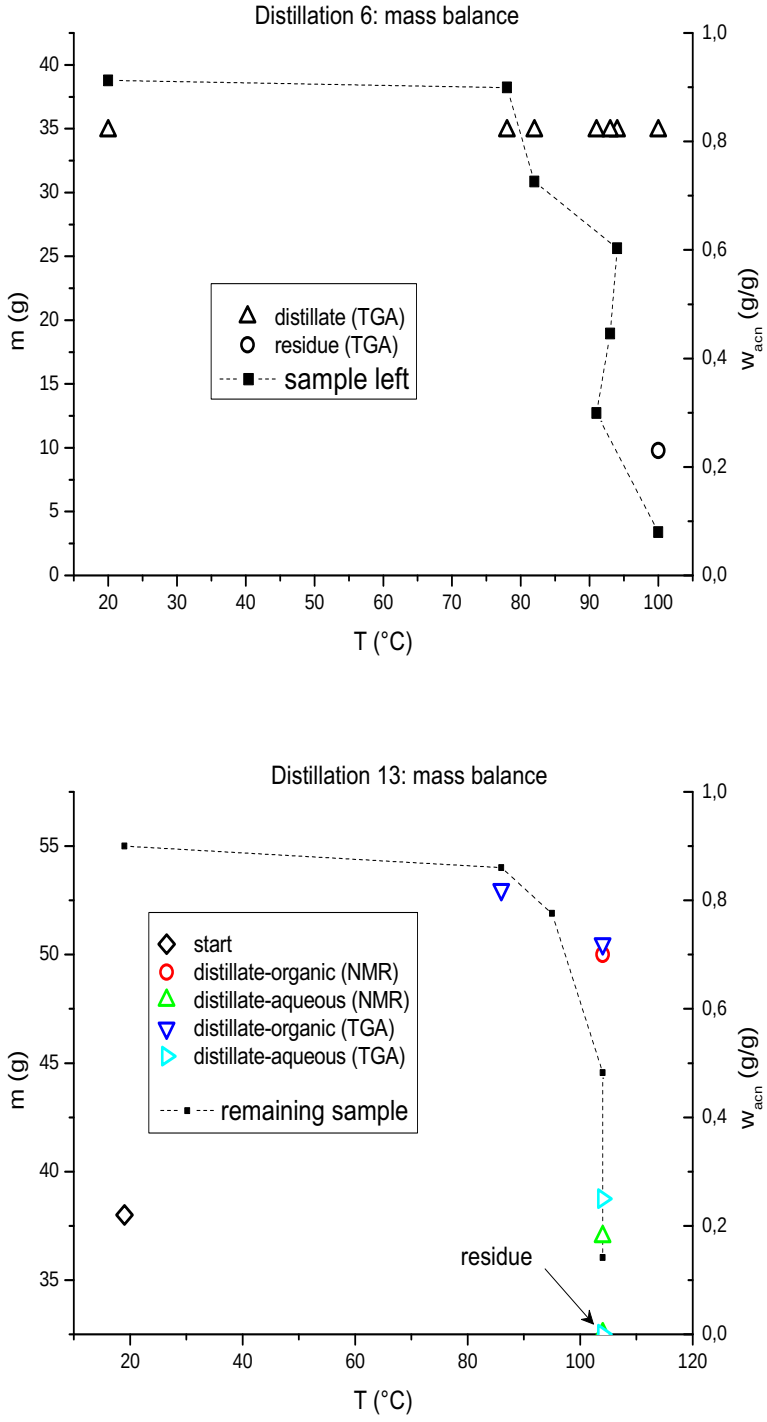

Figure 8.19: Mass balance of the batch distillation of the organic liquid n° 6 and aqueous n° 13. Methods: NMR-TGA (CH_3CN).

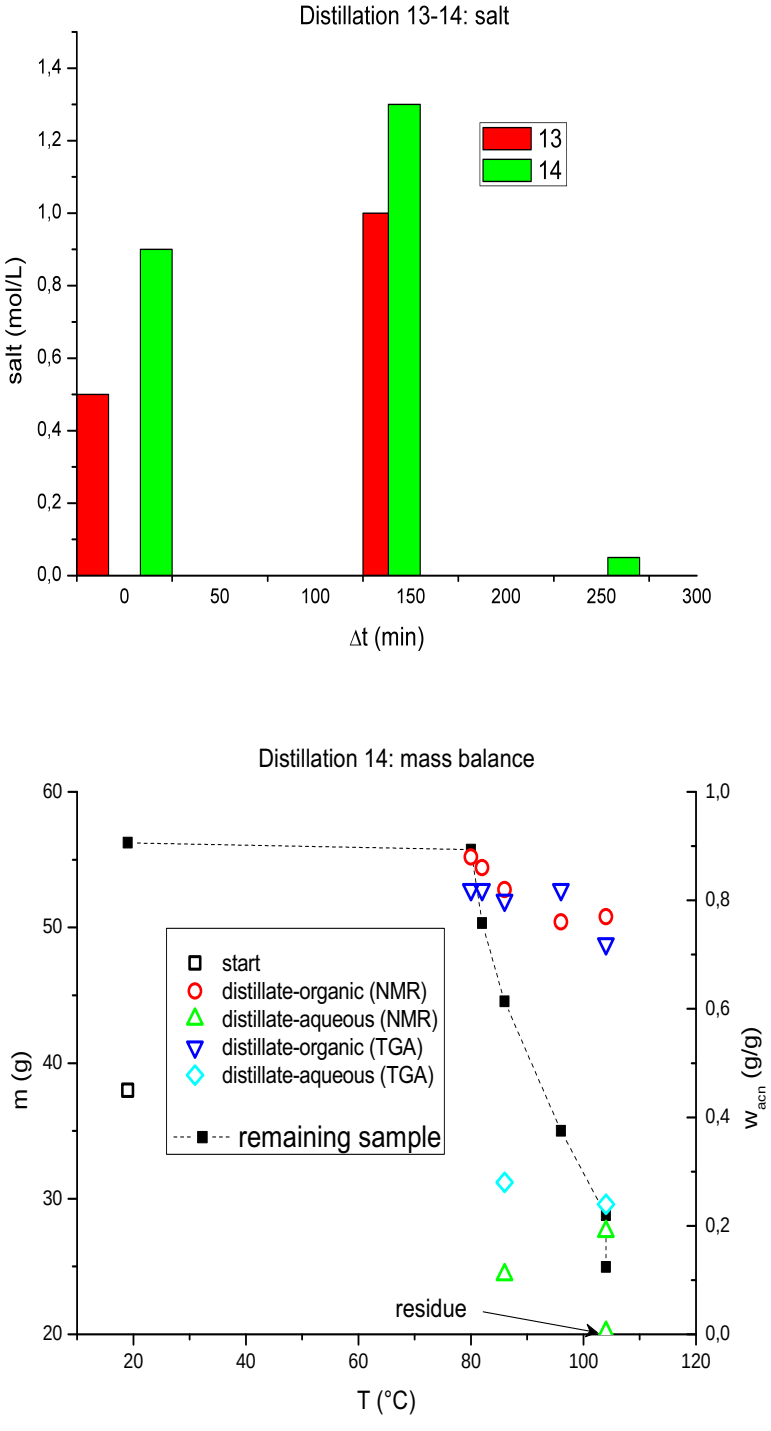

Figure 8.20: Acetonitrile (test n° 14) and ammonium bicarbonate (tests 13-14) contents of the samples taken over time. Methods: backtritration (salt), NMR-TGA (CH_3CN)

is properly set up with minimal losses.

A similar checksum for the distillation tests 13 and 14 is more complicated, because the starting batches are such as to yield multiple distillates in the split-region of the phase diagram. Nevertheless, it is worth noticing that at least a part of the starting acetonitrile can be recovered at azeotropic purity: almost $6 \times 0.82 = 4.9$ grams out of the initial $56 \times 0.45 = 25$ grams (20%) in test 14, with the salt blocked on the condenser wall or present as an insoluble solid at the bottom of the recovered overheads. When the average distillate composition becomes so rich in water as to bring along the solvated salt and yield a phase-split, the organic fraction (second collection of test 14) is still 2.5/5.8 (45%) grams, accounting for other 2 grams of acetonitrile.

Other Micro-Distillations

A final series of trials has been carried out to understand how any quantity of ethanol, still present in the acetontrile-water system after a possibly incomplete ammoxidation, can change the outcome of a batch distillation (and so how a real VLE-based separation would be affected). Tests in this sense have been carried out only at the micro-scale TGA level, with the outcomes reported in the graphs 8.21-8.22.

The ternary azeotrope composition is very close to the binary one between ethanol and acetontrile, and even closer in terms of saturation temperature [147]. Moreover, the latent heats of ethanol and its acetontrile-containing azeotropes are not so different as to yield separate trends within a thermo-gravimetry run. Of the samples rich in water, only one is successfully separable into a mixed overhead and pure bottom. The more sensitive DSC machine is able to separate the ternary azeotropes from the organics, bus also in this case the boiling points are confused when water is present.

Though these result may be improved by a more careful samples preparation and tests execution, they generally lead to the preliminary conclusion that the studied ammoxidation process should be operated without ethanol exiting the reactor, or the purification section is going to be altogether reworked.

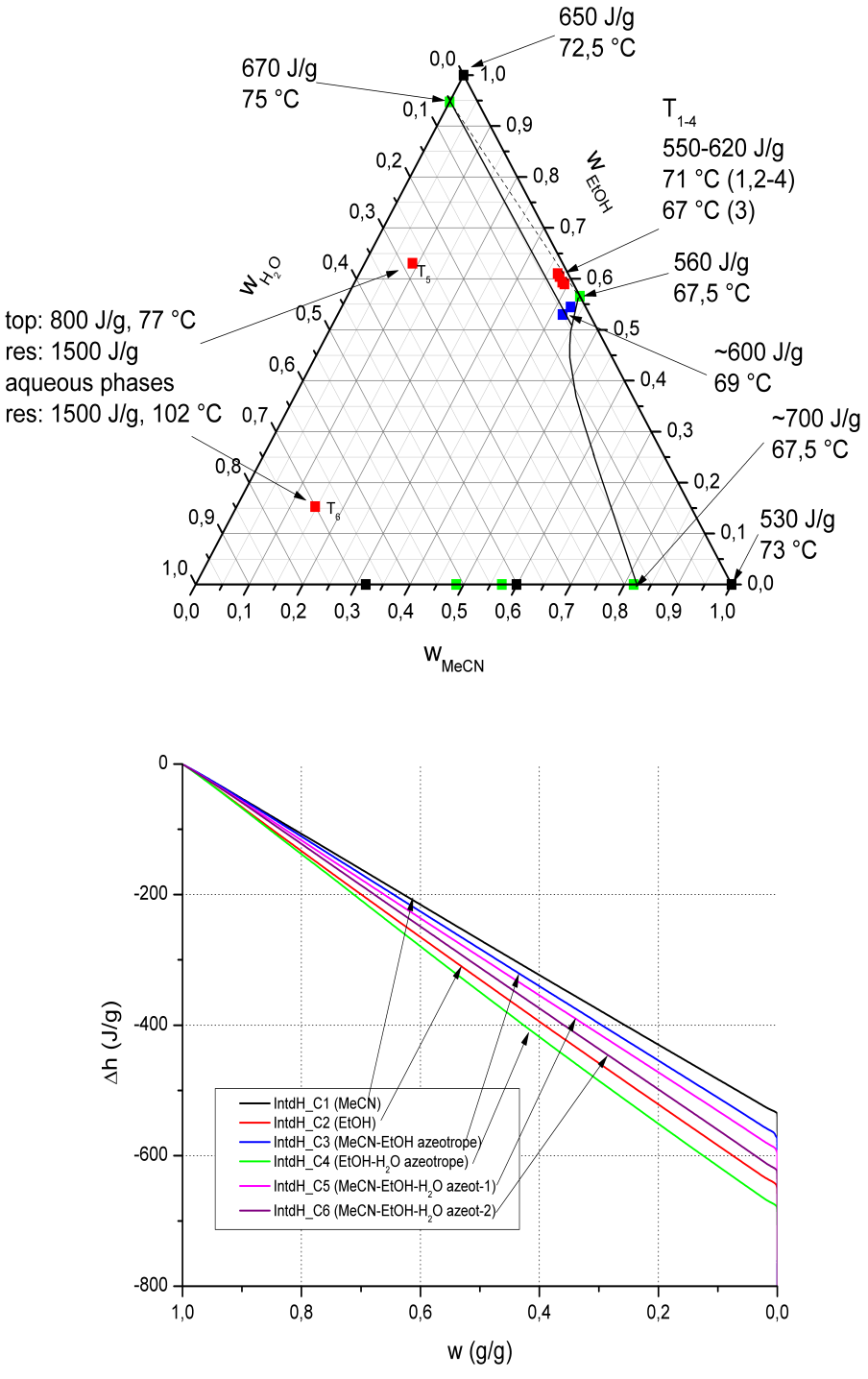

Figure 8.21: Tested ternary mixtures and TGA integrated signals for the calibrations (C) samples.

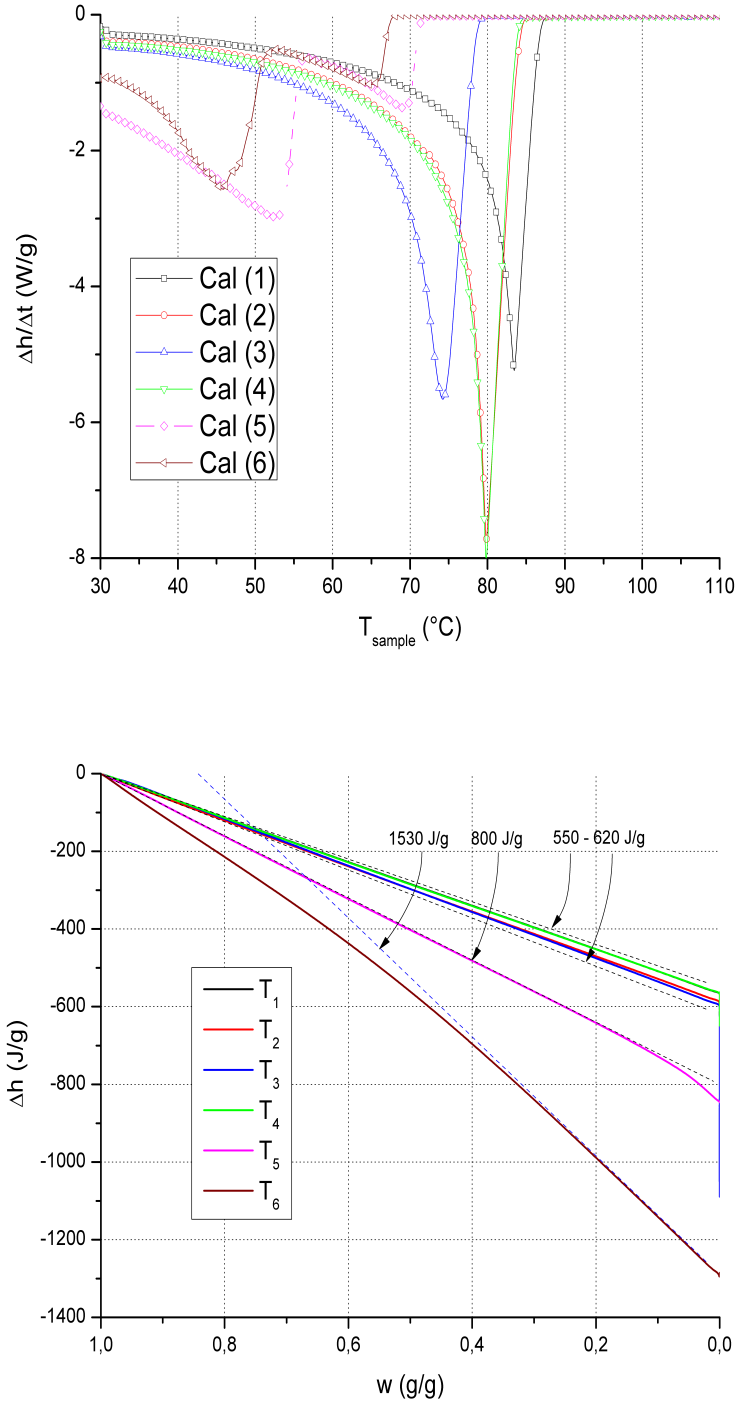

Figure 8.22: TGA integrated signals for the test (T) samples and C-samples boiling temperatures refined analysis via DSC.

8.6 Drying

The drying and decomposition tests of wet ammonium bicarbonate are used to foresee the behaviour of the relative block in the process (see chapter 4), but also to get more information on the salt itself and its interaction with the acetonitrile-water solvent.

Part of the drying experiments have been performed as dedicate tests, others using the solid phase recovered after a phase split trial with over-saturated mixtures. Manually recording the weight-loss over several days (or weeks) is a lengthy procedure, but has the advantage of monitoring the phenomenon at room temperature without dynamic effects. When the automatic thermo-gravimetric analysis is performed, instead, the data collection is very fast and the decomposition is brought to completion, but the temperature ramp quickly reaches values outside the range that would be used in the process. Other information are presented in section 9.4.

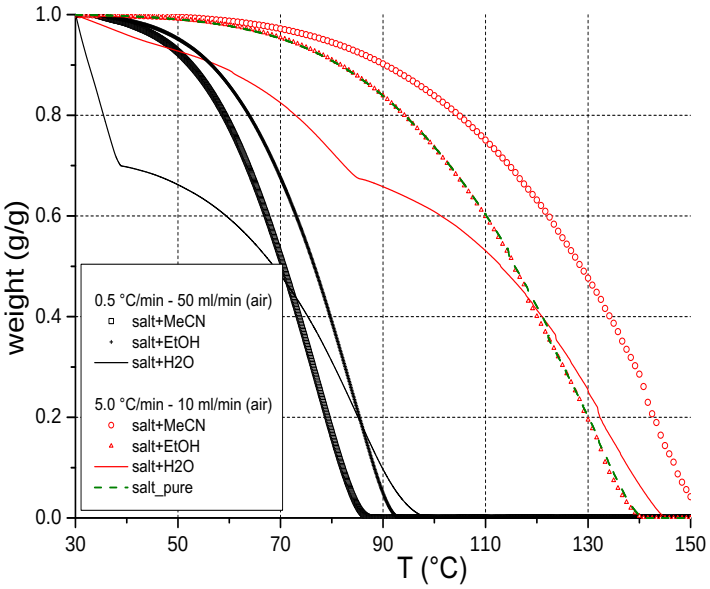

Figure 8.23: Drying and decomposition trends.

It is found that, when the salt is washed with ethanol or acetonitrile prior the experiment, its weight loss has the same shape of the decaying trend of the pure solid (Figure 8.23). When the salt is wet with water, instead, the initial weight loss is markedly more rapid, and is attributable to the evaporation of the moisture: once the 70% of the initial weight is reached, the dried salt decomposes like the pure sample.

Though the graphics 8.23 contain most of the needed information, the lengthy weight records at nearly constant temperature can catch the between the initial moisture-evaporating phase and the final slow decomposition [197], as exemplified in Figures 8.25-8.24 and table 8.2. The rapidity of the first loss decrease, when moisture evaporates, may be tentatively correlated directly to the quantity of liquid mother initially prepared as solvent and, inversely, to the quantity of ethanol used for the washing (parity plot 8.26).

Coming to the TGA-assisted rapid dryings, the graphics in Figure 8.27-8.28 clarify the effect of the sample preparation and protocol running time on the outcome if the analysis: generally, increasing the carrier gas flow results in a weight loss trend where the

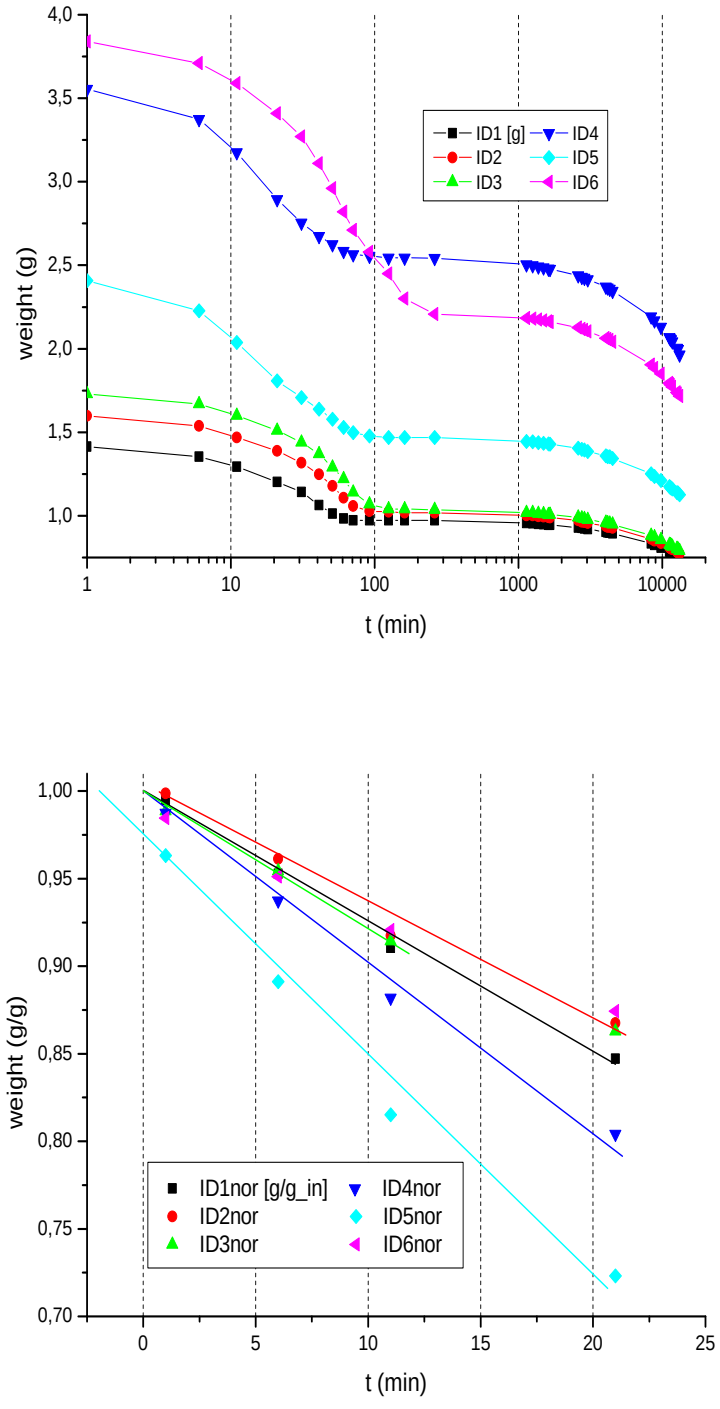

Figure 8.24: Drying trends recorded manually (Table 8.2), and relative short-time trends.

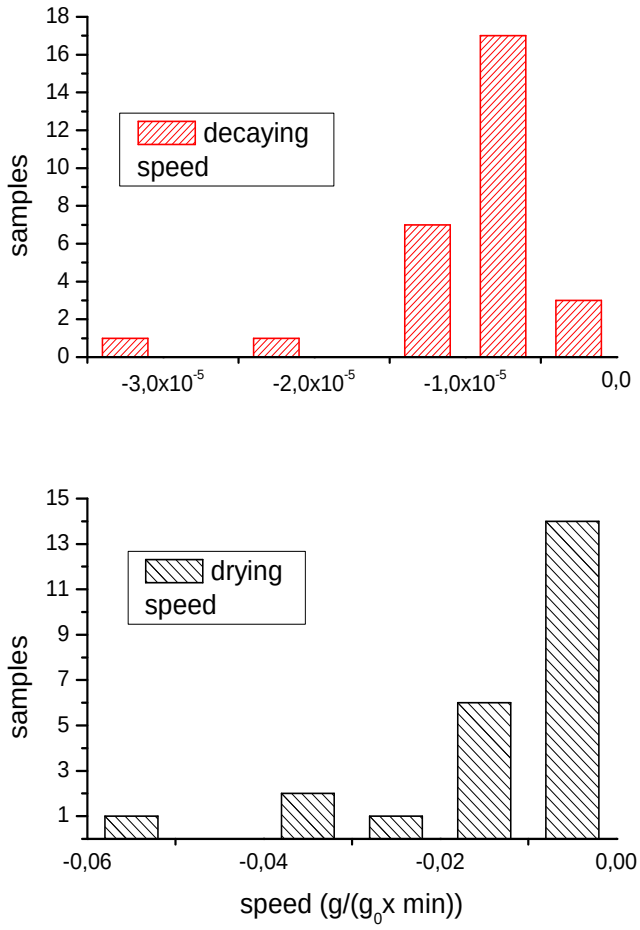

Figure 8.25: Distribution of decomposition velocity of the filtrated samples of Table 8.2 .

ID	Liquid mother (g)	CH_3CN:H_2O ratio (g/g)	salt (g)	Washing Ethanol (g)	Drying speed (min^{-1})	Decaying speed (min^{-1})
1	1.51	2	0.954	0.49	-7.48×10^{-3}	-1.17×10^{-5}
2	1.32	3	1	0.33	-6.57×10^{-3}	-1.17×10^{-5}
3	1.24	4	1.01	0.26	-7.78×10^{-3}	-1.07×10^{-5}
4	6.01	2	2.99	3.12	-9.68×10^{-3}	-1.20×10^{-5}
5	5.35	3	2.9	2.11	-1.20×10^{-2}	-1.05×10^{-5}
6	5.03	4	2.96	1.56	-7.48×10^{-3}	-9.83×10^{-6}
A	1.5	2	0.605	0.533	-1.98×10^{-2}	-1.02×10^{-5}
B	1.63	3	0.669	0.54	-1.30×10^{-2}	-1.06×10^{-5}
C	2.68	4	1.44	0.39	-1.10×10^{-2}	-3.11×10^{-5}
D	3.94	1.33	0.54	0	-1.50×10^{-2}	-2.02×10^{-5}
11a	4.96	–	0.906	2.15	-5.50×10^{-3}	-6.56×10^{-6}
12a	5.052	–	0.989	2.51	-6.00×10^{-2}	-7.89×10^{-6}
13a	4.68	2.61	0.794	0	-5.75×10^{-3}	-5.43×10^{-6}
14a	5.025	–	1.015	1.39	-3.77×10^{-3}	-5.49×10^{-6}
15a	3.97	0	0.777	1.4	-4.00×10^{-2}	-7.05×10^{-6}
6b	1.43	4	0.8	0.5	–	-7.37×10^{-6}
11b	3.93	–	1.652	1.7	-5.38×10^{-3}	-6.91×10^{-6}
12b	0.508	–	0.9	0.255	-2.50×10^{-2}	-8.35×10^{-6}
13b	3.93	2.61	0.612	0	-4.00×10^{-2}	-3.79×10^{-6}
14b	3.88	–	0.636	1.08	-8.00×10^{-3}	-5.29×10^{-6}
15b	3.79	0	0.662	1.33	–	-8.18×10^{-6}
11c	3.96	–	0.684	1.71	-7.14×10^{-3}	-7.48×10^{-6}
12c	2.01	–	0.45	1	–	-9.18×10^{-6}
13c	2.23	2.61	0.427	0	-1.13×10^{-2}	-3.71×10^{-6}
6c	1.417	4	0.73	0.27	-7.34×10^{-3}	-6.05×10^{-6}
1c	1.29	2	0.78	0.49	–	-7.29×10^{-6}
3c	1.46	4	0.96	0.258	–	-6.92×10^{-6}
13d	1.44	2.61	0.446	0	-7.00×10^{-3}	-3.27×10^{-6}
16	2.04	4.9	0.803	0.29	-4.30×10^{-3}	-6.19×10^{-6}

Table 8.2: Compositions of the centrifuged samples and recorded drying-decaying trends.

initial moisture evaporates together with some salt that starts to sublimate. At reduced carrier flow, the initial wetness evaporation becomes clearly separated by the eventual salt sublimation (the weight fraction still present at this point changes drastically according to the initial sample condition), then at 110 °C the salt melts and finishes to evaporate as a liquid. This passage is marked by the noise in the $\frac{dw}{dt}$ signal, save when the starting material is too wet (and its decomposition thus sensibly anticipated).

There are a few practical aspects that have to be considered: first, samples filtered from a liquor containing both water and ethanol do not show systematically the same drying trend of samples washed with only ethanol (or acetonitrile - graphics 8.23): second, the quantity of sample placed inside the TGA machine or a longer delay between the filtering and analysis start affect the result: third, the filtering and washing operations are not completely reproducible. This is evident in the last frame of graphs 8.28, where like samples treated with the same protocol yield very different decaying trends, essentially because of an unpredicted - yet critical - difference in the sample handling during the filtering.

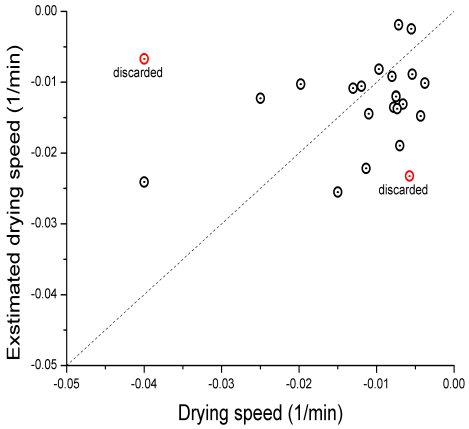

Figure 8.26: Tentative correlation to the initial moisture and ethanol content.

Despite the above mentioned shortcomings, it is generally observed that: shorter TGA runs and/or high initial moisture contents can mask the onset of the melting transition and: the decaying trends over days at constant temperature are essentially independent on the initial samples preparation, which confirm the fact that no moisture is present within the solid after the first drying phase (lasting 2-3 hours) has ended.

What is more important in the scope of this work, is that the energetic character of this decaying is much less sensitive to the various experiment conditions: the first frame of Figure 8.29 reports the latent heat released during the analysis, extrapolated by plotting the elaborated signals $\frac{\Delta h}{\Delta t}$: $\frac{\Delta w}{\Delta t}$, from the samples of Figure 8.23. Also for the samples of Figure 8.28-bottom, though the initial wetness evaporation (low-steep trend at low $\frac{dw}{dt}$ values) and the melting region (horizontal spikes) clearly distinguish the two processes, the heat release takes place, in both cases, along the same latent heat value.

Moreover, the more sensitive DSC analysis (same Fig. 8.29) shows that the enthalpy release of pure ammonium bicarbonate is very similar to that of water (and practically not distinguishable from it), probably because the energetic aspect of the decomposition is dominated by the one water mole present per mole of salt. This means that the whole process of the wet and dried salt decomposition (and eventual evaporation after melting) yield the same calorimetric signal of a water droplet.

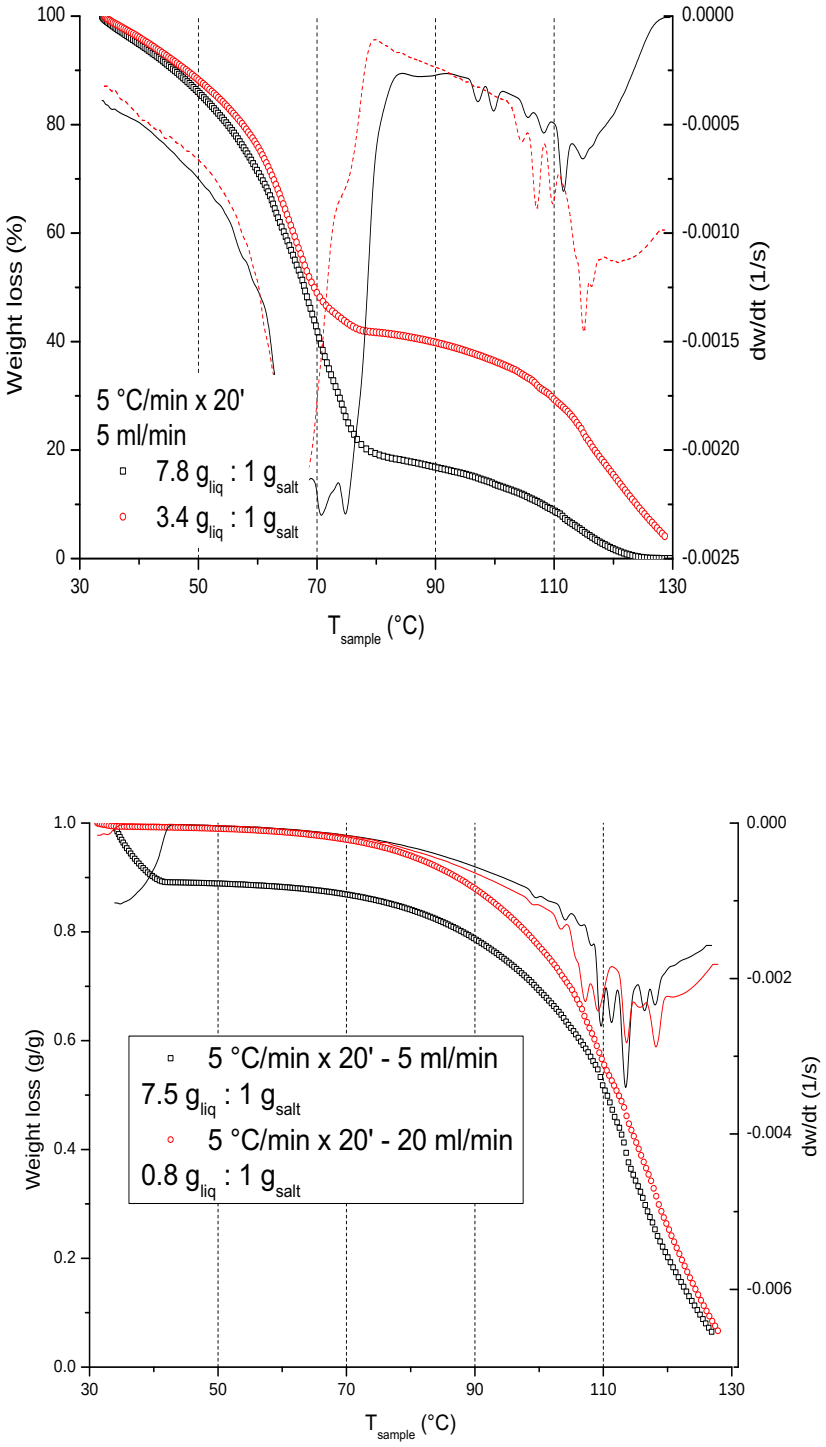

Figure 8.27: TGA-DSC trends for selected drying experiments, showing how the variation of a certain parameter affects the signal.

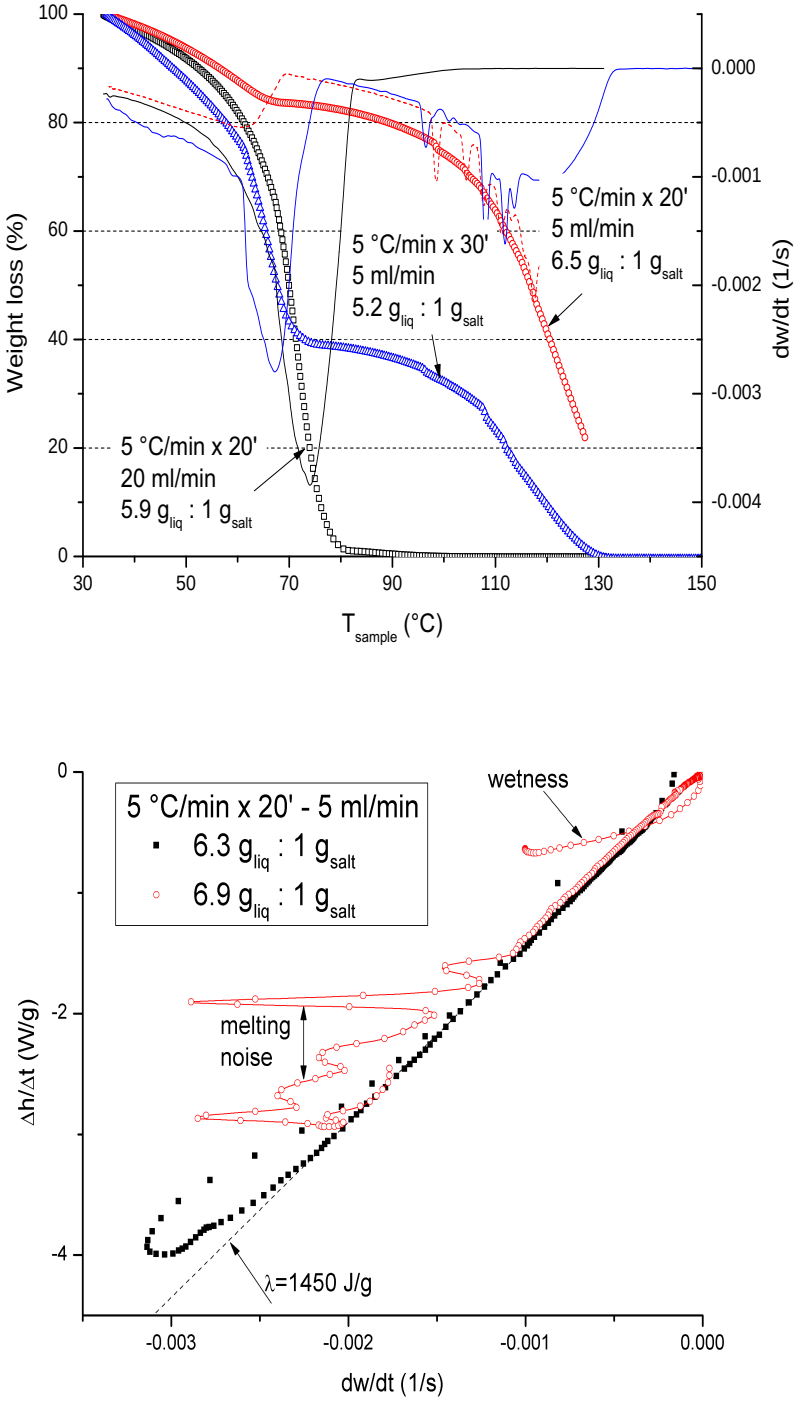

Figure 8.28: TGA-DSC trends for selected drying experiments, showing how the variation of a certain parameter affects the signal.

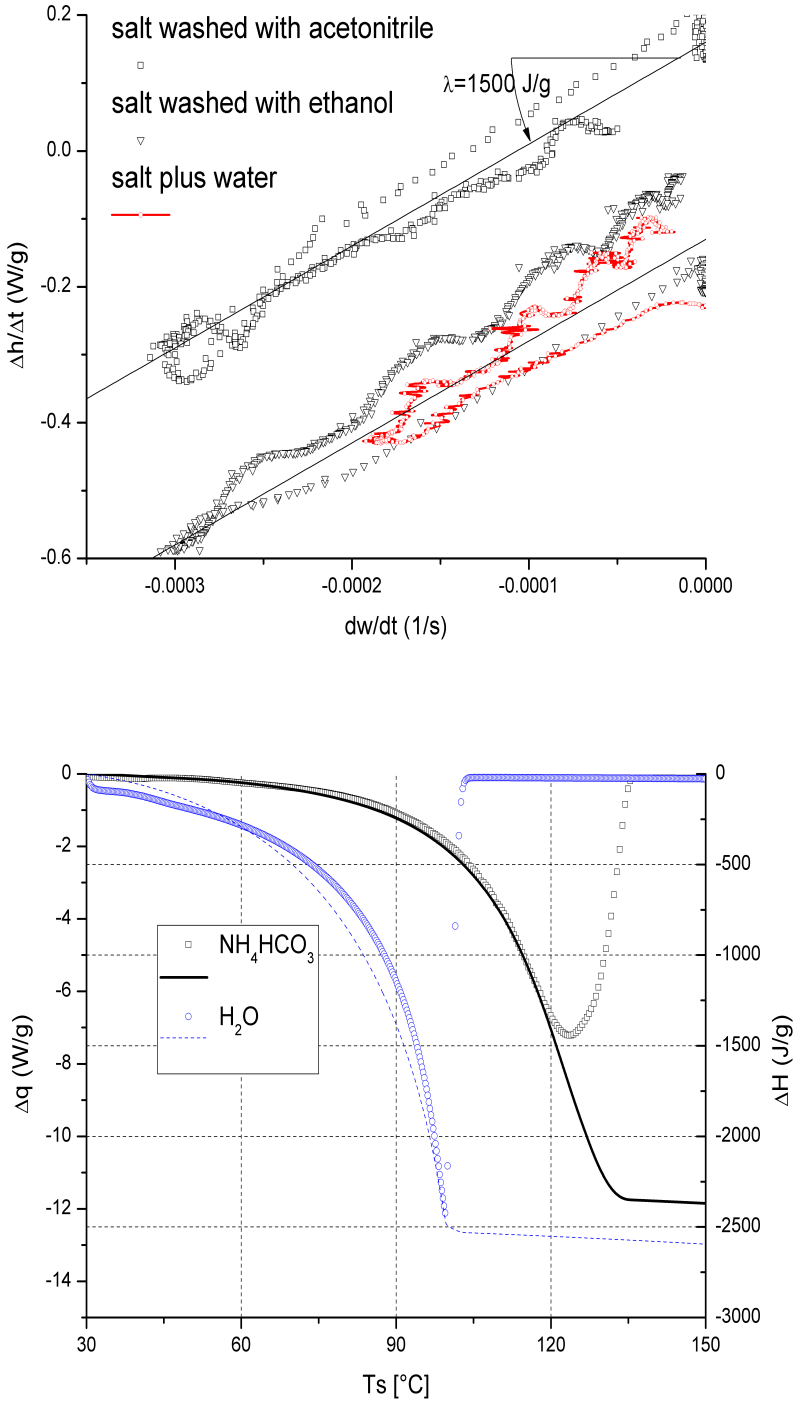

Figure 8.29: Latent heat for the salt filtered from different solvents and calorimetric essay of the pure solid compared to water.

Chapter 9

Methods of analysis

9.1 Backtritrations

The ammonium salt dissolved in the aqueous phases have always been quantified via backtritration, according to two different receipts. The pH values have been recorded with an AMEL-411/CGG/12 electrode, calibrated with the help of a neutral buffer plus a solution of acetic acid and sodium acetate 10^{-3} M. To have a more robust analysis, the conductimetric signal from an AMEL-2192 cell is recorded in parallel: this instrument has been calibrated with brine, so the used acid and base have been chosen coherently: this choice has granted very robust and reproducible conductimetric responses.

Ammonium backtritration

1) 5 ml of HCl (Sigma Aldrich) diluted to 1 M are prepared in a becher, and a weighted quantity of NH_4Cl is added[1];

2) a maximum of 1 ml of analyte is added: vigorous bubbling provides a first confirmation of the bicarbonate conversion to CO_2;

3) 2 to 3 mmoles of excess hydrochloric acid are still present in the becher, they are neutralized with known additions of a NaOH (Sigma Aldrich) solution 1M from a glass burette, and the actual backtritration of the ammonium follows until the pH rises above 11.

Ammonium-Bicarbonate backtritration

1) 5 ml of NaOH 1 M are prepared in a becher, and a weighted quantity of NH_4HCO_3 is added;

2) a maximum of 1 ml of analyte is added;

3) 1 to 2 mmoles of excess soda are still present in the becher, they are neutralized with known additions of HCl 1M from a glass burette until the ${CO_3}^{2-} \rightleftharpoons {HCO_3}^{-}$ buffer zone is entered ($pH \lesssim 11.5$): this is linked, without solution of continuity, to the $NH_3 \rightleftharpoons {NH_4}^{+}$ buffer, then a relatively sharper transition occurs followed by the ${HCO_3}^{-} \rightleftharpoons H_2CO_3 \longrightarrow CO_2$ range.

[1] All weightings have been done on a Gibertini E42S-B electronic scale.

This second approach has been adopted only after careful calibrations (see Figure 9.1), to exclude the risk of an early ammonia evaporation during the tritration time (20-30 minutes). This phenomenon has been found practically negligible at room temperature and with the used concentrations.

The advantage of this procedure is that it yields two comparable responses, because the first long buffer between 11.5 and 8 pH units requires twice the moles of tritratrant than the second zone (7 to 5 pH units), so a quick coherence check clarifies if the test is usable or some systematic error invalidates the analysis, moreover the comparison of the two zones can provide an error estimate beside the sensitivity limit.

The drawbacks are two: the first buffer is often a 10-20% shorter than what expected, probably because the pH metric curve doesn't fall very steeply at the first step (when carbonate starts to be converted): then, when the salt concentration is relatively high (from 0.7-1.0 M, beside the internal reference quantity), the vigorous bubbling of the formed CO_2 'blinds' the conductimeter just in the range where the bicarbonate buffer is ending. Nevertheless, the pH-meter has never been found affected from this phenomenon, as the CO_2 bubbles are always seen to nucleate first on the conductimeter stick and cell covering, and also on the teflon-covered stirred, rather than from the glass surfaces.

9.2 Hydrolysis

The first screening of the organic phase have been made via an approximate yet robust and cheap technique of hydrolysis followed by backtritration, that can be performed in-house within the same day of a phase split experiment. The more convenient analysis protocol has been defined as follows, after several trials and calibration where one or two conditions at a time were changed:

1) 4 grams of NaOH (Sigma Aldrich) are put in a 250 ml reacting flask, and 100 ml of distilled water are added;

2) a vertical condenser flushed with tap water is placed onto the flask, and the apparatus starts to be heated with a thermo-mantle;

3) 0.5-1 ml of analyte (a sample of organic phase) is added through one of the flask side taps - just after the addition, a 10 ml sample is sometimes drawn from the mixture with a glass pipette and backtritrated with Bromoscresole-Green and HCl 1 M for calibration purposes;

4) the mixture is kept boiling under reflux for 4-5 hours, then the thermo-mantle is switched off and the flask is left cooling;

5) 10 to 15 ml are drawn and backtritrated in presence of a weighted quantity (0.7-1.2 g) of $AcONa \cdot 3\,H_2O$ (vendor) as internal standard.

The hydrolysis of known quantities of acetonitrile into acetic acid has been found to be complete, in the above described conditions, thanks to the effective removal of ammonia (one test made in acidic environment showed, on the other hand, a conversion limited to 35%). Most of the times, however, traces of ammonia have still been detected as a short broadening of the pH trend, that doesn't fall sharply from 9 to 6 (see graph 9.1).

The molarity of reacting NaOH and tritrating HCl have been chosen to assure a minimal sensitivity of about 0.1 mmol using a class A burette with 0.1 ml ticks.

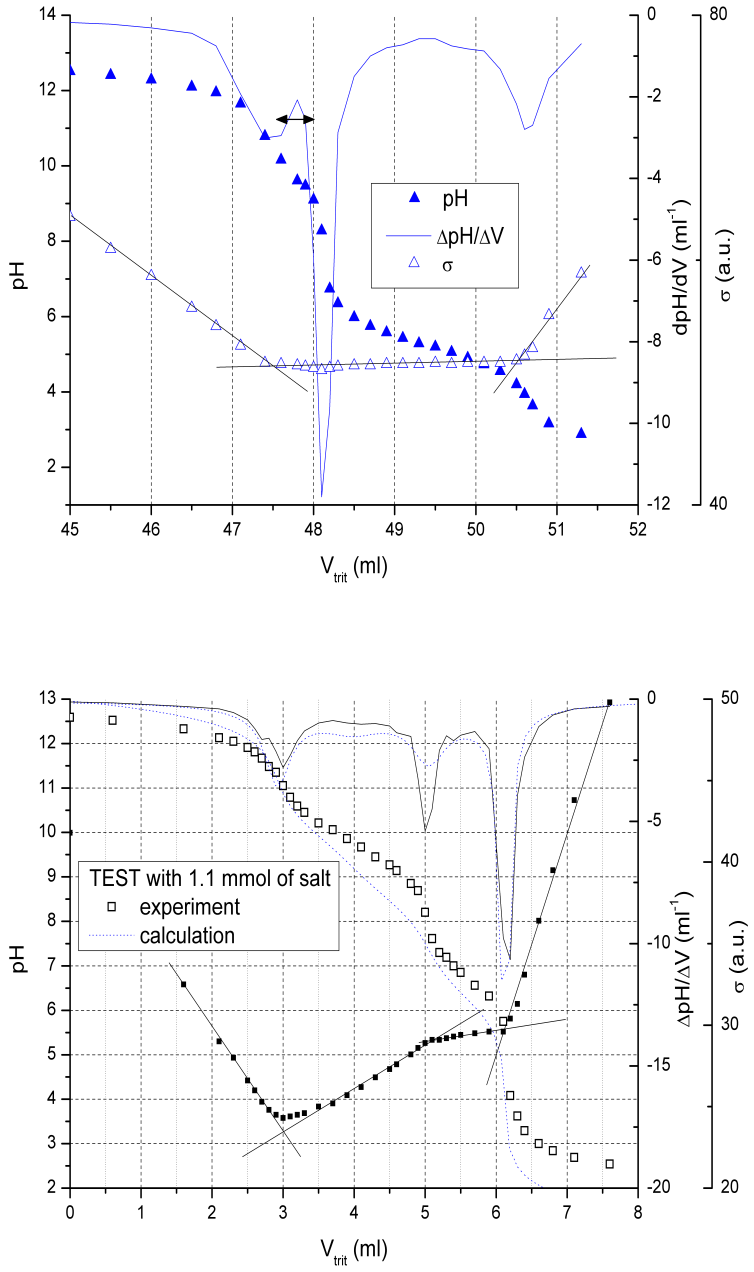

Figure 9.1: Up: typical acetate backtritration; bottom: test for the backtritration of ammonium bicarbonate.

9.3 Proton Magnetic Resonance

While the proton magnetic resonance technique (or, generally, nuclear magnetic resonance, NMR) is generally preferred for qualitative and identification purposes, its high sensitivity makes it a very accurate tool also for quantitative analysis. Usually, gas or liquid chromatograpy (GC-LC) are preferred, whenever possible, for several reasons:

- chromatography instruments are less expensive, easier to operate and available within most laboratories, while centralized NMR facilities have busier schedules;
- a properly calibrated GC/LC column yields quantitatively reliable results;
- the drawbacks of GC/LC columns in identifying some molecules with very close peaks are often balanced by spectra more easily readable (specially when the column is not followed by a mass-spectrum analyser);
- the deep insight into molecular structure offered by the NMR technique is best suited to purified samples and generally, not needed to quantify already known species.

Notwithstanding, most GC columns are permanently poisoned by ammonia, so the benchmark analysis to fix the relevant phase diagram points and calibrate the other methods' response have been obtained by NMR (with a Bruker-Avance equipment) according to the following workflow:

1) as quantitative analysis needs a reference internal analyte, this must be a NMR-active molecule with peaks sufficiently separated by the expected acetonitrile CH_3 one (2.1 ppm in CD_2Cl_2 [198]);
2) commonly employed solvents as CD_2Cl_2 or deuterated-DMSO are not miscible with water, leaving heavy water as the only viable choice;
3) the reference molecule (point 1) must then be miscible in water: this has led to exclude benzene and toluene (initially taken into consideration because of their clear signal around 6 ppm), as well as alkanes;
4) ethanol has been selected as reference because is fully miscible with water, D_2O and acetonitrile in any ratio, is not expensive, is readily available and does not require special handling cautions - the signal of its OH proton becomes assimilated into a unique broad peak with those of water and D_2O, but the signal of the $-CH_2-$ group can still be used for internal checks.

After this preliminary procedure, which has been carried out realizing calibration spectra and stability tests inside little vials, two modalities of sample preparation have been employed throughout the work.

I. For organic phases.

   a: the organic phase to analyse is collected and weighted into a vial;

   b: a weighted amount of ethanol is added;

   c: the vial is stirred, then some liquid is extracted and mixed with D_2O inside a NMR tube;

1: alternatively, the organic phase is added directly into a NMR tube containing already some D_2O, and the weights recorded after each addition;

2: ethanol is then added (and the weight recorded) and the tube sealed.

II. For aqueous phases.

a: the aqueous phase is sampled and weighted into a vial;

b: upon ethanol addition (and weighting), the ammonium bicarbonate still present flocculates and precipitates;

c: after waiting 30-60 minutes, some of the liquid surnatant is transferred into a separate vial, etc. In this way the acetontrile is actually sampled from the *liquid* part of the aqueous phase, but its content remains referred to the *total* sample because the weighting takes place before the salt is discarded via the ethanol-induced flocculation.

Once the ethanol and the acetontrile CH_3 peaks are recognized in the spectrum, their areas A_{etoh} and A_{acn} are integrated and the original acetontrile content in the sample is:

$$w_{acn} = \frac{A_{acn}}{A_{etoh}} \times \frac{MW_{acn}}{MW_{etoh}} \times \frac{m_{etoh}}{m_{liq}} \tag{9.1}$$

This working procedure has two drawbacks, first: the NMR sensitivity is limited by the scale one, because the peak areas correlation depends linearly from the phase:ethanol weights, second: to work with liquid quantities of the order of 0.01-0.1 grams means to reach a very high analyte:solvent ratio in the tube, that can lead to blurred spectra and is generally a non-recommended practice. An example of blurred spectrum is reported in Figure 9.2. The spectrum 9.3 shows instead a different unexpected feature occurring in many spectra recorded with good resolution, that's to say several side-bands and even split peaks.

The procedure for the aqueous phase has been initially devised in order to avoid interference from the free and exchanging protons of ammonium and bicarbonate ions. Nevertheless, the issue has been reconsidered in light of the fact that in aqueous environment the exchange is indeed complete, and so the N−H and -CO-OH protons are actually 'buried' in the water OH peak. The receipt (II) has then been modified following the same steps as in (I.1-2) for a organic phase directly inserted into a tube: extra care must be taken to use enough D_2O and a reduced amount of ethanol to overcome the anti-solvent effect and avoid precipitation within the tube.

A tabulation of the relevant data taken from the spectra is found in section C.3.2.

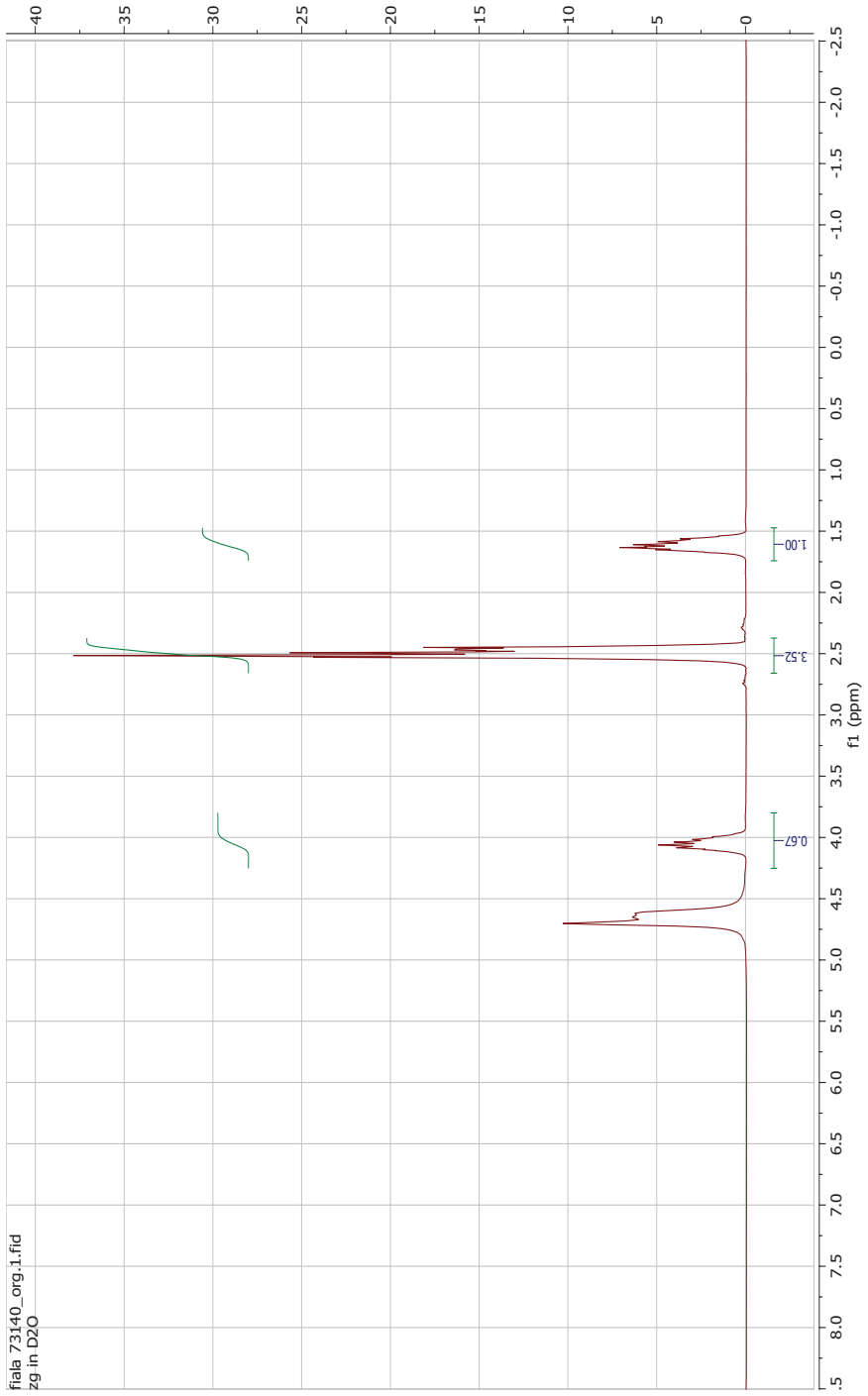

Figure 9.2: Example of organic-phase NMR spectrum: the poor resolution is due to a too concentrated sample.

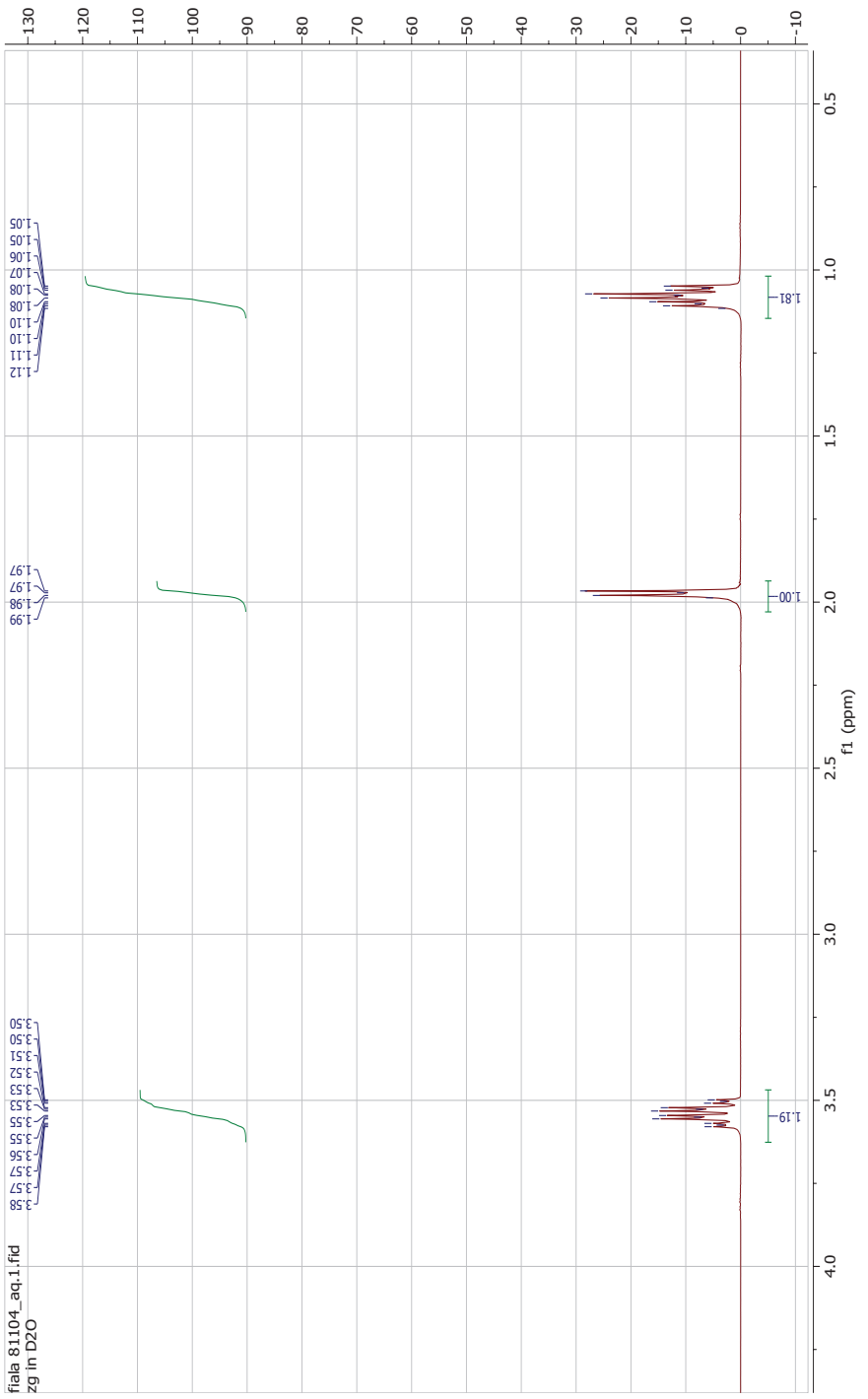

Figure 9.3: Example of aqueous-phase NMR spectrum: the automatic analysis highlights several peak-splits, more evident in the case of the acetonitrile singlet.

9.4 Salt Drying

The procedure to analyze the salt drying, melting and decomposition is as follows:

1) a liquid mother is prapared in a 10ml-vial, containing different proportions of water, ethanol and acetonitrile;

2) a weighted quantity of ammonium bicarbonate is added to the solvent;

3) the vial is sealed and centrifuged for 10' at 3000 rpm in an AHSI Biofuge Stratos machine;

4) the mixture is filtered and the wet salt is washed with some ethanol: a small quantity is placed within minutes into the sample holder of the automated TGA apparatus, while the remaining is weighted regularly until the difference between the drying and decaying trends becomes clear and quantitative.

The protocols adopted for the TGA machine are listed here. Most of them have been tested during the drying experiments and then discarded.

ID	Tstart (°C)	T-Ramp (°C/min)	time (min)	Gas flow (ml/min)	Sampling (data/sec)
B0	30	0.5	240	50 (air)	1
B1	30	0.75	120	50 (air)	2
B2	30	0.75	120	10 (air)	2
B3	30	0.75	120	50 (N_2)	2
B4	30	0.75	120	10 (N_2)	2
B5	30	0.5	180	10 (air)	2
B6	30	0.5	180	50 (N_2)	2
B7	30	0.5	180	10 (N_2)	2
B8	30	5	30	10 (N2)	1
B9	30	5	30	10 (aria)	1
B10	30	5	20	5 (aria)	1
B11	30	5	20	20 (aria)	1
B12	30	5	30	5 (aria)	1

Table 9.1: Tested TGA machine protocols.

9.5 Liquid Samples TGA

The thermal and gravimetric analysis (TGA) on the liquid mixtures have been carried out on three different instruments:

1) a Perkin-Elmer machine for thermo-gravimetry, equipped with an open-pan microscale (hanging from a suspended wire, with vertical carrier flow), used for calibration purposes only;

2) a Mettler-Toledo DSC3/500 machine for Differential Scanning Calorimetry (DSC): this instruments hoists the samples into a covered pan, and yields reliable sublimation and evaporation temperatures also thanks to the multiple sensors installed;

3) a Mettler-Toledo TGA/DSC/3+1100 machine for the combined analysis: this instruments has a double open pan (lever system, carrier gas in cross-flow), an additional sample holder is kept empty and the released heat is calculated by the temperature difference between the sample and dummy sockets.

The more convenient protocol has been established after 10-12 trials with different T-ramps and carrier gas flows, as reported in the previous Table 9.1.

The qualitative analysis of the data obtained by liquid samples proceeds as follows (refer to Figures 9.4 and 9.5):

1) the weight loss is adjusted subtracting any non-zero or offset or linear drift possibly present;

2) the recorded weight and its time derivative as a function of temperature are analyzed considering: the shape (broader in higher-boiling samples) : the number of derivative minima: their position.

The most important feature of the signal is the appearance of more than one peak in the weight loss speed, indicating that the mixture can be resolved in fractions with different boiling points (both the shape and position of the peaks depend on the measuring protocol and the instrument internals) [199]. The acetontrile-water 'Txy lens' is appreciably flat, and the boiling points of the azeotrope (76.5 °C [149]) and water sufficiently apart, to overcome sensitivity limitations and resolve the azeotropic and residual fractions for any sample with $0.4 \leq w_{acn} < 0.8\,(g/g)$ (Fig. 9.4).

It is interesting to see that this range corresponds roughly to the phase-split boundaries traced in the phase-diagram (Fig. 8.3): in other words, an acetonitrile-water mixture yielding two boiling points when examined via DSC or TGA is meant to yield also two liquid phases when ammonium bicarbonate is added. The more accurate NMR measurements indicate that the phase-split frontier is actually a little larger than the DSC-sensitive range, nonetheless the calorimetric analysis bears the whole qualitative meaning with acceptable approximation, if compared to the greater simplicity of the technique. As a mixture becomes poorer in acetontrile, the low-temperature maximum gets less pronounced, while the high-temperature one more marked; their position shifts upward because, as the absolute quantity of a given fraction increases, it becomes less sensitive to the early evaporation (at $T < T_{sat}$) caused by the open-pane apparatus. In this framework, it is also important to notice how the signal is modified after the salting-out: the upper and lower phases don't yield, in general, a multi-peak calorimetric essay[2]: this means that the split conditions tested bring the coexistence limit very near

[2]This behavior is showed by roughly one organic liquids out of ten tested.

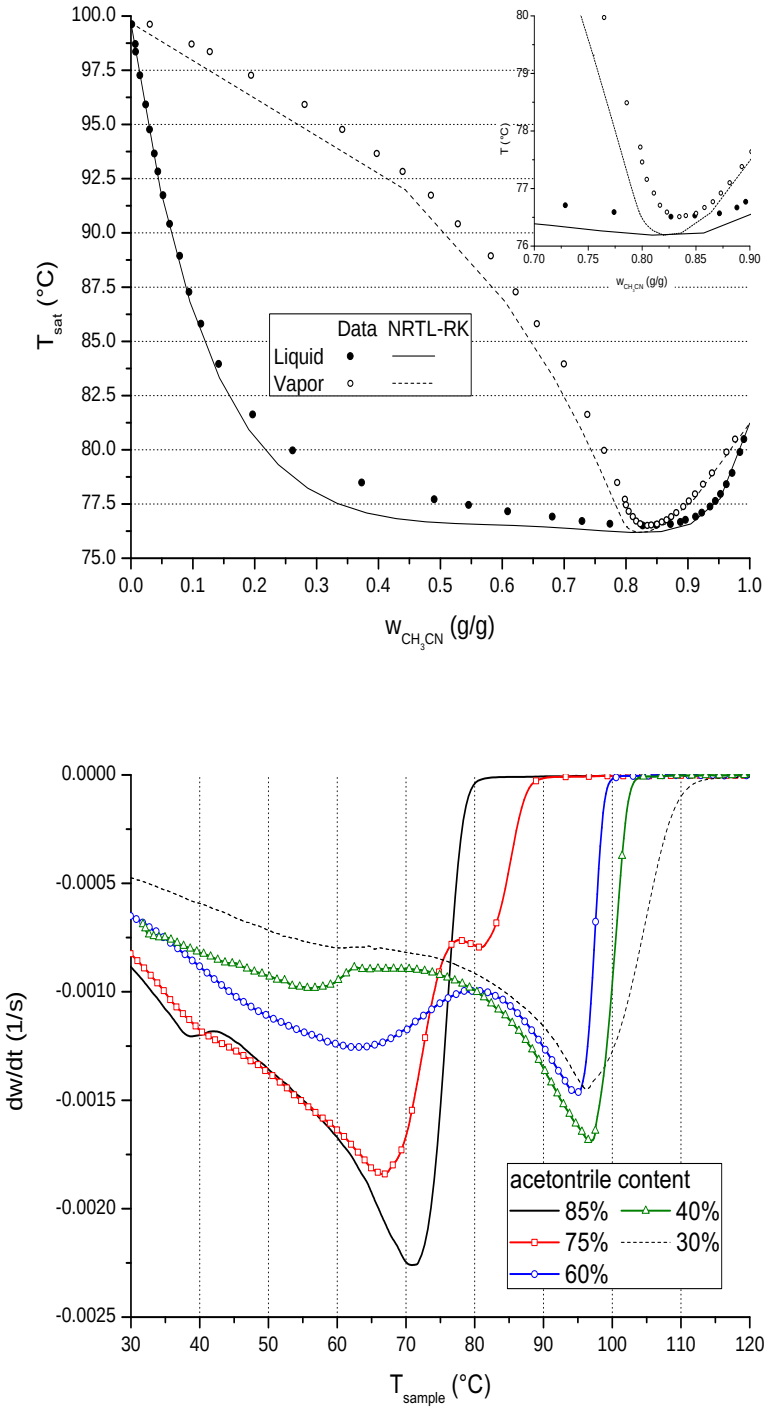

Figure 9.4: Up: VLE of acetonitrile-water; bottom: TGA signals of different mixtures.

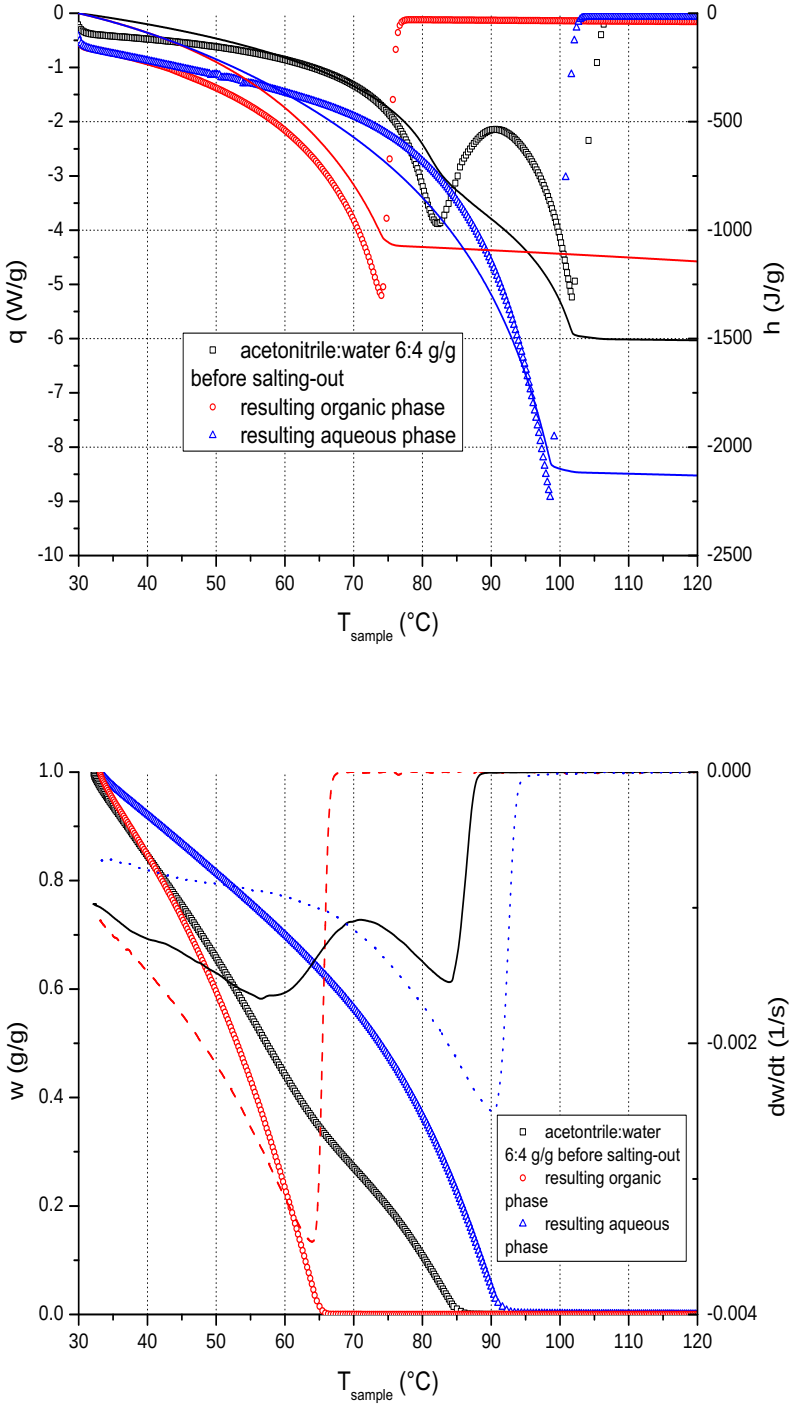

Figure 9.5: Left: DSC analysis of an acetonitrile-water mixture (60% wt of CH_3CN - points) and total released heat (lines); right: TGA analysis (points: weight loss - lines: evaporation speed).

the azeotropic composition (or just below) on one side, and below an acetonitrile content of 40% on the other.

The marked difference in the shape and peak temperature between an organic phase signal and a water-phase one contribute to assign at a glance the unknown mixture in one or the other phase diagram region after a 30' essay. It can finally be observed that:

- the shapes of the DSC and TGA-derivative signals are very similar, as expected employing equal temperature ramps: the lower-temperature DSC peaks appear shallower because they're already normalized by a lower latent heat value[3];
- the peak positions yielded by the closed-pan machine are closely matched to the boiling points expected for the assumed composition, while they are systematically underestimated by the open-pan instrument (also this behavior has already been observed [199]);
- the open-pan TGA machine performs less accurate temperature recordings than the DSC one (due essentially to a reduced number of sensors), that can result in shifted positions of the low-temperature and high-temperature peaks between different runs.

9.6 TGA Quantitative Treatment

Sensible and latent heat contributions

Both the sublimation of pure ammonium bicarbonate and the evaporation of liquids (water, acetonitrile or mixtures) are not treated with the same approach used for solid samples undergoing decomposition or phase changes at relatively high temperatures. In particular, it is noticed that:

a: peaks of the weight-loss speed $\partial w/\partial t$ are always relatively broad;

b: the function $ln\frac{\partial w(t)}{\partial t}$ plotted vs $1/T$ (having converted T in Kelvin) has the same trend regardless of the sample and, moreover, is defined over all the spanned T-range (see graphics 9.6);

c: plotting $ln\frac{\partial w(t)}{\partial t}$ against $ln\, w(t)$, no definite pseudo-order is recognized, and the signal trend let otherwise surmise the same implicit dependence of w on T.

Then it is not possible to identify a sublimation (or evaporation) 'activation energy' closely correlated to the chemical composition of samples themselves, because the process proceeds in the same fashion at *any* temperature, and its velocity increases just approaching the threshold represented by the melting (or boiling) point, which is the true distinctive feature in this regard (same Fig. 9.6).

At the same time, the poor stability of the samples at low temperatures prevents to discriminate between the sensible and latent heat contribution: more specifically, writing an expansion of the integrated calorimetric signal q (expressed in W/g) as:

$$q(t)\Delta t \;=\; \Delta h \;=\; \frac{\partial h}{\partial T}\Delta T + \frac{\partial h}{\partial w}\Delta w \;=\; c_p\Delta T + \lambda\Delta w \tag{9.2}$$

[3]This is a characteristic of the acetontrile-water mixture.

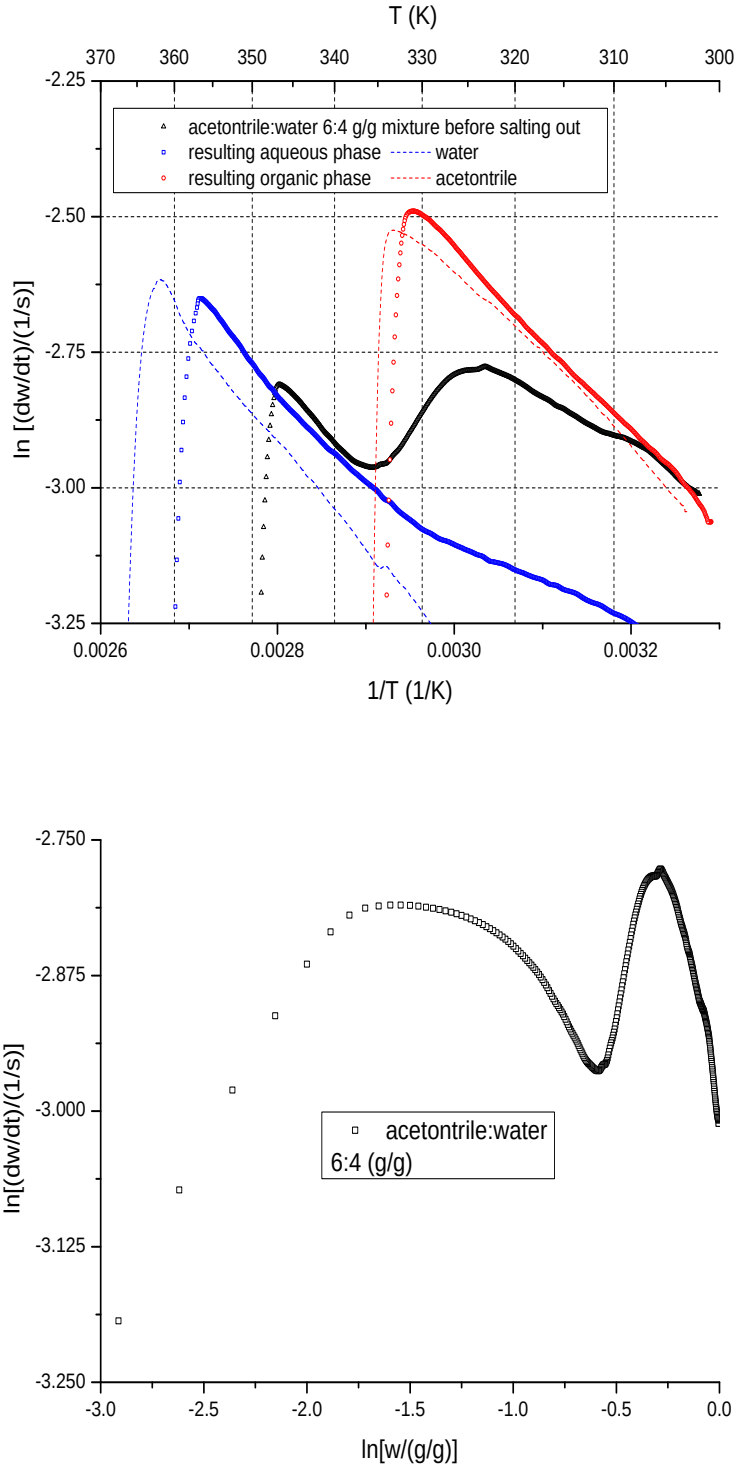

Figure 9.6: Separate representations of the quantity: $ln\frac{\partial w}{\partial}$ as $\frac{E}{T} + a\,ln\,w$: the first term (up) has the same shape for any sample, while the second (bottom) looks as not independent.

Range	$0.8 < w < 1$		$0.95 < w < 1$		$0.1 < w < 0.2$	
Model DF		2		2		2
Error DF		569		272		43
Total DF		571		274		45
F-Value		1.5×10^{13}		8.1×10^{6}		2.5×10^{8}
Δh_{tot} (J/g)	-1389.17	$\pm$ 0.5753	-1451.33	$\pm$ 6.733	-1911.41	$\pm$ 15.084
c_p (J/g°C)	-2.53	$\pm$ 0.0024	-2.38	$\pm$ 0.0171	2.06	$\pm$ 0.1467
λ (J/g)	1471.85	$\pm$ 0.4879	1529.18	$\pm$ 6.1691	1664.47	$\pm$ 2.8719

Table 9.2: Analysis of the sensible and latent heat contributions in the calorimetric signal of a water droplet according to eq. 9.2.

where T is in degrees Celsius (or Kelvin), w is the relative weight (in g/g) and c_p, λ are the specific heat and latent heat (in $\frac{J}{g^\circ C}$ and J/g respectively), it is found that $|c_p| << \lambda$ even in the range $w \leq 0.80$ (where $T < T_{sat}$)[4]. See for example the test results of Table 9.2 for the TGA analysis of a drop of water. The signal $q(t)$ is calculated automatically by the instrument software knowing: the thermal conductivity of the panes holder: and adding a correction for the convective dispersion for every gas-flow employed. The energy $\Delta h = \int_0^{\Delta t} q(t)dt$ is calculated once the data have been downloaded, performing the integration according to the trapezoid formula (Microcal OriginPro 8), then the unknown parameters of equation 9.2 are estimated performing a bi-linear regression (same software), under the verified assumption that they are nearly constant over limited ranges.

Notice that the picture doesn't change if the interpolation range is varied. This means that, even below the bubble point, the evaporation of the liquid (due to its negligible partial pressure in the carrier gas) is the dominant phenomenon in the energetic balance of the analysis. The negative impact of this fact is the very noisy signal resulting from the TGA instrument at low temperatures (when the evaporation is anyway slower, and thus the SNR low). The DSC machine always yields a good-shaped q trend, but doesn't provide any mass record.

This different behavior of the two instruments can be noticed by the fact that using the TGA with open pane the recorded latent heat for water increases apparently as the temperature rises, but seldom reaches the expected value of 2500 J/g, while the total released heat is in good accord with the literature when the DSC experiment is performed with the closed-pane (graph 9.7).

The analysis described can be applied also to the differential signal expanded as:

$$q(t) = \frac{\partial h}{\partial t} = c_p \frac{\partial T}{\partial t} + \lambda \frac{\partial w}{\partial t} \tag{9.3}$$

which in principle is an easier procedure, because the quantity $\frac{\partial T}{\partial t}$ is the temperature ramp fixed by the instrument, and the derivative $\frac{\partial w}{\partial t}$ is already calculated by its software (mixed-Euler formula). This method, nevertheless, is much less robust near the boiling points of the mixture, where the weight-loss rate changes much more rapidly than the weight itself and, on the other hand, the sample temperature varies very slowly, departing significantly by the assumed instrumental parameter.

[4]Note that c_p may assume negative values because, for liquid samples, the influence of the actual heat flow through the reference and measure panes is not negligible.

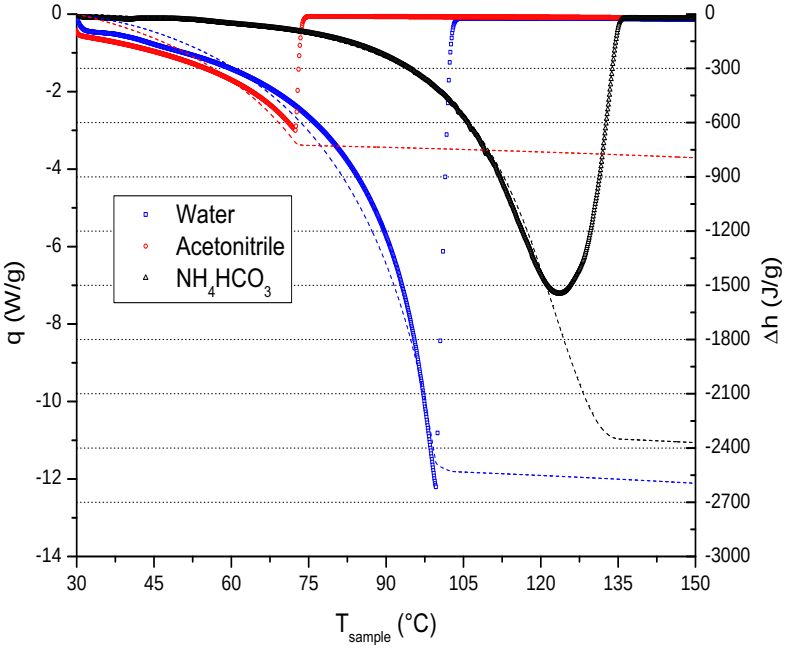

Figure 9.7: DSC signals for pure samples.

Signal shape and calibration

The differential analysis becomes a very useful qualitative and semi-quantitative tool just for the fact that it enhances discontinuities, making changes in the sample behavior or process regime become more visible. Moreover, since the noises affecting the thermal and weight signal share the same source (the early liquid samples evaporation determines also the instantaneous deviations $T_{sample} - T_{ref}$ because the latent heat contribution is dominant), considering the relative quantity $q/\frac{\partial w}{\partial t}$ becomes an effective way to reject the high-frequency and sampling noise (on times shorter than 2 seconds, with a 1 Hz acquisition protocol) and then have a reasonable estimation of $\lambda \simeq \frac{\partial h}{\partial t}$. The integral signal analysis (eq. 9.2) offers a smoother linear interpolation, because this low-pass filtering of the data is a more effective noise-rejection technique, but is less sensitive in identifying possible latent heat shifts.

These considerations can be visualized through Figures 9.8-9.9. Unlike the DSC closed-pan machine, the open-pan apparatus systematically underestimates the boiling points of acetonitrile and the overall enthalpy content of all samples (right to left); the coupling of the measured q and calculated $\frac{dw}{dt}$ is anyway useful to normalize the bumps in the signals and greatly enhances the impact of a λ-change on the data appearance (Figs. 9.9).

Unfortunately, the reliability of the DSC instrument in ascertaining the boiling points is not very useful to recognize differences in a sample's acetonitrile content lower than 10-15 % (due to the very shape of the Txy diagram), while the machine's accuracy yielding the total released heat is more valuable. Nonetheless, due also to the practical

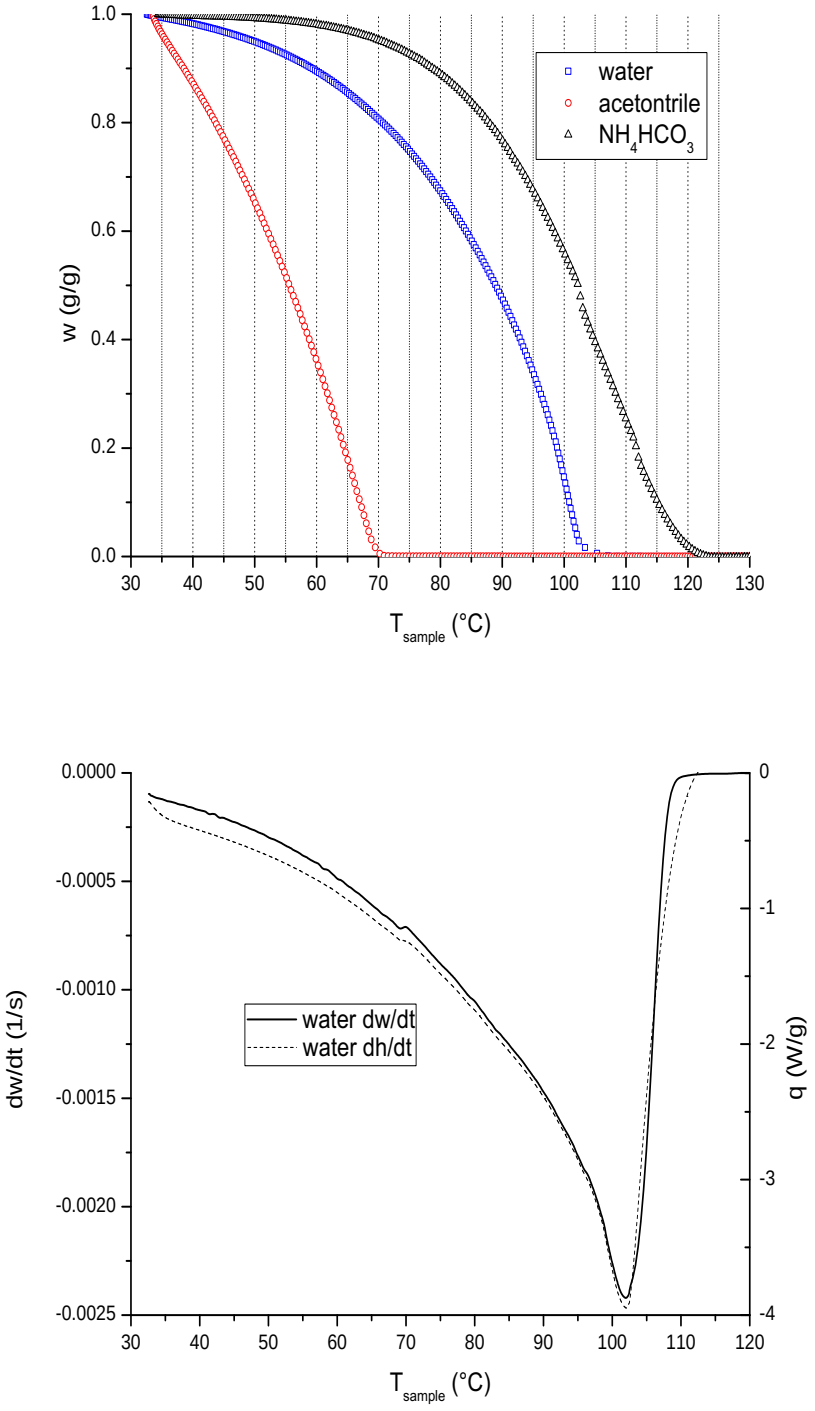

Figure 9.8: Calorimetry of pure samples.

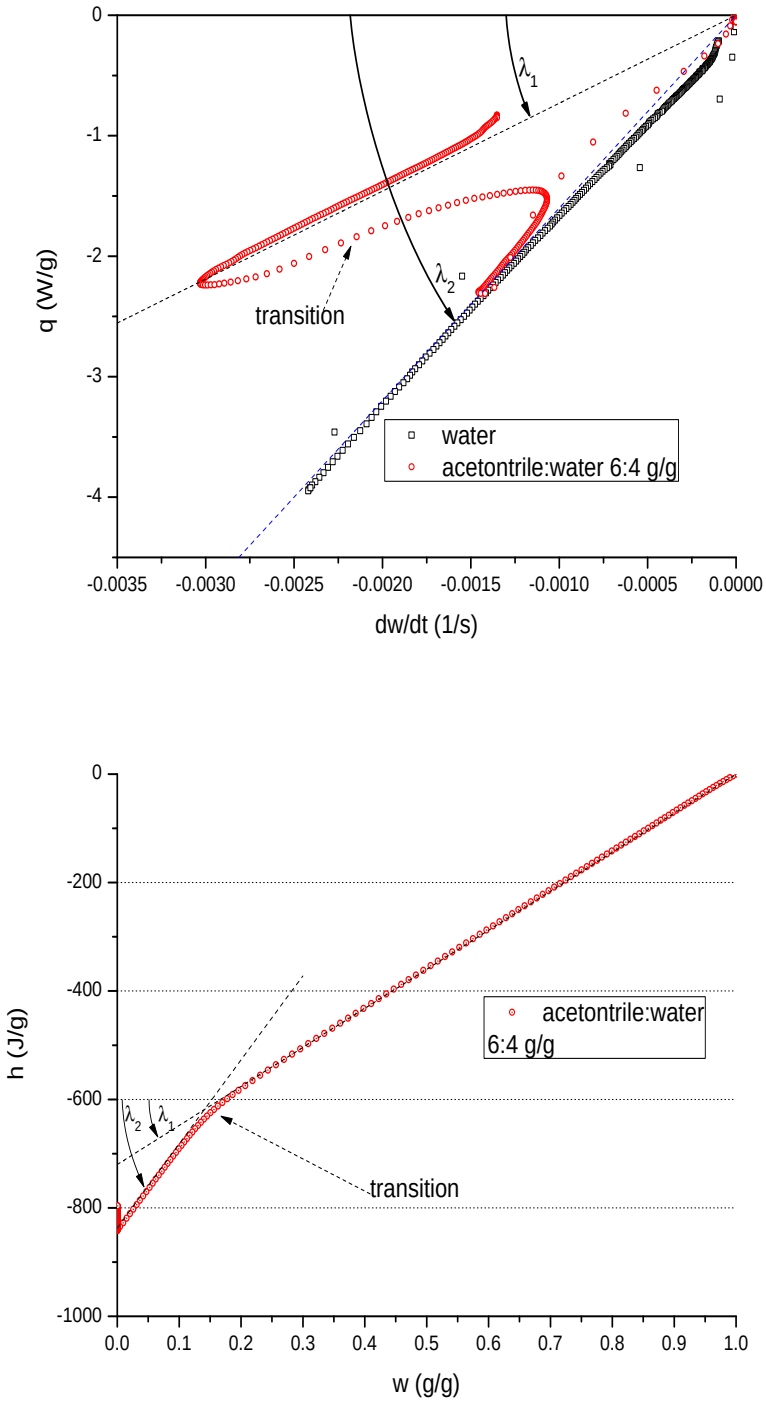

Figure 9.9: Latent heat and integrated heat for a 6:4 g/g acetontrile:water mixture.

management of the TGA/DSC instruments available[5] in the premises, the first has been preferred (whenever possible), due to the richer information derived from the coupled heat & mass signals.

Taking advantage of the energy calibration performed via DSC on one side, and of the fairly linear correlation of the TGA signals, the latter's data can be auto-calibrated finding and comparing the factors: $\frac{\Delta q}{\Delta(\partial w/\partial t)} : \lambda_{DSC,water}$ and $\frac{\Delta h}{\Delta w} : \lambda_{DSC,water}$ for the regions of the TGA signal clearly attributed to water's evaporation after the qualitative inspection. Samples that don't release *free* water are calibrated with the reference value $\lambda_{DSC,\,organic\,phase} \simeq \lambda_{azeotrope} \simeq 1000\,J/g$.

Signal interpolation

A TGA (or DSC) experiment can be considered as a micro-scale batch distillation with no reflux [200–202], that is described by the Rayleigh equation (being L the total liquid weight, and x, y^* the liquid-vapor acetonitrile mass fractions at equilibrium):

$$\frac{dL}{L} = \frac{dx}{y^* - x} \tag{9.4}$$

that can be integrated numerically (rectangle formula, fixing $dL \equiv 0.01$ and $L_i \equiv 1$)[6] yielding the equality:

$$lnL_f = \int_{x_i}^{0} \frac{dx}{y^*(x) - x} \tag{9.5}$$

that is a parametric function of the liquid fraction L_f (remaining when the acetonitrile has been stripped from the pan), for every starting acetonitrile fraction x_i, and can be represented in a graph like te one in figure 9.10:

In this way, retracing the data entry corresponding to the onset of the free water behavior (using graphical representations as those in Figure 9.8), the weight fraction of the initial sample still remaining at that point (upper x-axis in Fig. 9.10) can be correlated to the initial acetonitrile content of the mixture. This method has the advantage of being independent of the heat-value calibration factor needed to match TGA and DSC data, because resorts to the mass balance only.

As extracting the $w(x = 0)$ point from a $\Delta h/\Delta w$ representation (rather than from a $\Delta q/\frac{\Delta w}{\Delta t}$ one) is more practical, it is anyway convenient to use a calibration $h(w)$ curve for a direct comparison. Rewriting then the process energy balance as:

$$h_l(x)\,L + \Delta h_{exp} = h_l(x - dx)\,(L - dL) + h_v(y^*)dL \tag{9.6}$$

where Δh_{exp} is the heat duty recorded by the instruments any time a quantity dL of the sample is evaporated, under the assumption that the sensible heat flow is negligible. Rather than integrating the associated homogeneous equation: $\frac{dL}{L} = \frac{dh_l(x)}{\lambda(x)}$ and finding then parametric solutions fixing the boundary condition $h_{exp} = h_{DSC}$, it is more convenient to perform a step-wise calculation (Ms Excel) fixing $dL \equiv 0.01$ and calculating, for every x_i:

[5] A run of the second one is more expensive; moreover the machine underwent extended unscheduled maintenance right during this activity.

[6] The values of $y^*(x)$ are sampled from a polinomial fit of the VLE data.

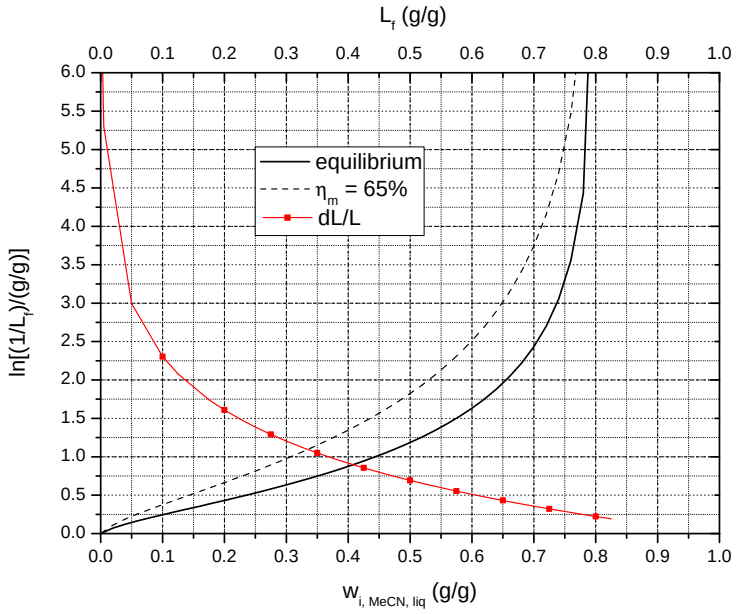

Figure 9.10: Integral representation of the right and left-hand sides of the Reyleigh equation for the acetonitrile-water system @ 1 atm (NRTL-RK model). The dashed curve has been obtained supposing that $y(x)/y^*(x) = \eta_M = 0.65$.

1) the quantities $y^*(x)$, $h_l(x)$, $h_v(y^*)$ from suitable interpolations of the NRTL-RK model;

2) the decrement dx according to equation 9.4, starting from $L_i \equiv 1$, then $h_l(x - dx)$;

3) the heat duty h_{exp} corresponding to a dL release (eq. 9.6);

4) the new values when L has reduced to $L - dL$ and x to $x - dx$, etc.

In this way the function $h_{exp}(L_f) = \Sigma_1^{w=L_f} \Delta h_{exp}$ can be tabulated and represented, for every x_i as in the graphics 9.11.

In this way it is not needed to use the nomogram 9.10. The fact that the quantity Δh_{exp} yielded by the TGA machine is different from that recorded by the DSC (which, in turn, is close to the calculated value but cannot be put in direct relation with the evaporated liquid) is just a minor issue, because the *shape* of the function $h_{exp}(w)$ is the same, so the horizontal extension of the steeper linear coda in the experimental and theoretical curves can be compared directly (as exemplified in Figure 9.11).

Once the apparent λ_{exp} for water or the azeotrope is estimated, anyway, the total heat released during a TGA run can be normalized as $h_{corr}(w) = h_{exp}(w)\frac{\lambda_{H_2O}}{\lambda_{exp}}$ and compared to the expected value via a calibration diagram such as the 9.12 one: for example, the test sample yielding the trend of graph 9.11-right has a recalibrated heat content of 1600 J/g ca., which matches closely the calculated value.

In this way, the acetonitrile content can be evaluated, for most of the sub-azeotropic mixtures obtained, averaging the x_i values retrieved from the diagrams 9.12, 9.11 and 9.10, provided they are consistent (otherwise, it is to one's experience to sort out the

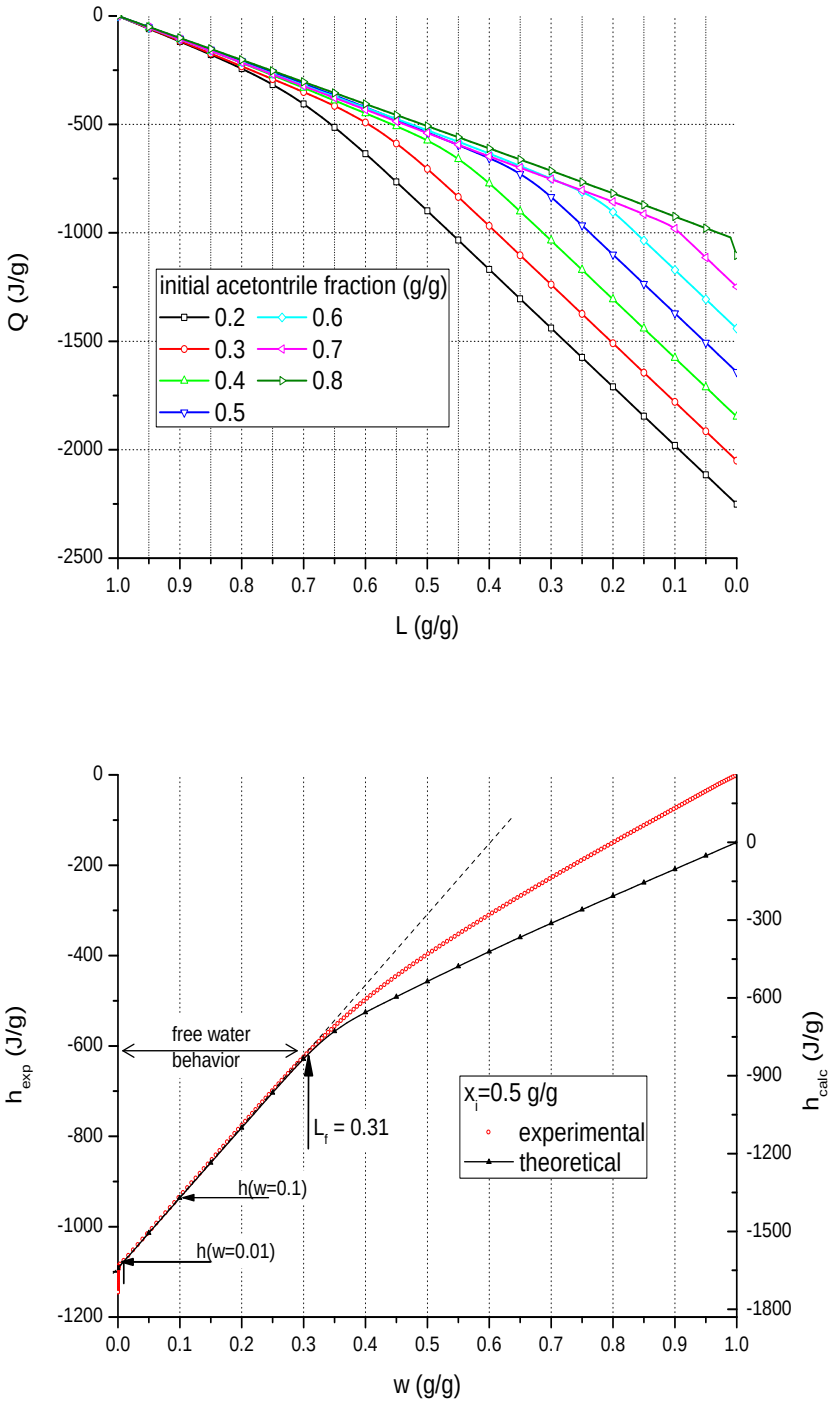

Figure 9.11: Diagrams correlating the total released heat to acetonitrile content, and y-scale re-calibration matching experimental and expected data around the x-axis pivot.

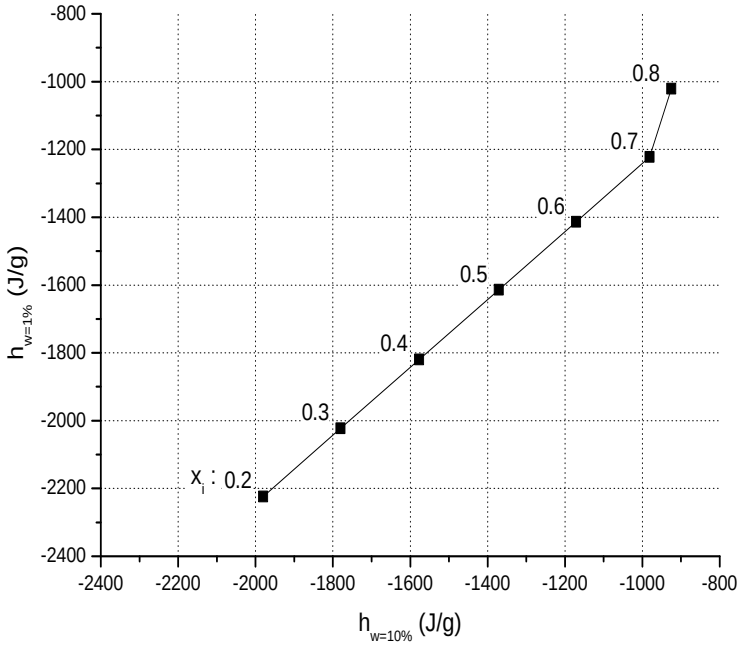

Figure 9.12: Diagram for for the correlation of released heat and initial acetonitrile content.

outlier). This method is not as accurate as the NMR, partly due to the actual non-equilibrium character of the evaporation from open-panes and partly to the non-negligible changes in the machine's response at this relatively low temperatures, slow rising ramps and very quick sample loss rates. The reliability of the data analysis can be improved evaporating a known mixture every 5-10 actual samples to have updated sets of calibration diagrams.

Salt Effect

The discussion so far is applicable to a binary mixture, but in principle it does not hold for the ternary mixture constituted by the aqueous phase. However, there are two peculiar features of the system under study that make possible a simplified analysis.

- first: the ammonium an bicarbonate ions solvated in an aqueous phase do not behave as the solid salt, but are actually evaporated from the sample before the saturation temperature is reached, both in the micro and bench-scale batch distillations - this is also what happens to the salt samples that undergo a temperature-ramp drying as in graphs 8.24;

- second: wet, dry and melted ammonium bicarbonate releases the same evaporation heat of a pure water sample (within the instruments sensitivity) over all its range of behaviors - this is shown in Figure 8.29 (DSC) and also in figure 9.13 (TGA).

In this context, one can assume that the total released heat $h_{exp}(w = 0.01)$ recorded

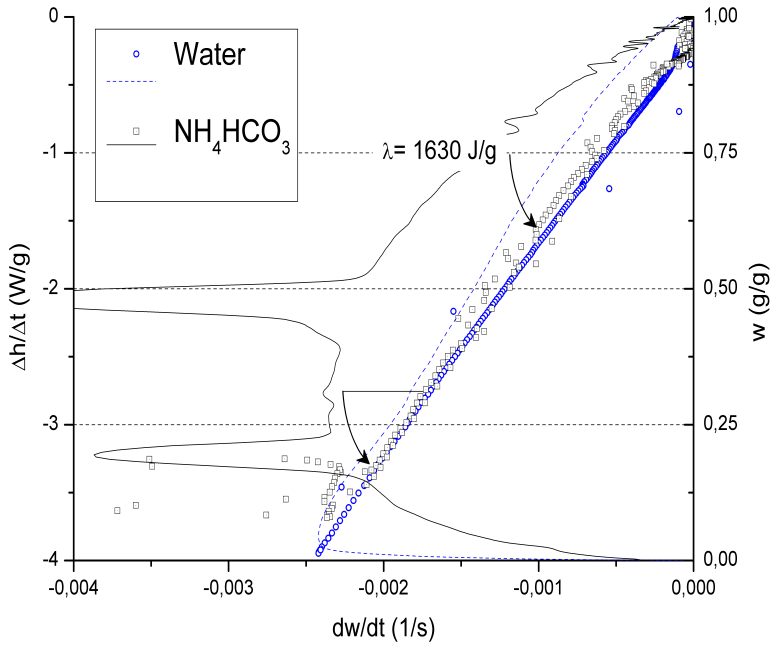

Figure 9.13: Comparison between the latent heat of pure ammonium bicarbonate and pure water.

during a TGA/DSC scan of a ternary mixture is equal to that of a binary acetonitrile-water system where the water fraction is apparently higher, but the acetonitrile fraction (on total) is the same.

On the other hand, the residual weight fraction $h_{exp}(w = L_f)$ where a sample starts to behave as free water remains more or less constant, because the solvated ions are converted to their neutral forms and evaporated just before, but the total acetonitrile fraction is apparently higher. This second assumption is verified for aqueous phases with a relatively high content of acetonitrile (e.g. ≥ 0.3), because in this case all the light species are lost within the saturation temperature of the acetonitrile-water azeotrope leaving enough water to develop a separated higher-temperature distillation regime.

Unfortunately, it has to be pointed out that a dedicated test revealed that the TGA analysis is not accurate enough to recognize systematically this phenomenon, and even the more sophisticated DSC machines yield only a qualitative information at the highest salt concentration reached (see Fig. 9.14, where are shown the integrated heats of four liquid samples saturated with salt at temperatures from 4 to 38 °C, which means covering a concentration span of 0.8 to 1.5 M - all the same, this method has been adopted for other mixtures [203]).

Nevertheless, considering the whole set of calorimetric runs, some insight on the phenomenon can be retrieved on a statistical ground. The parity plot 9.15 (left frame) shows the acetonitrile fractions (lower and higher) estimated by the released heat (according to the different calibration factors) or by the Rayleigh equation mass balance (at 100% or 65% evaporation efficiency), as a function of the value retrieved from the free-water

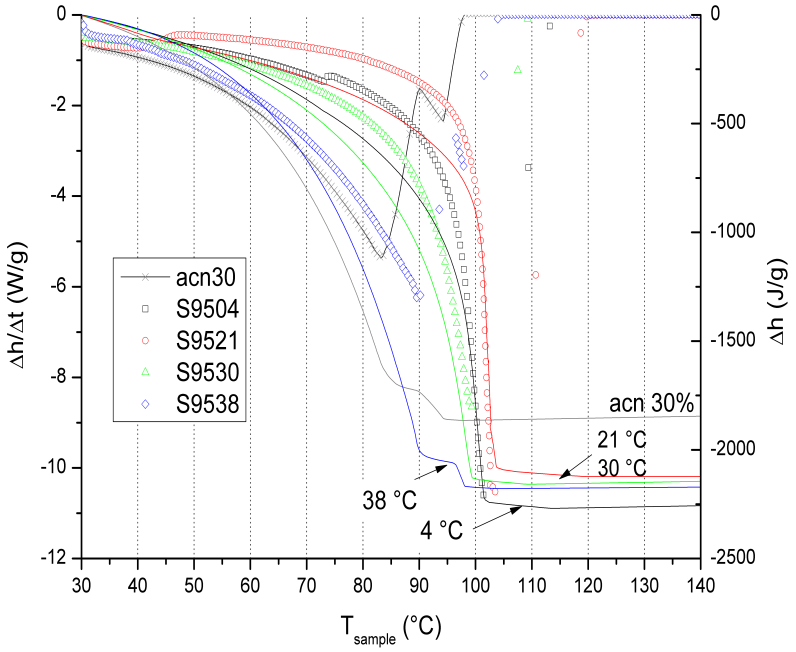

Figure 9.14: DSC response to the aqueous phase saturated with ammonium bicarbonate at different temperatures.

distillation onset. It can be noticed that the integral heat analysis yields generally lower values, hinting to the fact that the free water-point method actually accounts for an increased acetonitrile content; discounting the results coming from the organic phases (without salt), the described systematic bias of the salt-rich phases shows to be predominant (graph 9.15-right)

As the fork between the higher and lower registered heats depends critically on the calibration factor retrieved from the data, this effect must be sorted out. Basically, it is assumed that the part of the difference between the different data analysis methods: $\Delta w \equiv w_{acn(w_{tot}=L_f)} - w_{acn(\Delta h_{0.01})}$ (i.e. part of the spread of the cloud of points in Fig. 9.15-left below the parity line) comes from the distance $\nu \equiv \frac{1}{\lambda_{H_2O}} |\frac{\Delta h/\Delta t}{\Delta w/\Delta t} - \frac{\Delta h}{\Delta w}|$, so interpolating linearly :

$$\Delta w - a_1 \times \nu = a_0 + a_2 \times c$$

where c is the salt molar concentration retrieved independently by backtritration, one finds the results summarized in table 9.3, that highlight a positive correlation between Δw and the salt presence.

A synthetic comparison between the different techniques used is represented in graphic 9.16. It can be appreciated the generally good agreement between the NMR and calorimetric analysis: this latter suffers from a certain dispersion for the aqueous phases, due most likely for the sat-acetonitrile interplay. Also the hydrolysis-backtritration assay of the organics is reliable, though the procedure itself is more elaborate and depending on the operator.

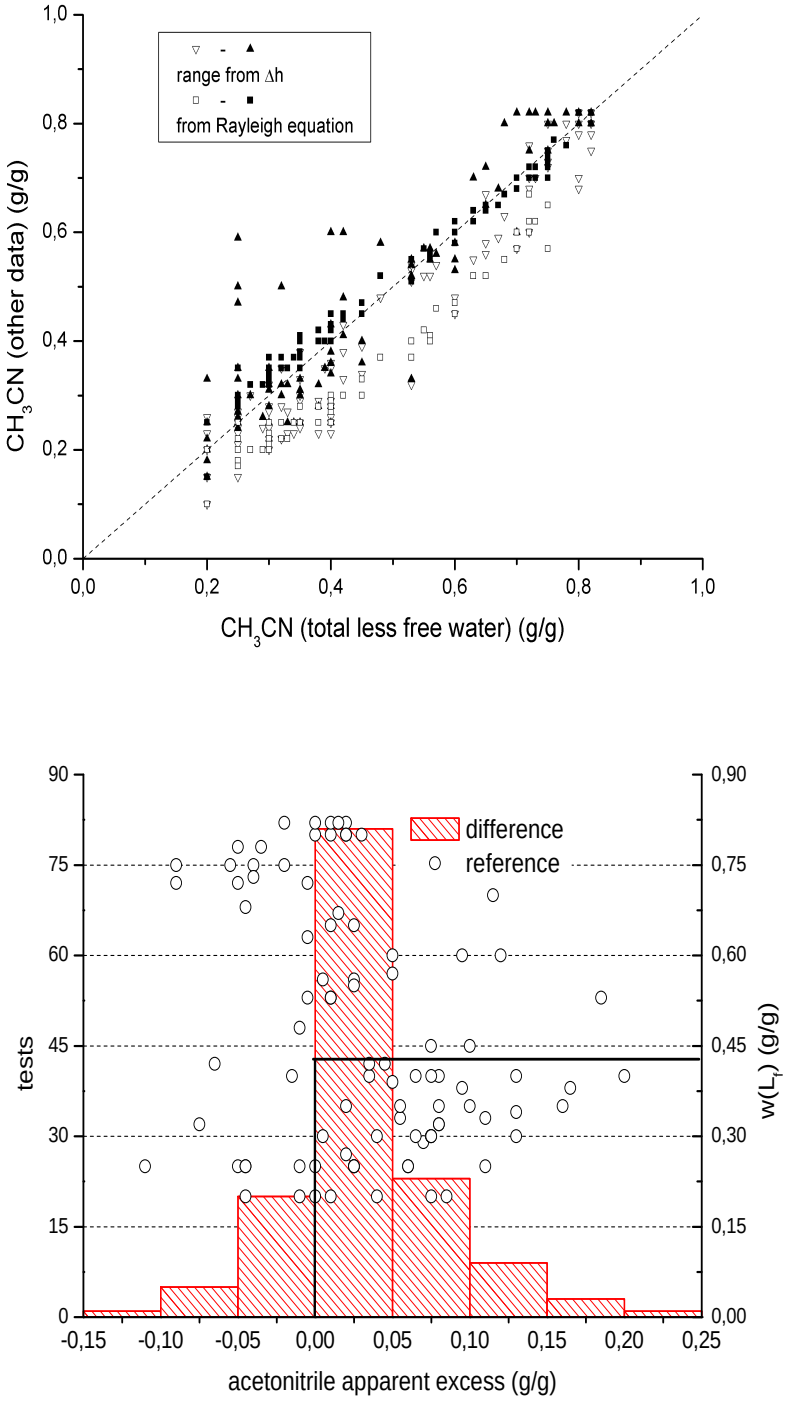

Figure 9.15: Up: comparison of the different ways (mass balance, filled marks - heat balance, void marks) of retrieving the acetonitrile content from calorimetric data; bottom: distribution of the difference between the mass-balance and heat-balance derived quantities.

Parameter	Value		Error
a_0	-0.0513		0.0209
a_1	0.0544		0.0239
a_2	0.0519		0.0113
	DF	Σres^2	$\Sigma res^2 / DF$	F Value
Model	2	0.0525	0.0263	12.94
Error	41	0.0832	0.0020	
Total	43	0.1357		

Table 9.3: Correlation between the salt content of a mixture and the acetonitrile fraction data dispersion.

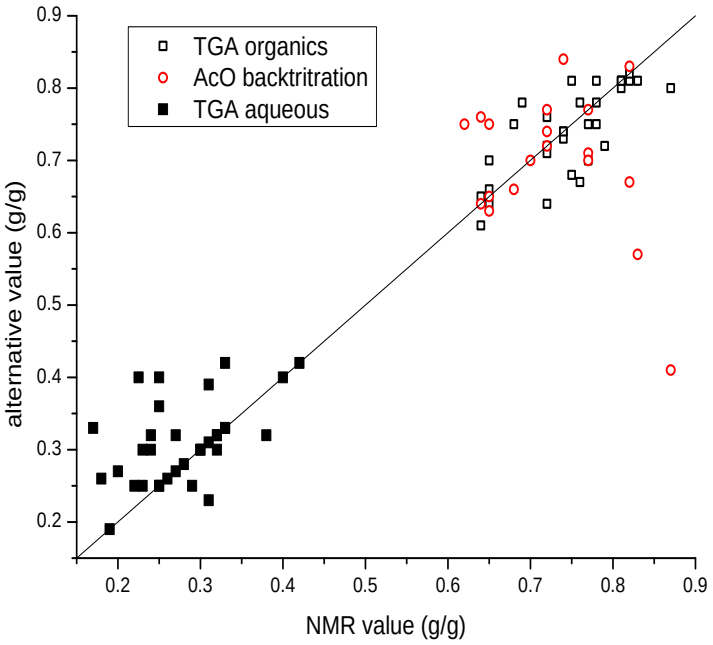

Figure 9.16: Response of three different analytical methods in quantifying the acetontrile content in water and in water plus ammonium bicarbonate solutions.

Part III

Supplementary Information

Appendix A

Streams and Duties Reports

The streams (and blocks) belonging to the processes are identified conventionally by a word of the type: AB-12-CD-34. The first two digits (1, 2) identify a plant section or the case-study, the second couple of digits (3, 4) numbers progressively the current. The general coding rules used throughout the process schemes are reported in the following Table A.1 for what concerns the alphabetic characters (AB-CD).

AB	**meaning**	**CD**	**meaning**
FR	Feed of reactants		
FT	Feed, Transformation		
SB	Separation of Byproducts	CS	Column, Stripper
SP	Separation of Products	CW	Column, Washer
SV,SW	Separation of Wastes	RK	Reactor with kinetic
QC	Auxiliaries, Cryogenic		
QW	Auxiliaries, Water		
TR	Transformation of Reactants	TA	Tube, atmospheric
TP	Transformation of Products	TP	Tube, pressurized

Table A.1: General scheme coding convention.

A.1 Ethanol Dehydration

Refer to the process schemes of section 1.3 for the stream names.

Stream	FR01TA09	FR01TA13	FR01TA15	TR01TA29	TR01TA17	TR01TA23	SP01TA31
Description							
Temp (°C)	25.00	96.03	360.00	318.78	256.41	278.99	300.00
Pres (bar)	1.20	1.20	1.20	0.99	1.15	1.08	0.99
Vapor (mol/mol)	0.00	0.83	1.00	1.00	1.00	1.00	1.00
Average MW (g/mol)	25.03	25.03	25.03	20.44	22.34	21.08	20.44
Mole Flows (kmol/h)	6592.43	6592.43	6592.43	8786.10	7384.76	8518.77	8786.10
Mass Flows (kg/h)							
TOTAL	165000.00	165000.00	165000.00	179568.62	165000.00	179568.62	179568.62
ETHANOL	75926.69	75926.69	75926.69	7820.60	38732.07	20104.16	7820.60
ACETLAD	0.00	0.00	0.00	0.51	0.08	0.42	0.51
ETOET	0.00	0.00	0.00	10.20	612.46	117.67	10.20
BUTYLEN	0.00	0.00	0.00	287.56	4.94	46.69	287.56
WATER	89073.31	89073.31	89073.31	125435.77	103418.54	120674.27	125435.77
CO	0.00	0.00	0.00	29.59	9.23	18.10	29.59
CO2	0.00	0.00	0.00	172.16	54.83	98.04	172.16
METHANE	0.00	0.00	0.00	79.48	25.27	45.88	79.48
H2	0.00	0.00	0.00	17.86	5.69	10.24	17.86
ETHYLENE	0.00	0.00	0.00	45714.90	22136.89	38453.16	45714.90
Mass Fractions							
ETHANOL	0.460	0.460	0.460	0.044	0.235	0.112	0.044
ACETLAD	0.000	0.000	0.000	0.000	0.000	0.000	0.000
ETOET	0.000	0.000	0.000	0.000	0.004	0.001	0.000
BUTYLEN	0.000	0.000	0.000	0.002	0.000	0.000	0.002
WATER	0.540	0.540	0.540	0.699	0.627	0.672	0.699
CO	0.000	0.000	0.000	0.000	0.000	0.000	0.000
CO2	0.000	0.000	0.000	0.001	0.000	0.001	0.001
METHANE	0.000	0.000	0.000	0.000	0.000	0.000	0.000
H2	0.000	0.000	0.000	0.000	0.000	0.000	0.000
ETHYLENE	0.000	0.000	0.000	0.255	0.134	0.214	0.255

Table A.2: Stream report for the reactive section.

Stream Description	SB02TA13	SB02TA14	SB02TA15	SB02TP21	SB02TP27	SB02TP31	QW01TA04	QW01TA08	QS01TA10
Temp (°C)	25.04	22.00	95.73	19.60	19.37	19.22	104.81	104.81	110.00
Pres (bar)	1.00	1.20	1.20	2.30	5.29	12.17	1.20	1.20	1.20
Vapor (mol/mol)	0.00	0.00	1.00	0.00	0.00	0.00	0.00	0.00	1.00
Average MW (g/mol)	18.64	18.67	26.49	19.95	23.16	30.07	18.02	18.02	18.02
Mole Flows (kmol/h)	7067.70	7127.10	550.00	40.77	11.69	6.94	6466.08	111.02	111.02
Mass Flows (kg/h)									
TOTAL	131764.28	133057.01	14568.62	813.49	270.60	208.64	116488.39	2000.00	2000.00
ETHANOL	7273.61	7636.07	7635.77	129.48	98.12	134.87	0.29	0.01	0.01
ACETLAD	0.22	0.25	0.25	0.01	0.01	0.02	0.00	0.00	0.00
ETOET	0.83	0.96	0.96	0.02	0.02	0.09	0.00	0.00	0.00
BUTYLEN	0.09	0.10	0.10	0.00	0.00	0.00	0.00	0.00	0.00
WATER	124468.73	125393.53	6905.44	683.49	171.63	69.68	116488.10	1999.99	1999.99
CO	0.00	0.00	0.00	0.00	0.00	0.00	0.00	0.00	0.00
CO2	0.54	0.63	0.63	0.01	0.02	0.06	0.00	0.00	0.00
METHANE	0.01	0.01	0.01	0.00	0.00	0.00	0.00	0.00	0.00
H2	0.00	0.00	0.00	0.00	0.00	0.00	0.00	0.00	0.00
ETHYLENE	20.26	25.46	25.46	0.48	0.79	3.93	0.00	0.00	0.00
Mass Fractions									
ETHANOL	0.055	0.057	0.524	0.159	0.363	0.646	0.000	0.000	0.000
ACETLAD	0.000	0.000	0.000	0.000	0.000	0.000	0.000	0.000	0.000
ETOET	0.000	0.000	0.000	0.000	0.000	0.000	0.000	0.000	0.000
BUTYLEN	0.000	0.000	0.000	0.000	0.000	0.000	0.000	0.000	0.000
WATER	0.945	0.942	0.474	0.840	0.634	0.334	1.000	1.000	1.000
CO	0.000	0.000	0.000	0.000	0.000	0.000	0.000	0.000	0.000
CO2	0.000	0.000	0.000	0.000	0.000	0.000	0.000	0.000	0.000
METHANE	0.000	0.000	0.000	0.000	0.000	0.000	0.000	0.000	0.000
H2	0.000	0.000	0.000	0.000	0.000	0.000	0.000	0.000	0.000
ETHYLENE	0.000	0.000	0.002	0.001	0.003	0.019	0.000	0.000	0.000

Table A.3: Stream report for the recycle section.

Description	SP01TA39	SP01TA41	SP01TA43	SP02TA45	SP02TP47	SP02TP53	SP02TP55	SP02TP61	SP02TP63	SP02TP67	SP02TP69	SP02TP71
Temp (°C)	85.00	55.00	25.00	25.04	92.60	19.60	88.31	19.37	92.06	19.22	100.91	20.00
Pres (bar)	0.99	0.99	0.99	1.00	2.30	2.30	5.29	5.29	12.17	12.17	27.98	27.98
Vapor (mol/mol)	0.49	0.22	0.20	1.00	1.00	1.00	1.00	1.00	1.00	1.00	1.00	0.99
Average MW (g/mol)	20.44	20.44	20.44	27.82	27.82	28.01	28.01	28.04	28.04	28.04	28.04	28.04
Mole Flows (kmol/h)	8786.10	8786.10	8786.16	1718.45	1718.45	1677.69	1677.69	1666.00	1666.00	1659.06	1659.06	1659.06
Mass Flows (kg/h)												
TOTAL	179568.62	179568.62	179570.43	47806.15	47806.15	46992.65	46992.65	46722.06	46722.06	46513.42	46513.42	46513.42
ETHANOL	7820.60	7820.60	7821.02	547.41	547.41	417.93	417.93	319.81	319.81	184.95	184.95	184.95
ACETLAD	0.51	0.51	0.51	0.30	0.30	0.29	0.29	0.28	0.28	0.26	0.26	0.26
ETOET	10.20	10.20	10.20	9.38	9.38	9.36	9.36	9.33	9.33	9.25	9.25	9.25
BUTYLEN	287.56	287.56	287.55	287.46	287.46	287.46	287.46	287.46	287.46	287.46	287.46	287.46
WATER	125435.77	125435.77	125435.57	966.84	966.84	283.35	283.35	111.72	111.72	42.04	42.04	42.04
CO	29.59	29.59	29.59	29.59	29.59	29.59	29.59	29.59	29.59	29.58	29.58	29.58
CO2	172.16	172.16	172.16	171.62	171.62	171.61	171.61	171.59	171.59	171.53	171.53	171.53
METHANE	79.48	79.48	79.48	79.47	79.47	79.47	79.47	79.47	79.47	79.47	79.47	79.47
H2	17.86	17.86	17.86	17.85	17.85	17.85	17.85	17.85	17.85	17.85	17.85	17.85
ETHYLENE	45714.90	45714.90	45716.48	45696.23	45696.23	45695.75	45695.75	45694.95	45694.95	45691.03	45691.03	45691.03
Mass Fractions												
ETHANOL	0.044	0.044	0.044	0.011	0.011	0.009	0.009	0.007	0.007	0.004	0.004	0.004
ACETLAD	0.000	0.000	0.000	0.000	0.000	0.000	0.000	0.000	0.000	0.000	0.000	0.000
ETOET	0.000	0.000	0.000	0.000	0.000	0.000	0.000	0.000	0.000	0.000	0.000	0.000
BUTYLEN	0.002	0.002	0.002	0.006	0.006	0.006	0.006	0.006	0.006	0.006	0.006	0.006
WATER	0.699	0.699	0.699	0.020	0.020	0.006	0.006	0.002	0.002	0.001	0.001	0.001
CO	0.000	0.000	0.000	0.001	0.001	0.001	0.001	0.001	0.001	0.001	0.001	0.001
CO2	0.001	0.001	0.001	0.004	0.004	0.004	0.004	0.004	0.004	0.004	0.004	0.004
METHANE	0.000	0.000	0.000	0.002	0.002	0.002	0.002	0.002	0.002	0.002	0.002	0.002
H2	0.000	0.000	0.000	0.000	0.000	0.000	0.000	0.000	0.000	0.000	0.000	0.000
ETHYLENE	0.255	0.255	0.255	0.956	0.956	0.972	0.972	0.978	0.978	0.982	0.982	0.982

Table A.4: Stream report for the water condensation section.

Stream Description	SP03TP10	SP03TP12	SP03TA14	SP03TA40	SP03TA42	SP03TP50	SP03TP20	SW03TA15
Temp (°C)	43.49	93.19	85.15	113.81	69.08	70.17	69.70	110.13
Pres (bar)	27.00	27.00	1.10	1.10	1.10	27.00	27.00	1.10
Vapor (mol/mol)	0.00	0.00	0.01	0.00	0.00	0.00	1.00	1.00
Average MW (g/mol)	22.18	22.17	22.12	21.01	21.01	21.40	27.89	20.32
Mole Flows (kmol/h)	292.28	292.42	293.02	313.32	313.32	284.31	2220.26	93.09
Mass Flows (kg/h)								
TOTAL	6481.48	6481.48	6481.48	6581.63	6581.63	6083.47	61918.62	1891.37
ETHANOL	184.95	184.95	184.95	0.00	0.00	0.00	0.00	184.95
ACETLAD	0.13	0.13	0.13	0.00	0.00	0.00	17.52	0.13
ETOET	0.47	0.47	0.47	0.00	0.00	0.00	55.76	0.47
BUTYLEN	0.04	0.04	0.04	0.00	0.00	0.00	383.13	0.04
WATER	4946.90	4949.40	4960.20	5477.21	5477.29	4950.34	396.59	1525.56
CO	0.00	0.00	0.00	0.00	0.00	0.00	39.43	0.00
CO2	0.44	6.55	32.95	0.00	0.00	0.00	19.13	158.12
METHANE	0.01	0.01	0.01	0.00	0.00	0.00	105.92	0.01
H2	0.00	0.00	0.00	0.00	0.00	0.00	23.80	0.00
ETHYLENE	22.07	22.07	22.07	0.00	0.00	0.00	60877.11	22.07
MDEA	646.74	681.24	753.54	1097.66	1096.99	1126.79	0.23	0.00
H3O+	0.00	0.00	0.00	0.00	0.00	0.00	0.00	0.00
OH-	0.00	0.00	0.01	0.22	0.14	0.14	0.00	0.00
HCO3-	207.10	207.85	171.67	1.56	0.96	1.07	0.00	0.00
CO3–	12.93	3.87	3.46	0.08	0.67	0.40	0.00	0.00
MDEA+	459.68	424.88	351.98	4.91	5.58	4.72	0.00	0.00
Mass Fractions								
ETHANOL	0.029	0.029	0.029	0.000	0.000	0.000	0.000	0.098
ACETLAD	0.000	0.000	0.000	0.000	0.000	0.000	0.000	0.000
ETOET	0.000	0.000	0.000	0.000	0.000	0.000	0.001	0.000
BUTYLEN	0.000	0.000	0.000	0.000	0.000	0.000	0.006	0.000
WATER	0.763	0.764	0.765	0.832	0.832	0.814	0.006	0.807
CO	0.000	0.000	0.000	0.000	0.000	0.000	0.001	0.000
CO2	6.86E-05	1.01E-03	5.08E-03	7.18E-08	2.08E-08	1.33E-08	3.09E-04	8.36E-02
METHANE	0.000	0.000	0.000	0.000	0.000	0.000	0.002	0.000
H2	0.000	0.000	0.000	0.000	0.000	0.000	0.000	0.000
ETHYLENE	0.003	0.003	0.003	0.000	0.000	0.000	0.983	0.012
MDEA	9.98E-02	1.05E-01	1.16E-01	1.67E-01	1.67E-01	1.85E-01	3.65E-06	3.56E-11
H3O+	1.76E-10	3.93E-10	4.19E-10	1.19E-11	1.50E-12	3.01E-12	0.00E+00	0.00E+00
OH-	2.70E-07	5.51E-07	8.76E-07	3.27E-05	2.19E-05	2.35E-05	0.00E+00	0.00E+00
HCO3-	3.20E-02	3.21E-02	2.65E-02	2.37E-04	1.46E-04	1.75E-04	0.00E+00	0.00E+00
CO3–	2.00E-03	5.97E-04	5.33E-04	1.18E-05	1.01E-04	6.61E-05	0.00E+00	0.00E+00
MDEA+	7.09E-02	6.56E-02	5.43E-02	7.46E-04	8.48E-04	7.76E-04	0.00E+00	0.00E+00

Table A.5: Stream report for the CO_2 capture section.

Stream Description	SP04TP01	SP04TP10	SP04TP12	SP04TP13	SP04TP15	SP04TP21	SP04TP40	SP04TP41	SP04TP44	SP04TP50
Temp (°C)	25.00	21.28	21.28	21.28	14.63	14.65	21.28	14.65	242.85	100.00
Pres (bar)	27.00	5.50	5.50	5.50	1.50	1.50	5.50	1.50	27.50	27.50
Vapor (mol/mol)	0.98	0.99	1.00	0.96	0.97	0.97	1.00	0.97	1.00	0.99
Average MW (g/mol)	27.89	27.89	27.97	27.66	27.64	27.64	27.97	27.64	27.64	27.65
Mole Flows (kmol/h)	2220.26	2220.26	1647.82	572.44	572.12	572.12	1647.82	572.12	572.18	571.81
Mass Flows (kg/h)										
TOTAL	61918.62	61918.62	46086.39	15832.23	15815.84	15815.84	46086.39	15815.84	15817.63	15810.77
ETHANOL	0.00	0.00	0.00	0.00	0.00	0.00	0.00	0.00	0.00	0.00
ACETLAD	17.52	17.52	0.00	17.52	0.87	0.87	0.00	0.87	0.90	17.40
ETOET	55.76	55.76	0.00	55.76	52.77	52.77	0.00	52.77	52.87	46.98
BUTYLEN	383.13	383.13	287.35	95.78	95.78	95.78	287.35	95.78	95.78	95.71
WATER	396.59	396.59	0.00	396.59	395.78	395.78	0.00	395.78	396.47	394.11
CO	39.43	39.43	29.57	9.86	9.86	9.86	29.57	9.86	9.86	9.85
CO2	19.13	19.13	14.35	4.78	5.14	5.14	14.35	5.14	6.12	5.95
METHANE	105.92	105.92	79.44	26.48	26.48	26.48	79.44	26.48	26.48	26.46
H2	23.80	23.80	17.85	5.95	5.95	5.95	17.85	5.95	5.95	5.94
ETHYLENE	60877.11	60877.11	45657.83	15219.28	15222.99	15222.99	45657.83	15222.99	15222.99	15208.15
Mass Fractions										
ETHANOL	0.000	0.000	0.000	0.000	0.000	0.000	0.000	0.000	0.000	0.000
ACETLAD	0.000	0.000	0.000	0.001	0.000	0.000	0.000	0.000	0.000	0.001
ETOET	0.001	0.001	0.000	0.004	0.003	0.003	0.000	0.003	0.003	0.003
BUTYLEN	0.006	0.006	0.006	0.006	0.006	0.006	0.006	0.006	0.006	0.006
WATER	0.006	0.006	0.000	0.025	0.025	0.025	0.000	0.025	0.025	0.025
CO	0.001	0.001	0.001	0.001	0.001	0.001	0.001	0.001	0.001	0.001
CO2	0.000	0.000	0.000	0.000	0.000	0.000	0.000	0.000	0.000	0.000
METHANE	0.002	0.002	0.002	0.002	0.002	0.002	0.002	0.002	0.002	0.002
H2	0.000	0.000	0.000	0.000	0.000	0.000	0.000	0.000	0.000	0.000
ETHYLENE	0.983	0.983	0.991	0.961	0.963	0.963	0.991	0.963	0.962	0.962

Table A.6: Stream report for the PSA section.

Stream Description	SP05FR00	SP05FR01	SP05TP01	SP05TP03	SP05TP05	SP05TP07	SP05TP10	SP05TP11
Temp (°C)	-103.14	-231.71	-13.72	-14.43	-62.01	-51.10	-70.54	-103.37
Pres (bar)	1.05	1.05	5.50	5.00	5.00	5.00	5.10	1.05
Vapor (mol/mol)	0.00	0.00	1.00	1.00	0.00	0.00	0.21	0.36
Average MW (g/mol)	28.05	27.56	27.97	27.97	28.03	35.24	28.03	28.03
Mole Flows (kmol/h)	178.23	1046.34	1647.82	1647.82	1432.48	20.00	1432.48	1432.48
Mass Flows (kg/h)								
TOTAL	5000.00	28832.54	46086.39	46086.39	40156.94	704.72	40156.94	40156.94
ETHANOL	0.00	0.00	0.00	0.00	0.00	0.00	0.00	0.00
ACETLAD	0.00	0.00	0.00	0.00	0.00	0.00	0.00	0.00
ETOET	0.00	0.00	0.00	0.00	0.00	0.00	0.00	0.00
BUTYLEN	0.00	0.00	287.35	287.35	0.00	287.35	0.00	0.00
WATER	0.00	0.00	0.00	0.00	0.00	0.00	0.00	0.00
CO	0.00	201.09	29.57	29.57	13.60	0.02	13.60	13.60
CO2	0.00	0.00	14.35	14.35	12.48	0.10	12.48	12.48
METHANE	0.00	552.97	79.44	79.44	34.70	0.07	34.70	34.70
H2	0.00	8.29	17.85	17.85	0.63	0.00	0.63	0.63
ETHYLENE	5000.00	28070.19	45657.83	45657.83	40095.52	417.17	40095.52	40095.52
Mass Fractions								
ETHANOL	0.000	0.000	0.000	0.000	0.000	0.000	0.000	0.000
ACETLAD	0.000	0.000	0.000	0.000	0.000	0.000	0.000	0.000
ETOET	0.000	0.000	0.000	0.000	0.000	0.000	0.000	0.000
BUTYLEN	0.000	0.000	0.006	0.006	0.000	0.408	0.000	0.000
WATER	0.000	0.000	0.000	0.000	0.000	0.000	0.000	0.000
CO	0.00E+00	6.97E-03	6.42E-04	6.42E-04	3.39E-04	3.11E-05	3.39E-04	3.39E-04
CO2	0.00E+00	7.61E-08	3.11E-04	3.11E-04	3.11E-04	1.45E-04	3.11E-04	3.11E-04
METHANE	0.00E+00	1.92E-02	1.72E-03	1.72E-03	8.64E-04	1.04E-04	8.64E-04	8.64E-04
H2	0.00E+00	2.87E-04	3.87E-04	3.87E-04	1.56E-05	1.23E-06	1.56E-05	1.56E-05
ETHYLENE	1.000	0.974	0.991	0.991	0.998	0.592	0.998	0.998

Table A.7: Stream report for the cryogenic section.

Steam Description	SP05TP12	SP05TP14	SP05TP15	SW05TP06	SW05TP08	SW05TP10	SW05TP12
Temp (°C)	-83.00	-103.32	-103.28	-62.01	-104.21	-51.54	-104.00
Pres (bar)	1.05	1.05	1.05	5.00	1.05	2.50	1.05
Vapor (mol/mol)	1.00	0.00	1.00	1.00	1.00	1.00	1.00
Average MW (g/mol)	28.03	28.06	28.06	26.75	28.02	28.02	27.56
Mole Flow (kmol/h)	1432.48	1365.58	1365.58	195.34	1507.56	1507.56	68.19
Mass Flows (kg/h)							
TOTAL	40156.94	38311.60	38311.60	5224.73	42240.07	42240.07	1879.53
ETHANOL	0.00	0.00	0.00	0.00	0.00	0.00	0.00
ACETLAD	0.00	0.00	0.00	0.00	0.00	0.00	0.00
ETOET	0.00	0.00	0.00	0.00	0.00	0.00	0.00
BUTYLEN	0.00	0.00	0.00	0.00	0.00	0.00	0.00
WATER	0.00	0.00	0.00	0.00	0.00	0.00	0.00
CO	13.60	1.38	1.38	15.95	35.55	35.55	11.21
CO2	12.48	8.07	8.07	1.76	0.12	0.12	0.00
METHANE	34.70	1.27	1.27	44.66	59.61	59.61	33.73
H2	0.63	0.00	0.00	17.22	0.63	0.63	0.63
ETHYLENE	40095.52	38300.88	38300.88	5145.14	42144.17	42144.17	1833.96
Mass Fractions							
ETHANOL	0.000	0.000	0.000	0.000	0.000	0.000	0.000
ACETLAD	0.000	0.000	0.000	0.000	0.000	0.000	0.000
ETOET	0.000	0.000	0.000	0.000	0.000	0.000	0.000
BUTYLEN	0.000	0.000	0.000	0.000	0.000	0.000	0.000
WATER	0.000	0.000	0.000	0.000	0.000	0.000	0.000
CO	3.39E-04	3.61E-05	3.61E-05	3.05E-03	8.42E-04	8.42E-04	5.96E-03
CO2	3.11E-04	2.11E-04	2.11E-04	3.37E-04	2.74E-06	2.74E-06	7.92E-07
METHANE	8.64E-04	3.31E-05	3.31E-05	8.55E-03	1.41E-03	1.41E-03	1.79E-02
H2	1.56E-05	5.72E-09	5.72E-09	3.30E-03	1.49E-05	1.49E-05	3.33E-04
ETHYLENE	0.998	1.000	1.000	0.985	0.998	0.998	0.976

Table A.8: Stream report for the cryogenic section (continued).

Stream	**Q** (kW)	**Tin** (°C)	**Tout** (°C)	Note
stream 1	6975	25	65	feed preheat
stream 2	22885	65	87.5	feed boil1
stream 3	372	87.5	88.5	feed boil2
stream 4	19997	87.5	91.5	feed boil3
stream 5	1330	91.5	92.5	feed boil4
stream 6	24086	92.5	97.5	feed boil 5
stream 7	24145	97.5	360	feed heat
stream 8	11219	244	350	2nd stage reheat
stream 9	1961	279	298	3rd stage reheat 1
stream 10	5670	298	350	3rd stage reheat 2
stream 11	1961	318	300	prod cool 1
stream 12	19997	299	99	prod cool 2
stream 13	372	99	95	prod cond 1 (still above dwpt)
stream 14	13700	95	91	prod cond 2
stream 15	10000	91	90	prod cond 3
stream 16	53119	90	55	prod cond 4
stream 17	8810	55	25	prod cond 5
stream 18	2096	93	20	cmpr1 cool
stream 19	1557	88	20	cmpr2 cool
stream 20	1474	92	20	cmpr3 cool
stream 21	1405	101	20	cmpr4 cool
stream 22	307	44	93	mdea preheat
stream 23	307	114	70	mdea cooldown
stream 24	21	111	110	stripper condenser
stream 25	1330	234	100	psa recycle
stream 26	979	71	25	psa cooldown
stream 27	807	21	-14	crio precool
stream 28	5625	-61	-62	crio condens
stream 29	807	-72	-71	cio revap
stream 30	3738	-103	-83	crio2 preheat
stream 31	6200	-51	-104	crio2 condens
stream 32	1253	105	110	stripper steam

Table A.9: Fluid List relevant to the assessment of the energetic balances.

A.2 Ethanol Reforming for Hydrogen Production

Stream reports for the ethanol steam reforming process: refer to section 1.3.

Stream	FR13TP03	FR13TP05	FR13TP07	FR13TP09	FR13TP60
Description					
Temp (°C)	50.00	148.25	425.88	470.00	25.00
Pres (bar)	12.20	12.20	12.20	12.20	1.20
Vapor (mol/mol)	0.00	0.00	1.00	1.00	0.00
Average MW (g/mol)	25.03	25.03	25.03	25.03	18.17
Mass Flows (kg/h)					
TOTAL	10000.00	10000.00	10000.00	10000.00	3000.00
ETHANOL	4601.62	4601.62	4601.62	4601.62	0.00
WATER	5398.38	5398.38	5398.38	5398.38	2969.97
METHANE	0.00	0.00	0.00	0.00	0.00
CO2	0.00	0.00	0.00	0.00	0.00
CO	0.00	0.00	0.00	0.00	0.00
HYDROGEN	0.00	0.00	0.00	0.00	0.00
OXYGEN	0.00	0.00	0.00	0.00	0.00
NITROGEN	0.00	0.00	0.00	0.00	0.00
ACETALD	0.00	0.00	0.00	0.00	0.00
Mass Fractions					
ETHANOL	0.46	0.46	0.46	0.46	0.00
WATER	0.54	0.54	0.54	0.54	0.99
METHANE	0.00	0.00	0.00	0.00	0.00
CO2	0.00	0.00	0.00	0.00	0.00
CO	0.00	0.00	0.00	0.00	0.00
HYDROGEN	0.00	0.00	0.00	0.00	0.00
OXYGEN	0.00	0.00	0.00	0.00	0.00
NITROGEN	0.00	0.00	0.00	0.00	0.00
ACETALD	0.00	0.00	0.00	0.00	0.00

Table A.10: Feeding streams.

Stream	TP13TP23	TP13TP25	TP13TP27	TP13TP29	TP13TP31	TR13TP11	TR13TP13	TR13TP15	TR13TP17	TR13TP19	TR13TP21
Description											
Temp (°C)	255.81	100.00	99.08	85.00	84.02	517.30	537.25	502.34	380.00	394.17	220.00
Pres (bar)	11.62	11.62	11.62	11.62	11.62	12.19	12.14	11.96	11.96	11.86	11.86
Vapor (mol/mol)	1.00	0.98	1.00	0.96	1.00	1.00	1.00	1.00	1.00	1.00	1.00
Average MW (g/mol)	13.53	13.53	13.43	13.43	13.23	22.66	16.34	13.69	13.69	13.53	13.53
Mass Flows (kg/h)											
TOTAL	10000.00	10000.00	9723.68	9723.68	9194.44	10000.00	10000.00	10000.00	10000.00	10000.00	10000.00
ETHANOL	181.69	181.69	178.19	178.19	166.49	3258.28	1087.24	276.59	276.59	181.69	181.69
WATER	1409.68	1409.68	1137.19	1137.19	620.38	5180.21	3419.67	2289.21	2289.21	1818.44	1818.44
METHANE	353.07	353.07	353.07	353.07	353.07	175.45	620.83	346.94	346.94	353.07	353.07
CO2	6490.27	6490.27	6489.96	6489.96	6489.23	508.07	3402.81	4432.32	4432.32	5491.71	5491.71
CO	627.47	627.47	627.47	627.47	627.46	14.68	739.79	1811.17	1811.17	1263.01	1263.01
HYDROGEN	937.82	937.82	937.81	937.81	937.81	85.48	506.29	826.94	826.94	892.08	892.08
OXYGEN	0.00	0.00	0.00	0.00	0.00	0.00	0.00	0.00	0.00	0.00	0.00
NITROGEN	0.00	0.00	0.00	0.00	0.00	0.00	0.00	0.00	0.00	0.00	0.00
ACETALD	0.00	0.00	0.00	0.00	0.00	777.84	223.37	16.83	16.83	0.00	0.00
Mass Fractions											
ETHANOL	0.02	0.02	0.02	0.02	0.02	0.33	0.11	0.03	0.03	0.02	0.02
WATER	0.14	0.14	0.12	0.12	0.07	0.52	0.34	0.23	0.23	0.18	0.18
METHANE	0.04	0.04	0.04	0.04	0.04	0.02	0.06	0.03	0.03	0.04	0.04
CO2	0.65	0.65	0.67	0.67	0.71	0.05	0.34	0.44	0.44	0.55	0.55
CO	0.06	0.06	0.06	0.06	0.07	0.00	0.07	0.18	0.18	0.13	0.13
HYDROGEN	0.09	0.09	0.10	0.10	0.10	0.01	0.05	0.08	0.08	0.09	0.09
OXYGEN	0.00	0.00	0.00	0.00	0.00	0.00	0.00	0.00	0.00	0.00	0.00
NITROGEN	0.00	0.00	0.00	0.00	0.00	0.00	0.00	0.00	0.00	0.00	0.00
ACETALD	0.00	0.00	0.00	0.00	0.00	0.08	0.02	0.00	0.00	0.00	0.00

Table A.11: Reactive Section (continued).

Stream Description	SB13TP01	SB13TP61	SB13TP63	SB13TP79	SP13TP33	SP13TP35	SP13TP37	SP13TP39	SP13TP41	SP13TP43	SP13TP51	SP13TP52
Temp (°C)	174.95	98.94	73.00	76.76	88.15	147.99	143.97	99.75	60.00	60.00	77.17	86.16
Pres (bar)	15.00	1.10	1.10	1.10	11.62	18.00	18.00	18.00	18.00	18.00	18.00	18.00
Vapor (mol/mol)	1.00	1.00	1.00	1.00	1.00	1.00	1.00	1.00	0.96	1.00	1.00	0.00
Average MW (g/mol)	29.41	27.94	34.74	10.13	13.23	13.23	13.23	13.23	13.23	12.99	5.18	27.57
Mass Flows (kg/h)												
TOTAL	29.47	6572.72	2343.83	2100.67	9194.44	9194.44	9194.44	9194.44	9194.44	8670.53	2753.98	88916.55
ETHANOL	16.32	120.63	4.10	0.00	166.49	166.49	166.49	166.49	166.49	124.73	0.00	124.75
WATER	10.30	2622.91	365.80	152.11	620.38	620.38	620.38	620.38	620.38	140.02	152.11	51075.13
METHANE	0.01	0.00	1.75	351.31	353.07	353.07	353.07	353.07	353.07	353.06	351.31	1.75
CO2	2.80	3829.16	1965.07	692.28	6489.23	6489.23	6489.23	6489.23	6489.23	6487.47	692.28	464.90
CO	0.01	0.00	2.52	624.93	627.46	627.46	627.46	627.46	627.46	627.46	624.93	2.53
HYDROGEN	0.02	0.01	4.49	279.99	937.81	937.81	937.81	937.81	937.81	937.79	933.30	4.50
OXYGEN	0.00	0.00	0.00	0.00	0.00	0.00	0.00	0.00	0.00	0.00	0.00	0.00
NITROGEN	0.00	0.00	0.00	0.00	0.00	0.00	0.00	0.00	0.00	0.00	0.00	0.00
ACETALD	0.00	0.00	0.00	0.00	0.00	0.00	0.00	0.00	0.00	0.00	0.00	0.00
MDEA	0.00	0.00	0.10	0.05	0.00	0.00	0.00	0.00	0.00	0.00	0.05	13534.51
MDEA+	0.00	0.00	0.00	0.00	0.00	0.00	0.00	0.00	0.00	0.00	0.00	15800.33
H3O+	0.00	0.00	0.00	0.00	0.00	0.00	0.00	0.00	0.00	0.00	0.00	0.00
OH-	0.00	0.00	0.00	0.00	0.00	0.00	0.00	0.00	0.00	0.00	0.00	0.02
HCO3-	0.00	0.00	0.00	0.00	0.00	0.00	0.00	0.00	0.00	0.00	0.00	7797.32
CO3–	0.00	0.00	0.00	0.00	0.00	0.00	0.00	0.00	0.00	0.00	0.00	110.81
Mass Fractions												
ETHANOL	0.55	0.02	0.00	0.00	0.02	0.02	0.02	0.02	0.02	0.01	0.00	0.00
WATER	0.35	0.40	0.16	0.07	0.07	0.07	0.07	0.07	0.07	0.02	0.06	0.57
METHANE	0.00	0.00	0.00	0.17	0.04	0.04	0.04	0.04	0.04	0.04	0.13	0.00
CO2	0.10	0.58	0.84	0.33	0.71	0.71	0.71	0.71	0.71	0.75	0.25	0.01
CO	0.00	0.00	0.00	0.30	0.07	0.07	0.07	0.07	0.07	0.07	0.23	0.00
HYDROGEN	0.00	0.00	0.00	0.13	0.10	0.10	0.10	0.10	0.10	0.11	0.34	0.00
OXYGEN	0.00	0.00	0.00	0.00	0.00	0.00	0.00	0.00	0.00	0.00	0.00	0.00
NITROGEN	0.00	0.00	0.00	0.00	0.00	0.00	0.00	0.00	0.00	0.00	0.00	0.00
ACETALD	0.00	0.00	0.00	0.00	0.00	0.00	0.00	0.00	0.00	0.00	0.00	0.00
MDEA	0.00	0.00	0.00	0.00	0.00	0.00	0.00	0.00	0.00	0.00	0.00	0.15
MDEA+	0.00	0.00	0.00	0.00	0.00	0.00	0.00	0.00	0.00	0.00	0.00	0.18
H3O+	0.00	0.00	0.00	0.00	0.00	0.00	0.00	0.00	0.00	0.00	0.00	0.00
OH-	0.00	0.00	0.00	0.00	0.00	0.00	0.00	0.00	0.00	0.00	0.00	0.00
HCO3-	0.00	0.00	0.00	0.00	0.00	0.00	0.00	0.00	0.00	0.00	0.00	0.09
CO3–	0.00	0.00	0.00	0.00	0.00	0.00	0.00	0.00	0.00	0.00	0.00	0.00

Table A.12: Separation section.

Stream	SP13TP53	SP13TP54	SP13TP55	SP13TP56	SP13TP57	SP13TP58	SP13TP59
Temp (°C)	73.00	73.00	90.00	115.32	85.10	60.00	60.57
Pres (bar)	1.10	1.10	1.10	1.10	1.10	1.10	18.00
Vapor (mol/mol)	0.02	0.00	0.02	0.00	0.00	0.00	0.00
Average MW (g/mol)	27.27	27.11	26.87	26.28	26.28	25.86	25.86
Mass Flows (kg/h)							
TOTAL	88916.55	86572.72	86572.72	80000.00	80000.00	83000.00	83000.00
ETHANOL	124.75	120.65	120.65	0.02	0.02	0.02	0.02
WATER	51708.62	51342.80	51870.31	50266.72	50267.46	53237.75	53237.74
METHANE	1.75	0.00	0.00	0.00	0.00	0.00	0.00
CO2	2012.50	47.38	1336.17	0.11	0.11	0.10	0.10
CO	2.53	0.00	0.00	0.00	0.00	0.00	0.00
HYDROGEN	4.50	0.01	0.01	0.00	0.00	0.00	0.00
OXYGEN	0.00	0.00	0.00	0.00	0.00	0.00	0.00
NITROGEN	0.00	0.00	0.00	0.00	0.00	0.00	0.00
ACETALD	0.00	0.00	0.00	0.00	0.00	0.00	0.00
MDEA	17633.94	17633.65	21286.41	28163.11	28144.90	28127.58	28129.19
MDEA+	11666.24	11666.43	7982.79	1047.96	1066.32	1114.05	1112.42
H3O+	0.00	0.00	0.00	0.00	0.00	0.00	0.00
OH-	0.03	0.03	0.08	1.23	0.53	0.26	0.26
HCO3-	5605.12	5605.18	3902.03	514.22	502.40	477.21	478.05
CO3–	156.55	156.57	74.25	6.63	18.25	43.04	42.21
Mass Fractions							
ETHANOL	0.00	0.00	0.00	0.00	0.00	0.00	0.00
WATER	0.58	0.59	0.60	0.63	0.63	0.64	0.64
METHANE	0.00	0.00	0.00	0.00	0.00	0.00	0.00
CO2	0.02	0.00	0.02	0.00	0.00	0.00	0.00
CO	0.00	0.00	0.00	0.00	0.00	0.00	0.00
HYDROGEN	0.00	0.00	0.00	0.00	0.00	0.00	0.00
OXYGEN	0.00	0.00	0.00	0.00	0.00	0.00	0.00
NITROGEN	0.00	0.00	0.00	0.00	0.00	0.00	0.00
ACETALD	0.00	0.00	0.00	0.00	0.00	0.00	0.00
MDEA	0.20	0.20	0.25	0.35	0.35	0.34	0.34
MDEA+	0.13	0.13	0.09	0.01	0.01	0.01	0.01
H3O+	0.00	0.00	0.00	0.00	0.00	0.00	0.00
OH-	0.00	0.00	0.00	0.00	0.00	0.00	0.00
HCO3-	0.06	0.06	0.05	0.01	0.01	0.01	0.01
CO3–	0.00	0.00	0.00	0.00	0.00	0.00	0.00

Table A.13: Separation section (continued).

Stream	SP13TP71	SP13TP73	SP13TP75	SP13TP76	SP13TP78	SP13TP80	SP13TP81	SP13TP83	SP13TP85
Temp (°C)	77.27	77.27	77.27	76.76	76.76	77.27	99.08	84.02	60.00
Pres (bar)	10.00	10.00	10.00	1.10	1.10	10.00	11.62	11.62	18.00
Vapor (mol/mol)	1.00	1.00	1.00	1.00	1.00	1.00	0.00	0.00	0.00
Average MW (g/mol)	5.18	2.02	10.13	10.13	10.13	2.02	18.17	18.27	18.97
Mass Flows (kg/h)									
TOTAL	2753.98	653.31	2100.67	2100.67	2100.67	653.31	276.32	529.25	523.91
ETHANOL	0.00	0.00	0.00	0.00	0.00	0.00	3.50	11.70	41.76
WATER	152.11	0.00	152.11	152.11	152.11	0.00	272.50	516.80	480.36
METHANE	351.31	0.00	351.31	351.31	351.31	0.00	0.00	0.00	0.01
CO2	692.28	0.00	692.28	692.28	692.28	0.00	0.31	0.73	1.76
CO	624.93	0.00	624.93	624.93	624.93	0.00	0.00	0.00	0.01
HYDROGEN	933.30	653.31	279.99	279.99	279.99	653.31	0.00	0.01	0.01
OXYGEN	0.00	0.00	0.00	0.00	0.00	0.00	0.00	0.00	0.00
NITROGEN	0.00	0.00	0.00	0.00	0.00	0.00	0.00	0.00	0.00
ACETALD	0.00	0.00	0.00	0.00	0.00	0.00	0.00	0.00	0.00
MDEA	0.05	0.00	0.05	0.05	0.05	0.00	0.00	0.00	0.00
MDEA+	0.00	0.00	0.00	0.00	0.00	0.00	0.00	0.00	0.00
H3O+	0.00	0.00	0.00	0.00	0.00	0.00	0.00	0.00	0.00
OH-	0.00	0.00	0.00	0.00	0.00	0.00	0.00	0.00	0.00
HCO3-	0.00	0.00	0.00	0.00	0.00	0.00	0.00	0.00	0.00
CO3- -	0.00	0.00	0.00	0.00	0.00	0.00	0.00	0.00	0.00
Mass Fractions									
ETHANOL	0.00	0.00	0.00	0.00	0.00	0.00	0.01	0.02	0.08
WATER	0.06	0.00	0.07	0.07	0.07	0.00	0.99	0.98	0.92
METHANE	0.13	0.00	0.17	0.17	0.17	0.00	0.00	0.00	0.00
CO2	0.25	0.00	0.33	0.33	0.33	0.00	0.00	0.00	0.00
CO	0.23	0.00	0.30	0.30	0.30	0.00	0.00	0.00	0.00
HYDROGEN	0.34	1.00	0.13	0.13	0.13	1.00	0.00	0.00	0.00
OXYGEN	0.00	0.00	0.00	0.00	0.00	0.00	0.00	0.00	0.00
NITROGEN	0.00	0.00	0.00	0.00	0.00	0.00	0.00	0.00	0.00
ACETALD	0.00	0.00	0.00	0.00	0.00	0.00	0.00	0.00	0.00
MDEA	0.00	0.00	0.00	0.00	0.00	0.00	0.00	0.00	0.00
MDEA+	0.00	0.00	0.00	0.00	0.00	0.00	0.00	0.00	0.00
H3O+	0.00	0.00	0.00	0.00	0.00	0.00	0.00	0.00	0.00
OH-	0.00	0.00	0.00	0.00	0.00	0.00	0.00	0.00	0.00
HCO3-	0.00	0.00	0.00	0.00	0.00	0.00	0.00	0.00	0.00
CO3- -	0.00	0.00	0.00	0.00	0.00	0.00	0.00	0.00	0.00

Table A.14: Separation section (continued).

Stream	AUX2	AUX4	AUX6	AUX8	AUX10	AUX12	AUX14	AUX18	AUX20	QA13FAIR	QA13FR00	QF13TA01	QP13TA03
Description													
Temp (°C)	431.61	456.08	198.29	198.29	25.00	198.29	198.29	198.31	198.39	22.30	76.75	20.00	1100.00
Pres (bar)	15.00	15.00	15.00	15.00	15.00	15.00	15.00	15.00	15.00	1.02	1.05	1.00	1.05
Vapor (mol/mol)	1.00	1.00	1.00	0.00	0.00	0.06	0.00	0.21	0.32	1.00	1.00	1.00	1.00
Average MW (g/mol)	18.07	18.07	18.07	18.07	18.02	18.02	18.07	18.07	18.07	28.85	10.14	28.85	27.18
Mass Flows (kg/h)													
TOTAL	5967.00	5967.00	5967.00	6900.00	7000.00	7000.00	6900.00	6900.00	6900.00	23000.00	2080.83	23000.00	25080.83
ETHANOL	29.27	29.27	29.27	33.87	0.00	0.00	33.87	33.87	33.87	0.00	0.00	0.00	0.00
WATER	5937.73	5937.73	5937.73	6866.13	7000.00	7000.00	6866.13	6866.13	6866.13	0.00	150.60	0.00	3408.87
METHANE	0.00	0.00	0.00	0.00	0.00	0.00	0.00	0.00	0.00	0.00	347.77	0.00	0.00
CO2	0.00	0.00	0.00	0.00	0.00	0.00	0.00	0.00	0.00	0.00	686.52	0.00	2612.74
CO	0.00	0.00	0.00	0.00	0.00	0.00	0.00	0.00	0.00	0.00	618.70	0.00	0.00
HYDROGEN	0.00	0.00	0.00	0.00	0.00	0.00	0.00	0.00	0.00	0.00	277.19	0.00	0.00
OXYGEN	0.00	0.00	0.00	0.00	0.00	0.00	0.00	0.00	0.00	5357.09	0.00	5357.09	1416.31
NITROGEN	0.00	0.00	0.00	0.00	0.00	0.00	0.00	0.00	0.00	17642.91	0.00	17642.91	17642.91
Mass Fractions													
ETHANOL	0.00	0.00	0.00	0.00	0.00	0.00	0.00	0.00	0.00	0.00	0.00	0.00	0.00
WATER	1.00	1.00	1.00	1.00	1.00	1.00	1.00	1.00	1.00	0.00	0.07	0.00	0.14
METHANE	0.00	0.00	0.00	0.00	0.00	0.00	0.00	0.00	0.00	0.00	0.17	0.00	0.00
CO2	0.00	0.00	0.00	0.00	0.00	0.00	0.00	0.00	0.00	0.00	0.33	0.00	0.10
CO	0.00	0.00	0.00	0.00	0.00	0.00	0.00	0.00	0.00	0.00	0.30	0.00	0.00
HYDROGEN	0.00	0.00	0.00	0.00	0.00	0.00	0.00	0.00	0.00	0.00	0.13	0.00	0.00
OXYGEN	0.00	0.00	0.00	0.00	0.00	0.00	0.00	0.00	0.00	0.23	0.00	0.23	0.06
NITROGEN	0.00	0.00	0.00	0.00	0.00	0.00	0.00	0.00	0.00	0.77	0.00	0.77	0.70

Table A.15: Auxiliary Streams.

Stream Description	QP13TA05	QP13TA07	QP13TA09	QP13TA11	QP13TA13	QP13TA15	QP13TA17	QP13TA19	QP13TA21	QP13TA23	QP13TA25	QP13TA27
Temp (°C)	1100.00	1100.00	1100.00	1090.00	730.12	830.00	796.84	786.84	546.63	500.00	480.00	350.00
Pres (bar)	1.05	1.05	1.05	1.05	1.05	1.05	1.05	1.05	1.05	1.05	1.05	1.05
Vapor (mol/mol)	1.00	1.00	1.00	1.00	1.00	1.00	1.00	1.00	1.00	1.00	1.00	1.00
Average MW (g/mol)	27.18	27.18	27.18	27.18	27.18	27.18	27.18	27.18	27.18	27.18	27.18	27.18
Mass Flows (kg/h)												
TOTAL	7524.25	15048.50	2508.08	2508.08	15048.50	7524.25	25080.83	25080.83	25080.83	25080.83	25080.83	25080.83
ETHANOL	0.00	0.00	0.00	0.00	0.00	0.00	0.00	0.00	0.00	0.00	0.00	0.00
WATER	1022.66	2045.32	340.89	340.89	2045.32	1022.66	3408.87	3408.87	3408.87	3408.87	3408.87	3408.87
METHANE	0.00	0.00	0.00	0.00	0.00	0.00	0.00	0.00	0.00	0.00	0.00	0.00
CO2	783.82	1567.64	261.27	261.27	1567.64	783.82	2612.74	2612.74	2612.74	2612.74	2612.74	2612.74
CO	0.00	0.00	0.00	0.00	0.00	0.00	0.00	0.00	0.00	0.00	0.00	0.00
HYDROGEN	0.00	0.00	0.00	0.00	0.00	0.00	0.00	0.00	0.00	0.00	0.00	0.00
OXYGEN	424.89	849.78	141.63	141.63	849.78	424.89	1416.31	1416.31	1416.31	1416.31	1416.31	1416.31
NITROGEN	5292.87	10585.75	1764.29	1764.29	10585.75	5292.87	17642.91	17642.91	17642.91	17642.91	17642.91	17642.91
Mass Fractions												
ETHANOL	0.00	0.00	0.00	0.00	0.00	0.00	0.00	0.00	0.00	0.00	0.00	0.00
WATER	0.14	0.14	0.14	0.14	0.14	0.14	0.14	0.14	0.14	0.14	0.14	0.14
METHANE	0.00	0.00	0.00	0.00	0.00	0.00	0.00	0.00	0.00	0.00	0.00	0.00
CO2	0.10	0.10	0.10	0.10	0.10	0.10	0.10	0.10	0.10	0.10	0.10	0.10
CO	0.00	0.00	0.00	0.00	0.00	0.00	0.00	0.00	0.00	0.00	0.00	0.00
HYDROGEN	0.00	0.00	0.00	0.00	0.00	0.00	0.00	0.00	0.00	0.00	0.00	0.00
OXYGEN	0.06	0.06	0.06	0.06	0.06	0.06	0.06	0.06	0.06	0.06	0.06	0.06
NITROGEN	0.70	0.70	0.70	0.70	0.70	0.70	0.70	0.70	0.70	0.70	0.70	0.70

Table A.16: Auxiliary Streams (continued).

Stream	QP13TA27	QP13TA29	QR13TA01	QR13TA02	QV13TA31	QW13TA39	QW13TA40	QW13TP01	QW13TP03	QW13TP05
Description										
Temp (°C)	350.00	270.00	120.00	120.00	182.79	76.75	182.57	60.00	78.29	193.13
Pres (bar)	1.05	1.05	1.05	1.02	1.05	1.05	1.05	11.60	15.00	15.00
Vapor (mol/mol)	1.00	1.00	1.00	1.00	1.00	1.00	1.00	0.00	0.00	0.00
Average MW (g/mol)	27.18	27.18	10.14	28.85	27.18	10.13	27.15	18.97	18.52	18.36
Mass Flows (kg/h)										
TOTAL	25080.83	25080.83	2080.83	23000.00	25080.83	21.01	25101.84	523.91	1329.47	1300.00
ETHANOL	0.00	0.00	0.00	0.00	0.00	0.00	0.00	41.76	56.96	40.64
WATER	3408.87	3408.87	150.60	0.00	3408.87	1.52	3410.39	480.36	1269.66	1259.36
METHANE	0.00	0.00	347.77	0.00	0.00	3.51	3.51	0.01	0.01	0.00
CO2	2612.74	2612.74	686.52	0.00	2612.74	6.92	2619.66	1.76	2.80	0.00
CO	0.00	0.00	618.70	0.00	0.00	6.25	6.25	0.01	0.01	0.00
HYDROGEN	0.00	0.00	277.19	0.00	0.00	2.80	2.80	0.01	0.02	0.00
OXYGEN	1416.31	1416.31	0.00	5357.09	1416.31	0.00	1416.31	0.00	0.00	0.00
NITROGEN	17642.91	17642.91	0.00	17642.91	17642.91	0.00	17642.91	0.00	0.00	0.00
Mass Fractions										
ETHANOL	0.00	0.00	0.00	0.00	0.00	0.00	0.00	0.08	0.04	0.03
WATER	0.14	0.14	0.07	0.00	0.14	0.07	0.14	0.92	0.96	0.97
METHANE	0.00	0.00	0.17	0.00	0.00	0.17	0.00	0.00	0.00	0.00
CO2	0.10	0.10	0.33	0.00	0.10	0.33	0.10	0.00	0.00	0.00
CO	0.00	0.00	0.30	0.00	0.00	0.30	0.00	0.00	0.00	0.00
HYDROGEN	0.00	0.00	0.13	0.00	0.00	0.13	0.00	0.00	0.00	0.00
OXYGEN	0.06	0.06	0.00	0.23	0.06	0.00	0.06	0.00	0.00	0.00
NITROGEN	0.70	0.70	0.00	0.77	0.70	0.00	0.70	0.00	0.00	0.00

Table A.17: Auxiliary Streams (continued).

Stream	**Q** (kW)	**Tin** (°C)	**Tout** (°C)	Note
stream 1	1100	50	146	feed preheat
stream 2	4100	146	177	feed boil
stream 3	1900	177	470	feed superheat
stream 4	770	470	517	reac1
stream 5	2100	517	537	reac2
stream 6	2180	502	537	reac3
stream 7	890	502	380	hx11
stream 8	1230	393	220	hx12
stream 9	1260	255	100	hx13
stream 10	430	99	85	hx14
stream 11	280	144	100	cmprcool
stream 12	570	100	60	prod cond
stream 13	2430	73	90	mdea preheat
stream 14	2430	115	85	mdea precool
stream 15	1880	85	60	mdea makeup
stream 16	7340	115	116	stripper reboil
stream 17	3250	100	99	stripper cond
stream 18	195	193	194	cond stripper
stream 19	490	197	198	SG dispersion
stream 20	710	22	120	fuel plus air preheat
stream 21	5690	1100	1090	radiative heat 1
stream 22	770	1100	830	hot flues reac1
stream 23	2100	1100	730	hot flues reac 2
stream 24	2180	793	783	hot flues steam
stream 25	2128	787	547	fot flues reac 3
stream 26	410	544	500	hot flues coolwater 1
stream 27	170	500	480	hot flues coolwater 2
stream 28	1110	480	350	hot flues feed
stream 29	670	350	270	hot flues coolwater 3
stream 30	705	270	183	hot flues preheat fuel
stream 31	430	25	78	feedwater preheat 1
stream 32	1250	78	198	feedwater preheat 2
stream 33	670	198	199	boil1
stream 34	180	198	199	boil2
stream 35	410	198	199	boil3
stream 36	1230	198	199	boil4
stream 37	890	198	433	steam sh 1
stream 38	90	433	458	steam sh 2
stream 39	4030	458	198	mp steam available
stream 40	690	198	135	mp steam available
stream 41	3500	199	198	mp steam ext
stream 42	5974	21	81	cooling air

Table A.18: Fluid list for the calculation of energetic balances.

A.3 Ethanol Reforming for DHPC

Block	**Temperature (°C)**		**Pressure (bar)**	**Duty (kW)**	**Hydrogen Flow (mol/h)**	
	In	Out			In	Out
Reformer	567	500 – 670	2.0	3 – 3.7	0	185 – 245
FPHX	105	111	2.0		0	0
AUTOHX	111	na	2.0 – 1.8	5.1 – 10	0	0
HTWGS	350	371	2.0	na	na	na
LTWGS	280	281	2.0	na	na	na
Methanator	210	216	2.0	na	na	202 – 261
Condenser	216	50 – 55	1.8	3.7 – 7.8	202 – 261	202 – 261
PEMFC	80	80	1.8	7.8 – 12.6	202 – 261	na
Burner	80	1050 – 1400	1.8	0	na	0
FLUEHX	240 – 860	80	1.8 – 1.0	1.3 – 10.4	0	0

Table A.19: Summary of the key specifications and results for the SR system fed with 420 mol/h of Ethanol. The ranges of varying parameter refer to the working cases discussed.

Case	Flues to SR	FC	E:W	Condenser		Fuel Cell			Flues	
	x			Heat	T	Power	Heat	T	Heat	T
n°	(mol/mol)			(kWth)	(°C)	(kWel)	(kWth)	(°C)	(kWth)	(°C)
1	0.425	0.8	1:5	3.9	50	4.9	7.4	80	5.6	544
4	0.3	0.5	1:5	3.8	50	3.1	4.7	80	10.4	863
2	0.475	0.8	1:7	5.8	50	5.0	7.5	80	2.7	296
5	0.35	0.5	1:7	5.7	50	3.3	4.9	80	8.1	699
3	0.525	0.7	1:9	7.6	50	4.9	7.3	80	1.3	179
6	0.275	0.6	1:9	7.8	50	3.5	5.3	80	3.8	359
7	0.4	0.9	1:5	4.1	50	5.0	7.6	80	4.4	455
8	0.4	0.9	1:7	6.1	50	5.0	7.5	80	1.9	242
11	0.425	0.8	1:5	3.8	55	4.9	7.4	80	5.6	537
41	0.3	0.5	1:5	3.7	55	3.1	4.7	80	10.4	860
21	0.475	0.8	1:7	5.7	55	5.0	7.5	80	2.8	297
51	0.35	0.5	1:7	5.5	55	3.3	4.9	80	8.1	695
31	0.525	0.7	1:9	7.4	55	4.9	7.3	80	1.4	183
61	0.275	0.6	1:9	7.7	55	3.5	5.3	80	3.8	360
71	0.4	0.9	1:5	4.0	55	5.0	7.6	80	4.4	451
81	0.4	0.9	1:7	5.9	55	5.0	7.5	80	1.9	240

Table A.20: Reference working points for the steady state of the cogeneration system.

Case	Radiator single element					Total		Dissipator		Condenser		Water Circuit	
	Water		Air	Heat		Heat		Air	Fan	Hot	Cold	Flow	RS1
n°	Tin (°C)	Tout (°C)	Tout (°C)	calc(*) (W)	ref(**) (W)	rad (kW)	diss (kW)	Tout (°C)	Work (W)	Tout (°C)	Tout (°C)	total (l/min)	split (l/l)
1	69.5	42.5	31.4	101	104	9.5	7.5	26.5	26.5	50	45.5	11.9	0.35
4	70.5	43.0	31.7	103	107	9.6	9.3	31.7	31.7	50	45.3	11.9	0.27
2	69.1	42.3	31.3	101	103	9.4	6.6	24.2	24.2	50	45.8	16.7	0.62
5	70.4	42.9	31.7	103	107	9.6	9.1	31.2	31.2	50	45.9	16.0	0.52
3	69.9	42.7	31.5	102	105	9.5	6.7	24.5	24.5	50	45.9	21.7	0.76
6	70.7	43.1	31.8	104	108	9.6	7.3	26.0	26.0	50	46.1	21.7	0.76
11	70.6	43.0	31.7	103	107	9.6	6.5	23.8	23.8	50	45.7	11.9	0.42
41	70.0	42.7	31.5	102	106	9.4	6.0	22.4	22.4	50	46.0	17.0	0.67
21	74.5	44.9	32.9	111	118	10.3	6.5	23.8	23.8	55	49.7	13.8	0.45
51	73.8	44.5	32.7	109	116	10.1	8.6	29.8	29.8	55	49.6	13.8	0.35
31	73.9	44.6	32.7	110	117	10.1	5.8	21.9	21.9	55	50.4	17.7	0.64
61	74.0	44.6	32.7	110	117	10.3	8.3	28.9	28.9	55	50.3	17.7	0.55
71	74.6	44.9	32.9	111	119	10.3	5.8	21.9	21.9	55	50.8	21.7	0.76
81	74.8	45.0	33.0	111	119	10.3	6.5	23.8	23.8	55	51.0	21.7	0.75

Table A.21: Performance of the cogeneration system in relation to the power outputs of Table A.20. The water flowrate in each radiator element is fixed at 3.3 l/h, and the total elements are 91 (the air flow is set to 18 cum/h for each element, and its lowest temperature is assumed to be 15 °C). The external cooling air for these winter cases is 5 °C. (*) Calculated according to Table B.9 – (**) Calculated at fixed water temperature (inlet) and fixed air temperature (20 °C)

A.4 Ammonia Synthesis

Stream reports for the ethanol-ammonia process: refer to chapter 3.3.

Stream	FR11TP01	FR11TP02	FR11TP03	FR13TP03	FR13TP05	FR13TP07	FR13TP09	FR13TP60
Description								
Temp (°C)	200	20	513.5346	50	137.4863	481.5638	470	25
Pres (bar)	12	1	12	12.2	12.2	12.2	12.2	1.2
Vapor (mol/mol)	1	1	1	0	0	1	1	0
Average MW (g/mol)	28.8504	28.8504	28.8504	25.02872	25.02872	25.02872	25.02872	18.16951
Mole Flows (kmol/h)	207.9694	103.9847	207.9694	399.541	399.541	399.541	399.541	27.51863
Mass Flows (kg/h)								
TOTAL	6000	3000	6000	10000	10000	10000	10000	500
ETHANOL	0	0	0	4601.618	4601.618	4601.618	4601.618	0
WATER	0	0	0	5398.382	5398.382	5398.382	5398.382	494.9952
OXYGEN	1397.502	698.751	1397.502	0	0	0	0	0
NITROGEN	4602.498	2301.249	4602.498	0	0	0	0	0
MDEA	0	0	0	0	0	0	0	4.968445
MDEA+	0	0	0	0	0	0	0	0.031821
H3O+	0	0	0	0	0	0	0	1.92E-10
OH-	0	0	0	0	0	0	0	0.004504
Mass Fractions								
ETHANOL	0	0	0	0.460162	0.460162	0.460162	0.460162	0
WATER	0	0	0	0.539838	0.539838	0.539838	0.539838	0.98999
OXYGEN	0.232917	0.232917	0.232917	0	0	0	0	0
NITROGEN	0.767083	0.767083	0.767083	0	0	0	0	0
MDEA	0	0	0	0	0	0	0	0.009937
MDEA+	0	0	0	0	0	0	0	6.36E-05
H3O+	0	0	0	0	0	0	0	3.84E-13
OH-	0	0	0	0	0	0	0	9.01E-06

Table A.22: Feed streams.

Description	TR13TP11	TR13TP13	TR13TP15	TR13TP17	TR13TP19	TR13TP21	TP13TP23	TP13TP25	TP13TP27	TP13TP29	TP13TP31
Temp (°C)	514.45	533.98	495.41	380.00	820.00	220.00	335.56	100.00	99.08	85.00	84.14
Pres (bar)	12.19	12.14	11.97	11.97	11.97	11.97	11.42	11.42	11.42	11.42	11.42
Vapor (mol/mol)	1.00	1.00	1.00	1.00	1.00	1.00	1.00	0.94	1.00	0.96	1.00
Average MW (g/mol)	22.69	16.46	13.94	13.94	17.09	17.09	17.09	17.09	17.03	17.03	16.99
Mole Flows (kmol/h)	440.81	607.36	717.16	717.16	936.14	936.14	936.14	936.14	877.90	877.90	842.61
Mass Flows (kg/h)											
TOTAL	10000.00	10000.00	10000.00	10000.00	16000.00	16000.00	16000.00	16000.00	14950.17	14950.17	14313.90
ETHANOL	3271.41	1109.42	303.33	303.33	0.00	0.00	0.00	0.00	0.00	0.00	0.00
WATER	5184.27	3463.56	2381.60	2381.60	4117.99	4117.99	2460.96	2460.96	1412.34	1412.34	776.99
METHANE	173.28	638.41	434.85	434.85	207.53	207.53	207.53	207.53	207.53	207.53	207.52
CO2	499.71	3373.71	4476.60	4476.60	3165.49	3165.49	7213.47	7213.47	7212.45	7212.45	7211.70
CO	14.20	689.55	1592.83	1592.83	3193.05	3193.05	616.68	616.68	616.67	616.67	616.67
HYDROGEN	84.30	493.25	790.70	790.70	693.35	693.35	878.77	878.77	878.76	878.76	878.75
OXYGEN	0.00	0.00	0.00	0.00	0.00	0.00	0.00	0.00	0.00	0.00	0.00
NITROGEN	0.00	0.00	0.00	0.00	4602.50	4602.50	4602.50	4602.50	4602.47	4602.47	4602.45
ACETALD	772.83	232.10	20.10	20.10	20.10	20.10	20.10	20.10	19.95	19.95	19.81
Mass Fractions											
ETHANOL	0.33	0.11	0.03	0.03	0.00	0.00	0.00	0.00	0.00	0.00	0.00
WATER	0.52	0.35	0.24	0.24	0.26	0.26	0.15	0.15	0.09	0.09	0.05
METHANE	0.02	0.06	0.04	0.04	0.01	0.01	0.01	0.01	0.01	0.01	0.01
CO2	0.05	0.34	0.45	0.45	0.20	0.20	0.45	0.45	0.48	0.48	0.50
CO	0.00	0.07	0.16	0.16	0.20	0.20	0.04	0.04	0.04	0.04	0.04
HYDROGEN	0.01	0.05	0.08	0.08	0.04	0.04	0.05	0.05	0.06	0.06	0.06
OXYGEN	0.00	0.00	0.00	0.00	0.00	0.00	0.00	0.00	0.00	0.00	0.00
NITROGEN	0.00	0.00	0.00	0.00	0.29	0.29	0.29	0.29	0.31	0.31	0.32
ACETALD	0.08	0.02	0.00	0.00	0.00	0.00	0.00	0.00	0.00	0.00	0.00

Table A.23: Bioethanol reforming section.

Description	SP13TP33	SP13TP35	SP13TP37	SP13TP39	SP13TP41	SP13TP43	SP13TP81	SP13TP83	SP13TP85
Temp (°C)	88.14	151.59	147.69	100.11	60.00	60.00	99.08	84.14	60.00
Pres (bar)	11.42	18.00	18.00	18.00	18.00	18.00	11.42	11.42	18.00
Vapor (mol/mol)	1.00	1.00	1.00	1.00	0.96	1.00	0.00	0.00	0.00
Average MW (g/mol)	16.99	16.99	16.99	16.99	16.99	16.94	18.03	18.03	18.05
Mole Flows (kmol/h)	842.61	842.61	842.61	842.61	842.61	809.20	58.24	35.29	33.40
Mass Flows (kg/h)									
TOTAL	14313.90	14313.90	14313.90	14313.90	14313.90	13710.99	1049.83	636.27	602.91
WATER	776.99	776.99	776.99	776.99	776.99	176.10	1048.62	635.35	600.89
METHANE	207.52	207.52	207.52	207.52	207.52	207.52	0.00	0.00	0.00
CO2	7211.70	7211.70	7211.70	7211.70	7211.70	7210.19	1.02	0.75	1.51
CO	616.67	616.67	616.67	616.67	616.67	616.67	0.01	0.00	0.01
HYDROGEN	878.75	878.75	878.75	878.75	878.75	878.75	0.01	0.01	0.01
OXYGEN	0.00	0.00	0.00	0.00	0.00	0.00	0.00	0.00	0.00
NITROGEN	4602.45	4602.45	4602.45	4602.45	4602.45	4602.42	0.03	0.02	0.03
ACETALD	19.81	19.81	19.81	19.81	19.81	19.35	0.15	0.14	0.46
Mass Fractions									
WATER	0.05	0.05	0.05	0.05	0.05	0.01	1.00	1.00	1.00
METHANE	0.01	0.01	0.01	0.01	0.01	0.02	0.00	0.00	0.00
CO2	0.50	0.50	0.50	0.50	0.50	0.53	0.00	0.00	0.00
CO	0.04	0.04	0.04	0.04	0.04	0.04	0.00	0.00	0.00
HYDROGEN	0.06	0.06	0.06	0.06	0.06	0.06	0.00	0.00	0.00
OXYGEN	0.00	0.00	0.00	0.00	0.00	0.00	0.00	0.00	0.00
NITROGEN	0.32	0.32	0.32	0.32	0.32	0.34	0.00	0.00	0.00
ACETALD	0.00	0.00	0.00	0.00	0.00	0.00	0.00	0.00	0.00

Table A.24: Reformate purification.

Stream	SP13TP51	SP13TP52	SP13TP53	SP13TP54	SP13TP55	SP13TP56	SP13TP57	SP13TP58	SP13TP59	SB13TP61	SB13TP63
Description											
Temp (°C)	60.55	85.18	73.22	73.22	90.00	115.03	86.01	60.00	60.55	96.74	73.22
Pres (bar)	18.00	18.00	1.10	1.10	1.10	1.10	1.10	1.10	18.00	1.10	1.10
Vapor (mol/mol)	1.00	0.00	0.02	0.00	0.02	0.00	0.00	0.00	0.00	1.00	1.00
Average MW (g/mol)	10.00	26.76	26.49	26.33	26.11	25.50	25.50	25.45	25.45	29.12	34.80
Mole Flows (kmol/h)	637.27	4394.95	4439.17	4355.04	4392.07	4207.70	4207.70	4235.22	4235.22	254.13	84.13
Mass Flows (kg/h)											
TOTAL	6375.17	117614.90	117614.90	114687.17	114687.17	107287.17	107287.17	107787.17	107787.17	7400.00	2927.73
WATER	90.04	70439.31	71235.98	70772.66	71439.69	70072.54	70073.37	70568.73	70568.72	2622.49	463.32
METHANE	206.41	1.11	1.11	0.00	0.00	0.00	0.00	0.00	0.00	0.00	1.11
CO2	2.95	553.33	2499.59	62.62	1692.28	0.21	0.19	0.15	0.15	4762.26	2436.97
CO	613.99	2.67	2.67	0.00	0.00	0.00	0.00	0.00	0.00	0.00	2.67
HYDROGEN	874.20	4.55	4.55	0.01	0.01	0.00	0.00	0.00	0.00	0.01	4.54
NITROGEN	4587.53	14.89	14.89	0.01	0.01	0.00	0.00	0.00	0.00	0.01	14.88
ACETALD	0.00	19.35	19.35	15.22	15.22	0.00	0.00	0.00	0.00	15.22	4.13
MDEA	0.04	16774.39	21937.24	21937.09	26552.20	35024.98	34998.87	34937.38	34939.57	0.00	0.11
MDEA+	0.00	19866.41	14659.92	14659.95	10005.83	1461.42	1487.75	1554.79	1552.59	0.00	0.00
H3O+	0.00	0.00	0.00	0.00	0.00	0.00	0.00	0.00	0.00	0.00	0.00
OH-	0.00	0.03	0.04	0.04	0.11	1.46	0.67	0.31	0.32	0.00	0.00
HCO3-	0.00	9795.43	7042.32	7042.32	4886.77	716.73	700.59	665.36	666.50	0.00	0.00
CO3- -	0.00	143.44	197.24	197.25	95.05	9.83	25.74	60.43	59.31	0.00	0.00
Mass Fractions											
WATER	0.01	0.60	0.61	0.62	0.62	0.65	0.65	0.65	0.65	0.35	0.16
METHANE	0.03	0.00	0.00	0.00	0.00	0.00	0.00	0.00	0.00	0.00	0.00
CO2	0.00	0.00	0.02	0.00	0.01	0.00	0.00	0.00	0.00	0.64	0.83
CO	0.10	0.00	0.00	0.00	0.00	0.00	0.00	0.00	0.00	0.00	0.00
HYDROGEN	0.14	0.00	0.00	0.00	0.00	0.00	0.00	0.00	0.00	0.00	0.00
NITROGEN	0.72	0.00	0.00	0.00	0.00	0.00	0.00	0.00	0.00	0.00	0.01
ACETALD	0.00	0.00	0.00	0.00	0.00	0.00	0.00	0.00	0.00	0.00	0.00
MDEA	0.00	0.14	0.19	0.19	0.23	0.33	0.33	0.32	0.32	0.00	0.00
MDEA+	0.00	0.17	0.12	0.13	0.09	0.01	0.01	0.01	0.01	0.00	0.00
H3O+	0.00	0.00	0.00	0.00	0.00	0.00	0.00	0.00	0.00	0.00	0.00
OH-	0.00	0.00	0.00	0.00	0.00	0.00	0.00	0.00	0.00	0.00	0.00
HCO3-	0.00	0.08	0.06	0.06	0.04	0.01	0.01	0.01	0.01	0.00	0.00
CO3- -	0.00	0.00	0.00	0.00	0.00	0.00	0.00	0.00	0.00	0.00	0.00

Table A.25: Reformate purification (continued).

Stream Description	TR41TP01	TR41TP02	TR41TP03	TR41TP04	TR41TP05	TR41TP06
From	HR41	TR41RK06	TR41HX11	TR41RK07	TR41HX01	HR41
To	TR41RK06	TR41HX11	TR41RK07	TR41HX01	HR41	TR41CA01
Temp (°C)	250.00	325.47	250.00	390.34	270.00	72.49
Pres (bar)	18.00	17.99	17.99	17.98	17.98	17.98
Vapor (mol/mol)	1.00	1.00	1.00	1.00	1.00	1.00
Average MW (g/mol)	10.00	10.29	10.29	10.74	10.74	10.74
Mole Flows (kmol/h)	637.27	619.43	619.43	593.42	593.42	593.42
Mass Flows (kg/h)						
TOTAL	6375.17	6375.17	6375.17	6375.41	6375.41	6375.41
ETHANOL	0.00	0.00	0.00	0.00	0.00	0.00
WATER	90.04	250.71	250.71	485.09	485.09	485.09
METHANE	206.41	349.49	349.49	558.21	558.21	558.21
CO2	2.95	2.95	2.95	2.95	2.95	2.95
CO	613.99	364.19	364.19	0.00	0.00	0.00
HYDROGEN	874.20	820.26	820.26	741.58	741.58	741.58
OXYGEN	0.00	0.00	0.00	0.00	0.00	0.00
NITROGEN	4587.53	4587.53	4587.53	4587.53	4587.53	4587.53
Mass Fractions						
ETHANOL	0.00	0.00	0.00	0.00	0.00	0.00
WATER	0.01	0.04	0.04	0.08	0.08	0.08
METHANE	0.03	0.05	0.05	0.09	0.09	0.09
CO2	0.00	0.00	0.00	0.00	0.00	0.00
CO	0.10	0.06	0.06	0.00	0.00	0.00
HYDROGEN	0.14	0.13	0.13	0.12	0.12	0.12
OXYGEN	0.00	0.00	0.00	0.00	0.00	0.00
NITROGEN	0.72	0.72	0.72	0.72	0.72	0.72

Table A.26: Ammonia synthesis.

Stream	TR41TP07	TR41TP09	TR41TP10	TR41TP11	TR41TP13	TR41TP15	TR41TP15
Description							
Temp (°C)	243.21	122.95	50.00	50.00	213.28	40.00	40.00
Pres (bar)	53.95	53.95	53.95	53.95	161.84	161.84	161.84
Vapor (mol/mol)	1.00	1.00	0.96	1.00	1.00	1.00	1.00
Average MW (g/mol)	10.74	10.74	10.74	10.42	10.42	10.42	10.42
Mole Flows (kmol/h)	593.42	593.42	593.42	568.06	568.06	568.06	568.06
Mass Flows (kg/h)							
TOTAL	6375.41	6375.41	6375.41	5918.58	5918.58	5918.58	5918.58
ETHANOL	0.00	0.00	0.00	0.00	0.00	0.00	0.00
WATER	485.09	485.09	485.09	28.45	28.45	28.45	28.45
METHANE	558.21	558.21	558.21	558.18	558.18	558.18	558.18
CO2	2.95	2.95	2.95	2.95	2.95	2.95	2.95
CO	0.00	0.00	0.00	0.00	0.00	0.00	0.00
HYDROGEN	741.58	741.58	741.58	741.56	741.56	741.56	741.56
OXYGEN	0.00	0.00	0.00	0.00	0.00	0.00	0.00
NITROGEN	4587.53	4587.53	4587.53	4587.43	4587.43	4587.43	4587.43
Mass Fractions							
ETHANOL	0.00	0.00	0.00	0.00	0.00	0.00	0.00
WATER	0.08	0.08	0.08	0.00	0.00	0.00	0.00
METHANE	0.09	0.09	0.09	0.09	0.09	0.09	0.09
CO2	0.00	0.00	0.00	0.00	0.00	0.00	0.00
CO	0.00	0.00	0.00	0.00	0.00	0.00	0.00
HYDROGEN	0.12	0.12	0.12	0.13	0.13	0.13	0.13
OXYGEN	0.00	0.00	0.00	0.00	0.00	0.00	0.00
NITROGEN	0.72	0.72	0.72	0.78	0.78	0.78	0.78

Table A.27: Ammonia synthesis (continued).

Stream	TR41TP21	TP41TP69	TP41TP70	TP41TP71	TP41TP73	TP41TP75	TP41TP77	TP41TP79	TR41TP25	TR41SP23
Description										
Temp (°C)	20.00	297.34	483.83	453.83	378.87	433.40	420.00	388.03	170.45	20.00
Pres (bar)	161.84	162.00	161.79	161.79	161.79	161.78	161.78	161.78	161.84	161.84
Vapor (mol/mol)	1.00	1.00	1.00	1.00	1.00	1.00	1.00	1.00	1.00	1.00
Average MW (g/mol)	10.40	20.50	17.56	17.56	18.95	19.63	19.63	19.87	16.44	10.12
Mole Flows (kmol/h)	566.64	840.22	1253.41	1253.41	2373.71	2290.54	2290.54	3130.77	1380.01	539.78
Mass Flows (kg/h)										
TOTAL	5893.02	17224.38	22005.77	22005.77	44971.61	44971.61	44971.61	62195.99	22686.36	5461.81
ETHANOL	0.00	0.00	0.00	0.00	0.00	0.00	0.00	0.00	0.00	0.00
WATER	2.92	0.00	0.00	0.00	0.00	0.00	0.00	0.00	0.00	0.00
METHANE	558.18	1366.04	1451.06	1451.06	3272.45	3272.45	3272.45	4638.49	1495.94	129.89
CO2	2.95	6.98	9.63	9.63	18.94	18.94	18.94	25.93	9.93	2.95
CO	0.00	176.95	171.64	171.64	407.57	407.57	407.57	584.52	176.95	0.00
HYDROGEN	741.56	368.52	819.15	819.15	1310.51	1059.02	1059.02	1427.55	1110.08	741.56
NITROGEN	4587.41	14462.63	17285.18	17285.18	36568.68	35403.74	35403.74	49866.37	19050.04	4587.41
AMMONIA	0.00	843.26	2269.11	2269.11	3393.45	4809.89	4809.89	5653.14	843.43	0.00
Mass Fractions										
ETHANOL	0.00	0.00	0.00	0.00	0.00	0.00	0.00	0.00	0.00	0.00
WATER	0.00	0.00	0.00	0.00	0.00	0.00	0.00	0.00	0.00	0.00
METHANE	0.09	0.08	0.07	0.07	0.07	0.07	0.07	0.07	0.07	0.02
CO2	0.00	0.00	0.00	0.00	0.00	0.00	0.00	0.00	0.00	0.00
CO	0.00	0.01	0.01	0.01	0.01	0.01	0.01	0.01	0.01	0.00
HYDROGEN	0.13	0.02	0.04	0.04	0.03	0.02	0.02	0.02	0.05	0.14
NITROGEN	0.78	0.84	0.79	0.79	0.81	0.79	0.79	0.80	0.84	0.84
AMMONIA	0.00	0.05	0.10	0.10	0.08	0.11	0.11	0.09	0.04	0.00

Table A.28: Ammonia synthesis (continued).

Stream	SP41TP51	SP41TP53	SP41TP22	SP41TP26	SP41TP27	SP41TP28
Description						
Temp (°C)	40.01	25.00	20.00	170.45	170.45	30.00
Pres (bar)	161.62	161.62	161.84	161.84	161.84	161.84
Vapor (mol/mol)	1.00	0.99	0.00	1.00	1.00	1.00
Average MW (g/mol)	20.30	20.30	16.05	16.44	16.44	16.44
Mole Flows (kmol/h)	3064.13	3064.13	26.86	41.40	1338.61	41.40
Mass Flows (kg/h)						
TOTAL	62195.99	62195.99	431.21	680.59	22005.77	680.59
ETHANOL	0.00	0.00	0.00	0.00	0.00	0.00
WATER	0.00	0.00	2.92	0.00	0.00	0.00
METHANE	4638.49	4638.49	428.29	44.88	1451.06	44.88
CO2	25.93	25.93	0.00	0.30	9.63	0.30
CO	584.52	584.52	0.00	5.31	171.64	5.31
HYDROGEN	1226.06	1226.06	0.00	33.30	1076.78	33.30
NITROGEN	48933.05	48933.05	0.00	571.50	18478.54	571.50
AMMONIA	6787.96	6787.96	0.00	25.30	818.12	25.30
Mass Fractions						
ETHANOL	0.00	0.00	0.00	0.00	0.00	0.00
WATER	0.00	0.00	0.01	0.00	0.00	0.00
METHANE	0.07	0.07	0.99	0.07	0.07	0.07
CO2	0.00	0.00	0.00	0.00	0.00	0.00
CO	0.01	0.01	0.00	0.01	0.01	0.01
HYDROGEN	0.02	0.02	0.00	0.05	0.05	0.05
NITROGEN	0.79	0.79	0.00	0.84	0.84	0.84
AMMONIA	0.11	0.11	0.00	0.04	0.04	0.04

Table A.29: Separation loop.

Stream	SP41TP29	SP41TP30	SP41TP31	SP41TP33	SP41TP35	SP41TP37	SP41TP39
Description							
Temp (°C)	15.00	0.00	380.00	420.51	400.00	316.79	260.00
Pres (bar)	161.62	155.00	161.84	161.62	161.62	161.62	161.62
Vapor (mol/mol)	1.00	1.00	1.00	1.00	1.00	1.00	1.00
Average MW (g/mol)	20.39	20.51	16.44	20.30	20.30	20.30	20.30
Mole Flows (kmol/h)	2971.84	2794.03	1338.61	3064.13	3064.13	3064.13	3064.13
Mass Flows (kg/h)							
TOTAL	60595.09	57293.26	22005.77	62195.99	62195.99	62195.99	62195.99
ETHANOL	0.00	0.00	0.00	0.00	0.00	0.00	0.00
WATER	0.00	0.00	0.00	0.00	0.00	0.00	0.00
METHANE	4658.89	4512.72	1451.06	4638.49	4638.49	4638.49	4638.49
CO2	24.85	22.90	9.63	25.93	25.93	25.93	25.93
CO	589.13	588.50	171.64	584.52	584.52	584.52	584.52
HYDROGEN	1258.65	1227.18	1076.78	1226.06	1226.06	1226.06	1226.06
NITROGEN	49478.36	48163.33	18478.54	48933.05	48933.05	48933.05	48933.05
AMMONIA	4585.22	2778.64	818.12	6787.96	6787.96	6787.96	6787.96
Mass fractions							
ETHANOL	0.00	0.00	0.00	0.00	0.00	0.00	0.00
WATER	0.00	0.00	0.00	0.00	0.00	0.00	0.00
METHANE	0.08	0.08	0.07	0.07	0.07	0.07	0.07
CO2	0.00	0.00	0.00	0.00	0.00	0.00	0.00
CO	0.01	0.01	0.01	0.01	0.01	0.01	0.01
HYDROGEN	0.02	0.02	0.05	0.02	0.02	0.02	0.02
NITROGEN	0.82	0.84	0.84	0.79	0.79	0.79	0.79
AMMONIA	0.08	0.05	0.04	0.11	0.11	0.11	0.11

Table A.30: Separation loop.

Stream	SP41TP40	SP41TP41	SP41TP42	SP41TP43	SP41TP44	SP41TP45	SP41TP46	SP41TP50	SP41TP51	SP41TP52
Description										
Temp (°C)	15.00	15.00	-10.00	-30.00	-14.13	-27.00	-26.47	-27.00	-27.00	-27.00
Pres (bar)	161.62	161.62	155.00	5.00	5.00	5.00	5.00	5.00	5.00	5.00
Vapor (mol/mol)	0.00	0.00	0.00	0.00	0.01	1.00	1.00	0.00	0.00	0.00
Average MW (g/mol)	17.07	17.07	17.06	17.04	17.06	18.05	18.05	17.04	17.04	17.04
Mole Flows (kmol/h)	222.99	133.80	294.32	5.76	294.32	7.08	6.72	293.00	5.76	228.54
Mass Flows (kg/h)										
TOTAL	3805.38	2283.23	5021.02	98.09	5021.02	127.73	121.34	4991.39	98.09	3893.28
METHANE	40.80	24.48	50.88	0.16	50.88	42.91	40.76	8.13	0.16	6.34
CO2	2.29	1.38	3.29	0.06	3.29	0.39	0.37	2.96	0.06	2.31
CO	1.22	0.73	1.43	0.00	1.43	1.40	1.33	0.03	0.00	0.03
HYDROGEN	1.18	0.71	1.31	0.00	1.31	1.30	1.23	0.01	0.00	0.01
NITROGEN	43.64	26.18	48.15	0.01	48.15	47.82	45.43	0.33	0.01	0.26
AMMONIA	3716.25	2229.75	4915.97	97.87	4915.97	33.91	32.22	4979.92	97.87	3884.34
Mass Fractions										
METHANE	0.01	0.01	0.01	0.00	0.01	0.34	0.34	0.00	0.00	0.00
CO2	0.00	0.00	0.00	0.00	0.00	0.00	0.00	0.00	0.00	0.00
CO	0.00	0.00	0.00	0.00	0.00	0.01	0.01	0.00	0.00	0.00
HYDROGEN	0.00	0.00	0.00	0.00	0.00	0.01	0.01	0.00	0.00	0.00
NITROGEN	0.01	0.01	0.01	0.00	0.01	0.37	0.37	0.00	0.00	0.00
AMMONIA	0.98	0.98	0.98	1.00	0.98	0.27	0.27	1.00	1.00	1.00

Table A.31: Separation loop (continued).

Stream Description	SP41TP60	SP41TP61	SP41TP62	SP41TP63	SP41TP64	SP41TP65
Temp (°C)	250.00	745.32	180.00	300.00	258.55	258.55
Pressure (bar)	155.00	162.00	5.00	162.00	162.00	162.00
Vapor (mol/mol)	1.00	1.00	1.00	1.00	1.00	1.00
Average MW (g/mol)	20.51	18.05	18.05	18.05	20.50	20.50
Mole Flows (kmol/h)	2794.03	6.72	6.72	6.72	2800.75	840.22
Mass Flows (kg/h)						
TOTAL	57293.26	121.34	121.34	121.34	57414.60	17224.38
METHANE	4512.72	40.76	40.76	40.76	4553.48	1366.04
CO2	22.90	0.37	0.37	0.37	23.27	6.98
CO	588.50	1.33	1.33	1.33	589.83	176.95
HYDROGEN	1227.18	1.23	1.23	1.23	1228.41	368.52
OXYGEN	0.00	0.00	0.00	0.00	0.00	0.00
NITROGEN	48163.33	45.43	45.43	45.43	48208.76	14462.63
AMMONIA	2778.64	32.22	32.22	32.22	2810.85	843.26
Mass Fractions						
METHANE	0.08	0.34	0.34	0.34	0.08	0.08
CO2	0.00	0.00	0.00	0.00	0.00	0.00
CO	0.01	0.01	0.01	0.01	0.01	0.01
HYDROGEN	0.02	0.01	0.01	0.01	0.02	0.02
OXYGEN	0.00	0.00	0.00	0.00	0.00	0.00
NITROGEN	0.84	0.37	0.37	0.37	0.84	0.84
AMMONIA	0.05	0.27	0.27	0.27	0.05	0.05

Table A.32: Separation loop (continued).

Stream	SP41TP66	SP41TP67	SP41TP68	SP41TP90	SP41TP91	SP41TP93	SV41TP91
Description							
Temp (°C)	258.55	293.57	258.55	18.24	0.00	0.00	18.24
Pres (bar)	162.00	162.00	162.00	161.62	155.00	155.00	161.62
Vapor (mol/mol)	1.00	1.00	1.00	1.00	0.00	0.00	1.00
Average MW (g/mol)	20.50	20.50	20.50	20.39	17.06	17.06	20.39
Mole Flows (kmol/h)	1120.30	1120.30	840.22	2897.54	267.54	160.52	74.30
Mass Flows (kg/h)							
TOTAL	22965.84	22965.84	17224.38	59080.21	4562.99	2737.79	1514.88
METHANE	1821.39	1821.39	1366.04	4542.41	44.00	26.40	116.47
CO2	9.31	9.31	6.98	24.23	3.20	1.92	0.62
CO	235.93	235.93	176.95	574.40	1.16	0.70	14.73
HYDROGEN	491.36	491.36	368.52	1227.19	1.00	0.60	31.47
OXYGEN	0.00	0.00	0.00	0.00	0.00	0.00	0.00
NITROGEN	19283.50	19283.50	14462.63	48241.40	36.61	21.97	1236.96
AMMONIA	1124.34	1124.34	843.26	4470.59	4477.03	2686.22	114.63
Mass Fractions							
METHANE	0.08	0.08	0.08	0.08	0.01	0.01	0.08
CO2	0.00	0.00	0.00	0.00	0.00	0.00	0.00
CO	0.01	0.01	0.01	0.01	0.00	0.00	0.01
HYDROGEN	0.02	0.02	0.02	0.02	0.00	0.00	0.02
OXYGEN	0.00	0.00	0.00	0.00	0.00	0.00	0.00
NITROGEN	0.84	0.84	0.84	0.82	0.01	0.01	0.82
AMMONIA	0.05	0.05	0.05	0.08	0.98	0.98	0.08

Table A.33: Separation loop (continued).

Stream	**Q** (kW)	**Tin** (°C)	**Tout** (°C)	Note
stream 1	1000	50	163	feed preheat
stream 2	3771	163	179	feed boil
stream 3	2150	179	470	feed superheat
stream 4	746	470	514	1st reac stage
stream 5	1990	514	534	2nd reac stage
stream 6	1870	495	537	3rd reac stage
stream 7	831	495	380	hx11
stream 8	5416	820	220	hx12fluid
stream 9	1918	336	114	hx13cool
stream 10	782	114	100	hx13cond
stream 11	518	99	85	hx14fluid
stream 12	359	148	100	1st cmpr cool
stream 13	687	100	60	1st cmpr cond
stream 14	3167	73	90	mdea preheat
stream 15	3167	115	86	mdea precool
stream 16	2788	86	60	mdea cool
stream 17	990	61	250	meth preheat
stream 18	138	325	250	1st meth cooljack
stream 19	396	325	250	1st meth aftercool
stream 20	55	390	250	2nd meth cooljack
stream 21	623	390	270	2nd meth aftercool
stream 22	138	22	185	feed air heat meth1
stream 23	55	185	248	feed air heat meth2
stream 24	128	248	98	feed air cool hx14
stream 25	559	514	200	feed air cool hx12
stream 26	990	270	72	meth reg cool
stream 27	609	243	123	2nd cmpr cool
stream 28	657	123	50	2nd cmpr cond
stream 29	853	213	40	3rd cmpr cool
stream 30	101	40	20	3rd cmpr cond
stream 31	2521	170	380	amm loop preheat
stream 32	368	484	454	amm 1st postcool
stream 33	306	433	420	amm 2nd postcool
stream 34	630	421	400	amm 3rd postcool
stream 35	2521	400	317	amm loop postcool
stream 36	1694	317	260	recycle cool 1
stream 37	6608	260	40	recycle cool 2
stream 38	563	40	25	recycle cool 3
stream 39	750	25	15	sep1 duty
stream 40	850	18	0	sep2 duty
stream 41	200	0	-30	sep3 duty
stream 42	114	15	-10	sep 3 precool
stream 43	14	-26	5	recycle heat 1
stream 44	6594	0	155	recycle heat 2
stream 45	368	259	294	recycle heat 3
stream 46	306	259	297	recycle heat 4
stream 47	2940	98	97	stripper cond
stream 48	7757	114	115	stripper reboil

Table A.34: Fluid list for the energetic balance.

A.5 Ethanol Ammoxidation

Stream report for the ethanol-acetonitrile process: refer to chapter 4.

Stream Description	FR61TA01 ethanol	FR61TA07 mixed feed	FR61TA08 heated feed	FR61TA06 quencher	FR61TA04 EtOH-air	FR61TA05 ammonia	P5 1st quarter	P11 2nd qt	P17 3rd qt	SP61TA10
Temp (°C)	20.00	108.93	360.00	20.00	150.00	20.00	390.80	412.21	455.87	380.00
Pres (bar)	1.00	1.00	1.00	1.00	1.00	1.00	1.00	1.00	1.00	1.00
Vapor (mol/mol)	0.00	1.00	1.00	1.00	1.00	1.00	1.00	1.00	1.00	1.00
Average MW (g/mol)	44.67	29.31	29.31	44.01	29.57	17.03	29.03	28.54	27.78	26.92
Mole Flows (kmol/h)	37.39	439.82	439.82	60.00	301.72	78.09	444.05	451.61	464.01	478.83
Mass Flows (kg/h)										
TOTAL	1670.00	12891.00	12891.00	2640.59	8920.41	1330.00	12891.00	12891.00	12891.00	12891.00
ETHANOL	1636.32	1636.32	1636.32	0.00	1636.32	0.00	1382.36	1005.53	443.72	0.07
WATER	33.68	681.13	681.13	0.00	681.13	0.00	868.04	1234.10	1842.39	2584.17
AMMONIA	0.00	1534.88	1534.88	0.00	204.88	1330.00	1496.99	1399.67	1230.67	1004.44
OXYGEN	0.00	1376.54	1376.54	0.00	1376.54	0.00	1243.12	1002.57	594.15	29.86
MECN	0.00	259.02	259.02	0.00	259.02	0.00	347.09	573.42	951.91	1388.13
ACH	0.00	0.00	0.00	0.00	0.00	0.00	126.76	206.96	258.89	39.55
ETHYLENE	0.00	0.00	0.00	0.00	0.00	0.00	6.91	18.32	37.89	63.28
CO	0.00	0.00	0.00	0.00	0.00	0.00	6.55	18.14	49.73	167.76
CO2	0.00	2869.64	2869.64	2640.59	229.05	0.00	2877.68	2892.23	2928.54	3027.32
HCN	0.00	0.00	0.00	0.00	0.00	0.00	1.91	5.53	12.15	3.99
NITROGEN	0.00	4533.46	4533.46	0.00	4533.46	0.00	4533.59	4534.53	4540.96	4582.41
Mass Fractions										
ETHANOL	0.98	0.13	0.13	0.00	0.18	0.00	0.11	0.08	0.03	0.00
WATER	0.02	0.05	0.05	0.00	0.08	0.00	0.07	0.10	0.14	0.20
AMMONIA	0.00	0.12	0.12	0.00	0.02	1.00	0.12	0.11	0.10	0.08
OXYGEN	0.00	0.11	0.11	0.00	0.15	0.00	0.10	0.08	0.05	0.00
MECN	0.00	0.02	0.02	0.00	0.03	0.00	0.03	0.04	0.07	0.11
ACH	0.00	0.00	0.00	0.00	0.00	0.00	0.01	0.02	0.02	0.00
ETHYLENE	0.00	0.00	0.00	0.00	0.00	0.00	0.00	0.00	0.00	0.00
CO	0.00	0.00	0.00	0.00	0.00	0.00	0.00	0.00	0.00	0.01
CO2	0.00	0.22	0.22	1.00	0.03	0.00	0.22	0.22	0.23	0.23
HCN	0.00	0.00	0.00	0.00	0.00	0.00	0.00	0.00	0.00	0.00
NITROGEN	0.00	0.35	0.35	0.00	0.51	0.00	0.35	0.35	0.35	0.36

Table A.35: Reactor section.

Stream Description	SP61TA12	SP61TA14	SP61TA16	SP61TA40	SP61TA18	SP61TA20	SP61TA21	SP61TA34	SP61TA35	Purge1	Purge2	Purge3
Temp (°C)	250.00	74.37	35.00	30.00	25.43	25.00	25.00	25.00	25.00	32.72	25.00	25.00
Pres (bar)	1.00	1.00	1.00	1.00	1.00	1.00	1.00	1.00	1.00	1.00	1.00	1.00
Vapor (mol/mol)	1.00	1.00	0.54	0.00	0.00	0.00	0.00	0.00	0.00	1.00	1.00	1.00
Average MW (g/mol)	26.92	26.92	31.96	18.02	22.92	27.32	31.11	21.69	49.58	29.34	25.62	41.37
Mole Flows (kmol/h)	478.83	478.83	403.35	336.00	562.01	1403.35	672.51	518.12	100.10	206.56	0.01	0.87
Mass Flows (kg/h)												
TOTAL	12891.00	12891.00	12889.15	6053.13	12881.36	38344.82	20921.86	11237.07	4962.73	6060.92	0.21	35.87
ETHANOL	0.07	0.07	0.12	0.00	0.12	0.12	0.00	0.00	0.00	0.00	0.00	0.12
WATER	2584.17	2584.17	1720.30	6053.13	7622.10	13326.84	5228.77	6356.50	553.80	186.31	0.00	0.00
AMMONIA	1004.44	1004.44	120.30	0.00	42.21	1038.44	0.00	1237.38	95.12	0.00	0.04	0.00
OXYGEN	29.86	29.86	30.81	0.00	0.01	0.01	0.00	0.00	0.00	30.80	0.00	0.01
MECN	1388.13	1388.13	1387.81	0.00	1369.55	18925.76	15693.09	2973.65	259.02	18.26	0.02	0.00
ACH	39.55	39.55	40.69	0.00	32.01	32.01	0.00	0.00	0.00	8.68	0.00	32.01
ETHYLENE	63.28	63.28	63.22	0.00	0.09	0.09	0.00	0.00	0.00	63.13	0.00	0.09
CO	167.76	167.76	167.36	0.00	0.03	0.02	0.00	0.00	0.00	167.33	0.01	0.02
CO2	3027.32	3027.32	921.50	0.00	3.08	1.39	0.00	0.02	0.26	1003.87	0.00	0.00
HCN	3.99	3.99	4.03	0.00	3.28	3.28	0.00	0.00	0.00	0.75	0.00	3.28
NITROGEN	4582.41	4582.41	4582.26	0.00	0.48	0.35	0.00	0.00	0.00	4581.78	0.13	0.35
H3O+	0.00	0.00	0.00	0.00	0.00	0.00	0.00	0.00	0.00	0.00	0.00	0.00
NH4+	0.00	0.00	439.46	0.00	1014.25	1487.71	0.00	233.50	116.25	0.00	0.00	0.00
AMMON(S)	0.00	0.00	2172.85	0.00	16.20	0.00	0.00	0.00	3622.32	0.00	0.00	0.00
HCO3-	0.00	0.00	998.36	0.00	2146.17	2073.96	0.00	93.71	241.16	0.00	0.00	0.00
OH-	0.00	0.00	0.00	0.00	0.00	0.02	0.00	0.04	0.00	0.00	0.00	0.00
CO3- -	0.00	0.00	240.09	0.00	631.77	1454.81	0.00	342.26	74.79	0.00	0.00	0.00
Mass Fractions												
ETHANOL	0.00	0.00	0.00	0.00	0.00	0.00	0.00	0.00	0.00	0.00	0.00	0.00
WATER	0.20	0.20	0.13	1.00	0.59	0.35	0.25	0.57	0.11	0.03	0.01	0.00
AMMONIA	0.08	0.08	0.01	0.00	0.00	0.03	0.00	0.11	0.02	0.00	0.19	0.00
OXYGEN	0.00	0.00	0.00	0.00	0.00	0.00	0.00	0.00	0.00	0.01	0.00	0.00
MECN	0.11	0.11	0.11	0.00	0.11	0.49	0.75	0.26	0.05	0.00	0.12	0.00
ACH	0.00	0.00	0.00	0.00	0.00	0.00	0.00	0.00	0.00	0.00	0.00	0.89
ETHYLENE	0.00	0.00	0.00	0.00	0.00	0.00	0.00	0.00	0.00	0.01	0.00	0.00
CO	0.01	0.01	0.01	0.00	0.00	0.00	0.00	0.00	0.00	0.03	0.03	0.00
CO2	0.23	0.23	0.07	0.00	0.00	0.00	0.00	0.00	0.00	0.17	0.00	0.00
HCN	0.00	0.00	0.00	0.00	0.00	0.00	0.00	0.00	0.00	0.00	0.00	0.09
NITROGEN	0.36	0.36	0.36	0.00	0.00	0.00	0.00	0.00	0.00	0.76	0.64	0.01
H3O+	0.000	0.000	0.000	0.000	0.000	0.000	0.000	0.000	0.000	0.000	0.000	0.000
NH4+	0.000	0.000	0.034	0.000	0.079	0.039	0.000	0.021	0.023	0.000	0.000	0.000
AMMON(S)	0.000	0.000	0.169	0.000	0.001	0.000	0.000	0.000	0.730	0.000	0.000	0.000
HCO3-	0.000	0.000	0.077	0.000	0.167	0.054	0.000	0.008	0.049	0.000	0.000	0.000
OH-	0.000	0.000	0.000	0.000	0.000	0.000	0.000	0.000	0.000	0.000	0.000	0.000
CO3- -	0.000	0.000	0.019	0.000	0.049	0.038	0.000	0.030	0.015	0.000	0.000	0.000

Table A.36: Separation Section.

Stream Description	SP61ATA23	SP61TA26	SP61TA28	SP61TA29	MECN	SP61TA38	SP61TA39	Bicarbon	Air	FR61TA02	FR01TA03	SP61TA36
Temp (°C)	25.25	186.49	30.29	20.00	209.65	78.69	30.00	5.30	20.00	20.00	5.30	110.02
Pres (bar)	18.00	18.00	1.00	1.00	18.00	1.00	1.00	1.00	1.00	1.00	1.00	1.00
Vapor (mol/mol)	0.00	0.00	0.00	0.00	0.00	1.00	0.41	0.00	1.00	1.00	0.72	0.00
Average MW (g/mol)	31.11	30.58	30.58	41.05	41.05	26.70	27.64	79.06	28.85	44.01	30.08	18.02
Mole Flows (kmol/h)	672.51	638.51	638.51	7.50	26.50	204.13	197.21	45.82	204.85	5.00	296.52	321.23
Mass Flows (kg/h)												
TOTAL	20921.86	19526.14	19526.14	307.89	1087.82	5449.98	5449.98	3622.32	5910.00	220.05	8920.41	5787.09
ETHANOL	0.00	0.00	0.00	0.00	0.00	0.00	0.00	0.00	0.00	0.00	1636.32	0.00
WATER	5228.77	5228.71	5228.71	0.00	0.06	699.87	575.21	0.00	0.00	0.00	587.48	5787.09
AMMONIA	0.00	0.00	0.00	0.00	0.00	1457.84	1299.90	0.00	0.00	0.00	95.12	0.00
OXYGEN	0.00	0.00	0.00	0.00	0.00	0.00	0.00	0.00	1376.54	0.00	1376.54	0.00
MECN	15693.09	14297.43	14297.43	307.89	1087.76	2973.65	2973.65	0.00	0.00	0.00	259.02	0.00
ACH	0.00	0.00	0.00	0.00	0.00	0.00	0.00	0.00	0.00	0.00	0.00	0.00
ETHYLENE	0.00	0.00	0.00	0.00	0.00	0.00	0.00	0.00	0.00	0.00	0.00	0.00
CO	0.00	0.00	0.00	0.00	0.00	0.00	0.00	0.00	0.00	0.00	0.00	0.00
CO2	0.00	0.00	0.00	0.00	0.00	318.61	14.09	0.00	0.00	220.05	0.26	0.00
HCN	0.00	0.00	0.00	0.00	0.00	0.00	0.00	0.00	0.00	0.00	0.00	0.00
NITROGEN	0.00	0.00	0.00	0.00	0.00	0.00	0.00	0.00	4533.46	0.00	4533.46	0.00
H3O+	0.00	0.00	0.00	0.00	0.00	0.00	0.00	0.00	0.00	0.00	0.00	0.00
NH4+	0.00	0.00	0.00	0.00	0.00	0.00	167.29	0.00	0.00	0.00	116.25	0.00
AMMON(S)	0.00	0.00	0.00	0.00	0.00	0.00	0.00	3622.32	0.00	0.00	0.00	0.00
HCO3-	0.00	0.00	0.00	0.00	0.00	0.00	278.55	0.00	0.00	0.00	241.16	0.00
OH-	0.00	0.00	0.00	0.00	0.00	0.00	0.01	0.00	0.00	0.00	0.00	0.00
CO3- -	0.00	0.00	0.00	0.00	0.00	0.00	141.29	0.00	0.00	0.00	74.79	0.00
Mass Fractions												
ETHANOL	0.00	0.00	0.00	0.00	0.00	0.00	0.00	0.00	0.00	0.00	0.18	0.00
WATER	0.25	0.27	0.27	0.00	5.259E-05	0.13	0.11	0.00	0.00	0.00	0.07	1.00
AMMONIA	0.00	0.00	0.00	0.00	0.00	0.27	0.24	0.00	0.00	0.00	0.01	0.00
OXYGEN	0.00	0.00	0.00	0.00	0.00	0.00	0.00	0.00	0.23	0.00	0.15	0.00
MECN	0.75	0.73	0.73	1.00	9.999E-01	0.55	0.55	0.00	0.00	0.00	0.03	0.00
ACH	0.00	0.00	0.00	0.00	0.00	0.00	0.00	0.00	0.00	0.00	0.00	0.00
ETHYLENE	0.00	0.00	0.00	0.00	0.00	0.00	0.00	0.00	0.00	0.00	0.00	0.00
CO	0.00	0.00	0.00	0.00	0.00	0.00	0.00	0.00	0.00	0.00	0.00	0.00
CO2	0.00	0.00	0.00	0.00	0.00	0.06	0.00	0.00	0.00	1.00	0.00	0.00
HCN	0.00	0.00	0.00	0.00	0.00	0.00	0.00	0.00	0.00	0.00	0.00	0.00
NITROGEN	0.00	0.00	0.00	0.00	0.00	0.00	0.00	0.00	0.77	0.00	0.51	0.00
H3O+	0.000	0.000	0.000	0.000	0.00	0.000	0.000	0.000	0.000	0.000	0.000	0.000
NH4+	0.000	0.000	0.000	0.000	0.00	0.000	0.031	0.000	0.000	0.000	0.013	0.000
AMMON(S)	0.000	0.000	0.000	0.000	0.00	0.000	0.000	1.000	0.000	0.000	0.000	0.000
HCO3-	0.000	0.000	0.000	0.000	0.00	0.000	0.051	0.000	0.000	0.000	0.027	0.000
OH-	0.000	0.000	0.000	0.000	0.00	0.000	0.000	0.000	0.000	0.000	0.000	0.000
CO3- -	0.000	0.000	0.000	0.000	0.00	0.000	0.026	0.000	0.000	0.000	0.008	0.000

Table A.37: Separation Section (continued).

Stream	**Q** (kW)	**Tin** (°C)	**Tout** (°C)	Note
stream 1	1260	110	360	cofeed preheat
stream 2	54	378	360	stage 1 jack
stream 3	57	383	378	stage 2 jack
stream 4	73	383	370	stage 2 aftercool
stream 5	57	391	370	stage 3 jack
stream 6	114	391	370	stage 3 aftercool
stream 7	58	406	370	stage 4 jack
stream 8	171	406	375	stage 4 aftercool
stream 9	59	404	375	stage 5 jack
stream 10	161	404	375	stage 5 aftercool
stream 11	59	412	375	stage 6 jack
stream 12	204	412	375	stage 6 aftercool
stream 13	61	427	375	stage 7 jack
stream 14	286	427	375	stage 7 aftercool
stream 15	62	435	375	stage 8 jack
stream 16	329	435	375	stage 8 aftercool
stream 17	88	456	375	stage 9 jack
stream 18	421	459	380	stage 9 aftercool
stream 19	103	453	380	stage 10 jack
stream 20	295	453	400	stage 10 aftercool
stream 21	162	605	400	stage 11 jack
stream 22	1280	605	380	stage 11 aftercool
stream 23	687	380	250	prod cool1
stream 24	862	250	74	prod cool2
stream 25	3638	74	35	prod cond
stream 26	652	26	25	mix cool
stream 27	17763	209	210	rectifier reboiler
stream 28	14688	187	186	rectifier condenser
stream 29	6520	109	110	stripper reboiler
stream 30	3696	80	79	stripper condenser
stream 31	1084	79	50	recycled vapor condenser
stream 32	324	50	30	recycle cool 1
stream 33	2814	186	30	azeotrope cool
stream 34	600	30	20	recycle cool 2
stream 35	1546	5	150	damp air preheat
stream 36	487	110	30	process water recycle
stream 37	411	210	20	mecn conditioning
stream 38	1900	25	190	reac coolant preheat
stream 39	4700	231	198	LPS steam available
stream 40	1630	198	45	LPS steam cond
stream 41	4154	190	198	LPS generation
stream 42	687	198	231	LPS superheating

Table A.38: Fluid List relevant to the assessment of the energetic balances.

A.6 Carbon Dioxide Methanation

The reported streams refer to the scheme in figure 5.5.

Stream	SP51TA20	SP51TA21	SP51TA22	SP51TA23	SP51TP25	SP51TP26	SP51TP30
Description							
Temp (°C)	165.78	97.03	80.00	79.80	200.00	160.00	80.00
Pres (bar)	1.09	1.09	1.09	1.09	17.00	17.00	17.00
Vapor (mol/mol)	1.00	1.00	0.54	1.00	1.00	0.92	1.00
Average MW (g/mol)	19.34	19.34	19.34	20.46	20.46	20.46	22.18
Mole Flows (kmol/h)	903.20	903.20	903.20	487.80	487.80	487.80	285.61
Mass Flows (kg/h)							
TOTAL	17464.24	17464.24	17464.24	9980.26	9980.26	9980.26	6333.68
CARBO-01	2878.46	2878.46	2878.46	2877.87	2877.87	2877.87	2870.72
HYDRO-01	12.96	12.96	12.96	12.96	12.96	12.96	12.96
METHA-01	3290.12	3290.12	3290.12	3290.08	3290.08	3290.08	3289.53
WATER	11282.69	11282.69	11282.69	3799.35	3799.35	3799.35	160.48
Mass fractions							
CARBO-01	0.16482	0.16482	0.16482	0.288356	0.288356	0.288356	0.453247
HYDRO-01	0.000742	0	0	0	0.001298	1.30E-03	0.002046
METHA-01	0	0	0	0	0.329659	3.30E-01	0.51937
WATER	1	1	1	0	0.380687	3.81E-01	0.025337

Table A.39: Water condensation.

Stream Description	SP52TP32	SP52TP33	SP52TP34	SP53TP35	SP52TP40	SP52TP41	SP52TA44	SP52TA46
Temp (°C)	70.78	70.00	80.70	25.00	70.00	84.01	86.94	100.48
Pres (bar)	17.00	17.00	17.00	17.00	2.00	17.00	1.00	1.00
Vapor (mol/mol)	0.99	1.00	1.00	1.00	0.00	0.00	0.01	0.00
Average MW (g/mol)	22.18	15.66	15.71	15.64	19.48	19.52	19.45	19.07
Mole Flow (kmol/h)	285.61	69.98	285.93	277.87	5957.00	5971.51	5966.84	5942.69
Mass Flows (kg/h)								
TOTAL	6333.68	1095.94	4492.23	4346.92	116040.72	116580.31	116040.72	113335.91
CARBO-01	2870.72	2.32	9.26	9.26	293.47	666.59	726.22	0.58
HYDRO-01	12.96	4.24	16.97	16.97	0.01	0.23	0.01	0.00
METHA-01	3289.53	1077.10	4308.41	4308.41	2.00	58.22	2.00	0.00
WATER	160.48	12.28	157.59	12.28	102361.93	102378.24	102538.79	103180.81
POTAS-01	0.00	0.00	0.00	0.00	0.00	0.00	0.00	0.00
H3O+	0.00	0.00	0.00	0.00	0.00	0.00	0.00	0.00
K+	0.00	0.00	0.00	0.00	5317.29	5317.29	5317.29	5184.36
OH-	0.00	0.00	0.00	0.00	0.04	0.04	0.31	9.33
HCO3-	0.00	0.00	0.00	0.00	7841.26	8025.67	6642.25	1964.79
CO3- -	0.00	0.00	0.00	0.00	224.72	134.03	813.85	2996.04
Mass Fractions								
CARBO-01	0.453	0.002	0.002	0.002	0.003	0.006	0.006	0.000
HYDRO-01	0.002	0.004	0.004	0.004	0.000	0.000	0.000	0.000
METHA-01	0.519	0.983	0.959	0.991	0.000	0.000	0.000	0.000
WATER	0.025	0.011	0.035	0.003	0.882	0.878	0.884	0.910
POTAS-01	0.000	0.000	0.000	0.000	0.000	0.000	0.000	0.000
H3O+	0.000	0.000	0.000	0.000	0.000	0.000	0.000	0.000
K+	0.000	0.000	0.000	0.000	0.046	0.046	0.046	0.046
OH-	0.000	0.000	0.000	0.000	0.000	0.000	0.000	0.000
HCO3-	0.000	0.000	0.000	0.000	0.068	0.069	0.057	0.017
CO3- -	0.000	0.000	0.000	0.000	0.002	0.001	0.007	0.026

Table A.40: Carbon Dioxide separation.

Stream Description	SP52TA47	SP52TA48	SP52TP50	SB52TA58	SB52TA59	SB52TA60
Temp (°C)	100.48	80.00	80.67	100.48	70.00	93.54
Pres (bar)	1.00	1.00	17.00	1.00	2.00	1.00
Vapor (mol/mol)	0.00	0.00	0.00	0.00	1.00	1.00
Average MW (g/mol)	19.07	19.07	19.09	19.07	33.68	23.28
Mole Flow (kmol/h)	6095.13	5942.69	5951.79	152.38	16.02	270.48
Mass Flows (kg/h)						
TOTAL	116242.97	113335.91	113642.92	2906.07	539.59	6297.75
CARBO-01	0.59	0.40	0.39	0.01	439.62	2413.26
HYDRO-01	0.00	0.00	0.00	0.00	0.22	0.01
METHA-01	0.00	0.00	0.00	0.00	56.22	2.54
WATER	105827.48	103185.87	103257.58	2645.69	43.53	3881.94
POTAS-01	0.00	0.00	0.00	0.00	0.00	0.00
H3O+	0.00	0.00	0.00	0.00	0.00	0.00
K+	5317.29	5184.36	5317.29	132.93	0.00	0.00
OH-	9.57	4.49	4.81	0.24	0.00	0.00
HCO3-	2015.18	1947.92	1949.11	50.38	0.00	0.00
CO3- -	3072.86	3012.88	3113.74	76.82	0.00	0.00
Mass fractions						
CARBO-01	0.000	0.000	0.000	0.000	0.815	0.383
HYDRO-01	0.000	0.000	0.000	0.000	0.000	0.000
METHA-01	0.000	0.000	0.000	0.000	0.104	0.000
WATER	0.910	0.910	0.909	0.910	0.081	0.616
POTAS-01	0.000	0.000	0.000	0.000	0.000	0.000
H3O+	0.000	0.000	0.000	0.000	0.000	0.000
K+	0.046	0.046	0.047	0.046	0.000	0.000
OH-	0.000	0.000	0.000	0.000	0.000	0.000
HCO3-	0.017	0.017	0.017	0.017	0.000	0.000
CO3- -	0.026	0.027	0.027	0.026	0.000	0.000

Table A.41: Carbon Dioxide separation (continued).

Stream Description	SP53TA44	SP53TA38	SP53TA46	SP53TP35	SP53TP41	SP53TP43	SP53TP50
Temp (°C)	25.00	25.00	25.00	25.00	25.00	25.00	25.00
Pres (bar)	1.00	1.00	1.00	17.00	17.00	17.00	17.00
Vapor (mol/mol)	1.00	1.00	1.00	1.00	1.00	1.00	1.00
Average MW (g/mol)	15.66	15.66	15.66	15.64	15.64	15.64	15.64
Mole Flow (kmol/h)	69.98	69.98	69.98	277.87	277.87	207.89	207.89
Mass Flows (kg/h)							
TOTAL	1095.94	1095.94	1095.94	4346.92	4346.92	3250.98	3250.98
CARBO-01	2.32	2.32	2.32	9.26	9.26	6.95	6.95
HYDRO-01	4.24	4.24	4.24	16.97	16.97	12.73	12.73
METHA-01	1077.10	1077.10	1077.10	4308.41	4308.41	3231.31	3231.31
WATER	12.28	12.28	12.28	12.28	12.28	0.00	0.00
Mass Fractions							
CARBO-01	0.002	0.002	0.002	0.002	0.002	0.002	0.002
HYDRO-01	0.004	0.004	0.004	0.004	0.004	0.004	0.004
METHA-01	0.983	0.983	0.983	0.991	0.991	0.994	0.994
WATER	0.011	0.011	0.011	0.003	0.003	0.000	0.000

Table A.42: PSA dehydration section.

Stream	QS50TP10	QS50TP12	QS50TP14	QS50TP19	QW50TA01	QW50TP05	QW50TP07	QW50TP21	SB51TA01
Description									
Temp (°C)	100.17	100.49	100.49	100.49	15.00	72.41	95.00	100.18	79.80
Pres (bar)	1.02	1.02	1.02	1.02	1.00	1.10	1.10	1.02	1.09
Vapor (mol/mol)	1.00	1.00	1.00	1.00	0.00	0.00	0.00	0.00	0.00
Average MW (g/mol)	18.03	18.03	18.03	18.03	18.02	18.02	18.02	18.02	18.02
Flows (kmol/h)	399.21	5.55	360.58	33.08	44.41	662.00	662.00	262.79	415.41
Mass Flows (kg/h)									
TOTAL	7196.39	100.00	6500.00	596.39	800.00	11930.56	11930.56	4734.17	7483.98
CARBO-01	7.74	0.11	6.99	0.64	0.00	7.74	7.74	0.00	0.59
HYDRO-01	0.00	0.00	0.00	0.00	0.00	0.00	0.00	0.00	0.00
METHA-01	0.60	0.01	0.54	0.05	0.00	0.60	0.60	0.00	0.04
WATER	7188.05	99.88	6492.46	595.70	800.00	11922.21	11922.21	4734.17	7483.34
Mass Fractions									
CARBO-01	0.001	0.001	0.001	0.001	0.000	0.001	0.001	0.000	0.000
HYDRO-01	0.000	0.000	0.000	0.000	0.000	0.000	0.000	0.000	0.000
METHA-01	0.000	0.000	0.000	0.000	0.000	0.000	0.000	0.000	0.000
WATER	0.999	0.999	0.999	0.999	1.000	0.999	0.999	1.000	1.000

Table A.43: Water streams and main recycle.

Stream	SB51TA04	SB51TA32	SB51TP02	SB52TA62
Description				
Temp (°C)	75.00	100.00	80.00	92.09
Pres (bar)	1.05	1.20	17.00	1.00
Vapor (mol/mol)	0.00	1.00	0.00	1.00
Average MW (g/mol)	18.04	23.60	18.04	23.87
Mole Flow (kmol/h)	202.19	298.05	202.19	286.50
Mass Flows (kg/h)				
TOTAL	3646.58	7033.45	3646.58	6837.34
CARBO-01	7.15	2941.02	7.15	2852.89
HYDRO-01	0.00	8.29	0.00	0.23
METHA-01	0.55	58.77	0.55	58.76
WATER	3638.87	4025.37	3638.87	3925.47
Mass Fractions				
CARBO-01	0.002	0.418	0.002	0.417
HYDRO-01	0.000	0.001	0.000	0.000
METHA-01	0.000	0.008	0.000	0.009
WATER	0.998	0.572	0.998	0.574

Table A.44: Water streams and main recycle (continued).

Stream Description	FR51TA01	TR51TA10 1st stage	TR51TA13 2nd stage	TR51TA15 3rd stage	TR51TA17 4th stage	FR51TA09	FR51TA10	SP52FR09
From		PFR1	PFR2	PFR3	PFR4			
To		PFR2	PFR3	PFR4	PFR5			
Temp (°C)	60.00	309.89	444.51	395.48	307.57	200.00	80.00	25.00
Pres (bar)	1.30	1.17	1.16	1.15	1.12	1.20	1.30	1.10
Vapor (mol/mol)	1.00	1.00	1.00	1.00	1.00	1.00	1.00	0.00
Average MW (g/mol)	10.35	10.78	15.41	17.12	18.76	10.35	16.01	45.78
Mole Flow (kmol/h)	1008.00	967.58	1133.38	1020.15	931.07	1008.00	6.00	6.71
Mass Flows (kg/h)								
TOTAL	10430.79	10430.79	17464.24	17464.24	17464.24	10430.79	96.08	307.01
CARBO-01	8801.96	7912.53	7943.46	5451.90	3491.69	8801.96	88.02	0.00
HYDRO-01	1628.83	1465.87	940.97	484.47	125.31	1628.83	8.06	0.00
METHA-01	0.00	324.22	1443.80	2352.04	3066.59	0.00	0.00	0.00
WATER	0.00	728.17	7136.01	9175.83	10780.65	0.00	0.00	70.74
K+	0.00	0.00	0.00	0.00	0.00	0.00	0.00	39.32
K2CO3(S)	0.00	0.00	0.00	0.00	0.00	0.00	0.00	160.39
KHCO3(S)	0.00	0.00	0.00	0.00	0.00	0.00	0.00	7.33
OH-	0.00	0.00	0.00	0.00	0.00	0.00	0.00	1.25
HCO3-	0.00	0.00	0.00	0.00	0.00	0.00	0.00	0.02
CO3- -	0.00	0.00	0.00	0.00	0.00	0.00	0.00	27.96
Mass Fractions								
CARBO-01	0.844	0.759	0.455	0.312	0.200	0.844	0.916	0.000
HYDRO-01	0.156	0.141	0.054	0.028	0.007	0.156	0.084	0.000
METHA-01	0.000	0.031	0.083	0.135	0.176	0.000	0.000	0.000
WATER	0.000	0.070	0.409	0.525	0.617	0.000	0.000	0.230
K+	0.000	0.000	0.000	0.000	0.000	0.000	0.000	0.128
K2CO3(S)	0.000	0.000	0.000	0.000	0.000	0.000	0.000	0.522
KHCO3(S)	0.000	0.000	0.000	0.000	0.000	0.000	0.000	0.024
OH-	0.000	0.000	0.000	0.000	0.000	0.000	0.000	0.004
HCO3-	0.000	0.000	0.000	0.000	0.000	0.000	0.000	0.000
CO3- -	0.000	0.000	0.000	0.000	0.000	0.000	0.000	0.091

Table A.45: Feed streams and reactive section.

Stream	**Q** (kW)	**Tin** (°C)	**Tout** (°C)	Note
stream 1	802	60	152	feed preheat 1
stream 2	282	152	120	feed intercool 1
stream 3	865	120	217	feed preheat 2
stream 4	603	217	150	feed intercool 2
stream 5	518	150	208	feed preheat 3
stream 6	429	208	160	feed intercool 3
stream 7	377	160	202	feed preheat 4
stream 8	20	202	200	feed intercool 4
stream 9	671	256	200	prod intercool 2nd stage
stream 10	377	445	200	2nd stage cool
stream 11	2918	445	190	prod intercool 3rd stage
stream 12	518	395	190	3rd stage cool
stream 13	2305	395	180	prod intercool 4th stage
stream 14	865	308	180	4th stage cool
stream 15	1270	308	180	prod intercool 5th stage
stream 16	802	180	166	5th stage cool
stream 17	629	166	97	prod cool 1
stream 18	4950	97	80	prod cool 2
stream 19	444	193	110	cmpr cool 1
stream 20	351	224	160	cmpr cool 2
stream 21	480	283	200	cmpr cool 3
stream 22	638	200	160	prod cool 3
stream 23	2300	160	80	prod cool 4
stream 24	92	80	71	prod cool 5
stream 25	1639	84	70	rich solvent degas
stream 26	2414	70	90	rich solvent reheat
stream 27	2414	100	80	lean solvent cool
stream 28	267	81	25	psa precool
stream 29	314	72	95	feedwater preheat 1
stream 30	210	99	100	feedwater preheat 2
stream 31	3944	100	101	feedwater boil
stream 32	456	101	100	SG dispersion
stream 33	3226	114	30	high T crio exchanger

Table A.46: Fluid List relevant to the assessment of the energetic balances.

Appendix B

Computational Details

B.1 Thermodynamic parameters

The following parameters in Table B.1 have been used to correct the predicted acetaldehyde(i)-water(j) VLE in the ethanol dehydration simulation, after regression using the data of [38], with the NRTL model as reworked within the Aspen Plus package:

$$ln\gamma_i = \frac{\Sigma_j x_j \tau_{ji} G_{ji}}{\Sigma_k x_k G_{ki}} + \Sigma_j \frac{x_j G_{ij}}{\Sigma_k x_k G_{kj}} \left(\tau_{ij} - \frac{\Sigma_m x_m \tau_{mj} G_{mj}}{\Sigma_k x_k G_{kj}} \right) \quad \text{(B.1)}$$

$$G_{ij} = exp(-\alpha_{ij}\tau_{ij}) \qquad G_{ii} = 1 \quad \text{(B.2)}$$

$$\tau_{ij} = A_{ij} + B_{ij}/T \qquad \tau_{ii} = 0 \quad \text{(B.3)}$$

$$\alpha_{ij} = C_{ij} \quad \text{(B.4)}$$

where higher order parameters are omitted since they are kept at the default value of 0.

The Henry constant temperature dependence is represented as:

$$lnH = a + b/T + clnT + dT \quad \text{(B.5)}$$

and the parameters in Table B.1 are used, instead the default ones, if acetaldehyde is to be treated with this approach.

Parameter	A_{ij}	A_{ji}	B_{ij}	B_{ji}	C_{ij}
Value	17.10	-1.133	-4681	569.7	0.3

Table B.1: Henry constant parameters for acetaldehyde in water.

Table B.2 has other two Henry constant corrections for the ethylene process.

Specie	Solvent	A	B	C	D
Ethylene	Ethanol	5.134	0	0	0
Butylene	Water	26.30	-5000	0	0

Table B.2: Henry constant parameters for ethylene and butylene.

The ethanol dehydration and reforming processes need another correction, regarding the Henry constant of carbon monoxide, as per Table B.3.

Parameter	corrected	APV90 BINARY
A bar/(mol/mol)	152.2	171.775
B (K)	-8150	-8297
C	-20.015	-23.,3372
D	0	0
Tmin		-0.15
Tmax		79.85

Table B.3: Heuristic Henry constant correction for carbon monoxide in water.

Also the correlation for methane solubility into potassium carbonate solutions has been corrected heuristically using a modified Henry constant, with coefficients are in Table B.4.

Parameter	A	B	C	D
Value	184.05	-9111.7	-25.038	0.000143

Table B.4: Heuristic Henry constant correction for methane in water plus potassium carbonate.

B.2 Pressure Swing Schemes

The pressure-swing calculation has been performed using the Aspen Adsorption software: this allows to choose the proper model equations and numerical solution algorithms between a wide range of options, without the need of rewriting them explicitly. The chosen equations are:

$$\epsilon \frac{\partial c}{\partial t} = -\frac{\partial (v\, c)}{\partial z} - \rho_s \frac{\partial w}{\partial t} \tag{B.6}$$

$$\frac{\partial w}{\partial t} = (MTC) \times (w - w_{eq}) \tag{B.7}$$

$$w_{eq} = f(P, P_{sat}, T) \tag{B.8}$$

$$\frac{\partial P_{tot}}{\partial z} = \frac{-0.0015 \mu \, (1-\epsilon)^2}{4 r^2 \epsilon^3} \, v + 1.75 \times 10^{-5} (MW) \rho \frac{1-\epsilon}{2 r \epsilon^3} \, v^2 \tag{B.9}$$

$$c = f(P, T) \tag{B.10}$$

where v is the gas velocity, ϵ the total bed void fraction, r the solid particles radius and z the spatial coordinate. MTC (Mass-transfer coefficient) is considered constant.

Ethylene dehydration

According to the reviewed literature [204, 205], adsorption data for ethylene and water have been interpolated using the software built-in Langmuir-Freundlich equilibrium model (in place of the general formula B.8), where p are adjustable parameters:

$$w_{eq} = \frac{p_1 \, p_2 \, P^{p_3} \, exp\,(p_4/T)}{1 + p_5 \, P^{p_3} \, exp\,(p_6/T)} \tag{B.11}$$

See also graph B.1 for a comparison between the available and re-calculated data. This step is necessary because the authors provide different correlation to fit their data for ethylene and water on the same material, while the Aspen Adsorption algorithm requires one model for each adsorbent, equal for every chemical in the calculation.

The input data are presented in Table B.5, the bed height, diameter and packing have been adjusted to grant a limited pressure drop with the gas flow given by the steady-state simulation. After evaluating the breakthrough time, in the simpler configuration 2 beds have been connected and scheduled as reported in scheme B.2 and Table B.6.

Parameter	Value	Units	Description
Hb	0.5	m	Height of adsorbent layer
Db	0.5	m	Internal diameter of adsorbent layer
ϵ	0.35	m3 void/m3 bed	Inter-particle voidage
ρ_s	650	kg/m3	Bulk solid density of adsorbent
r	0.002	m	Adsorbent particle radius
MTC("ETHYLENE")	1	1/s	Constant mass transfer coefficients
MTC("WATER")	1	1/s	Constant mass transfer coefficients
p_1(1."ETHYLENE")	0.148	n/a	Isotherm parameter
p_1(1."WATER")	11.9	n/a	Isotherm parameter
p_2(2."ETHYLENE")	1	n/a	Isotherm parameter
p_2(2."WATER")	1	n/a	Isotherm parameter
p_3(3."ETHYLENE")	0.6	n/a	Isotherm parameter
p_3(3."WATER")	1.4	n/a	Isotherm parameter
p_4(4."ETHYLENE")	0	n/a	Isotherm parameter
p_4(4."WATER")	0	n/a	Isotherm parameter
p_5(5."ETHYLENE")	0.0315	n/a	Isotherm parameter
p_5(5."WATER")	0.84	n/a	Isotherm parameter
p_6(6."ETHYLENE")	0	n/a	Isotherm parameter
p_6(6."WATER")	0	n/a	Isotherm parameter

Table B.5: Inputs for the ethylene-water adsorption bed in Aspen Adsorption.

step	t (s)	VCON	VF1	VF2	VP1	VP2	VW1	VW2
1	480	Cv	OPENED	CLOSED	Flow	CLOSED	CLOSED	OPENED
2	20	CLOSED	CLOSED	Cv	CLOSED	CLOSED	Cv	CLOSED
3	480	Cv	CLOSED	OPENED	CLOSED	Flow	OPENED	CLOSED
4	20	CLOSED	Cv	CLOSED	CLOSED	CLOSED	CLOSED	Cv

Table B.6: Valve positions schedule ('Cv' stands for pressure driven operation where the linear bound: $Flow = C_v \times \Delta P$ is applied.)

Notice that the feed, product and purge (i.e. the inlet/outlet ports for the calculation) are separated (and their specifications set equal) because, in this way, the software doesn't need to solve the dynamic mass and pressure balances of the 3-way connectors that would be otherwise present, and the calculation results easier while the information on the relevant process blocks (i.e. the beds and outlet streams) is kept.

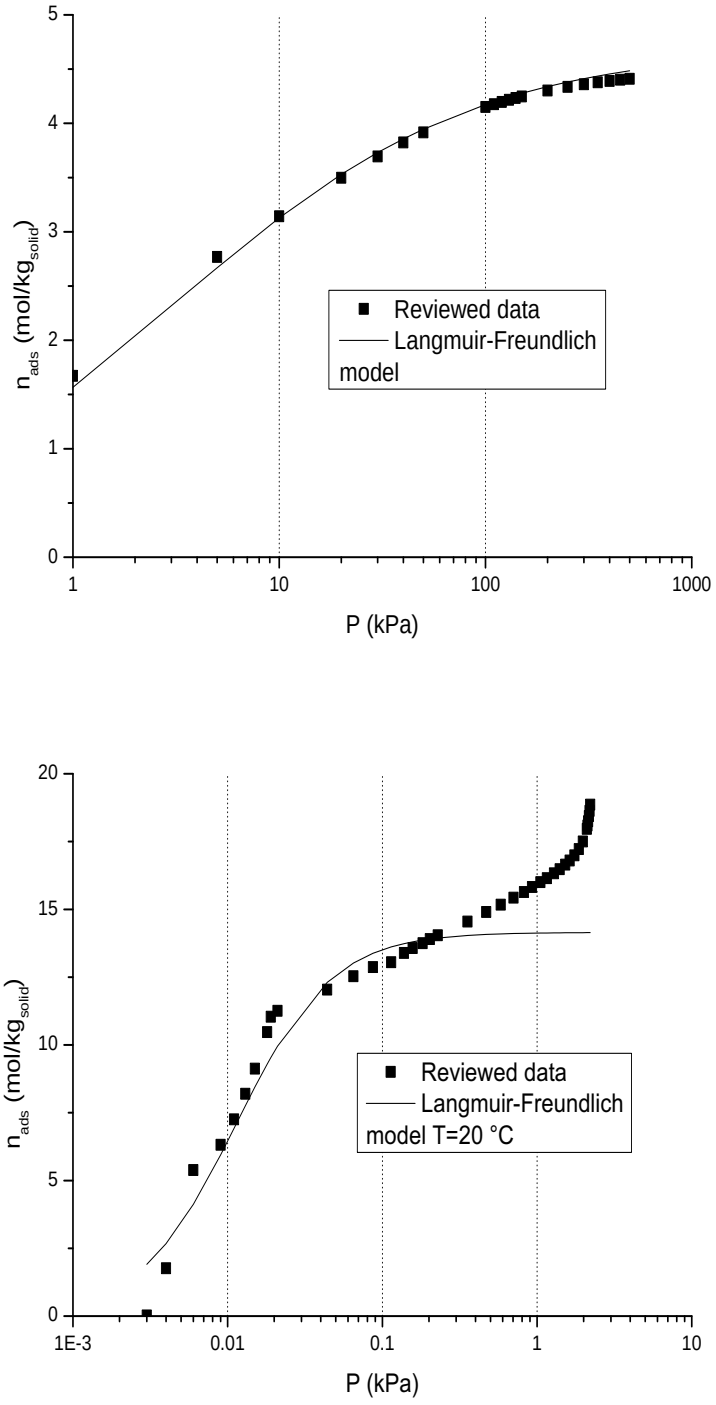

Figure B.1: Data and interpolation for ethylene and water adsorption on the solid bed. The model doesn't fit the range of water condensation, that anyway is not relevant for the simulated conditions.

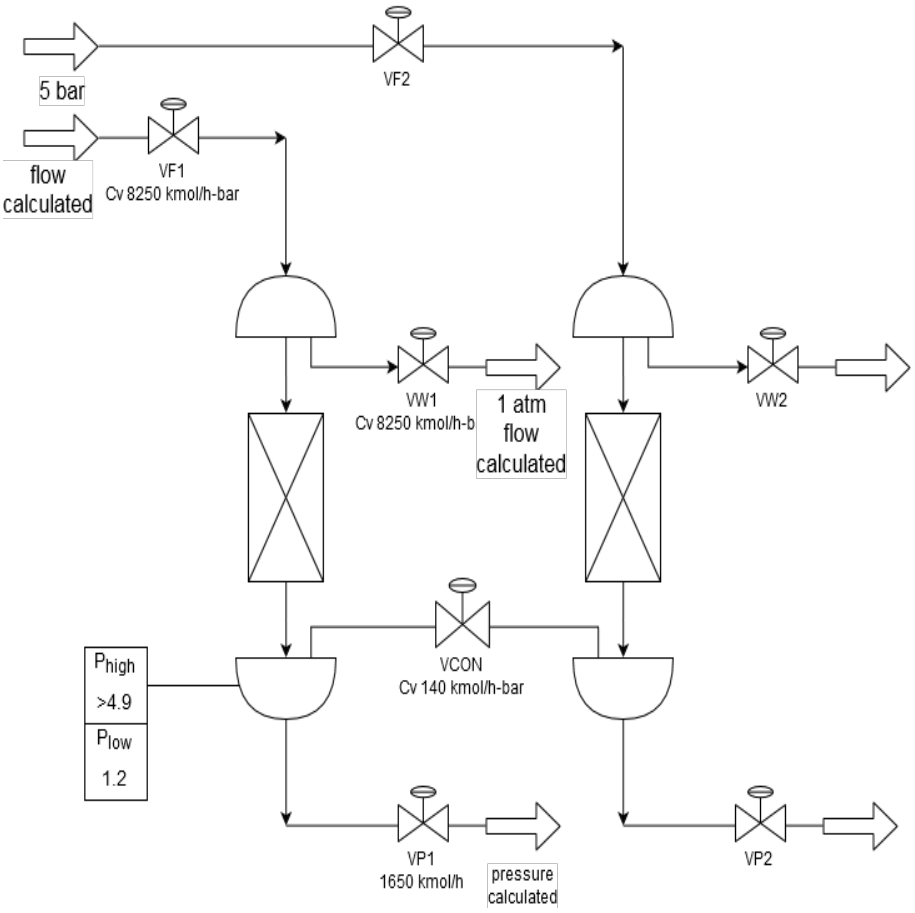

Figure B.2: Scheme for the ethylene-water adsorption bed in Aspen Adsorption.

Methane dehydration

In this case, the data from [206] and [207] are interpolated replacing eq. B.8 via a simple Langmuir model, as shown in the Figure B.3:

$$w_{eq} = \frac{p_1 P}{1 + p_2 P} \tag{B.12}$$

The range of very low water pressure is not reproduced correctly, but the error in defective should result in a conservative calculation.

The same procedure has been followed to build the scheme B.4 and the input data (Tables B.7 and B.8), but in this case a numerical solution has been tried and found with a fully connected layout.

Parameter	Value	Units	Description
Hb	0.5	m	Height of adsorbent layer
Db	0.4	m	Internal diameter of adsorbent layer
ϵ	0.5	m3 void/m3 bed	Inter-particle voidage
ϵ_p	0.7	m3 void/m3 bead	Intra-particle voidage
ρ_s	1920	kg/m3	Bulk solid density of adsorbent
r	0.001	m	Adsorbent particle radius
MTC("METHANE")	10	1/s	Constant mass transfer coefficients
MTC("WATER")	10	1/s	Constant mass transfer coefficients
p_1(1."METHANE")	0.001	n/a	Isotherm parameter
p_1(1."WATER")	3.5	n/a	Isotherm parameter
p_2(2."METHANE")	2.2	n/a	Isotherm parameter
p_2(2."WATER")	2500	n/a	Isotherm parameter

Table B.7: Inputs for the methane-water adsorption bed in Aspen Adsorption.

step	t (s)	VCON	VF1	VF2	VP1	VP2	VW1	VW2
1	45	Cv	OPENED	CLOSED	Flow	CLOSED	CLOSED	Cv
2	5	CLOSED	CLOSED	Cv	CLOSED	CLOSED	Cv	CLOSED
3	45	Cv	CLOSED	OPENED	CLOSED	Flow	Cv	CLOSED
4	5	CLOSED	Cv	CLOSED	CLOSED	CLOSED	CLOSED	Cv

Table B.8: Valve positions schedule ('Cv' stands for pressure driven operation where the linear bound: $Flow = C_v \times \Delta P$ is applied.)

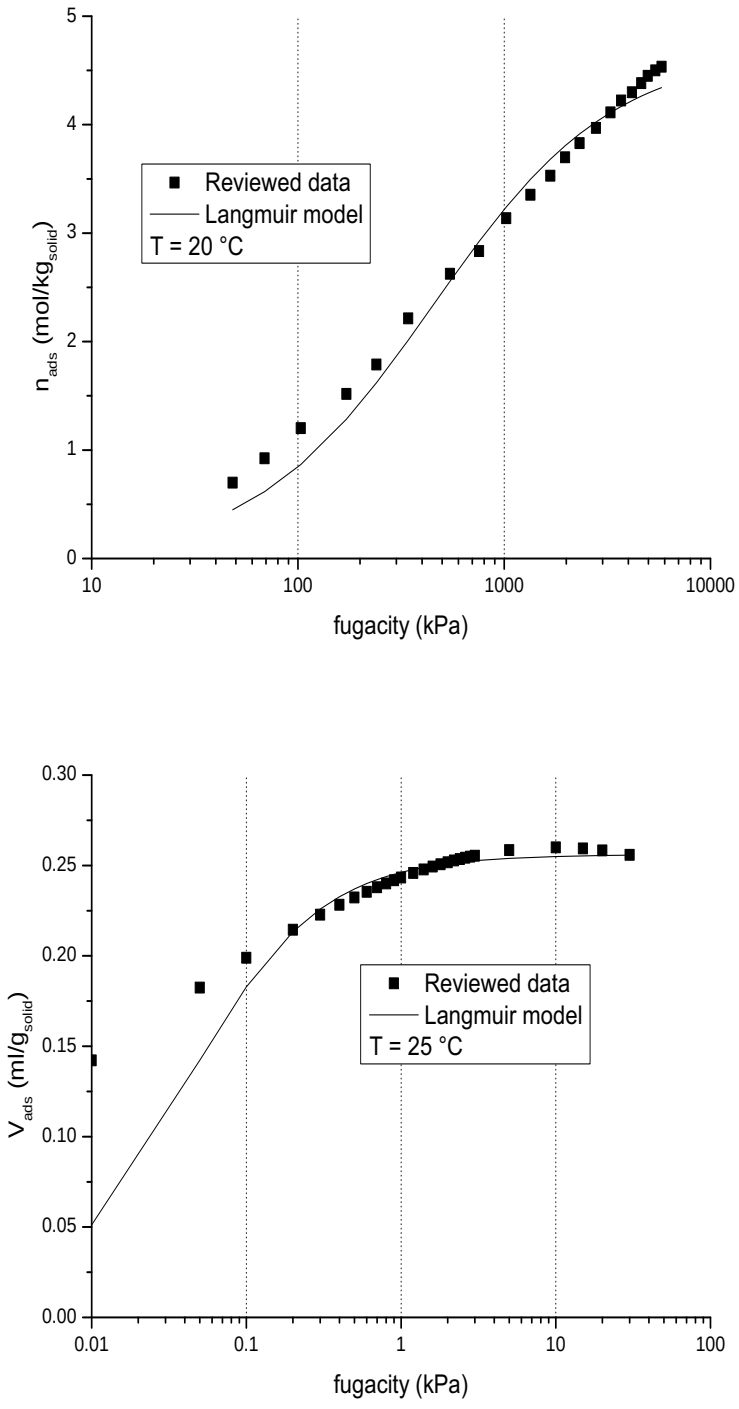

Figure B.3: Data and interpolation for methane and water adsorption on the bed.

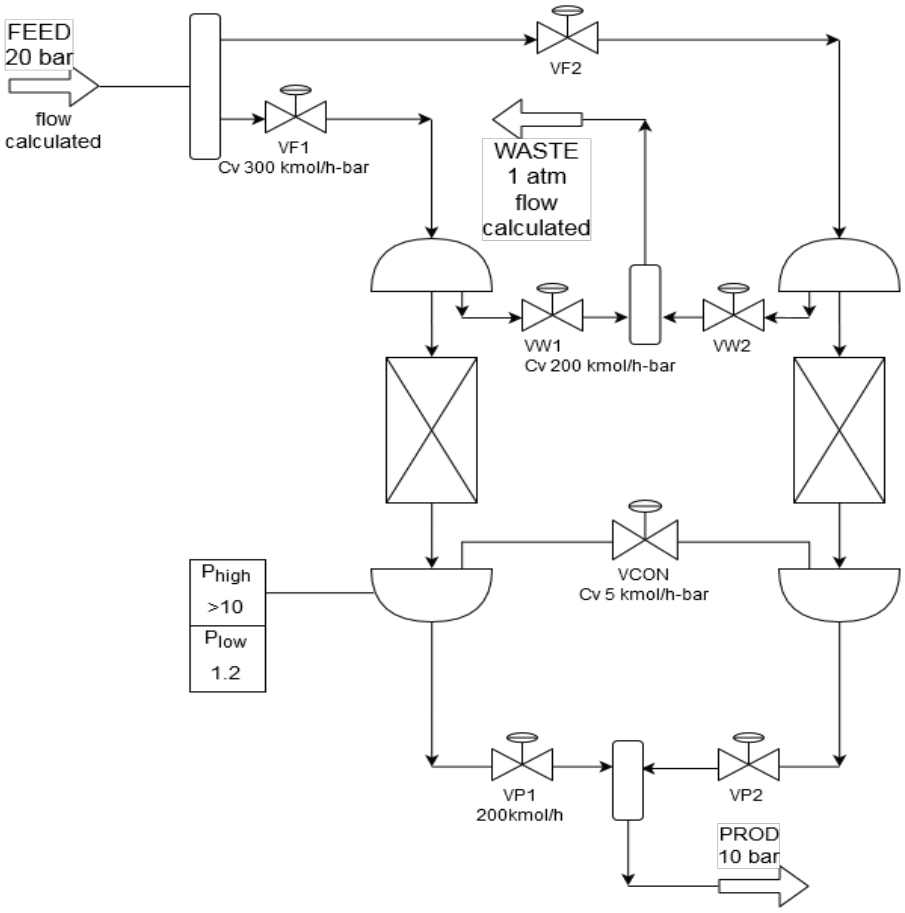

Figure B.4: Scheme for the methane-water adsorption bed in Aspen Adsorption.

B.3 Customized Blocks Simulation

Ethanol Reforming for DHPC

The following calculations (Table A.21) are used to find the heat-exchange parameters relative to the radiators of the steady-state cogeneration section of scheme 2.12.

Step	**T_{water}**	**Tair (°C)**	**ΔT**	**ΔT∗**	**Heat (ΔT) (W)**	**Heat(ΔT*)**	**U(ΔT) (W/°C)**	**U(ΔT*)**
0	69.5	31.0	38.5	49.5	114.1	159.8	3.0	3.2
1	66.8	29.4	37.4	46.8	109.8	148.3	2.9	3.2
2	64.1	27.8	36.3	44.1	105.5	136.9	2.9	3.1
3	61.4	26.2	35.2	41.4	101.2	125.8	2.9	3.0
4	58.7	24.6	34.1	38.7	97.0	114.9	2.8	3.0
5	56.0	23.0	33.0	36.0	92.8	104.3	2.8	2.9
6	53.3	21.4	31.9	33.3	88.7	94.0	2.8	2.8
7	50.6	19.8	30.8	30.6	84.6	83.9	2.7	2.7
8	47.9	18.2	29.7	27.9	80.6	74.1	2.7	2.7
9	45.2	16.6	28.6	25.2	76.6	64.7	2.7	2.6
10	42.5	15.0	27.5	22.5	72.7	55.6	2.6	2.5
Mean	56	23	33	36	93.1	105.7	2.8	2.9
Water Flow (l/h)					3.0	3.6		
Air Flow (cum/h)					17.4	19.8		
Length (m)			0.8		Surface (m^2)			0.65
β			0.0033		μ/ρ			1.6e-5
Gr			2.13e9		k ($\frac{W}{m\,K}$)			0.026
c_p ($\frac{J}{kg\,K}$)			1200					

Table B.9: Relevant parameters for a single radiator element calculation, used to compile the AP forms. The values refer to a radiator power of 162 W for $< dT >= 50°C$. $\Delta T* = T_{water} - 20°C$.

The second report (Table B.10), that presents the heating duty for a civil building, has been obtained with the DOCET[1] spreadsheet developed by to be used in the civil energetic assessments.

The relations and values in Table B.11 have been employed to solve dynamically the DHPC problem. The software used to integrate the partial differential equations under the algebraic and logical constraints is Matlab. Letter 'T' indicates a temperature, 'Q' a thermal power, 'M' a mass, 'C' and 'c' gross and specific heat capacities, and the other letters stand for the currents' mass flows.

[1]http://www.docet.itc.cnr.it/. The code is compliant to norms: UNI TS 11300 p. 1-2: 2014, UNI TS 11300 p. 3: 2010 and UNI TS 11300 p. 4-5: 2016.

House general data					
Location		Milan	Italy		
Climate	Code	E 2404			
Type		Detached house			
Building period		1986	– 1991		
External color		Medium gradation			
Non-heated spaces					
Underfloor		Cellar	car box		
Ceiling		Roof			
Floor level		Staircase			
Building Storey		**number**	**Height (m)**		
		2	3		
Surface (m2)		100			
Plant dimensions		**N**	**E**	**S**	**W**
Equivalent length (m)		10	10	10	10
Walls	**U** $(\frac{\mathbf{W}}{\mathbf{m^2K}})$		**A** $(\mathbf{m^2})$		
		N	**E**	**S**	**W**
Walls	1.14	56	53	54	54
Windows	2.9	3.9	6.9	5.9	5.9
Staircases	1.11	24			
Floor	1.25	120			
Ceiling	1.50	120			
Total	**Volume (m3)**		**A (m2)**		
	823		554		
Summary		587			
Conductive dispersion (W/K)		587			
Convective dispersion (W/K)		30			
House time constant (h)		41.9			
	total	**Dec-Feb**	**Mar-May**	**Jun-Aug**	**Sept-Nov**
Heating power required(kWh)	30160	18710	4760	0	6690
Classification: 439 kWh/m2 per year (F)					

Table B.10: Summary of the key parameters and results ofthe calculation of a model house in the northern Italy climate. Data relative to the summer cooling requirements have been omitted, but they are nevertheless included in the classification result according to the methodology adopted.

Block	**Balances**	**Constraints**
Reservoir (R)	$\frac{\partial T_R}{\partial t} = \frac{1}{M_R}\left(R_5T_5 + R_7T_7 - R_1T_R - \frac{Q_{RS}}{c_p} - \frac{Q_{R-ext}}{c_p}\right)$	$M_r \equiv M_{R0}$ $R_7 = R_5(1-D)$
Condenser HX (C)	$\frac{\partial T_{RC}}{\partial t} = \frac{1}{M_{RC}}\left(R_0T_R - R_2T_2 + \frac{Q_{cond}}{c_p}\right)$ $\frac{\partial T_C}{\partial t} = \frac{1}{M_C}\left(CT_{C,in} - CT_{C,out} - \frac{Q_{cond}}{c_p}\right)$ $T_2 = T_{R,C} + \frac{Q'/c_p}{R_2} \qquad T_{C,out} = T_C - \frac{Q''/c_p}{C}$	$R_2 = R_0$ $Q_{cond} = Q' + Q''$
Fuel Cell HX (FC)	$\frac{\partial T_{RFC}}{\partial t} = \frac{1}{M_{RFC}}\left(R_2T_2 - R_3T_3 + \frac{Q_{FC}}{c_p}\right)$ $\frac{\partial T_{FC}}{\partial t} = \frac{1}{M_{FC}}\left(FCT_{FC,in} - FCT_{FC,out} - \frac{Q_{FC}}{c_p}\right)$ $T_3 = T_{R,FC} + \frac{Q'/c_p}{R_2} \qquad T_{FC,out} = T_{FC} - \frac{Q''/c_p}{FC}$	$R_3 = R_2$ $Q_{FC} = Q' + Q''$
Flue Gas HX (G)	$\frac{\partial T_{RG}}{\partial t} = \frac{1}{M_{RG}}\left(R_3T_3 - R_3T_5 + \frac{Q_{gas}}{c_p}\right)$ $\frac{\partial T_G}{\partial t} = \frac{1}{M_G}\left(GT_{G,in} - GT_{G,out} - \frac{Q_{gas}}{c_{p,gas}}\right)$ $T_5 = T_{RG} + \frac{Q'/c_p}{R_3} \qquad T_{G,out} = T_G - \frac{Q''/c_{p,gas}}{G}$	$R_5 = R_3$ $Q_{gas} = Q' + Q''$
Sanitary HX (X)	$\frac{\partial T_{RX}}{\partial t} = \frac{1}{M_{RX}}\left(R_6T_3 - R_6T_5 - \frac{Q_X}{c_p}\right)$ $\frac{\partial T_{SX}}{\partial t} = \frac{1}{M_{SX}}\left(S_1T_S - S_2T_{SX} + \frac{Q_X}{c_p}\right)$ $T_5 = T_{RX} - \frac{Q'/c_p}{R_6} \qquad T_{S2} = T_{SX} + \frac{Q''/c_p}{S1}$	$R_6 = R_5D$ $S_2 = S_1 = S_3MIX$ $Q_X = Q' + Q''$
Sanitary Water (S)	$\frac{\partial T_S}{\partial t} = \frac{1}{M_S}\left(S_4T_{S4} - S_4T_S + \frac{Q_{RS}}{cp}\right)$ $\frac{\partial M_S}{\partial S_1} = S_4 - S_1$	$S_4 = S_3\left[MIX\,(1-0.95)\right]$ $S_2 = S_1 \qquad M_S \geq M_{S0}/2$
D-regulator	$\frac{\partial D}{\partial t} = -\rho\,(T_{S2} - T_{set})$	$0.1 < D < 0.95$

Table B.11: Mathematical model for the cogeneration – sanitary system dynamic simulation. Refer to Figures 2.14 for the block and stream names. Other computational details can be found in [109].

Block	Water Inventory	Water Flowrate	Working Temperatures	Heat exchange coeff. UA
Water Reservoir	800	8 - 20	40 - 45	200 (sanitary) 10 (dispersion)
Sanitary reservoir	300	10	5 - 45	200 (Reservoir) 500 (Heater)
Condenser	5	8 - 20	40 - 50	600
FC	1	8 - 20	45 - 70	250
Flues	5	8 - 20	50 - 80	20
Sanitary Heater	5	8 - 10	20 -60	500

Table B.12: Nominal specifications for the cogeneration system. UA values are first-guesses and are adjusted within the calculation to meet the specified heat duties.

Acetontrile-Water Salting Out

The calculation of a decanter working in accord to the phase diagrams of section 8 takes place via an Excel spreadsheet used a shell to pass the input parameters to (and list the outputs from) a serie of Visual Basic routines. Aspen Plus features the option to automatically link specific process blocks to such Excel files, that are thus executed when needed during the simulation.

The relevant calculation steps are:

1) Temperature, pH, acetontrile content in the phases and moisture content of the cake are the parametric inputs, while the mass flows of the specie entering the virtual decanter are the variable inputs;

2) the input stream is divided in two: the organic, and the total aqueous (i.e. aqueous liquid plus cake), this split is obtained with tentative split-fractions for every specie;

3) part of the ammonia and CO_2 (plus the corresponding water) are 'converted' into ammonium bicarbonate, then the partition of the carbonated and azotated species remaining in the aqueous phase is adjusted by the pH and the equilibrium constants;

4) the aqueous stream is again divided (solid plus a liquid part determined by the moisture parameter, and liquid only);

5) if the obtained acetontrile fractions in the organic and clear aqueous liquids and the cake moisture are in line with the parameters, the calculation ends, otherwise:

   a- acetontrile' split fraction is adjusted to reach the desired values in the aqueous phase (with the Excel Solver plug-in);

   b- water' split fraction is tuned to achieve the desired organic liquid;

   c- conversion of ions into salt is modified to achieve to proper solubility product (that depends only on temperature and acetonitrile presence);

   d- the split of step 4) is modified, and the check of step 5) performed again.

The Visual Basic code that implements the above said passages is listed here with reference to the Excel spreadsheet of Figure B.5.

```
Sub SolverMacro()
' SolverMacro Macro
'
Worksheets("Sep").Activate

Dim err_tol, max_err As Double
Dim err_y, err_x As Double
Dim i, j As Integer

err_tol = Range("A4").Value
max_err = 1
err_y = Range("C5").Value
i = 1
```

```
Do While max_err > err_tol And i <= 10
        Range("G5").Value = i 'iteration  count
        max_err = Range("F5").Value
        err_x = Range("D5").Value 'MeCN in aq.phase error
        'MsgBox (max_err)
        corr = Range("Q9").Value 'tentative split fraction correction
        'for MeCN org/tot
        corr = corr + err_x / 2
        Range("Q9").Value = corr

        ' adjust the salt solubility
        SolverReset
        ' constraint
        SolverAdd CellRef:="$N$18", Relation:=3, FormulaText:="0"
        SolverAdd CellRef:="$N$18", Relation:=1, FormulaText:="L4"
        ' solution
        SolverOk SetCell:="$E$5", MaxMinVal:=3, ValueOf:="0", ByChange:="$N$18"
        SolverSolve True

        ' adjust the acn content in the phases
        SolverReset
        ' constraint
        SolverAdd CellRef:="$Q$9", Relation:=3, FormulaText:="0"
        SolverAdd CellRef:="$Q$9", Relation:=1, FormulaText:="1"
        ' solution aqueous
        SolverOk SetCell:="$D$5", MaxMinVal:=3, ValueOf:="0", ByChange:="$Q$9"

        SolverReset
        ' constraint
        SolverAdd CellRef:="$Q$10", Relation:=3, FormulaText:="0"
        SolverAdd CellRef:="$Q$10", Relation:=1, FormulaText:="1"
        ' solution organic
        SolverOk SetCell:="$C$5", MaxMinVal:=3, ValueOf:="0", ByChange:="$Q$10"
        SolverSolve True

        ' adjust the moisture
        SolverReset
        ' constraint
        SolverAdd CellRef:="$A$2", Relation:=3, FormulaText:="0"
        SolverAdd CellRef:="$A$2", Relation:=1, FormulaText:="1"
        ' solution
        SolverOk SetCell:="$B$5", MaxMinVal:=3, ValueOf:="0", ByChange:="$A$2"
        SolverSolve True
        i = i + 1
Loop

End Sub
```

sfZ:X	moist	y*	x*		pK	pK	pK	pK									
	(g/g)	(g/g)	(g/g)	KPS	amm	carb1	carb2	water	T_X	pH_X	N_X	C_X	O_X				
0,08013		0,25	0,75	0,26	4,74606	9,32	10,5	6,5	14	25	8	93,05802	7,8702	391,446			
toler		0,25	0,75	0,2599	4,7468	20,893	316,228	0,0316	1E+06			max N-C					
0,01				0,3142	0,17283							143,45					
0,00016		0	-4,9E-15	-0,0003	0,00016	0,00031	1										
<err>	err moist		err org	err aq	err KPS	max err											
PM	mass	W	Y	X	Z	X'				moles	W	Y	X	Z	X'	sfY:W	
	TOT	37218,62	20897	16402,4	4976,39	11426,1				TOT	1402,439	672,51	621,513	96,156	525,36		
41 acn		18901,53	15673	3228,53	258,691	2969,84				acn	461,01	382,27	78,7447	6,3095	72,435	0,82919	
18 water		13314,79	5224,3	7046,04	564,574	6481,46				water	739,71	290,24	391,446	31,365	360,08	0,39237	
17 OH		0	0	1,7E-05	1,4E-06	1,6E-05				OH	0,00	0	1E-06	8E-08	9E-07	0	
19 H3O		0	0	1,9E-07	1,5E-08	1,7E-07				H3O	0,00	0	1E-08	8E-10	9E-09	0	
17 NH3		2438,681	0	72,26	5,78995	66,4701				NH3	143,45	0	4,25059	0,3406	3,91	0	
18 NH4		0	0	1598,53	128,085	1470,45				NH4	0,00	0	88,8074	7,1158	81,692	0	
44 CO2		2563,615	0	10,5824	0,84793	9,73451				CO2	58,26	0	0,24051	0,0193	0,2212	0	
61 HCO3		0	0	463,941	37,174	426,767				HCO3	0,00	0	7,6056	0,6094	6,9962	0	
60 CO3		0	0	1,44306	0,11563	1,32743				CO3	0,00	0	0,02405	0,0019	0,0221	0	
79 NH4HCO3		0	0	3981,11	3981,11	0				NH4HCO3	0,00	0	50,3938	50,394	0	0	
TOT		1	1	1	1	1											
acn		0,507852	0,75	0,19683	0,05198	0,25992				TOT	0,328722	0,5684	0,1267	0,0656	0,1379		
water		0,357745	0,25	0,42957	0,11345	0,56725				acn	0,328722	0,5684	0,1267	0,0656	0,1379		
OH		0	0	1E-09	2,7E-10	1,4E-09				water	0,527446	0,4316	0,62983	0,3262	0,6854		
H3O		0	0	1,2E-11	3,1E-12	1,5E-11				OH	0	0	1,6E-09	8E-10	2E-09		
NH3		0,065523	0	0,00441	0,00116	0,00582				H3O	0	0	1,6E-11	8E-12	2E-11		
NH4		0	0	0,09746	0,02574	0,12869				NH3	0,102287	0	0,00684	0,0035	0,0074		
CO2		0,06888	0	0,00065	0,00017	0,00085				NH4	0	0	0,14289	0,074	0,1555		
HCO3		0	0	0,02828	0,00747	0,03735				CO2	0,041545	0	0,00039	0,0002	0,0004		
CO3		0	0	8,8E-05	2,3E-05	0,00012				HCO3	0	0	0,01224	0,0063	0,0133		
NH4HCO3		0	0	0,24271	0,8	0				CO3	0	0	3,9E-05	2E-05	4E-05		
										NH4HCO3	0	0	0,08108	0,5241	0		

Figure B.5: Excel spreadsheet that hosts the stream entering the decanter as calculated by Aspen Plus (column 'TOT') and elaborates the resulting organic ('Y'), aqueous ('X') and solid ('Z') phases that are then exported ot the relative Aspen Plus streams.

Kinetic Data Interpolation

The retro-fits of laboratory data to asses a kinetic model parameters have been carried out using a custom-made Matlab script. The program (that is not reported, but is available on request) proceeds through the following essential steps.

1) Data Load

   For every catalytic test, a structure is created with the variables: 'T', 'P', 'F' (gas flow), 'g' (weighted catalyst), '$\underline{y0}$' and '$\underline{y}$' (chemicals fractions at the inlet and outlet of the reactor).

2) Reaction Parameters

   They are collected into two matrices: $\underline{\underline{S}}$ contains the stoichiometric coefficients for the chemicals (by row) in every reaction (columns), $\underline{\underline{D}}$ has the reaction orders (same arrangement), and one array $\underline{k}$ lists by columns the result of the Ahrrenius expression: $r = exp\left(lnk_0 + \frac{E_a}{RT_0} - \frac{E_a}{RT}\right)$ given $k0$, E_a and T_0 for every reaction.

3) Reactor Balance

   Under the hypothesis of negligible diffusion and thermal changes (as obtained in laboratory tests), and with the inert gas flow making up for at least the 90% of the total molar flow, the steady balance of plug-flow reactor can be written as:

$$\frac{dy_i}{dz} = \frac{1}{v}\,\Sigma_j\, r_{ij}$$

   along the spatial coordinate z, for any specie i, reaction j and flowrate v, provided that v and k_0 are expressed in coherent units.

4) Balance Integration

   The non-linear set of equations above is automatically solved using a built-in variant of Runge-Kutta algorithm, that accepts $\underline{y0}$ as boundary condition and an array $\underline{\frac{dy}{dx}(x,y)}$ of formulas to calculate the derivatives at any (automatically chosen) integration step. The high-level coding syntax of Matlab is particularly well suited to perform calculations over data already organized into matrices.

5) Parameters adjustment

   Once the result $\underline{y_r}$ for any $\underline{y0}$ and set of matrices is calculated, it is possible to obtain the square residuals $S_t = \Sigma_i \left(\underline{y_r} - \underline{y}\right)^2$ for every test t: a built-in optimization tool based on the simplex method is capable of iteratively modifying the matrices content until the sum $\Sigma_t S_t$ is minimal.

Pinch Analysis

Here is listed the core function of the Matlab scripts used to: draw the composite curves, calculate the heat duties and pinch temperatures starting from matrices representing the fluid lists. For clarity, the code lines relative to the loading, arrangement and video output are abridged.

The code has been developed using as a base those published by dr. Andrea Chiarelli[2] and by ph.d. Matteo Morandin[3].

```
% inits
%dTmin = 25; this is already defined in the input masks
Tin_star = Tin;
Tout_star = Tout;
Duty_in = 0;
Duty_out = 0;
for i=1:nfluid
    if Tin(i)>Tout(i) % this is an hot stream
        type(i)='h';
        Tin_star(i)=Tin(i)-dTmin/2;
        Tout_star(i)=Tout(i)-dTmin/2;
    else
        type(i)='c'; % se non è zuppa... è pan bagnato
        Tin_star(i)=Tin(i)+dTmin/2;
        Tout_star(i)=Tout(i)+dTmin/2;
    end
end
%% basic analysis
Table = [M, Tin_star, Tout_star, M(:,2).*(Tout-Tin)];
Temp=[Tin_star, Tout_star];
Tscale=unique(Temp);
Tscale=sort(Tscale, 'descend');
intervals = [Tscale(1:end-1) Tscale(2:end)] ; % intervals
% find al the useful intervals
for i=1:length(Tscale)-1 %delta temperature in each interval of T*
    DELTA(i)=Tscale(i)-Tscale(i+1);
end
DH=zeros(length(Tscale)-1, nfluid+6);
%% cycles the fluid list and updates the stream chart
for i=1:nfluid
    %Calculating the sum of all the G*cp in each interval
    if type(i)=='h'
        for j=1:length(Tscale)-1
            if Tin_star(i)>=Tscale(j) && Tout_star(i)<=Tscale(j+1)
                DH(j,i)=DH(j,i)-F(i)*DELTA(j); % DH is released
                DH(j,nfluid+1)=DH(j,nfluid+1)-F(i)*DELTA(j);
```

[2]https://chiarelliandrea.com/computational-methods/.

[3]Matteo Morandin (2020). cascade.m (https://www.mathworks.com/matlabcentral/fileexchange/47743-cascade-m), MATLAB Central File Exchange.

```
            else
                % this fluid is after the present Tscale interval
                DH(j,i)=DH(j,i);
            end
        end
    end % end hot fluid
    if type(i)=='c'
        for j=1:length(Tscale)-1
            if Tout_star(i)>=Tscale(j) && Tin_star(i)<=Tscale(j+1)
                DH(j,i)=DH(j,i)+F(i)*DELTA(j); % DH is absorbed
                DH(j,nfluid+2)=DH(j,nfluid+2)+F(i)*DELTA(j);
            else
                DH(j,i)=DH(j,i);
            end
        end
    end % end cold fluid
end % end cycle on fluids
DH(:,nfluid+3) = DH(:,nfluid+1)+DH(:,nfluid+2);
%% finds the cumulative heats
DH(1,nfluid+4) = -DH(1,nfluid+1); % cumulative hot
DH(1,nfluid+5) = +DH(1,nfluid+2); % cumulative cold
DH(1,nfluid+6) = -DH(1,nfluid+3); % cumulative tot
% treat released heat as positive, i.e. in view of the cold sink
for j=2:length(Tscale)-1
    DH(j,nfluid+4) = DH(j-1,nfluid+4)-DH(j,nfluid+1);
    DH(j,nfluid+5) = DH(j-1,nfluid+5)+DH(j,nfluid+2);
    DH(j,nfluid+6) = DH(j-1,nfluid+6)-DH(j,nfluid+3);
end
%% main results
duty = [M(:,2).*abs(M(:,4)-M(:,3))].*M(:,5);
Duty_in = sum(0.5*(duty.*[M(:,5)+1])); % this rules out the hot fluids
Duty_out = sum(0.5*(duty.*[M(:,5)-1])); % this rules out the cold fluids
HU = min(DH(DH(:,nfluid+6)<0,nfluid+6)); %
if isempty(HU) % threshold problem
    HU = 0;
    TPINCH = intervals(1,1);
    fprintf(1,'THRESHOLD CASCADE!');
else
    TPINCH = Tscale(DH(:,nfluid+6)==HU,1);% hot pinch point
    HU = abs(HU); % MER hot utility
end
GCC=DH(:,nfluid+6)+HU; % MER cascade
CU=GCC(end); % MER cold utility
```

B.4 Reactors Cooling

Here are presented the actual block schemes used to model the reactor cooling in the Sabatier and acetonitrile processes (diagrams B.6 and B.7respectively). The overall references schemes are shown in Figures 5.5 and 4.6.

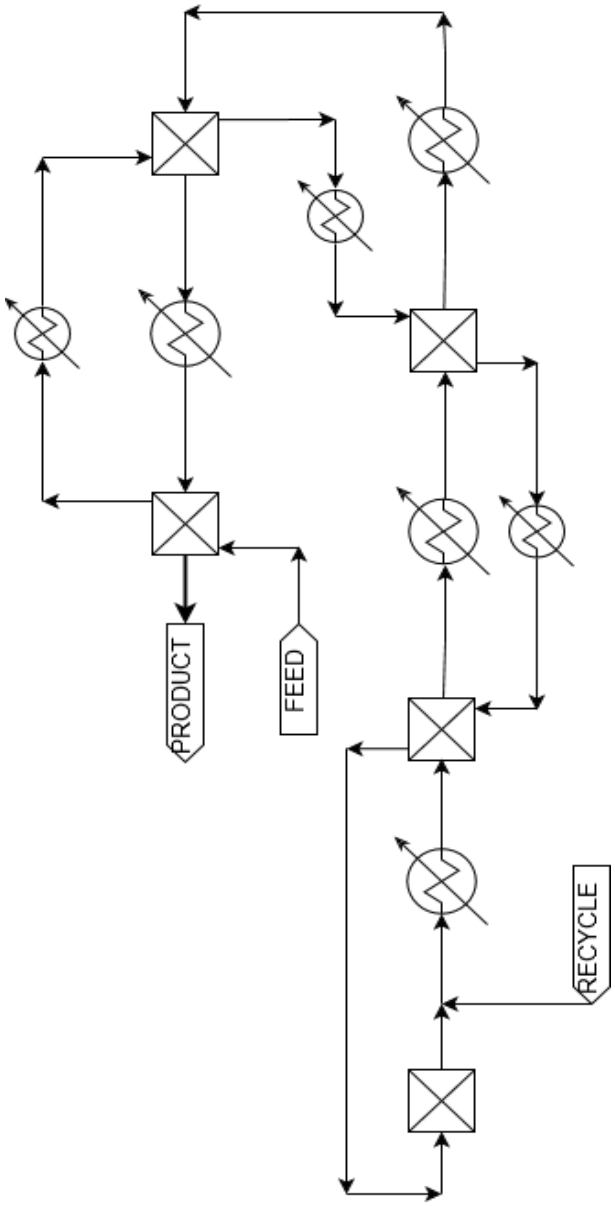

Figure B.6: Actual Aspen Plus calculation scheme of the methanation reactor cooling.

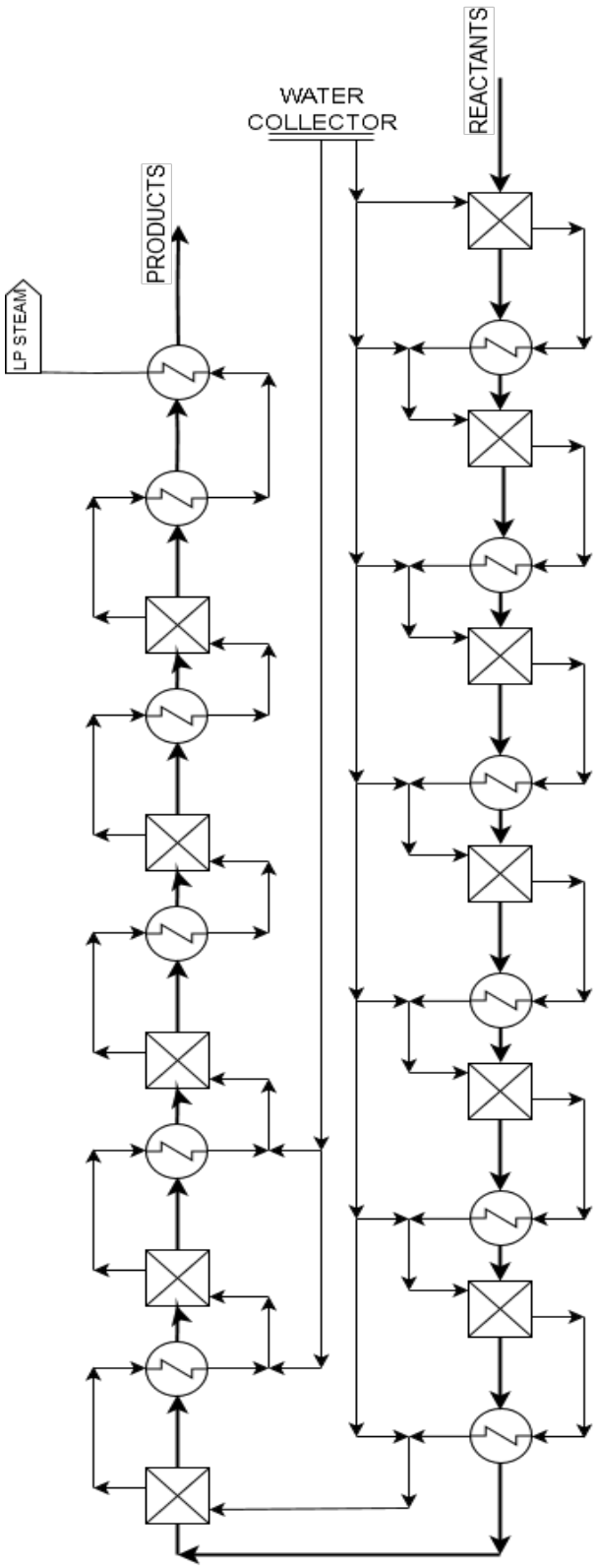

Figure B.7: Actual Aspen Plus calculation scheme of the ammoxidation reactor cooling.

Appendix C

Laboratory Data

C.1 Ethanol Dehydration

The Figures C.2-C.3-C.4-C.5 display the more relevant results of the kinetic model employed to calculate the ethylene production from ethanol. The underlying laboratory test are summarized in Tables C.1 and C.2.

In the scheme C.1 is pictured the experimental apparatus used for the activity and kinetic tests.

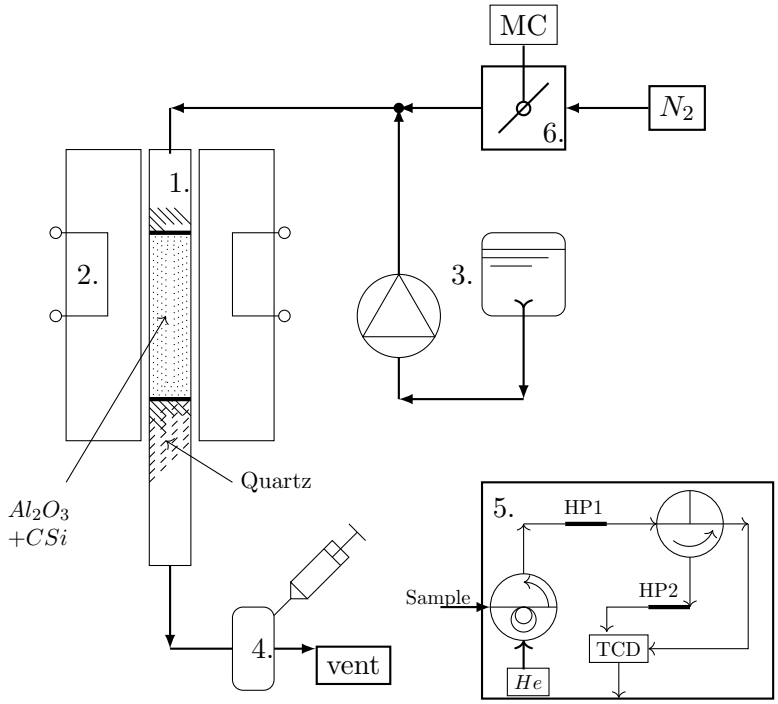

Figure C.1: 1: reactor; 2: cylindrical oven with thermoelements and controller; 3: HPLC pump and hydroalcoholic reservoir; 4: heated gas trap; 5: gas chromatograph; 6: mass flow controller.

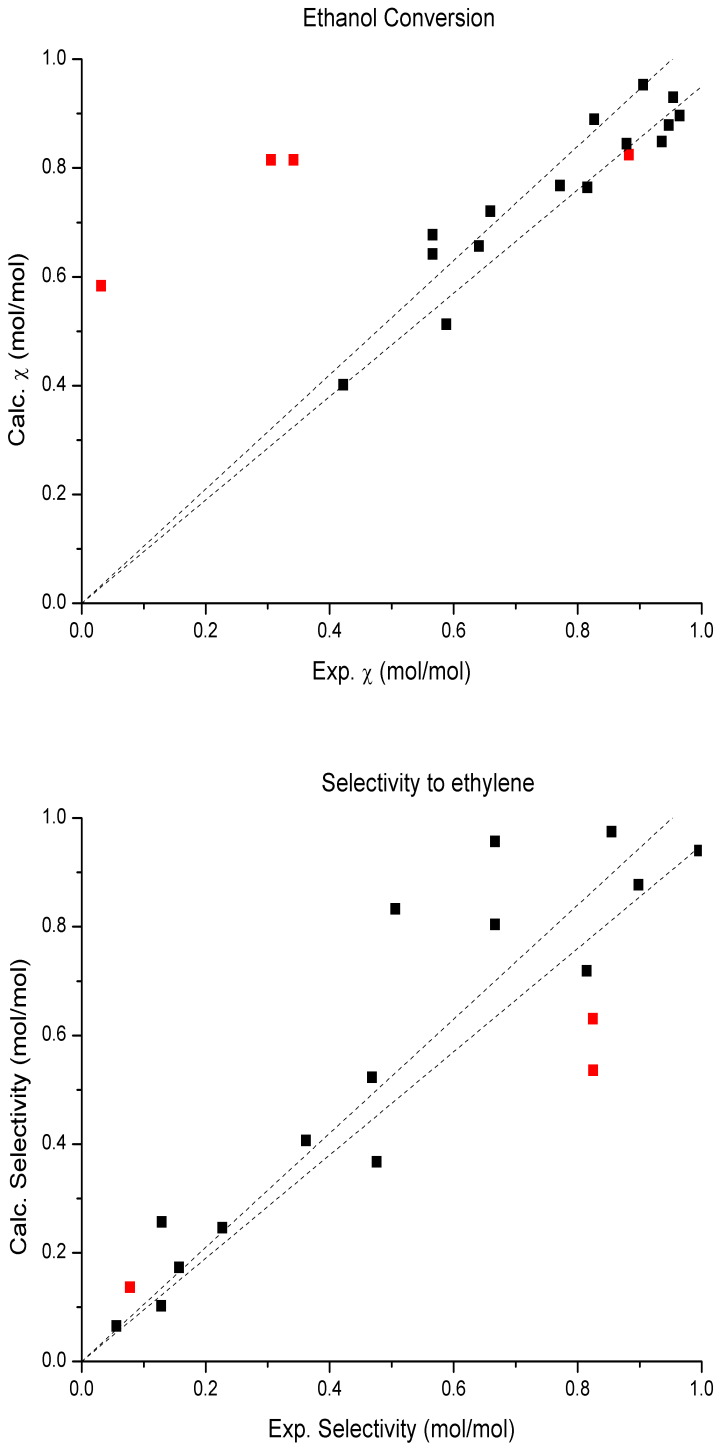

Figure C.2: Experimental and calculated conversion and selectivity (1).

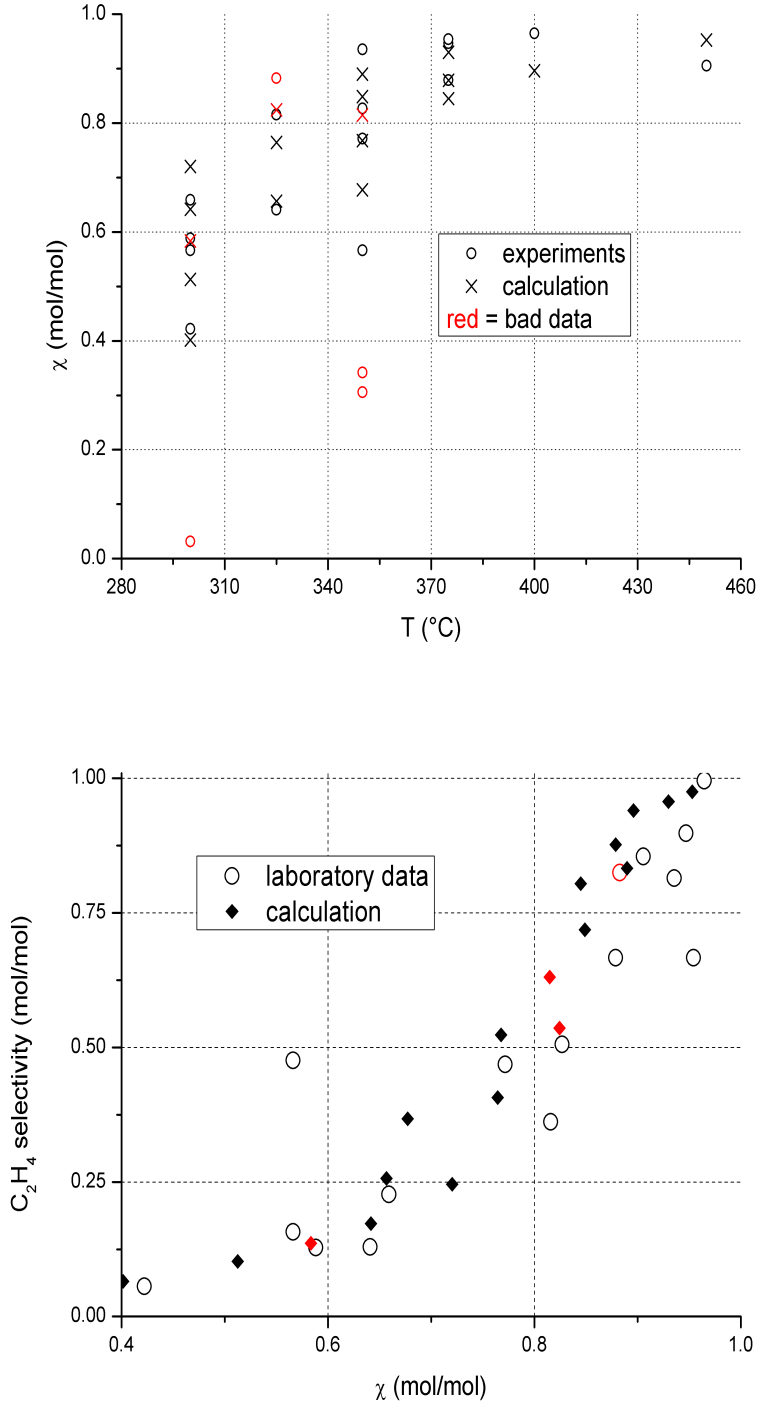

Figure C.3: Experimental and calculated conversion and selectivity (2).

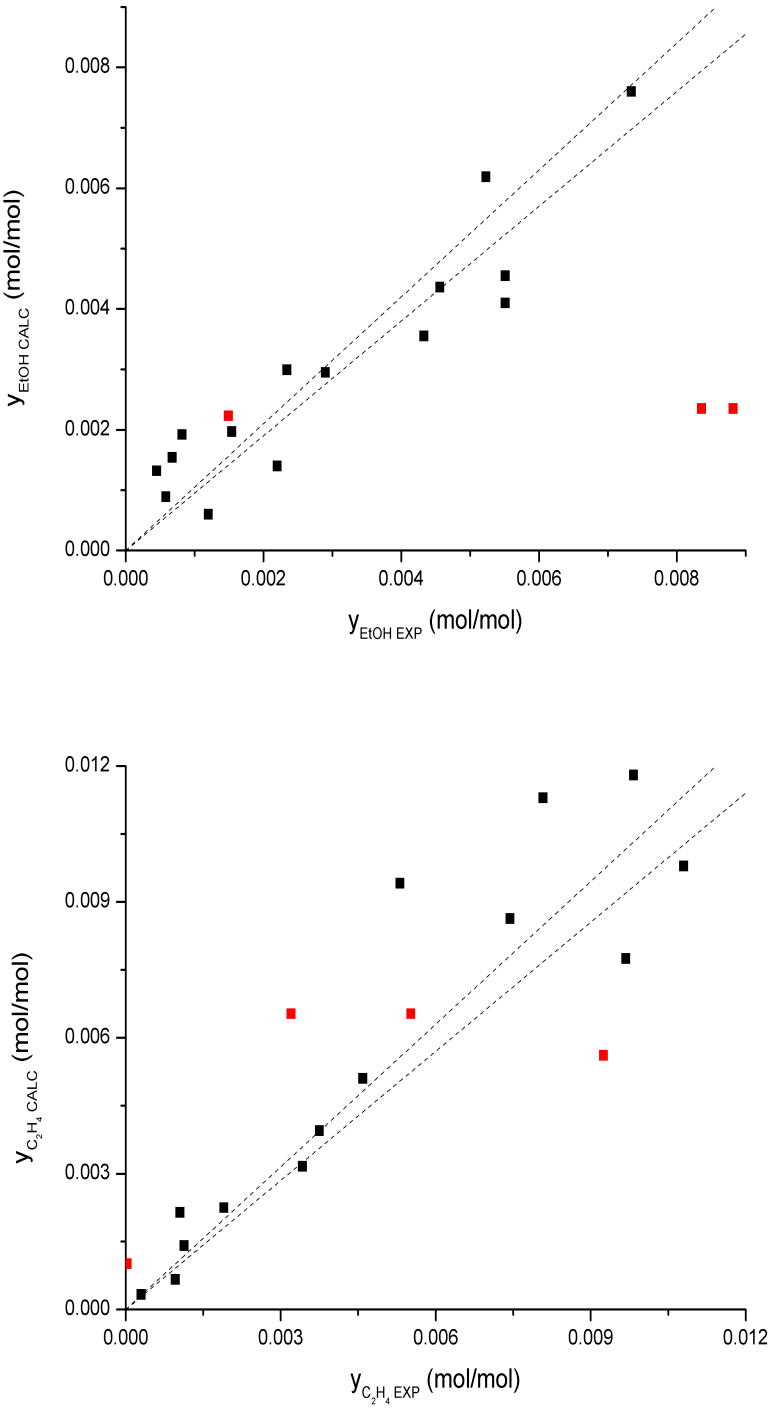

Figure C.4: Model capability of reproducing the ethanol consumption and ethylene production (1).

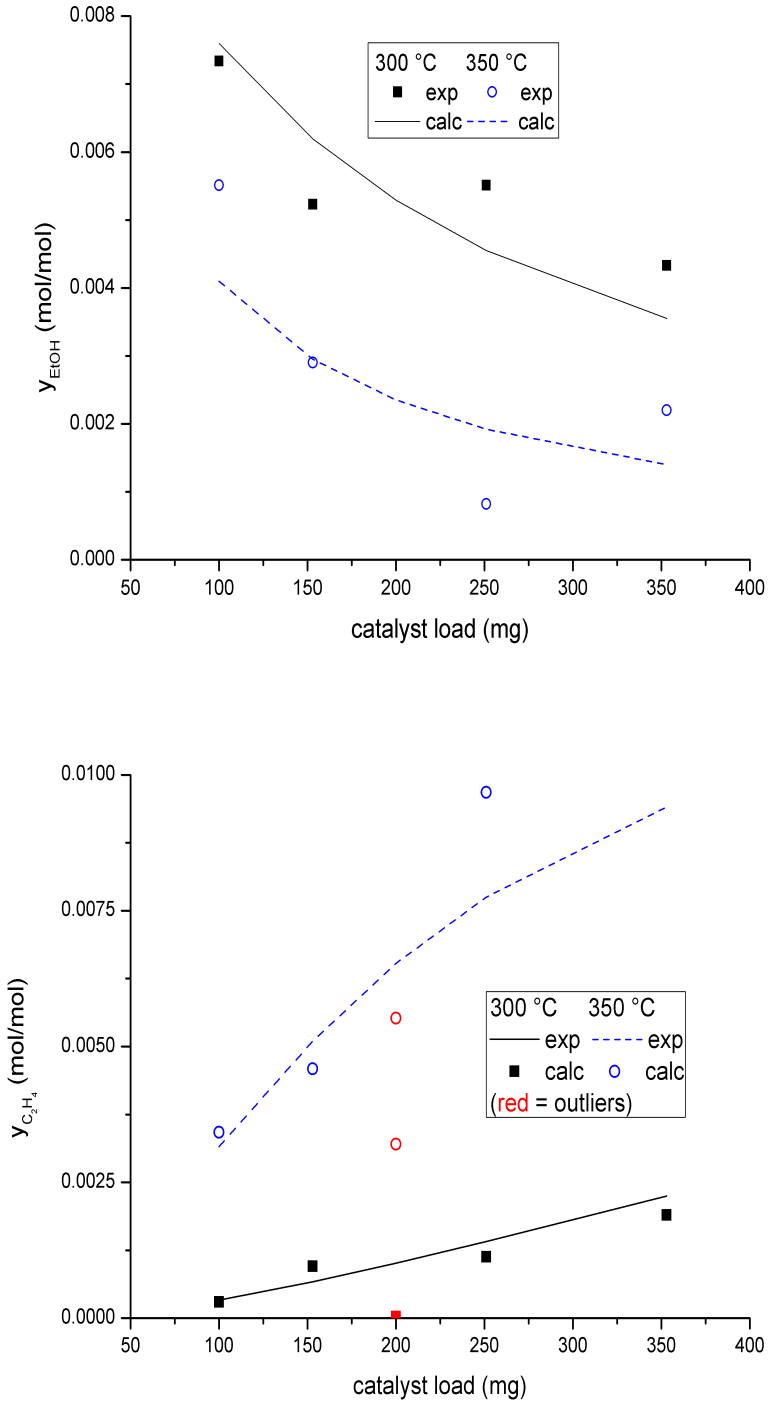

Figure C.5: Model capability of reproducing the ethanol consumption and ethylene production (2).

Id	**T**	**n** (mol/s)	**load** g	EtOHin (mol/mol)	H2Oin	N2in	EtOHout	H2Oout	C2H4out	AcHout	EtOEtout	**C-balance**
1	300	2.37E-4	100	0.0127	0.0383	0.949	0.00734	0.041	3.01E-4	1.08E-4	0.00129	0.145
2	300	2.37E-4	153	0.0127	0.0383	0.949	0.00523	0.0417	9.58E-4	0	0.00212	0.125
3	300	2.37E-4	200	0.0127	0.0383	0.949	0.0123	0.0373	3.12E-5	0	3.03E-4	0.0466
4	300	2.37E-4	251	0.0127	0.0383	0.949	0.00551	0.0404	0.00113	7.62E-5	0.00292	0.0322
5	300	2.37E-4	353	0.0127	0.0383	0.949	0.00433	0.0402	0.0019	8.69E-5	0.00351	0.031
6	325	2.37E-4	153	0.0127	0.0383	0.949	0.00456	0.0432	0.00105	1.1E-4	0.00104	0.119
7	325	2.37E-4	251	0.0127	0.0383	0.949	0.00234	0.0412	0.00375	1.23E-4	0.00255	0.0105
8	325	2.37E-4	353	0.0127	0.0383	0.949	0.00149	0.039	0.00925	1.74E-4	9.31E-5	0.0696
9	350	2.37E-4	100	0.0127	0.0383	0.949	0.00551	0.0378	0.00342	3.01E-4	0.00297	0
10	350	2.37E-4	153	0.0127	0.0383	0.949	0.0029	0.0407	0.00459	1.99E-4	0.00157	0.125
11	350	2.37E-4	200	0.0127	0.0383	0.949	0.00836	0.0318	0.00552	1.16E-4	0.00417	0
12	350	2.37E-4	200	0.0127	0.0383	0.949	0.00882	0.0341	0.0032	9.62E-5	0.00377	0.0254
13	350	2.37E-4	251	0.0127	0.0383	0.949	8.18E-4	0.039	0.00968	1.6E-4	2.9E-4	0.0393
14	350	2.37E-4	353	0.0127	0.0383	0.949	0.0022	0.0407	0.00531	1.45E-4	0.00162	0.00774
15	375	2.37E-4	153	0.0127	0.0383	0.949	0.00154	0.0397	0.00744	4.33E-4	9.2E-4	0.0261
16	375	2.37E-4	200	0.0127	0.0383	0.949	6.74E-4	0.0381	0.0108	2.82E-4	8.75E-5	0.00341
17	375	2.37E-4	353	0.0127	0.0383	0.949	5.83E-4	0.0412	0.00808	1.67E-4	0	0.071
18	400	2.37E-4	153	0.0127	0.0383	0.949	4.49E-4	0.0371	0.0122	2.05E-4	0	0.0165
19	450	2.37E-4	153	0.0127	0.0383	0.949	0.0012	0.0386	0.00983	3.81E-4	0	0

Table C.1: Experimental Data for ethanol dehydration with an Al_2O_3 catalyst.

Id	EtOHcalc	H2Ocalc	C2H4calc	AcHcalc	EtOEtcalc	H2calc	SSR	ncalc	Xsper	Ssper	Xcalc	Scalc
1	0.0076	0.0409	3.32E-4	6.13E-5	0.00234	6.13E-5	0.648	2.37E-4	0.42205	0.05616	0.40157	0.0651
2	0.00619	0.0418	6.67E-4	8.49E-5	0.00287	8.49E-5	0.248	2.37E-4	0.58819	0.12825	0.5126	0.10246
3	0.00529	0.0424	0.00101	1.03E-4	0.00314	1.03E-4	0	2.37E-4	0.0315	0.078	0.58346	0.1363
4	0.00455	0.043	0.00141	1.19E-4	0.0033	1.19E-4	0.295	2.37E-4	0.56614	0.15716	0.64173	0.17301
5	0.00355	0.0439	0.00225	1.47E-4	0.00337	1.47E-4	0.333	2.37E-4	0.65906	0.227	0.72047	0.2459
6	0.00436	0.0434	0.00214	1.2E-4	0.00303	1.2E-4	1.43	2.37E-4	0.64094	0.12899	0.65669	0.25659
7	0.00299	0.045	0.00395	1.6E-4	0.00279	1.6E-4	0.138	2.38E-4	0.81575	0.36197	0.76457	0.4068
8	0.00223	0.0462	0.00561	1.9E-4	0.00232	1.9E-4	3.81	2.38E-4	0.88268	0.82516	0.82441	0.53582
9	0.0041	0.0441	0.00316	1.23E-4	0.00265	1.23E-4	0.809	2.37E-4	0.56614	0.47566	0.67717	0.36744
10	0.00295	0.0456	0.0051	1.57E-4	0.00224	1.57E-4	0.189	2.38E-4	0.77165	0.46837	0.76772	0.52308
11	0.00235	0.0466	0.00653	1.8E-4	0.00181	1.8E-4	0	2.38E-4	0.34173	1.272	0.81496	0.63092
12	0.00235	0.0466	0.00653	1.8E-4	0.00181	1.8E-4	0	2.38E-4	0.30551	0.82474	0.81496	0.63092
13	0.00192	0.0474	0.00775	2,00E-04	0.0014	2,00E-04	2.43	2.38E-4	0.93559	0.81468	0.84882	0.71892
14	0.0014	0.0485	0.00941	2.31E-4	8.16E-4	2.31E-4	1.15	2.39E-4	0.82677	0.50571	0.88976	0.83274
15	0.00197	0.0478	0.00863	1.93E-4	9.45E-4	1.93E-4	0.672	2.39E-4	0.87874	0.66667	0.84488	0.80429
16	0.00154	0.0486	0.00979	2.16E-4	5.68E-4	2.16E-4	0	2.39E-4	0.94693	0.89805	0.87874	0.87724
17	8.89E-4	0.0497	0.0113	2.68E-4	1.31E-4	2.68E-4	0.496	2.39E-4	0.95409	0.66683	0.93	0.95674
18	0.00132	0.0492	0.0107	2.26E-4	2.12E-4	2.26E-4	0.992	2.39E-4	0.96465	0.99584	0.89606	0.94025
19	5.98E-4	0.0501	0.0118	2.83E-4	1.47E-5	2.83E-4	0.567	2.39E-4	0.90551	0.85478	0.95291	0.97505

Table C.2: Main quantities calculated after the laboratory data (Table C.1), according to the model presented in section 1.1. 'X' stands for conversion and 'S' for selectivity.

C.2 Ethanol Ammoxidation

The following Figures refers only to the kinetic model used for the simulation of this thesis, the full tabulation of the reaction outcomes for all the tested catalysts can be found in the already published works: [144–146]. The original data come from the group of professor F. Cavani, Alma Mater Studiorum University of Bologna.

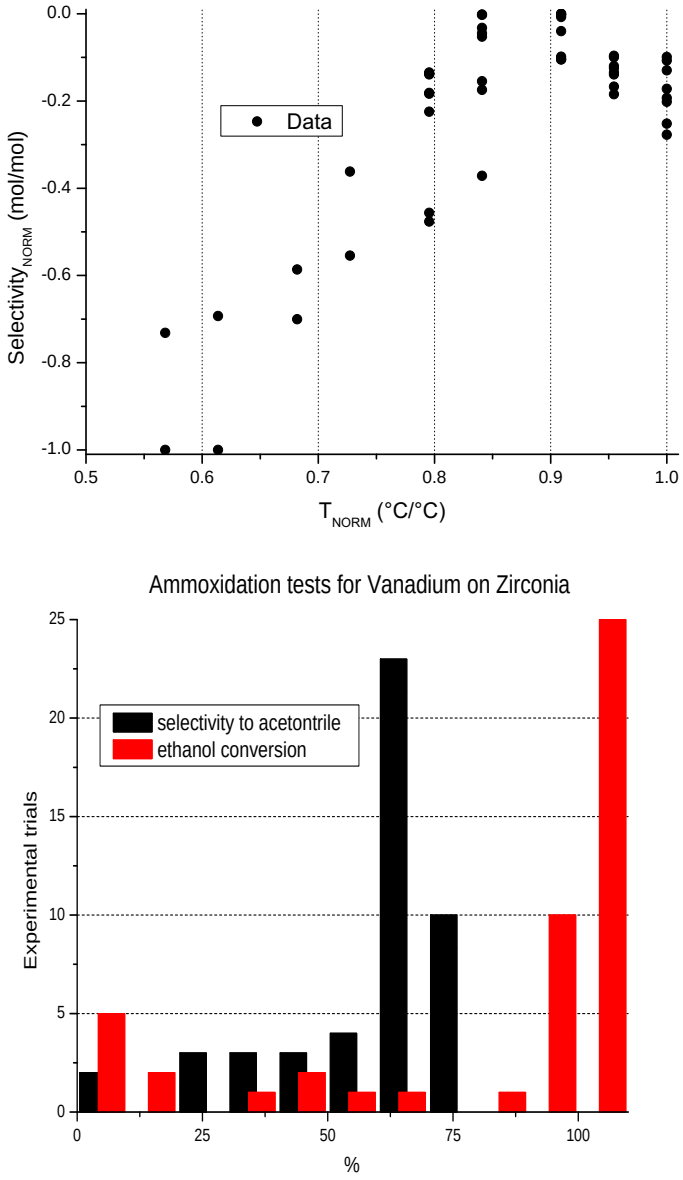

Figure C.6: Model capability of reproducing the reactants consumption and acetonitrile production (1).

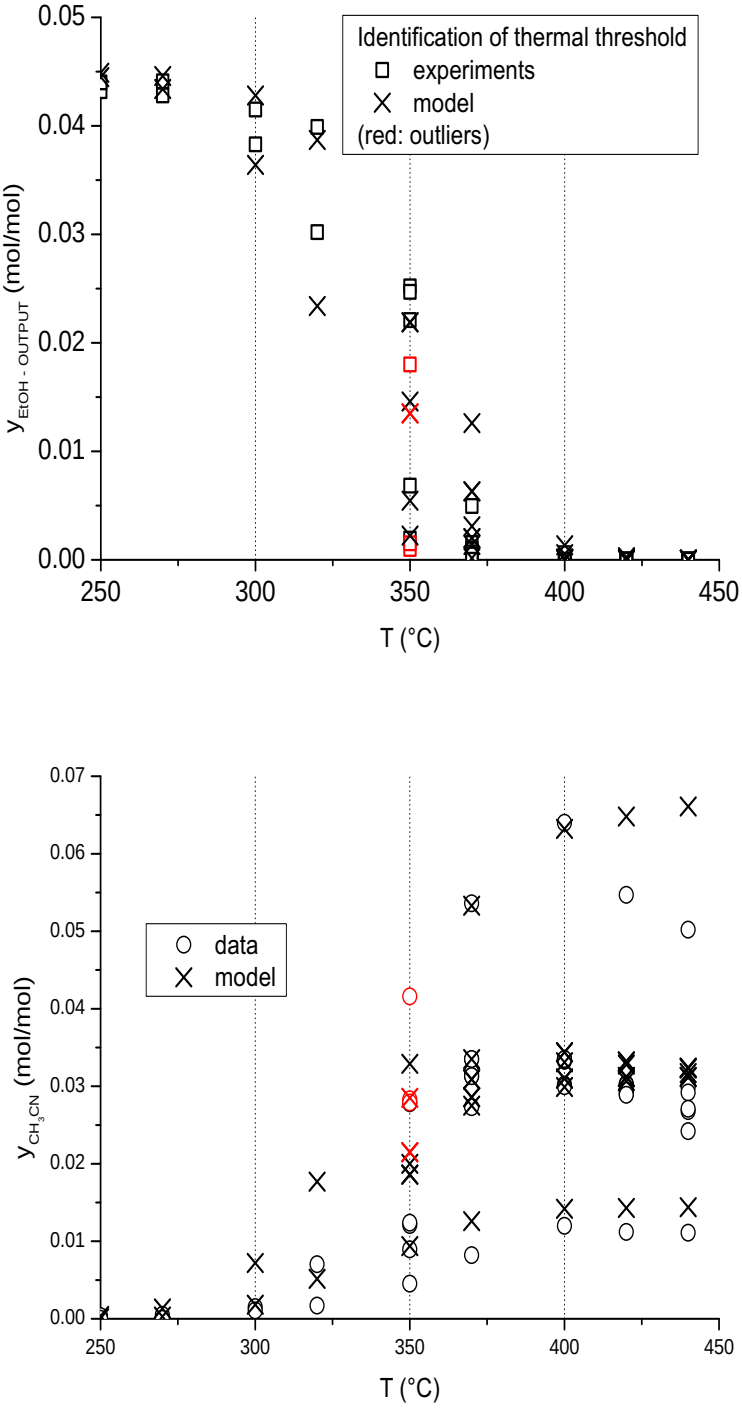

Figure C.7: Model capability of reproducing the reactants consumption and acetonitrile production (2).

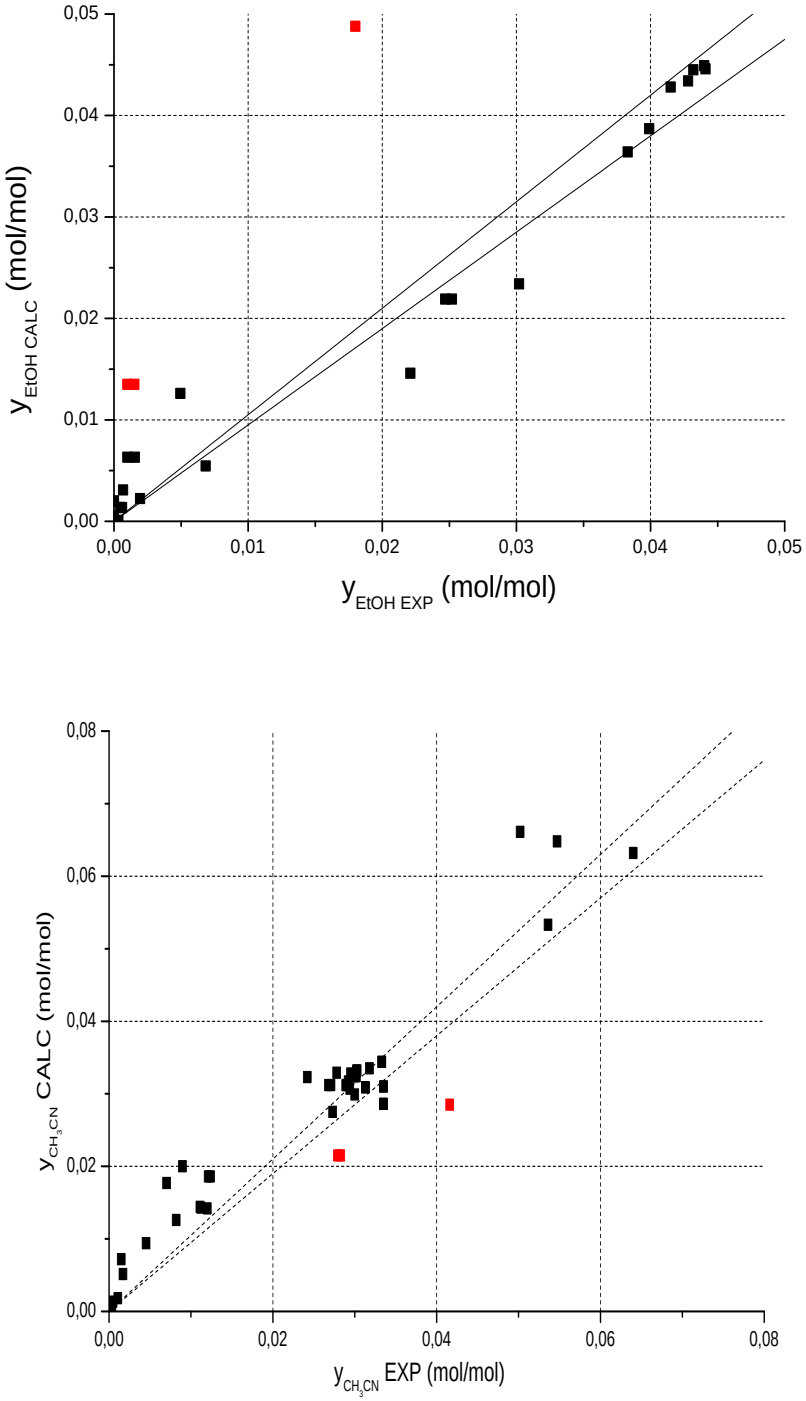

Figure C.8: Model capability of reproducing the reactants consumption and acetonitrile production (3).

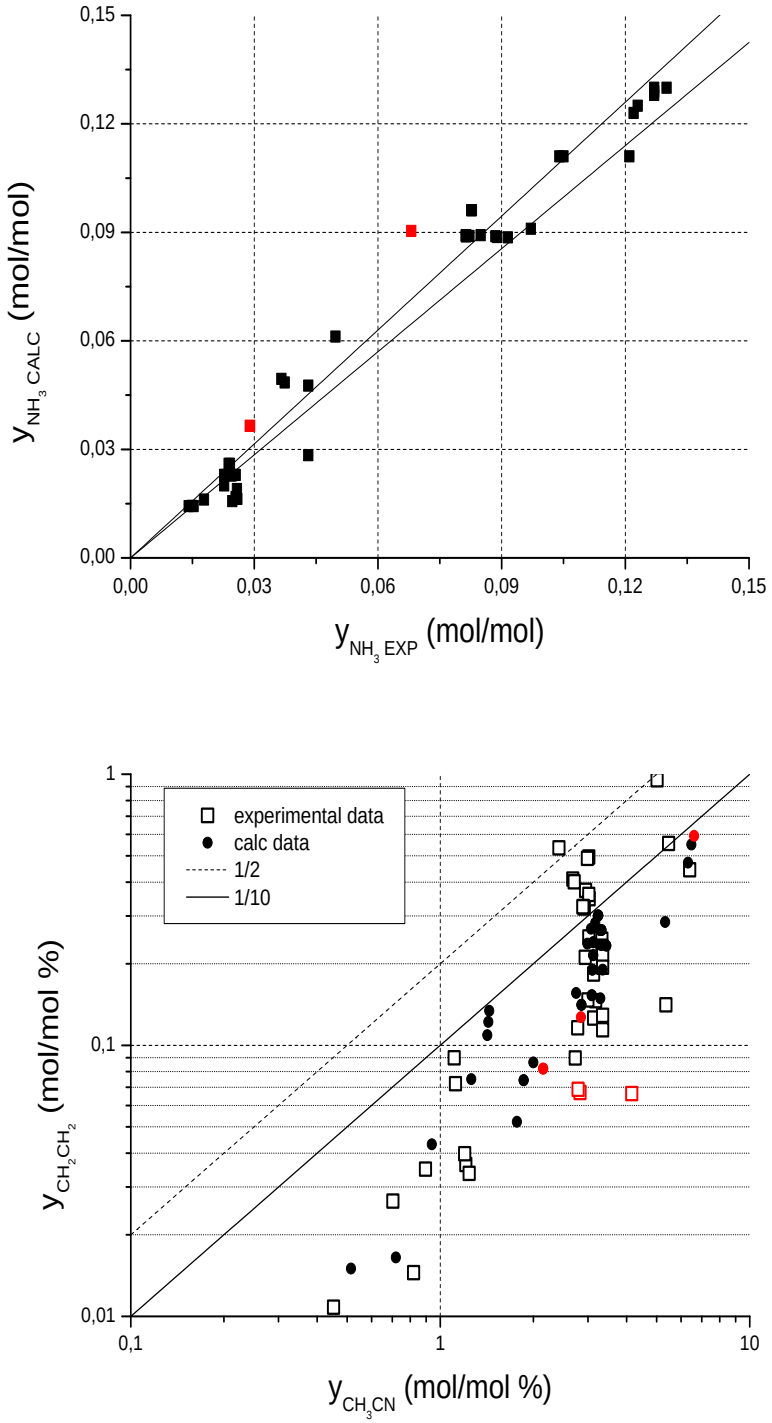

Figure C.9: Model capability of reproducing the reactants consumption and acetonitrile production (4).

C.3 Acetonitrile-Water-Ammonium Bicarbonate Mixtures

C.3.1 Thermo-Gravimetry

The extraction of data from a TGA log file has been performed with Origin v.8., and begins with the baseline subtraction. This operation is performed manually. The Tables C.3-C.6 header is compiled as:

Tp1,2:	temperature of the first and second peak of the weight-loss derivative
Tend:	temperature of complete sample disappearance from pan
L1,2:	specific heats of the various evaporation regimes
Q001,010:	total heat releases at 1% and 10% of initial weight
wq1,2:	minimum and maximum acetonitrile fractions calculated from Q
Lf:	weight remaining at the onset of the free water regime
wLf:	initial acetonitrile calculated from Lf according to the diagrams in figure 9.11
w0R,w1R:	minimum and maximum acetonitrile fractions from graph 9.10
w0A:	similar to w1R, but with a different numeric integration method
Tp...:	peak temperatures of a DSC signal
Q1,Qtot:	DSC integrated heat at the above said temperatures
wq,w2:	initial acetonitrile calculated from Q1 or Qtot
cal1,2,3:	calibrations derived from L2, Q001 or Qtot with respect to pure water analysis

C.3.2 Nuclear Magnetic Resonance

The extraction of data from a NMR log file has to be made with specific software: at first MestreNova v.9 (Mestrelab Research) has been used, and then TopSpin 3.6.1 (Bruker). Sometimes, a virtual phase correction on the downloaded data has been applied, beside the adjustment already operated during the signal acquisition. The Tables C.7-C.10 headers are as:

prel:	sampled quantity (organic phase unless specified)
etoh:	ethanol addition
CH_3,CH_2(a):	peak areas for the metyles or CH_2
CH_3,CH_2(d):	chemical shifts for the metyles or CH_2
acalc:	calculated molar ratio of acetonitrile to ethanol
wMeCN:	calculated weight fraction of acetonitrile in the sample
err:	deviation of ethanol peak areas from the 3:2 ratio

The loogboks of the backtritrations are not reported, because this kind of analysis remains somehow more dependent on the operator's action and judgement, and also more affected by changes in the adopted conditions.

ID	Tp1 °C	Tp2 °C	Tend °C	L1 J/g	L2 J/g	Q001 J/g	Q010 J/g	wq1 g/g	wq2 g/g	Lf g/g	wLf g/g	w0R	w1R	w0A	Tp1 °C	Tp2 °C	Tend °C	Q1 J/g	Qtot J/g	wq g/g	w2 g/g	cal1 J/J	cal2 J/J
200	62	–	–	–	530	-595	–	0.95		–	0.2	–		–	67	67	72	-867	-1018	–			
300	70	–	75	710	–	-666	-624	0.8		–	0.82	–	0.82	0.8	–	–	–	–	–	–			
400	60	82	87	750	1600	-847	-710	0.6		0.075	0.72	0.62	0.72	0.75	–	–	–	–	–	–		0.59	
402	76	–	79	710	–	-699	-363	0.8		–	0.82	–	0.82	0.8	–	–	–	–	–	–		0.59	
500	60	91	94	760	1600	-1028	-883	0.45	0.55	0.22	0.6	0.47	0.62	0.65	–	–	–	–	–	–		0.67	
501or	66	–	74	700	–	-672	-610	0.8	–	–	0.82	–	0.82	0.8	–	–	–	–	–	–		0.67	0.7
501aq	–	96	102	–	1600	-1361	-1222	0.25	0.3	0.52	0.25	0.2	0.3	0.25	–	–	–	–	–	–		0.64	0.64
513or	68	–	74	730	–	-707	-642	0.8	–	–	0.8	–	0.82	0.8	–	–	–	–	–	–		0.67	0.66
513aq	–	100	107	–	1600	-1495	-1308	0.23	0.25	0.48	0.25	0.22	0.35	0.3	–	–	–	–	–	–		0.67	0.7
520	–	–	–	–	–	–	–	–	–	–	–	–	–	–	82	102	107	-970	-1495	0.7	0.57	–	–
521or	64	–	70	620	–	-617	-563	0.8	–	–	0.8		0.82	0.8	74	–	77	-1070	-1100	0.8	0.8	0.64	0.62
521aq	–	90	95	–	1530	-1335	-1199	0.24	0.26	0.5	0.29	0.2	0.32	0.25	98	–	103	-2110	-2120	0.25	–	0.64	0.62
5220or	57	79	87	–	–	-1515	-1266	0.57	0.6	0.08	0.7	0.6	0.7	0.7	75	89	91	-720	-1145	0.7	0.6	–	–
5220aq	–	93	109	–	2600	-2357	-2113	0.15	0.18	0.6	0.2	0.15	0.25	0.2	–	98	103	-1980	-1980	0.3	–	1.1	1
600	53	80	80	800	1600	-1112	-960	0.48	0.58	0.31	0.48	0.37	0.52	0.48	–	–	–	–	–	–	–	0.67	0.8
620	–	–	–	–	–	–	–	–	–	–	–	–	–	–	67	88	92	-718	-1670	0.48	0.52	–	–
603or	62	83	87	730	1600	-796	-662	0.7	–	0.07	0.72	0.62	0.72	0.75	–	–	–	–	–	–	–	0.66	0.73
603aq	–	96	103	–	1580	-1340	-1197	0.28	0.3	0.43	0.32	0.25	0.37	0.35	–	–	–	–	–	–	–	0.66	–
615or	63	–	70	730	–	-737	-669	0.78	0.8	–	0.8	–	0.82	0.8	–	–	–	–	–	–	–	0.71	0.75
615aq	–	102	110	–	1630	-1459	-1311	0.28	0.32	0.5	0.3	0.21	0.34	0.28	–	–	–	–	–	–	–	0.71	0.75
617or	70	–	75	720	–	-670	-609	0.8	–	–	0.8	–	0.82	0.8	–	–	–	–	–	–	–	0.7	0.66
617aq	–	101	109	–	1580	-1372	-1233	0.27	0.32	0.45	0.3	0.25	0.37	0.35	–	–	–	–	–	–	–	0.66	–
621or	69	–	78	730	–	-703	-637	0.78	0.82	–	0.8	–	0.82	0.8	78	83	85	-896	-1035	0.78	–	0.73	0.67
621aq	–	94	100	–	1600	-1441	-1300	0.29	0.32	0.4	0.38	0.25	0.4	0.4	–	–	–	–	–	–	–	–	–
6301or	67	87	101	1700	2800	-1860	-1594	–	–	0.15	0.63	0.52	0.64	0.65	–	–	–	–	–	–	–	1.7	–
6301aq	–	95	110	1700	2500	-2138	-1912	0.29	0.31	0.4	0.35	0.25	0.4	0.4	–	–	–	-1810	-1840	0.38	–	1.2	1
6506aq	–	95	114	–	2700	-2412	-2163	0.24	0.24	0.52	0.25	0.2	0.3	0.27	–	–	–	–	–	–	–	1.1	–
6508or	65	78	87	1200	–	-1373	-1143	0.7	0.75	0.075	0.72	0.62	0.72	0.72	–	–	–	–	–	–	–	1.25	1.2
6508aq	–	97	117	–	2900	-2275	-2040	0.25	0.25	0.43	0.35	0.28	0.41	0.35	–	–	–	–	–	–	–	1.1	1.2
6512or	68	79	92	1200	2900	-1170	-1403	0.73	0.75	0.09	0.75	0.57	0.7	0.75	–	–	–	–	–	–	–	1.2	1.26
6512aq	–	93	105	–	2900	-2347	-2108	0.25	0.25	0.38	0.4	0.3	0.45	0.42	–	–	–	–	–	–	–	1.1	–
700	58	97	102	–	1600	-1203	-1062	0.39	0.4	0.33	0.45	0.33	0.47	0.41	–	–	–	–	–	–	–	0.67	–
702or	63	–	70	730	–	-694	-627	0.8	0.82	–	0.8	–	0.82	0.82	–	–	–	–	–	–	–	0.73	0.7
700	54	96	101	–	1600	-1276	-1126	0.36	0.34	0.36	0.4	0.3	0.43	0.42	–	–	–	–	–	–	–	0.67	–
703aq	–	97	103	–	1650	-1365	-1219	0.27	0.28	0.46	0.3	0.23	0.35	0.32	–	–	–	–	–	–	–	0.67	–
712or	67	–	76	730	–	-732	-662	0.78	0.8	–	0.82	–	0.8	0.82	–	–	–	–	–	–	–	0.73	0.69
712aq	–	99	104	–	1650	-1477	-1329	0.2	0.22	0.5	0.3	0.22	0.34	0.3	–	–	–	–	–	–	–	0.67	0.68
721or	68	–	71	700	–	-688	-628	0.82	0.82	–	0.82	–	0.8	0.8	78	81	9	-1025	-1123	0.75	0.8	0.7	0.68

Table C.3: Report of the calorimetric experiments and more important data derived.

721aq	–	94	99	–	1600	-1360	-1220	0.23	0.28	0.72	0.38	0.28	0.42	0.4	–	100	103	-2050	-2070	0.27	–	0.67	0.64
730	–	–	–	–	–	–	–	–	–	–	–	–	–	–	75	100	104	-940	-2700	0.4	–	1.4	–
731org	62	–	72	730	–	-733	-662	0.75	0.82	–	0.82	–	0.8	0.8	63	73	75	-650	-978	0.67	0.7	0.73	0.75
731aq	–	101	105	–	1700	-1420	-1275	0.24	0.25	0.5	0.3	0.2	0.32	0.3	–	96	98	-2111	-2147	0.25	–	0.71	0.64
7322aq	–	–	–	–	–	–	–	–	–	–	–	–	–	–	–	102	111	-1900	-1900	0.2	0.3	–	–
7323or	64	87	91	640	1500	-500	-403	0.67	–	–	0.65	–	0.65	–	–	–	–	–	–	–	–	0.5	0.64
7323aq	–	–	–	–	–	–	–	–	–	–	–	–	–	–	–	101	112	-1910	-1930	0.2	0.3	–	–
7411or	56	79	86	1500	3000	-1501	-1252	0.68	0.82	0.08	0.72	0.6	0.7	0.75	83	101	102	-900	-1100	0.7	0.75	1.5	1.2
7411aq	–	93	105	–	3000	-2405	-2155	0.3	0.3	0.52	0.27	0.2	0.32	0.3	–	103	119	-1900	-1955	0.32	–	1.2	–
7413or	61	85	95	1600	3000	-1963	-1670	0.55	0.7	0.18	0.63	–	0.62	0.6	67	88	90	-830	-1370	0.63	0.65	1.6	1.3
7413aq	58	96	113	–	3000	-2377	-2129	0.27	0.32	0.45	0.33	–	0.35	0.3	–	–	–	–	–	–	–	1.2	1.15
7415or	64	84	92	1350	3000	-1608	-1360	0.59	0.68	0.13	0.67	–	0.65	0.67	82	99	102	-950	-1200	0.68	–	1.3	1.15
7415aq	–	97	110	–	3000	-2495	-2248	0.21	0.27	0.57	0.25	0.25	0.3	0.27	–	102	115	–	-1600	–	–	1.2	1.15
7410or	65	83	91	1500	3000	-1747	-1748	0.56	0.72	0.14	0.65	–	0.65	0.65	76	94	97	-950	-1302	0.67	0.6	1.5	1.25
800	–	96	101	–	1600	-1319	-1175	0.33	0.33	0.47	0.35	–	0.35	0.33	–	–	–	–	–	–	–	0.67	0.67
801or	61	67	70	730	1600	-725	-635	0.8	0.82	0.4	0.78	–	0.76	0.7	–	–	–	–	–	–	–	0.73	–
801aq	–	94	99	–	1600	-1378	-1236	0.26	0.28	0.42	0.4	0.25	0.4	0.4	–	–	–	–	–	–	–	0.67	0.66
803or	65	74	76	730	1600	-759	-662	0.77	0.82	0.04	0.78	–	0.76	0.7	–	–	–	–	–	–	–	0.73	–
803aq	–	97	102	–	1600	-1406	-1265	0.23	0.25	0.46	0.33	0.22	0.35	0.33	–	–	–	–	–	–	–	0.67	0.65
811or	69	–	73	730	–	-717	-652	0.82	0.82	–	0.8	–	0.82	0.82	–	–	–	–	–	–	–	0.73	–
811aq	–	99	104	–	1600	-1352	-1214	0.24	0.3	0.47	0.35	–	0.35	0.33	–	–	–	–	–	–	–	0.67	0.64
821or	52	62	64	730	1600	-806	-673	0.76	0.82	0.08	0.72	0.67	0.7	0.75	–	–	–	–	–	–	–	0.73	–
821aq	–	92	96	–	1600	-1400	-1257	0.23	0.25	0.45	0.34	0.25	0.37	0.3	–	–	–	–	–	–	–	0.67	0.66
8410aq	–	95	110	–	3000	-2473	-2223	0.22	0.32	0.48	0.32	0.25	0.35	0.3	–	–	–	–	–	–	–	1.25	1.15
8412aq	–	95	107	–	3000	-2491	-2245	0.22	0.31	0.5	0.3	0.21	0.33	0.28	–	–	–	–	–	–	–	1.25	1.14
S6Taq	–	100	104	–	1250	-731	-639	0.43	0.6	0.38	0.42	0.3	0.45	0.41	–	–	–	–	–	–	–	0.52	0.43
S7Tor	63	84	87	550	1250	-315	-254	0.8	0.82	0.06	0.75	–	0.72	–	–	–	–	–	–	–	–	0.55	0.46
S7Taq	–	106	110	–	1250	-757	-668	0.35	0.38	0.4	0.4	–	0.4	0.38	–	–	–	–	–	–	–	0.52	0.41
S88or	–	–	–	–	–	–	–	–	–	–	–	–	–	–	58	69	70	-680	-713	–	0.78	–	–
S88aq	–	102	107	–	1250	-681	-590	0.33	0.48	0.37	0.42	0.3	0.44	–	–	–	–	–	–	–	–	0.52	0.42
S09or	59	88	90	550	1150	-393	-313	–	0.82	0.1	0.7	0.57	0.68	0.72	–	–	–	–	–	–	–	0.55	0.28
S09aq	–	112	118	–	1150	-847	-757	0.28	0.43	0.38	0.4	0.29	0.42	0.35	–	–	–	–	–	–	–	0.48	0.42
S10or	76	79	81	500	1360	-319	-276	–	0.82	0.05	0.75	0.65	0.74	0.82	–	–	–	–	–	–	–	0.5	0.35
S10aq	–	102	107	–	1360	-760	-667	0.23	0.6	0.4	0.4	0.27	0.4	0.4	–	–	–	–	–	–	–	0.57	0.35
S12or	70	83	86	550	1200	-375	-306	0.75	0.82	0.07	0.75	–	0.73	0.75	–	–	–	–	–	–	–	0.55	0.37
S12aq	–	84	87	–	1200	-597	-517	0.35	0.5	0.48	0.32	0.22	0.35	0.35	–	–	–	–	–	–	–	0.5	0.37
S13aq	64	87	94	1600	3000	-1691	-1457	0.52	0.55	0.25	0.56	0.41	0.56	0.47	56	76	78	-721	-1177	–	0.61	1.25	1.3
S15or	–	–	–	–	–	–	–	–	–	–	–	–	–	–	67	70	71	-918	-960	0.75	0.77	–	–
S15aq	–	–	–	–	–	–	–	–	–	–	–	–	–	–	–	116	117	–	-2230	–	–	–	–
F2	–	98	110	–	2800	-2385	-2147	0.21	0.35	0.55	0.25	0.18	0.28	0.28	–	–	–	–	–	–	–	1.2	1.1

Table C.4: Report of the calorimetric experiments (continued).

1250	2450	-1134	-1334	0.58	0.65	0.15	0.65	0.52	0.64	0.64	72	86	87	-950	-983	0.78	0.8	1	1.25			
–	2450	-2007	-1804	0.23	0.59	0.57	0.25	0.25	0.3	0.28	–	100	108	–	-1880	0.25	–	1.2	–			
1150	2900	-1274	-1067	0.63	0.8	0.12	0.68	0.55	0.67	0.7	79	94	97	-920	-1100	0.7	0.75	1.15	1.2			
–	2900	-2006	-1803	0.23	0.47	0.56	0.25	0.2	0.3	0.25	–	100	108	–	-1880	0.25	–	1.2	–			
630	–	-628	-573	0.78	0.82	–	0.82	–	0.8	0.72	–	–	–	–	–	–	–	0.63	0.61			
630	–	-639	-582	0.8	0.8	–	0.82	–	0.8	0.8	–	–	–	–	–	–	–	0.63	–			
630	–	-622	-567	0.8	0.8	–	0.82	–	0.8	0.8	–	–	–	–	–	–	–	0.63	0.61			
630	–	-620	-565	0.8	0.8	–	0.82	–	0.8	0.8	–	–	–	–	–	–	–	0.63	0.61			
630	–	-649	-591	0.8	0.8	–	0.82	–	0.8	0.8	–	–	–	–	–	–	–	0.63	0.65			
650	1600	-1309	-1165	0.3	0.33	0.45	0.35	0.25	0.37	0.3	–	–	–	–	–	–	–	0.65	0.67			
550	–	-579	-532	0.68	0.82	–	–	–	–	–	–	–	–	–	–	–	–	0.6	0.51			
550	–	-593	-547	0.68	0.8	–	–	–	–	–	–	–	–	–	–	–	–	0.6	0.52			
–	1600	-1342	-1200	0.28	0.3	–	–	–	–	–	–	–	–	–	–	–	–	0.66	0.65			
720	–	-697	-631	0.8	0.82	–	–	–	–	–	–	–	–	–	–	–	–	0.72	0.73			
–	1600	-1444	-1303	0.2	0.22	0.6	0.2	0.15	0.25	–	–	–	–	–	–	–	–	0.69	0.65			
–	1600	-1507	-1370	0.1	0.17	–	–	–	–	–	–	–	–	–	–	–	–	0.66	0.62			
–	1600	-1635	-1493	0.1	–	–	–	–	–	–	–	–	–	–	–	–	–	0.66	0.63			
–	1600	-1597	-1457	0.1	–	–	–	–	–	–	–	–	–	–	–	–	–	0.66	0.65			
750	1550	-995	-855	0.53	0.55	0.26	0.53	0.4	0.55	–	–	–	–	–	–	–	–	0.65	0.75			
750	1600	-993	-853	0.54	0.56	0.2	0.57	0.46	0.6	–	–	–	–	–	–	–	–	0.67	0.65			
750	1600	-1007	-865	0.54	0.54	0.25	0.53	0.4	0.55	–	–	–	–	–	–	–	–	0.67	0.66			
750	1550	-962	-828	0.52	0.57	0.22	0.55	0.42	0.57	–	–	–	–	–	–	–	–	0.65	0.62			
650	1350	-813	-700	0.52	0.57	0.25	0.56	0.4	0.55	–	–	–	–	–	–	–	–	0.56	0.52			
650	1350	-880	-758	0.51	0.52	0.28	0.53	0.37	0.51	–	–	–	–	–	–	–	–	0.65	0.56			
–	1600	-1573	-1430	0.1	0.15	–	0.2	0.2	–	–	–	–	–	–	–	–	–	0.67	0.66			
–	1600	-1640	-1500	0.1	–	–	0.2	0.2	–	–	–	–	–	–	–	–	–	0.67	0.64			
–	1600	-1481	-1342	0.1	0.2	0.7	0.2	0.1	0.15	–	–	–	–	–	–	–	–	0.67	0.64			
–	1600	-1481	-1342	0.1	0.2	0.7	0.2	0.1	0.15	–	–	–	–	–	–	–	–	0.67	0.64			
–	1600	-1441	-1308	0.1	0.22	0.7	0.2	0.1	0.15	–	–	–	–	–	–	–	–	0.67	0.61			
–	1600	-1543	-1402	0.1	–	–	–	–	–	–	–	–	–	–	–	–	–	0.67	0.65			
700	–	-672	-610	–	0.82	–	0.8	–	–	–	–	–	–	–	–	–	–	0.7	0.69			
700	–	-687	-625	–	0.8	–	0.8	–	–	–	–	–	–	–	–	–	–	0.7	0.69			
–	1630	-1422	-1278	0.23	0.25	0.62	0.2	0.15	0.25	–	–	–	–	–	–	–	–	0.68	0.67			
700	–	-656	-603	0.68	0.82	–	0.8	–	–	–	–	–	–	–	–	–	–	0.7	0.59			
700	–	-683	-626	0.7	0.82	–	0.8	–	–	–	–	–	–	–	–	–	–	0.7	0.63			
700	–	-687	-626	0.8	0.82	–	0.8	–	–	–	–	–	–	–	–	–	–	0.7	0.68			
700	–	-700	-637	–	0.8	–	0.8	–	–	–	–	–	–	–	–	–	–	0.7	–			
700	–	-656	-598	0.8	0.82	–	0.8	–	–	–	–	–	–	–	–	–	–	0.7	0.64			
650	–	-440	-402	–	0.82	–	0.8	–	–	–	–	–	–	–	–	–	–	0.65	0.42			
650	1400	-637	-532	–	0.82	0.08	0.73	–	0.7	–	–	–	–	–	–	–	–	0.65	0.49			

Table C.5: Report of the calorimetric experiments (continued).

–	1400	-1188	-1063	0.26	0.27	0.5	0.25	0.2	0.29	–	–	–	–	–	–	–	–	–	–	0.58	0.58	0.58	0.58
–	1400	-1358	-1233	0.1	–	–	–	–		–	–	–	–	–	–	–	–	–	–	0.58	0.58	0.58	0.58
650	–	-604	-550	–	0.8	–	–	–	–	–	–	–	–	–	–	–	–	–	–	0.7	0.7	0.6	0.6
700	–	-685	-617	–	0.8	–	–	–	–	–	–	–	–	–	–	–	–	–	–	0.7	0.7	0.75	0.75
700	1550	-1041	-903	0.48	0.53	0.2	0.6	0.45	0.6	–	–	–	–	–	–	–	–	–	–	0.7	0.7	0.64	0.64
–	1550	-1562	-1421	0.1	–	–	–	–	–	–	–	–	–	–	–	–	–	–	–	0.65	0.65	0.65	0.65
700	1550	-1269	-1129	0.32	0.33	0.3	0.53	0.37	0.51	–	–	–	–	–	–	–	–	–	–	0.65	0.65	–	–
–	1550	-1587	-1454	0.1	–	–	–	–	–	–	–	–	–	–	–	–	–	–	–	0.65	0.65	0.62	0.62
650	–	-561	-492	–	0.8	0.05	0.75	0.65	0.75	–	–	–	–	–	–	–	–	–	–	0.65	0.65	0.75	0.75
–	1550	-1155	-1034	0.29	0.36	0.4	0.4	0.28	0.4	–	–	–	–	–	–	–	–	–	–	0.63	0.63	0.57	0.57
650	–	-482	-444	–	0.8	–	–	–	0.8	–	–	–	–	–	–	–	–	–	–	0.65	0.65	0.4	0.4
750	1600	-862	-735	0.48	0.58	0.22	0.6	0.45	0.58	–	–	–	–	–	–	–	–	–	–	0.7	0.7	0.6	0.6
500	–	-483	-455	0.68	0.82	–	–	–	–	–	–	–	–	–	–	–	–	–	–	0.5	0.5	0.31	0.31
500	–	-309	-280	–	0.82	–	–	–	–	–	–	–	–	–	–	–	–	–	–	0.5	0.5	0.32	0.32
–	1550	-1191	-1067	0.27	0.33	0.55	0.25	0.18	0.29	–	–	–	–	–	–	–	–	–	–	0.64	0.64	0.57	0.57
650	1550	-546	-499	–	0.82	–	–	–	–	–	–	–	–	–	–	–	–	–	–	0.65	0.65	0.52	0.52
650	1550	-576	-518	–	0.82	–	–	–	–	–	–	–	–	–	–	–	–	–	–	0.65	0.65	0.64	0.64
–	1550	-1204	-1078	0.26	0.33	0.6	0.2	0.15	0.25	–	–	–	–	–	–	–	–	–	–	0.62	0.62	0.58	0.58
–	–	–	–	–	–	–	–	–	–	–	–	102	114	–	–	-2450	0	–	–	–	–	–	–
650	–	-563	-508	–	0.82	–	0.82	–	0.8	–	–	–	–	–	–	–	–	–	–	0.65	0.65	0.62	0.62
500	650	-400	-327	0.7	0.82	0.08	0.73	0.62	0.72	–	–	–	–	–	–	–	–	–	–	0.65	0.65	0.33	0.33
–	1400	-1044	-922	0.38	–	0.45	0.35	0.25	0.38			–	–	–	–	–	–	–		0.58	0.58	0.56	0.56
1350	–	-1410	-1192	0.72	0.8	0.05	0.75	–	0.74			–	–	–	–	–	–	–		1.35	1.35	1.25	1.25
1400	2700	-2035	-1790	0.38	0.41	0.37	0.42	–	0.44			–	–	–	–	–	–	–		1.12	1.12	1.13	1.13
1400	2700	-2160	-1917	0.35	0.35	0.41	0.39	–	0.4			–	–	–	–	–	–	–		1.12	1.12	1.12	1.12
1350	–	-1350	-1180	–	0.8	0.03	0.76	–	0.77			–	–	–	–	–	–	–		1.35	1.35	1.25	1.25
1800	2800	-2340	-2095	0.32	0.35	0.5	0.3	0.2	0.34			–	–	–	–	–	–	–		1.2	1.2	1.13	1.13
1800	2800	-2245	-1999	0.34	0.36	0.36	0.45	0.3	0.45			–	–	–	–	–	–	–		1.2	1.2	1.14	1.14
	2200	-2073	-1783	0.15	0.5	0.55	0.25	0.17	0.28			–	101	112	–	-2260	0.1			0.92	0.92	1.3	1.3
	2200	-2136	-1930	0.15	0.2	0.6	0.2	0.15	0.25			–	103	119	–	-2120	0.15			0.92	0.92	0.95	0.95
	2200	-2073	-1783	0.15	0.5	0.55	0.25	0.17	0.28			–	99	108	–	-2136	0.15			0.92	0.92	1.3	1.3
	2200	-2073	-1783	0.15	0.5	0.55	0.25	0.17	0.28			90	98	103	-2056	-2174	0.1			0.92	0.92	1.3	1.3
	2200	-1916	-1720	0.25	0.26	0.55	0.25	0.17	0.28			83	94	97	-1732	-1859	0.3			0.92	0.92	0.91	0.91

Table C.6: Report of the calorimetric experiments (continued).

ID	prel g default: org	etoh g	CH3-R(a) area ethanol	CH2(a) area ethanol	CH3CN(a) area MeCN	CH3-R(d) ppm ethanol	CH2(d) ppm ethanol	CH3CN(d) ppm MeCN	acalc mol/mol MeCN: Ethanol	wMeCN g/g	err % ethanol peaks	Notes
402	0.524	0.23	1	0.67	2.13	1.5	3.92	2.38	2.13	0.83	0.5	
512	0.406	0.234	1	0.67	1.64	1.47	3.91	2.36	1.64	0.84	0.5	
513	0.72	0.173	1.65	1.09	5.27	1.49	3.93	2.38	3.194	0.68	0.9	
5214	0.388	0.537	1	0.66	0.63	1.21	3.66	2.1	0.63	0.78	1	
615	1.01	0.207	1	0.66	4.74	1.63	4.07	2.51	4.74	0.87	1	
61704	0.633	0.313	1	0.67	1.84	1.48	3.92	2.36	1.84	0.81	0.5	
62140	1.267	0.237	1	0.66	4.87	1.39	3.84	2.29	4.87	0.81	1	not very good peaks
62140_aq	0.694	0.237	1	0.65	0.56	1.04	3.5	1.93	0.56	0.17	2.5	aq. phases weights corrected for salt 0.27 g/g
712	0.285	0.084	1	0.66	3.14	1.49	3.94	2.38	3.14	0.83	1	–
7214	0.291	0.658	1	0.66	0.4	1.26	3.7	2.15	0.4	0.81	1	–
73140	0.939	0.233	1	0.67	3.52	1.16	4.05	2.5	3.52	0.78	0.5	MeCN peak split multiple
73140_aq	0.327	0.236	1	0.65	0.44	1.07	3.53	1.95	0.44	0.28	2.5	aq. phases weights corrected for salt of 0.19 g/g
7322	0.086	0.189	1	0.664	0.356	1.08	3.56	1.99	0.356	0.7	0.4	–
7322_aq	0.127	0.22	1	0.671	0.16	1.07	3.56	1.97	0.16	0.25	0.6	correct salt fraction
7323	0.126	0.206	1	0.671	0.448	1.1	3.56	1.99	0.448	0.65	0.6	–
7323_aq	0.217	0.145	1	0.671	0.479	1.07	3.54	1.97	0.479	0.29	0.6	correct salt fraction
7410	0.077	0.203	1	0.668	0.278	1.07	3.52	1.95	0.278	0.65	0.2	–
7410_aq	0.089	0.246	1	0.67	0.15	1.07	3.49	1.94	0.15	0.37	0.5	phase sample directly into tube
7413	0.039	0.071	1	0.666	0.395	1.08	3.55	1.97	0.395	0.64	0.1	–
7413_aq	0.09	0.208	1	0.665	0.182	1.07	3.52	1.95	0.182	0.38	0.3	phase sample directly into tube
7411	0.276	0.142	1	0.667	1.57	1.15	3.62	2.04	1.57	0.72	0.1	–
7411_aq	0.091	0.159	1	0.665	0.207	1.09	3.55	2	0.207	0.32	0.3	phase sample directly into tube
7415	0.223	0.228	1	0.664	0.836	1.14	3.61	2.03	0.836	0.76	0.4	–
7415_aq	0.116	0.192	1	0.664	0.158	1.07	3.53	1.96	0.158	0.23	0.4	phase sample directly into tube
803	0.286	0.19	1	0.67	1.28	1.44	3.88	2.32	1.28	0.76	0.5	–
81104	0.215	0.163	1	0.66	1.11	1.33	3.67	2.21	1.11	0.75	1	–
81104_aq	1.3	0.643	1.81	1.19	1	1.08	3.54	1.975	0.552	0.24	1.4	aq. phases weights corrected for salt 0.07 g/g
82140	0.146	0.072	1	0.67	1.68	1.23	3.68	2.12	1.68	0.74	0.5	smeared peaks
82140_aq	1.56	0.38	1.84	1.2	1.96	1.08	3.54	1.97	1.065	0.23	2.2	aq. phases weights corrected for salt 0.13 g/g
S6tot	0.544	0.384	1	0.659	1.15	1.14	3.62	2.05	1.15	0.72	1.1	–
S7tot	0.322	0.24	1	0.663	1.02	1.32	3.78	2.24	1.02	0.68	0.5	–
S7tot_aq	0.908	0.713	1	0.66	0.437	1.09	3.56	1.98	0.437	0.31	1	missing correction for salt content
S8tot	0.083	0.132	1	0.671	0.434	1.05	3.52	1.94	0.434	0.62	0.6	–
S8tot_aq1	0.67	0.321	1	0.666	1.66	1.07	3.57	1.95	1.66	0.71	0.1	MeCN added: correction 0.303
S8tot_aq2	0.283	0.394	1	0.663	0.232	0.982	3.482	1.9	0.232	0.29	0.5	–
S88tot	0.089	0.106	1	0.665	0.645	1.16	3.62	2.07	0.645	0.69	0.3	–

Table C.7: Full report of the NMR measures, with the relevant data.

S88tot_aq	0.122	0.115	1	0.664	0.388	1.05	3.52	1.97	0.388	0.33	0.4	total phase sample directly into tube
S9tot	0.15	0.225	1	0.667	0.485	1.12	3.58	2.02	0.485	0.65	0.1	–
S9tot_aqA	0.181	0.417	1	0.664	0.124	1.02	3.49	1.92	0.124	0.25	0.4	not corrected for salt solubility - MeCN on total
S9tot_aqB	0.059	0.316	1	0.664	0.0521	1	3.48	1.92	0.052	0.25	0.4	surnatant re-sampled - result is MeCN on liquid
S10tot	0.636	0.738	1	0.665	0.74	1.32	3.74	2.21	0.74	0.77	0.3	–
S10tot_aqA	0.0175	0.24	100	64.4	2.04	1.39	3.53	1.95	0.02	0.25	3.4	surnatant re-sampled - result is MeCN on liquid
S10tot_aqB	0.0178	0.314	1	0.667	0.0128	1.04	3.5	1.92	0.013	0.2	0.1	surnatant re-sampled MeCN on liquid: 15% by comparative analysis
S12tot_aq	0.096	0.354	1	0.665	0.0437	1.03	3.54	1.94	0.044	0.14	0.3	not corrected for salt content
S13tot	0.153	0.211	1	0.666	0.63	1.17	3.62	2.05	0.63	0.78	0.1	–
S13tot_aq1	0.046	0.132	1	0.664	0.0758	1.04	3.5	1.91	0.076	0.19	0.4	entire phase sample directly into the tube
S13tot_aq2	0.097	0.352	1	0.667	0.0581	1.08	3.56	1.973	0.058	0.19	0.1	surnatant only. one sampling
S15tot	0.305	0.191	1	0.663	1.28	1.12	3.57	2	1.28	0.72	0.5	–
S15tot_aqS	0.146	0.733	1	0.666	0.038	1.03	3.5	1.88	0.038	0.17	0.1	surnatant only. one sampling
S15tot_aq	0.048	0.032	1	0.663	0.325	1.06	3.54	1.94	0.325	0.19	0.5	entire phase sample directly into the tube
S50	0.636	0.094	1	0.66	5.86	1.25	3.71	2.19	5.86	0.77	1	–
S50_aq	0.19	0.224	1	0.663	0.295	1.08	3.54	1.99	0.295	0.31	0.5	entire phase sample directly into the tube
S60	0.438	0.125	1	0.662	2.52	1.2	3.66	2.08	2.52	0.64	0.7	–
S60_aq	0.064	0.09	1	0.664	0.266	1.07	3.53	1.95	0.266	0.33	0.4	entire phase sample directly into the tube
7410aq	0.089	0.246	1	0.67	0.1496	1.067	3.49	1.945	0.15	0.37	0.5	entire phase sample directly into the tube
7410org	0.077	0.203	1	0.6685	0.278	1.069	3.517	1.95	0.278	0.65	0.3	–
7413aq	0.09	0.208	1	0.665	0.182	1.067	3.52	1.95	0.182	0.38	0.3	entire phase sample directly into the tube
7413org	0.039	0.071	1	0.666	0.395	1.077	3.547	1.97	0.395	0.64	0.1	–
7411aq	0.091	0.159	1	0.665	0.2068	1.109	3.55	2	0.207	0.32	0.3	entire phase sample directly into the tube
7411org	0.276	0.142	1	0.667	1.57	1.149	3.62	2.04	1.57	0.72	0.1	–
7415aq	0.116	0.192	1	0.665	0.158	1.07	3.53	1.96	0.158	0.23	0.3	entire phase sample directly into the tube
7415org	0.223	0.228	1	0.664	0.836	1.14	3.61	2.03	0.836	0.76	0.4	–
6506aq	0.087	0.143	1	0.665	0.536	1.13	3.59	2.04	0.536	0.79	0.3	–
8410aq	0.091	0.372	1	0.662	0.073	1.102	3.54	2.01	0.073	0.27	0.7	entire phase sample directly into the tube
8412org	0.107	0.138	1	0.664	0.72	1.13	3.602	2.041	0.72	0.83	0.4	–
8412aq	0.083	0.271	1	0.661	0.0685	1.075	3.526	1.959	0.069	0.2	0.8	entire phase sample directly into the tube
F2	0.276	0.217	1	0.656	0.26	1.092	3.53	1.969	0.26	0.18	1.6	entire phase sample directly into the tube
6512org	0.037	0.253	1	0.665	0.163	1.12	3.58	2.04	0.163	0.99	0.3	unrealistic
6512aq	0.094	0.325	1	0.662	0.082	1.1	3.54	2	0.082	0.25	0.7	entire phase sample directly into the tube
6508org	0.036	0.193	1	0.665	0.166	1.157	3.59	2.05	0.166	0.79	0.3	–
6508aq	0.046	0.078	1	0.663	0.156	1.1	3.57	1.99	0.156	0.24	0.5	entire phase sample directly into the tube
M7	0.78	0.395	1	0.67	1.89	1.67	4.11	2.54	1.89	0.85	0.5	weight extrapolated
M8	0.64	0.733	1	0.65	0.79	1.2	3.65	2.1	0.79	0.81	2.5	vyborne
6510org	0.038	0.088	1	0.666	0.363	1.1	3.57	1.98	0.363	0.75	0.1	entire phase sample directly into the tube
6510aq	0.044	0.178	1	0.667	0.0613	1.03	3.48	1.92	0.061	0.22	0.1	entire phase sample directly into the tube
6515org	0.037	0.136	1	0.667	0.247	1.07	3.55	1.99	0.247	0.81	0.1	entire phase sample directly into the tube

Table C.8: Full report of the NMR measures, with the relevant data (continued).

6515aq	0.048	0.205	1	0.664	0.0431	1.06	3.53	1.93	0.043	0.16	0.4	entire phase sample directly into the tube
T203	0.57	0.093	1	0.656	5.73	1.19	3.66	2.08	5.73	0.83	1.6	entire phase sample directly into the tube
7911org	0.184	0.089	1	0.665	1.67	1.22	3.68	2.13	1.67	0.72	0.3	–
7911aq	0.146	0.355	1	0.672	0.118	1.08	3.54	1.97	0.118	0.26	0.8	entire phase sample directly into the tube
2R13	0.803	0.226	1.81	1.19	0	1.02	3.48		0	0	0.83	
2D12	1.564	0.48	2.99	1.98	0.03	1	3.465	2.03	0.01	0.003	0.67	
2D7	0.281	0.237	1	0.66	0.31	1.02	3.49	1.92	0.31	0.233	0.33	
2D5_aq	0.97	0.5	1	0.66	0.44	1.03	3.485	1.93	0.44	0.202	0.33	
2D5_org	0.408	0.322	1	0.67	1.16	1.37	3.8	2.25	1.16	0.817	-0.17	–
2D4_org	0.619	0.327	1	0.67	1.95	1.53	3.95	2.4	1.95	0.919	-0.17	impurities in the fluid
2D4_aq	–	–	–	–	–	–	–	–	–	–	–	not usable
2D3_org	0.64	0.312	– 1	0.67	2.16	1.47	3.91	2.35	2.16	0.94	-0.17	impurities in the fluid peaks with tail to the right
2D3_aq	–	–	–	–	–	–	–	–	–	–	–	not usable
1R0	0.454	0.31	1	0.67	1.29	1.43	3.86	2.32	1.29	0.786	-0.17	impurities in the fluid peaks with tail to the right
1R7	0.726	0.31	1	0.67	0.96	1.11	3.57	2	0.96	0.366	-0.17	impurities in the fluid, smeared peaks, two small MeCN sidebands
1D1	1.362	0.31	1	0.66	4.01	1.52	3.96	2.41	4.01	0.814	0.33	clear!
1D2	0.96	0.31	1	0.66	2.8	1.54	3.97	2.42	2.8	0.807	0.33	broad. smeared peaks with tail to the right
1D3	0.865	0.31	1	0.66	2.48	1.38	3.83	2.28	2.48	0.793	0.33	broad. smeared peaks with tail to the left
1D4	0.892	0.31	1	0.66	2.63	1.57	4.01	2.46	2.63	0.816	0.33	defined peaks. possible phase problems across MeCN
1D5	1.352	0.31	1	0.66	4.03	1.68	4.11	2.55	4.03	0.825	0.33	baseline oscillations and curvatures
1D6	0.755	0.31	1	0.66	2.24	1.38	3.82	2.27	2.24	0.821	0.33	broad. smeared peaks
3R1	0.515	0.203	10	6.6	4.1	1.05	3.52	1.95	0.41	0.144	3.33	–
3R2	0.708	0.555	10	6.6	1.9	1.03	3.5	1.92	0.19	0.133	3.33	–
3R3	0.691	0.345	10	6.6	2.6	1.05	3.53	1.94	0.26	0.116	3.33	–
4R1	0.614	1.13	10	6.6	3.7	1.18	3.62	2.07	0.37	0.608	3.33	1.25 mol/l. density 0.97
												0.163 g of MeCN added after flocculation, so a 0.6 frac is 0.55
4R2	0.548	0.967	10	6.6	1.9	1.06	3.5	1.96	0.19	0.299	3.33	1.25 by tritration. Assume solubility of 0.4 mol/l.
												no flocculate was observed
4R3	0.469	0.868	10	6.6	1.2	1.05	3.51	1.94	0.12	0.198	3.33	0.4 mol/l. density 0.97
4R5	0.692	1.225	10	6.6	0.9	1.02	3.48	1.92	0.09	0.142	3.33	0.36 mol/l. density 0.97
RecOrg2602	0.168	0.462	1	0.659	0.257	1.13	3.6	0.258	0.257	0.631	0.38	–
RecOrg2702	0.172	0.234	1	0.666	0.524	1.17	3.61	2.07	0.524	0.636	0.03	–
9V0	0.53	0.244	1	0.617	0.778	1.13	2.05	3.63	0.778	0.32	2.48	–
9V5	0.56	0.585	1	0.643	0.0096	0.934	3.41	1.9	0.01	0.009	1.18	–
9V6	0.657	0.251	1	0.684	0.0018	0.979	3.43	1.85	0.002	0.001	-0.87	–
13D3_org	1.319	0.561	1	0.665	1.85	1.25	3.7	2.14	1.85	0.702	0.08	phase correction needed - baseline blurred
13D3_aq	0.47	0.583	1	0.665	0.165	1.11	3.56	1.98	0.165	0.183	0.08	phase correction needed - baseline blurred
13R1	0.803	0.206	1	0.666	0.0039	1.1	3.57	1.99	0.004	0.001	0.03	phase correction needed - baseline blurred
14D5_acq	0.976	0.397	1	0.659	0.531	1.12	3.56	2	0.531	0.193	0.38	phase correction needed - baseline blurred
14D5_org	0.786	0.373	1	0.667	1.81	1.13	3.59	2.01	1.81	0.767	-0.02	phase correction needed - baseline blurred
14D_REC1	0.961	0.281	1	0.664	0.016	1.04	3.5	1.92	0.016	0.004	0.13	–
14D4	0.825	0.382	1	0.669	1.83	1.2	3.65	2.06	1.83	0.756	-0.12	–

Table C.9: Full report of the NMR measures, with the relevant data (continued).

14D3_org	1.205	0.709	1	0.667	1.57	1.11	3.57	2.02	1.57	0.824	-0.02	split in J-peaks
14D3_acq	0.406	0.311	1	0.666	0.168	1.03	3.5	1.93	0.168	0.115	0.03	good
14D2	0.844	0.455	1	0.666	1.78	1.29	3.76	2.19	1.78	0.856	0.03	clear
14D1	1.185	0.779	1	0.671	1.5	1.33	3.78	2.26	1.5	0.88	-0.22	broad. smeared peaks
10D1	0.2	0.39	1	0.663	0.514	1.06	3.52	1.94	0.514	0.894	0.18	–
10D1_REC	0.184	0.281	1	0.665	0.152	1.03	3.5	1.91	0.152	0.207	0.08	record not checked
PL3	0.081	0.146	1	0.657	0.507	1.06	3.54	1.97	0.507	0.816	0.48	phase corr
PL5org	0.08	0.145	1	0.666	0.433	1.1	3.54	1.99	0.433	0.7	0.03	phase corr
PL5aq	0.096	0.015	1	0.666	2.39	1.04	3.52	1.94	2.39	0.333	0.03	good
PL7	0.086	0.148	1	0.664	0.407	1.02	3.49	1.91	0.407	0.625	0.13	phase corr

Table C.10: Full report of the NMR measures (continued).

Bibliography

[1] F. Cherubini. The biorefinery concept: Using biomass instead of oil for producing energy and chemicals. *Energy Conversion and Management*, 51:1412–1421, 2010.

[2] M. Ni, D. Leung, and M. Leung. A review on reforming bio-ethanol for hydrogen production. *International Journal of Hydrogen Energy*, 32:3238–3247, 2007.

[3] B. Schuster and M. Chinn. Consolidated bioprocessing of lignocellulosic feedstocks for ethanol fuel production. *Bioenergy Resources*, pages 416–435, 2013.

[4] Ethylene from ethanol. http://chematur.se/technologies/bio-chemicals/bio-ethylene-ethene/.

[5] D. Cook, S. Hodge, and C. Moffatt. Ethanol-to-ethylene process provides alternative pathway to plastics. *Hydrocarbon Processing*, 2014.

[6] I. S. Yakovleva, E. V. Banzaraktsaeva, S. P.and Ovchinnikova, V. A. Chumachenko, and L. A. Isupova. Catalytic dehydration of bioethanol to ethylene. review. *Catalysis in Industry*, 16:27–73, 2016.

[7] J. Jernberg, Ø. Nørregård, M. Olofsson, C. Hulteberg, and Hans Karlsson. Ethanol dehydration to green ethylene. Master's thesis, Lund University of technology, 2015.

[8] J. Gallo, J. Bueno, and Ulf Schuchardt. Catalytic transformations of ethanol for biorefineries. *Journal of Brazilian Chemical Society*, 25(12):2229–2243, 2014.

[9] J. Althoff, K. Biesheuvel, A. De Kok, H. Pelt, M. Ruitenbeek, G. Spork, J. Tange, and Ronald Wevers. Economic feasibility of the sugar beet-to-ethylene value chain. *ChemSusChem*, 6(9):1622–1630, 2013.

[10] P. Haro, P. Ollero, and F. Trippe. Technoeconomic assessment of potential processes for bio-ethylene production. *Fuel Processing Technology*, 114:35–48, 2013.

[11] I. Rossetti, M. Compagnoni, E. Finocchio, G. Ramis, A. Di Michele, Y. Millot, and Stanislaw Dzwigaj. Ethylene production via catalytic dehydration of diluted bioethanol: A step towards an integrated biorefinery. *Applied Catalysis B: Environmental*, 210:407–420, 2017.

[12] I. Rossetti, M. Compagnoni, G. De Guido, L. Pellegrini, G. Ramis, and Stanislaw Dzwigaj. Ethylene production from diluted bioethanol solutions. *Canadian Journal of Chemical Engineering*, 95(9):1752–1759, 2017.

[13] A. Morschbacker. Bio-ethanol based ethylene. *Polymer Reviews*, 49(2), 2009.

[14] G. Ondrey. The launch of a new bioethylene-production process. *Chemical Engineering*, 2014.

[15] D. Fan, D. J. Dai, and H. S. Wu. Ethylene formation by catalytic dehydration of ethanol with industrial considerations. *Materials*, 6:101–115, 2013.

[16] A. Mohsenzadeh, A. Zamani, and J. Taherzadeh Mohammad. Bioethylene production from ethanol: A review and techno-economical evaluation. *ChemBioEng Reviews*, 4(2):75–91, 2017.

[17] A. Tripodi, M. Belotti, and Rossetti Ilenia. Bioethylene production: From reaction kinetics to plant design. *ACS Sustainable Chemistry & Engineering*, 7(15):13333–13350, 2019.

[18] M. Zhang and Yingzhe Yu. Dehydration of ethanol to ethylene. *Industrial and Engineering Chemistry Research*, 52(28):9505–9514, 2013.

[19] J. Becerra, E. Quiroga, E. Tello, M. Figueredo, and Martha Cobo. Kinetic modeling of polymer-grade ethylene production by diluted ethanol dehydration over H-ZSM-5 for industrial design. *Journal of Environmental Chemical Engineering*, 6(5):6165–6174, 2018.

[20] C. B. Phillips and Ravindra Datta. Production of ethylene from hydrous ethanol on H-ZSM-5 under mild conditions. *Industrial and Engineering Chemistry Research*, 36(11):4466–4475, 1997.

[21] I. Takahara, M. Saito, M. Inaba, and K. Murata. Dehydration of ethanol into ethylene over solid acid catalysts. *Catalysis Letters*, 105:249–252, 2005.

[22] X. Zhang, R. Wang, X. Yang, and F. Zhang. Comparison of four catalysts in the catalytic dehydration of ethanol to ethylene. *Microporous and Mesoporous Materials*, 116:210–215, 2008.

[23] Joseph F. DeWilde, Hsu Chiang, Daniel A. Hickman, Christopher R. Ho, and Aditya Bhan. Kinetics and mechanism of ethanol dehydration on Al_2O_3: The critical role of dimer inhibition. *ACS Catalysis*, 3(4):798–807, 2013.

[24] Joseph F. DeWilde, Christopher J. Czopinski, and Aditya Bhan. Ethanol dehydration and dehydrogenation on Al_2O_3: Mechanism of acetaldehyde formation. *ACS Catalysis*, 4(12):4425–4433, 2014.

[25] M. Christiansen, G. Mpourmpakis, and Dimitros Vlachos. DFT-driven multisite microkinetic modeling of ethanol conversion to ethylene and diethyl ether on Al_2O_3(1 1 1). *Journal of Catalysis*, 323(111):121–131, 2015.

[26] K. Alexopoulos, M. John, K. Borght, V. Galvita, M. Reyniers, and Guy B. Marin. DFT-based microkinetic modeling of ethanol dehydration in H-ZSM-5. *Journal of Catalysis*, 339:173–185, 2016.

[27] K. Borght, R. Batchu, V. Galvita, K. Alexopoulos, M. Reyniers, J. Thybaut, and Guy B. Marin. Insights into the reaction mechanism of ethanol conversion into hydrocarbons on H-ZSM-5. *Angewandte Chemie International Edition*, 2016.

[28] W. Knaeble and E. Iglesia. Kinetic and theoretical insights into the mechanism of alkanol dehydration on solid bronsted acid catalysts. *Journal of Physical Chemistry C*, 2016.

[29] M. Kang and A. Bhan. Kinetics and mechanisms of alcohol dehydration pathways on alumina. *Catalysis Science & Technology*, 6:6667–6678, 2016.

[30] T. K. Phung and G. Busca. Diethyl ether cracking and ethanol dehydration: Acid catalysis and reaction paths. *Chemical Engineering Journal*, 272:92–101, 2015.

[31] A. Tripodi, M. Compagnoni, R. Martinazzo, G. Ramis, and Rossetti Ilenia. Process simulation for the design and scale up of heterogeneous catalytic process: Kinetic modeling issues. *Catalysts*, 7(5), 2017.

[32] A. Tripodi, M. Compagnoni, and Ilenia Rossetti. Kinetic modeling and reactor simulation for ethanol steam reforming. *ChemCatChem*, 8(24):3804–3813, 2016.

[33] M. Llano-Restrepo and Y. Muñoz Muñoz. Combined chemical and phase equilibrium for the hydration of ethylene to ethanol calculated by means of the Peng-Robinson-Stryjek-Vera equation of state and the Wong-Sandler mixing rules. *Fluid Phase Equilibria*, 307(1):45–57, 2011.

[34] H. Walter, editor. *IUPAC Solubility Data Series - Ethene*, volume 57. 1994.

[35] Y. Munoz-Munoz and M. Llano-Restrepo. Vapor-liquid equilibria for the binary systems ethylene+water, ethylene+ethanol, and ethanol+water, and the ternary system ethylene+water+ethanol from gibbs-ensemble molecular simulation. *Fluid Phase Equilibria*, 394:1–11, 2015.

[36] H. K. Bae and K. Nagahama. Measurement and correlation of high vapor-liquid equilibria for the systems ethylene-1-butene and ethylene-propylene. *Journal of Chemical Engineering of Japan*, 14(1):1–6, 1981.

[37] M. A. Villamanan, A. J. Allawi, and C. H. Van Ness. Vapor-liquid-liquid equilibrium and heats of mixing for diethyl ether-water at 35 degrees C. *Journal of Chemical Engineering Data*, 29(4):431–435, 1984.

[38] V. Bareggi, S. Mori, P. Schwarza, and P. Beltrame. Equilibrio liquido-vapore del sistema acetaldeide-acqua sotto pressione. *La Chimica e L'Industria*, 50(11):1224–1226, 1968.

[39] M. C. C. Serra and A. M. F. Palavra. Solubility of 1-butene in water and in a medium for cultivation of a bacterial strain. *Journal of Solution Chemistry*, 32:527–534, 2003.

[40] R. Sander. Compilation of Henry's law constants (version 4.0) for water as solvent. *Atmospheric Chemistry and Physics*, 15(8):4399–4381, 2015.

[41] A. Muhammad and Y. GadelHak. Simulation based improvement techniques for acid gases sweetening by chemical absorption: A review. *International Journal of Greenhouse Gas Control*, 37:481–491, 2015.

[42] S. Lange, S. Moioli, and Laura Pellegrini. Vapor-liquid equilibrium and enthalpy of asbsorption of the CO_2-MEA-H_2O system. *Chemical Engineering Transactions*, 43:1975–1980, 2015.

[43] S. Moioli, L. Pellegrini, and Simone Gamba. Simulation of CO_2 capture by MEA scrubbing with a rate-based model. *Procedia Engineering*, 42:1651–1661, 2012.

[44] J. Vivier, S. Kamalpour, and Mehablia Amine. Thermodynamics of CO_2-MDEA using eNRTL with differential evolution algorithm. *journal of Thermodynamics & Catalysis*, 3(2), 2012.

[45] I. Kim, H. F. Svendsen, and E. Borresen. Ebulliometric determination of vapor-liquid equilibria for pure water, Monoethanolamine, n-Methyldiethanolamine, 3-(methylamino)-propylamine, and their binary and ternary solutions. *Journal of Chemical Engineering Data*, 53:2521–2531, 2008.

[46] M. Xiao, H. Liu, H. Gao, and Zhiwu Liang. CO_2 absorption with aqueous tertiary amine solutions: Equilibrium solubility and thermodynamic modeling. *Journal of Chemical Thermodynamics*, 122:170–182, 2018.

[47] N. K. Kochar, T. Merims, and A. S. Padia. Ethylene from ethanol. *Chemical Engineering Progress*, 77(6):66–70, 1981.

[48] Y. Hu. Unconventional olefin processes. *Hydrocarbon Processing*, 1983.

[49] J. Maia, R. Demuner, A. Secchi, P. Melo, R. Carmo, and G. Gusmao. Process modeling and simulation of an industrial-scale plant for green ethylene production. *Industrial and Engineering Chemistry Research*, 57(18):6401–6416, 2018.

[50] A. Kagyrmanova, V. Chumachenko, V. Korotkikh, V. Kashkin, and Noskov A. Catalytic dehydration of bioethanol to ethylene: Pilot-scale studies and process simulation. *Chemical Engineering Journal*, 176:188–194, 2011.

[51] J. Becerra, M. Figueredo, and Martha Cobo. Thermodynamic and economic assessment of the production of light olefins from bioethanol. *Journal of Environmental Chemical Engineering*, 5(2):1554–1564, 2017.

[52] G. Cameron, L. Le, N. Nagulapalli, and Julie Levine. Process design for the production of ethylene from ethanol. Technical Report 29, University of Pennsylvania, 2012.

[53] M. Arvidsson and B. Lundin. Process integration study of a biorefinery producing ethylene from lignocellulosic feedstock for a chemical cluster. Technical report, Chalmers University of Technology, Goteborg, SE, 2011.

[54] Moran, D. Cellulosic ethanol biorefineries at commercial scale, 2017. [Online; accessed 4-4-2019].

[55] G. De Guido, M. Compagnoni, L. Pellegrini, and Rossetti Ilenia. Mature versus emerging technologies for CO_2 capture in power plants: Key open issues in post-combustion amine scrubbing and in chemical looping combustion. *Frontiers of Chemical Science and Engineering*, 12(2):315–325, 2018.

[56] M. Simo, C. J. Brown, and V. Hlavacek. Simulation of pressure swing adsorption in fuel ethanol production process. *Computers and Chemical Engineering*, 32(7):1635–1649, 2008.

[57] C. Chang, A. Devera, and D. Miller. A lumped kinetic model for dehydration of ethanol to hydrocarbons over H-ZSM-5. *Chemical Engineering Communications*, 95(1):27–39, 1990.

[58] I. C. Kemp. *Pinch Analysis and Process Integration: A User Guide on Process Integration for the Efficient Use of Energy*. Butterworth-Heinemann, an imprint of Elsevier, Linacre House, Jordan Hill, Oxford OX2 8DP, UK 30, second edition edition, 2007.

[59] V. Kirillov, V. Meshcheryakov, V. Sobyanin, V. Belyaev, Y. Amosov, N. Kuzin, and A Bobrin. Bioethanol as a promising fuel for fuel cell power plants. *Theoretical Foundations of Chemical Engineering*, 42(1):1–11, 2008.

[60] J. Xuan, M. Leung, D. Leung, and M. Ni. A review of biomass-derived fuel processors for fuel cell systems. *Renewable and Sustainable Energy Reviews*, 13:1301–1313, 2009.

[61] J. Wang, C. Lee, and M. Lin. Mechanism of ethanol reforming: Theoretical foundations. *Journal of Physical Chemistry C*, 113(16):6681–6688, 2009.

[62] J. Sutton, P. Panagiotopoulou, X. Verykios, and D. Vlachos. Combined DFT, microkinetic, and experimental study of ethanol steam reforming on pt. *Journal of Physical Chemistry C*, 117(9):4691–4706, 2013.

[63] J. R. Rostrup-Nielsen, J. Sehested, and J. K. Norskv. Hydrogen and synthesis gas by steam and C_{02} reforming. *Advances in Catalysis*, 47:65–139, 2002.

[64] I. Rossetti, J. Lasso, V. Nichele, M. Signoretto, E. Finocchio, G. Ramis, and Alessandro Di Michele. Silica and zirconia supported catalysts for the low-temperature ethanol steam reforming. *Applied Catalysis B: Environmental*, 150:257–267, 2014.

[65] A. Vizcaino, P. Arena, G. Baronetti, A. Carrero, J. Calles, M. Laborde, and N. Amadeo. Ethanol steam reforming on Ni/Al_2O_3 catalysts: Effect of Mg addition. *International Journal of Hydrogen Energy*, 33(13):3489–3492, 2008.

[66] L. Barattini, G. Ramis, C. Resini, G. Busca, M. Sisani, and U. Costantino. Reaction path of ethanol and acetic acid steam reforming over Ni-Zn-Al catalysts. flow reactor studies. *Chemical Engineering Journal*, 153:43–49, 2009.

[67] J. Liberatori, R. Ribeiro, D. Zanchet, F. Noronha, and J. Bueno. Steam reforming of ethanol on supported nickel catalysts. *Applied Catalysis A: General*, 327(2):197–204, 2007.

[68] Y. J. Wu, J. C. Santos, P. Li, J. G. Yu, A. F. Cunha, and A. E. Rodrigues. Simplified kinetic model for steam reforming of ethanol on a Ni/Al_2O_3 Ni/Al_2O_3 catalyst. *Canadian Journal of Chemical Engineering*, 92:116–130, 2014.

[69] M. Compagnoni, A. Tripodi, and Ilenia Rossetti. Parametric study and kinetic testing for ethanol steam reforming. *Applied Catalysis B: Environmental*, 203:899–909, 2016.

[70] M. Compagnoni, A. Tripodi, A. Di Michele, P. Sassi, M. Signoretto, and Rossetti Ilenia. Low temperature ethanol steam reforming: new Ni/M_xO-ZrO_2 active and stable catalysts prepared by flame spray pyrolysis. *International Journal of Hydrogen Energy*, 42(47):28193–28213, 2017.

[71] C. Resini, T. Montanari, L. Barattini, G. Ramis, G. Busca, S. Presto, P. Riani, R. Marazza, M. Sisani, F. Marmottini, and U. Costantino. Hydrogen production by ethanol steam reforming over ni catalysts derived from hydrotalcite-like precursors: Catalyst characterization, catalytic activity and reaction path. *Applied Catalysis A: General*, 355:83–93, 2009.

[72] A. Furtado, C. Alonso, M. Cantao, and N. Fernandes-Machado. Bimetallic catalysts performance during ethanol steam reforming: Influence of support materials. *International Journal of Hydrogen Energy*, 34(17):7189–7196, 2009.

[73] C. Graschinsky, M. Laborde, N. Amadeo, A. Le Valant, N. Bion, F. Epron, and Daniel Duprez. Ethanol steam reforming over $Rh(1\%)MgAl_2O_4/Al_2O_3$: A kinetic study. *Industrial and Engineering Chemistry Research*, 49:12383–12389, 2010.

[74] J. Xu and G. Froment. Methane steam reforming: Intrinsic kinetics. *AIChE Journal*, 35(1):88–96, 1989.

[75] V. Mas, R. Kipreos, N. Amadeo, and M. Laborde. Thermodynamic analysis of ethanol/water system with the stoichiometric method. *International Journal of Hydrogen Energy*, 31(1):21–28, 2006.

[76] V. Mas, M. L. Bergamini, G. Baronetti, N. Amadeo, and M. Laborde. A kinetic study of ethanol steam reforming using a nickel based catalyst. *Topics in Catalysis*, 51:39–48, 2008.

[77] I. Rossetti, M. Compagnoni, and Torli M. Process simulation and optimisation of H_2 production from ethanol steam reforming and its use in fuel cells. 1. Thermodynamic and kinetic analysis. *Chemical Engineering Journal*, 281:1024–1035, 2015.

[78] C. Bartholomew. Mechanisms of catalyst deactivation. *Applied Catalysis A: General*, 212:17–60, 2001.

[79] Andre L. Alberton, M. M. V. M. Souza, and Martin Schmal. Carbon formation and its influence on ethanol steam reforming over Ni/Al_2O_3 catalysts. *Catalysis Today*, 123(257-264), 2007.

[80] A. Akande, A. Aboudheir, R. Idem, and A. Dalai. Kinetic modeling of hydrogen production by the catalytic reforming of crude ethanol over a co-precipitated $Ni-Al_2O_3$ catalyst in a packed bed tubular reactor. *International Journal of Hydrogen Energy*, 31(12):1707–1715, 2006.

[81] I. Llera, V. Mas, M. Bergamini, M. Laborde, and Amadeo N. Bio-ethanol steam reforming on Ni-based catalyst. kinetic study. *Chemical Engineering Science*, 71:356–366, 2012.

[82] S. Freni, N. Mondello, S. Cavallaro, G. Cacciola, V. Parmon, and V. Sobyanin. Hydrogen production by steam reforming of ethanol: A two step process. *Reaction Kinetics and Catalysis Letters*, 71(1):143–152, 2000.

[83] S. Patel and K. K. Pant. Kinetic modeling of oxidative steam reforming of methanol over $Cu/ZnO/CeO_2/Al_2O_3$ catalyst. *Applied Catalysis A: General*, 356:189–200, 2009.

[84] A. N. Fatsikostas and X. E. Verykios. Reaction network of steam reforming of ethanol over ni-based catalysts. *Journal of Catalysis*, 225(2):439–452, 2004.

[85] Y. Wu, P. Li, J. Yu, A. Cunha, and A. Rodrigues. Sorption-enhanced steam reforming of ethanol on nimgal multifunctional materials: Experimental and numerical investigation. *Chemical Engineering Journal*, 231:36–48, 2013.

[86] Y. Choi and H. Stenger. Water gas shift reaction kinetics and reactor modeling for fuel cell grade hydrogen. *Journal of Power Sources*, 124(2):432–439, 2003.

[87] C. L. Young and H. L. Clever, editors. *Solubility Data Series - Methane*, volume 27-28. 1994.

[88] R. Wilhelm, E.and Battino and R. J. Wilcock. Low-pressure solubility of gases in liquid water. *Chemical Reviews*, 77(2):219–262, 1977.

[89] A. Valtz, A. Chapoy, C. Coquelet, P. Paricaud, and Dominique Richon. Vapour-liquid equilibria in the carbon dioxide-water system, measurement and modelling from 278.2 to 318.2 k. *Fluid Phase Equilibria*, 226:333–344, 2004.

[90] R. Crovetto, R. Fernandez-Prini, and M. L. Japas. Solubilities of inert gases and methane in H_2O and in D_2O in the temperature range of 300 to 600 k. *Journal of Chemical Physics*, 76(2), 1982.

[91] C. L. Young, editor. *Solubility Data Series - Hydrogen and Deuterium*, volume 5-6. Pergamon Press, 1981.

[92] M. Compagnoni, A. Tripodi, E. Mostafavi, N. Mahinpey, and Ilenia Rossetti. Hydrogen production by steam reforming of bio-ethanol: Process design and economic assessment. *DGMK Tagungsbericht*, 2:5–11, 2017.

[93] M. Compagnoni, E. Mostafavi, A. Tripodi, N. Mahinpey, and Ilenia Rossetti. Techno-economic analysis of a bioethanol to hydrogen centralized plant. *Energy and Fuels*, 31(11):12988–12996, 2017.

[94] A. Carrara, A. Perdichizzi, and G. Barigozzi. Simulation of an hydrogen production steam reforming industrial plant for energetic performance prediction. *International Journal of Hydrogen Energy*, 35(8):3499–3508, 2010.

[95] A. Miltner, W. Wukovits, T. Proll, and A. Friedl. Renewable hydrogen production: A technical evaluation based on process simulation. *Journal of Cleaner Production*, 18 (SUPPL 1):S51–S52, 2010.

[96] P. Lang, F. Denes, and L. Hegely. Comparison of different amine solvents for the absorption of CO_2. *Chemical Engineering Transactions*, 61:1105–1110, 2017.

[97] F. Lopes, C. A. Grande, A. M. Ribeiro, J. M. Loureiro, O. Evaggelos, V. Nikolakis, and A. E. Rodrigues. Adsorption of H_2, CO_2, CH_4, CO, N_2 and H_2O in activated carbon and zeolite for hydrogen production. *Separation Science and Technology*, 44:1045–1073, 2009.

[98] S. Yang, D. Choi, S. Jang, S. Kim, and D. Choi. Hydrogen separation by multi-bed pressure swing adsorption of synthesis gas. *Adsorption*, 14:583–590, 2008.

[99] C. Chou, F. Chen, Y. Huang, and H. Yang. Carbon dioxide capture and hydrogen purification from synthesis gas by pressure swing adsorption. *Chemical Engineering Transactions*, 32:1855–1860, 2013.

[100] A. Aden, M. Ruth, K. Ibsen, J. Jechura, K. Neeves, J. Sheehan, and B. Wallace. Lignocellulosic biomass to ethanol process design and economics utilizing co-current dilute acid prehydrolysis and enzymatic hydrolysis for corn stover. *National Renewable Energy Laboratory - Technical Report*, TP-510-32438, 2002.

[101] O. Pardo-Planas, H. Atiyeh, J. Phillips, C. Aichele, and S. Mohammad. Process simulation of ethanol production from biomass gasification and syngas fermentation. *journal*, 245:925–932, 2017.

[102] M. Dias, A. Ensinas, S. Nebra, F. R. Maciel, C. Rossell, and M. Maciel. Production of bioethanol and other bio-based materials from sugarcane bagasse: Integration to conventional bioethanol production process. *Chemical Engineering Research and Design*, 87(9):1206–1216, 2009.

[103] Toyo reforming process. https://www.toyo-eng.com/jp/en/products/petrochmical/hydrogen/.

[104] Ammonia dual pressure process by Uhde. http://www.processengineer.info/petrochemical/ammonia-dual-pressure-process.html.

[105] I. Rossetti, J. Lasso, M. Compagnoni, G. De Guido, and Laura Pellegrini. H_2 production from bioethanol and its use in fuel-cells. *Chemical Engineering Transactions*, 43, 2015.

[106] A. Tripodi, M. Compagnoni, G. Ramis, and Ilenia Rossetti. Process simulation of hydrogen production by steam reforming of diluted bioethanol. *International Journal of Hydrogen Energy*, 42(37):23776–23783, 2017.

[107] A. Tripodi, A. Pizzonia, E. Bahadori, and Ilenia Rossetti. Integrated plant layout for Heat and Power Cogeneration from diluted bioethanol. *ACS Sustainable Chemistry and Engineering*, 6(4):5358–5369, 2018.

[108] I. Rossetti, M. Compagnoni, and M. Torli. Process simulation and optimization of H_2 production from ethanol steam reforming and its use in fuel cells. 2. Process analysis and optimization. *Chemical Engineering Journal*, 281:1036–1044, 2015.

[109] A. Tripodi, E. Bahadori, G. Ramis, and Ilenia Rossetti. Feasibility assessment, process design and dynamic simulation for cogeneration of heat and power by steam reforming of diluted bioethanol. *International Journal of Hydrogen Energy*, 44(1):2–22, 2019.

[110] J. Le Dréau and P. Heiselberg. Energy flexibility of residential buildings using short term heat storage in the thermal mass. *Energy*, 111:991–1002, 2016.

[111] M. Temkin and V. Pyzhev. Kinetics of ammonia synthesis on promoted iron catalysts. *Acta Physicochimica URSS*, 12, 1940.

[112] D. Brown, T. Edmonds, R. Joyner, J. McCarroll, and S. Tennison. The genesis and development of the commercial BP doubly promoted catalyst for ammonia synthesis. *Catalysis Letters*, 144(4):545–552, 2014.

[113] N. Cherkasov, A. Ibhadon, and P. Fitzpatrick. A review of the existing and alternative methods for greener nitrogen fixation. *Chemical Engineering and Processing: Process Intensification*, 90:24–33, 2015.

[114] P. Arora, A. Hoadley, S. Mahajani, and A. Ganesh. Small-scale ammonia production from biomass: A techno-enviro-economic perspective. *Industrial and Engineering Chemistry Research*, 55:6422–6434, 2016.

[115] M. Reese, C. Marquart, M. Malmali, K. Wagner, E. Buchanan, A. McCormick, and E. Cussler. Performance of a small-scale Haber process. *Industrial and Engineering Chemistry Research*, 55:3742–3750, 2016.

[116] N. Pernicone, F. Ferrero, I. Rossetti, L. Forni, P. Canton, P. Riello, G. Fagherazzi, M. Signoretto, and F. Pinna. Wustite as a new precursor of industrial ammonia synthesis catalysts. *Applied Catalysis A: Genera*, 251(1):121–129, 2003.

[117] I. Rossetti, N. Pernicone, F. Ferrero, and Lucio Forni. Kinetic study of ammonia synthesis on a promoted Ru/C catalyst. *Industrial and Engineering Chemistry Research*, 45(12):4150–4155, 2006.

[118] L. Forni, D. Molinari, I. Rossetti, and N. Pernicone. Carbon-supported promoted ru catalyst for ammonia synthesis. *Applied Catalysis A: General*, 185(2):269–275, 1999.

[119] L. Gillespie and J. Beattie. The thermodynamic treatment of chemical equilibria in system composed of real gases. I. An approximate equation for the mass-action function applied to the existing data on the haber equilibrium. *Physical Review*, 36:743–753, 1930.

[120] A. Tripodi, M. Compagnoni, E. Bahadori, and Rossetti Ilenia. Process simulation of ammonia synthesis over optimized Ru/C catalyst and multibed Fe+Ru configurations. *Journal of Industrial and Engineering Chemistry*, 66:176–186, 2018.

[121] Aspen Technology Inc. Aspen Plus ammonia model. www.aspentech.com, 2008.

[122] C. Alesandrini, A. Sherman, and S. Lynn. Removal of argon and methane from ammonia plant synthesis gas. *Industrial and Engineering Chemistry Process Design and Development*, 12(3):217–220, 1973.

[123] C. Vancini. *La sintesi dell'Ammoniaca*. Hoepli, Milano, 1961.

[124] M. Sawant, A. Patwardhan, V. Gaikar, and M. Bhaskaran. Phase equilibria analysis of the binary N_2-NH_3 and H_2-NH_3 systems and prediction of ternary phase equilibria. *Fluid Phase Equilibria*, 239(1):52–62, 2006.

[125] A. Michels, G. F. Skelton, and E. Dumoulin. Gas-liquid phase equilibrium in the system ammonia-hydrogen-nitrogen. *Physica*, 16(11):831–838, 1950.

[126] K. Reddy and A. Husain. Vapor-liquid equilibrium relationship for ammonia in presence of other gases. *Industrial and Engineering Chemistry Process Design and Development*, 19(4):580–586, 1980.

[127] A. Larson and C. Black. Solubility of a mixture of hydrogen and nitrogen in liquid ammonia. *Industrial & Engineering Chemistry*, 17(7):715–716, 1925.

[128] A. Larson and C. Black. The concentration of ammonia in a compressed mixture of hydrogen and nitrogen over liquid ammonia. *Journal of the American Chemical Society*, 47(4):1015–1020, 1925.

[129] R. Wiebe and V. Gaddy. The solubility in liquid ammonia of hydrogen at 0 degrees C and of nitrogen at 0, 50, 75, 90 and 100 degrees C at pressures to 1000 atmospheres. critical phenomena of ammonia-nitrogen mixtures. *Journal of the American Chemical Society*, 59(10):1984–1987, 1937.

[130] A. AL-Dhfeery and A. Jassem. Modeling and simulation of an industrial secondary reformer reactor in the fertilizer plants. *International Journal of Industrial Chemistry*, 3(1):1–8, 2012.

[131] J. Klose and M. Baerns. Kinetics of the methanation of carbon monoxide on an alumina-supported nickel catalyst. *Journal of Catalysis*, 85(1):105–116, 1984.

[132] A. Araujo and S. Skogestad. Control structure design for the ammonia synthesis process. *Computers & Chemical Engineering*, 32(12):2920–2932, 2008.

[133] B. Babu and R. Angira. Optimal design of an auto-thermal ammonia synthesis reactor. *Computers and Chemical Engineering*, 29(5):1041–1045, 2005.

[134] Fei Quan. A study on the application of computer process simulation technology in ammonia synthesis. *Chemical Engineering Transactions*, 59:589–594, 2017.

[135] William Luyben. Plantwide control of a coupled reformer-ammonia process. *Chemical Engineering Research and Design*, 134:518–527, 2018.

[136] J. Sun and Y. Wang. Recent advances in catalytic conversion of ethanol to chemicals. *ACS Catalysis*, 4:1078–1090, 2014.

[137] D. Cespi, F Passarini, E. Neri, I. Vassura, L. Ciacci, and F. Cavani. Life cycle assessment comparison of two ways for acrylonitrile production: The SOHIO process and an alternative route using propane. *Journal of Cleaner Production*, 69:17–25, 2014.

[138] R. Grasselli. *Journal of Chem. Educ.*, (Selective Oxidation and ammoxidation of olefins by heterogeneus catalysis):216–221, 1981.

[139] F. Ayari, M. Mhamdi, J. Alvarez-Rodriguez, A. Guerrero-Ruiz, G. Delahay, and Abdelhamid Ghorbel. Ammoxidation of ethylene over low and over-exchanged Cr-ZSM-5 catalysts. *Applied Catalysis A: General*, 415:132–140, 2012.

[140] B. Rhimi, M. Mhamdi, A. Ghorbel, V. Kalevaru, A. Martin, M. Perez-cadenas, and A. Guerrero-ruiz. Ammoxidation of ethylene to acetonitrile over vanadium and molybdenum supported zeolite catalysts prepared by solid-state ion exchange. *Journal of Molecular Catalysis. A, Chemical*, 416:127–139, 2016.

[141] Y. Hu, J. Cao, J. Deng, B. Cui, M. Tan, J. Li, and H. Zhang. Synthesis of acetonitrile from ethanol via reductive amination over Cu/Al_2O_3. *Reaction Kinetics, Mechanisms and Catalysis*, 106(1):127–139, 2012.

[142] C. Feng, Y. Zhang, Y. Zhang, Y. Wen, and J. Zhao. Study on alumina-supported cobalt-nickel oxide catalyst for synthesis of acetonitrile from ethanol. *Catalysis Letters*, 141:168–177, 2011.

[143] C. Hamill, H. Driss, A. Goguet, R. Burch, L. Petrov, M. Daous, and D. Rooney. Mild temperature palladium-catalyzed ammoxidation of ethanol to acetonitrile. *Applied Catalysis A: General*, 506:261–267, 2015.

[144] Federico Folco. *Catalytic processes for the transformation of ethanol into acetonitrile*. PhD thesis, Alma Mater Studiorum University of Bologna, 2013.

[145] F. Folco, J.V. Ochoa, F. Cavani, L. Ott, and M. Janssen. Ethanol gas-phase ammoxidation to acetonitrile. *Catal. Sci. Technol.*, 7:200–212, 2017.

[146] A. Tripodi, D. Ripamonti, R. Martinazzo, F. Folco, T. Tabanelli, F. Cavani, and Ilenia Rossetti. Kinetic model for the ammoxidation of ethanol to acetonitrile. *Chemical Engineering Science*, 207:862–875, 2019.

[147] H. L. Horsley, editor. *Azeotropic Data*, volume III. American Chemical Society, 1973.

[148] D. Sutter and M. Mazzotti. Solubility and growth kinetics of ammonium bicarbonate in aqueous solution. *Crystal Growth and Design*, 17:3048–3054, 2017.

[149] J. Acosta, A. Arce, E. Rodil, and A. Soto. A thermodynamic study on binary and ternary mixtures of acetonitrile, water and butyl acetate. *Fluid Phase Equilibria*, 203:83–98, 2002.

[150] P. Mathias, S. Reddy, and J. Connell. Quantitative evaluation of the aqueous-ammonia process for CO_2 capture using fundamental data and thermodynamic analysis. *Energy Procedia*, 1(1):1227–1234, 2009.

[151] K. Nagahama and M. Hirata. Binary vapor-liquid equilibria at elevated pressures: C_5-hydrocarbon-acetonitrile and acetonitrile-water. *Bulletin of The Japan Petroleum Institute*, 18(1):79–85, 1976.

[152] W. L. Luyben. Pressure-swing distillation for minimum and maximum-boiling homogeneous azeotropes. *Industrial & Engineering Chemistry Reasearch*, 51:10881–10886, 2012.

[153] B. H. Jennings and F. P. Shannon. Tables of the properties of aqua-ammonia solutions. Technical report, Lehigh University, Bethlehem, Pennsylvania, 1938.

[154] D.R. Lide, editor. *CRC Handbook of Chemistry and Physics 88th Edition*, volume 57. CRC Press, Taylor & Francis, Boca Raton, FL, 2007.

[155] Z. Zhang, J. Li, Y. Feng, S. Bi, and Wu W. Physical and chemical properties of a durably efficacious ammonium bicarbonate as a fertilizer and its yield-increasing mechanism. *Science in China, Series B: Chemistry*, 40(1):105–112, 1997.

[156] Q. Zhuang, B. Clements, and Y. Li. From ammonium bicarbonate fertilizer production process to power plant CO_2 capture. *International Journal of Greenhouse Gas Control*, 10:56–3, 2012.

[157] M. Gazzani, D. Sutter, and M. Mazzotti. Improving the efficiency of a chilled ammonia CO_2 capture plant through solid formation: a thermodynamic analysis. *Energy Procedia*, 63:1084–1090, 2014.

[158] D. Sutter, M. Gazzani, and M. Mazzotti. A low-energy chilled ammonia process exploiting controlled solid formation for post-combustion CO_2 capture. *Faraday Discussions*, 192:59–83, 2016.

[159] A. Tripodi, E. Bahadori, D. Cespi, F. Passarini, F. Cavani, T. Tabanelli, and Ilenia Rossetti. Acetonitrile from bioethanol ammoxidation: Process design from the grass-roots and Life Cycle Analysis. *ACS Sustainable Chemistry and Engineering*, 2018(4):5441–5451, 6.

[160] A. Tripodi, D. Manzini, M. Compagnoni, G. Ramis, and Rossetti Ilenia. Alternative integrated distillation strategies for the purification of acetonitrile from ethanol ammoxidation. *Journal of Industrial and Engineering Chemistry*, 59:35–49, 2018.

[161] A. Tripodi, M. Compagnoni, G. Ramis, and Ilenia Rossetti. Pressure-swing or extractive distillation for the recovery of pure acetonitrile from ethanol ammoxidation process: A comparison of efficiency and cost. *Chemical Engineering Research and Design*, 127:92–102, 2017.

[162] O. Levenspiel. *Chemical Reaction Engineering.* John Wiley & Sons, 1999.

[163] M. Jacobson. Evaluation of coal and natural gas with carbon capture as proposed solutions to global warming, air pollution, and energy security. *In "100for Everything", Cambridge University Press*, 2019.

[164] P. Collet, E. Flottes, A. Favre, L. Raynal, H. Pierre, S. Capela, and C. Peregrina. Techno-economic and Life Cycle Assessment of methane production via biogas upgrading and power to gas technology. *Applied Energy*, 192:282–295, 2017.

[165] O. Buchholz, A. Van Der Ham, R. Veneman, D. Brilman, and S. Kersten. Power-to-gas: Storing surplus electrical energy, a design study. *Energy Procedia*, 63:7993–8009, 2014.

[166] J. Baier, G. Schneider, and Andre Heel. A cost estimation for CO_2 reduction and reuse by methanation from cement industry sources in switzerland. *Frontiers in Energy Research*, 6, 2018.

[167] M. Gotz, J. Lefebvre, F. Mors, Koch A. McDaniel, F. Graf, S. Bajohr, R. Reimert, and T. Kolb. Renewable power-to-gas: A technological and economic review. *Renewable Energy*, 85:1371–1390, 2016.

[168] M. Bailera, P. Lisbona, L. Romeo, and Espatolero S. Power to gas projects review: Lab, pilot and demo plants for storing renewable energy and CO_2. *Renewable and Sustainable Energy Reviews*, 69:292–312, 2016.

[169] M. Beaudin, H. Zareipour, A. Schellenberglabe, and W. Rosehart. Energy storage for mitigating the variability of renewable electricity sources: An updated review. *Energy for Sustainable Development*, 14(4):302–314, 2010.

[170] S. Fujita and N. Takezawa. Difference in the selectivity of CO and CO_2 methanation reactions. *Chemical Engineering Journal*, 68:63–68, 1997.

[171] M. Duyar, A. Ramachandran, C. Wang, and R. Farrauto. Kinetics of CO_2 methanation over Ru/ γ - Al_2O_3 and implications for renewable energy storage applications. *Journal of CO_2 Utilization*, 12:27–33, 2015.

[172] K. Brooks, J. Hu, H. Zhu, and R. Kee. Methanation of carbon dioxide by hydrogen reduction using the Sabatier process in microchannel reactors. *Chemical Engineering Science*, 62(4):1161–1170, 2007.

[173] A. Karelovic and P. Ruiz. Mechanistic study of low temperature CO_2 methanation over Rh/TiO_2 catalysts. *Journal of Catalysis*, 301:141–153, 2013.

[174] K. Ghaib, K. Nitz, and F. Ben-Fares. Chemical methanation of CO_2: A review. *ChemBioEng Reviews*, 3(6):266–275, 2016.

[175] H. Sagara, Y. Arai, and Shozaburo Saito. Vapor-liquid equilibria of binary and ternary systems containing hydrogen and light hydrocarbons. *J. Chem. Eng. Of Japan*, 4(5):339–348, 1972.

[176] D. Quyn, A. Rayer, J. Gouw, I. Indrawan, K. Mumford, C. Anderson, B. Hooper, and G. Stevens. Results from a pilot plant using un-promoted potassium carbonate for carbon capture. *Energy Procedia*, 37:448–454, 2013.

[177] G. Hu, K. Smith, S. Wu, Y. and0 Kentish, and G. Stevens. Recent progress on the performance of different rate promoters in potassium carbonate solvents for CO_2 capture. *Energy Procedia*, 114:2279–2286, 2017.

[178] R. Ramazani, S. Mazinani, Hafizi. A., A. Jahanmiri, V. Van Der bruggen, and S. Darvishmanesh. Solubility and absorption rate enhancement of CO_2 in K_2CO_3. *Separation Science and Technology*, 5(2):327–338, 2016.

[179] F. Isa, H. Zabiri, N. K. S. Ng, and A. M. Shariff. Purification of CO_2 removal via promoted potassium carbonate: A review on modeling & simulation techniques. *International Journal of Greenhouse Gas Control*, 76:236–265, 2017.

[180] R. K. Stoessell and Patricia A. Byrne. Salting-out of methane in single-salt solutions at 25 degrees C and below 800 psia. *Geochimica et Cosmochimica Acta*, 46(8):1327–1332, 1982.

[181] A. P. Kamps, E. Meyer, B. Rumpf, and Gerd Maurer. Solubility of CO_2 in aqueous solutions of KCl and in aqueous solutions of K_2CO_3. *J. Chem. Eng. Data*, 3(52):817–832, 2007.

[182] T. Schaaf, J. Grunig, M. Schuster, and A. Orth. Speicherung von elektrischer energie im erdgasnetz - methanisierung von CO_2-haltigen gasen. *Chemie-Ingenieur-Technik*, 86(4):476–485, 2014.

[183] K. Muller, M. Fleige, F. Rachow, and D. Schmeisser. Sabatier based CO_2-methanation of flue gas emitted by conventional power plants. *Energy Procedia*, 40:240–248, 2013.

[184] A. Lazdans, E. Dace, and J. Gusca. Development of the experimental scheme for methanation process. *Energy Procedia*, 95:540–545, 2016.

[185] A. Witkowski, A. Rusin, M. Majkut, and Stolecka K. Analysis of compression and transport of the methane/hydrogen mixture in existing natural gas pipelines. *International Journal of Pressure Vessels and Piping*, 166:24–34, 2018.

[186] D. Adolfo, C. Carcasci, C. Falchetti, and Pietro Lubello. Thermo-economic analysis of a natural gas liquefaction plant. *Energy Procedia*, 148:42–49, 2018.

[187] K. Buhner, G. Maurer, and E. Bender. Pressure-enthalpy diagrams for methane, ethane, propane, ethylene and propylene. *Cryogenics*, 100:157–164, 1981.

[188] Z. Liu and I. Karimi. Simulating combined cycle gas turbine power plants in Aspen HYSYS. *Energy Conversion and Management*, 171:1213–1225, 2018.

[189] V. Darde, W. Van Well, E. Stenby, and K. Thomsen. CO_2 capture using aqueous ammonia: Kinetic study and process simulation. *Energy Procedia*, 4:1443–1450, 2011.

[190] AAVV. A guide to HPLC and LC-MS buffer selection. https://www.hplc.eu/Downloads/ACE_Guide_BufferSelection.pdf.

[191] AAVV. Bridging the performance gap from analytical to prep. https://www.waters.com/webassets/cms/library/docs/720002117en.pdf.

[192] L. Peng, I. Rustamov, L. Loo, and T. Farkas. Improved results for LC/MS of basic compounds using high ph mobile phase on a Gemini C18 column. www.Phenomenex.com/TechNotes/1031.

[193] AAVV. Buffers and solutions for in gel digests. https://www.biotech.wisc.edu/services/massspec/protocols/buffers.

[194] AAVV. Use of Agilent Poroshell HPH C18columns at elevated ph as a tool for method development. https://www.agilent.com/cs/library/technicaloverviews/public/5991-4893EN.pdf.

[195] D. N. Pence and Tingyue Gu. Liquid-liquid equilibrium of the acetontrile-water system for protein purification. *Separations Technology*, 6:261–264, 1996.

[196] Yukio Nagaosa. Salting-out of polar solvents from aqueous solution and its application to ion-pair extractions. *Analytica Chimica Acta*, 120:279–287, 1980.

[197] W. Kuu, R. Chilamkurti, and C. Chen. Effect of relative humidity and temperature on moisture sorption and stability of sodium bicarbonate powder. *International Journal of Pharmaceutics*, 166:167–175, 1998.

[198] H. Gottlieb, V. Kotlyar, and A. Nudelman. NMR chemical shifts of common laboratory solvents as trace impurities. *Journal of Organic Chemistry*, 62(21):7512–7515, 1997.

[199] Aboul-Gheit A. K. Volatility characteristics of petroleum fractions by differential scanning calorimetry. *Thermochimica Acta*, 176:107–117, 1991.

[200] D. B. Van Dongene and M. F. Doherty. On the dynamics of distillation processes - VI. Batch distillation. *Chemical Engineering Science*, 40(11):2087–2093, 1985.

[201] B. T. Safrit. Synthesis of azeotropic batch distillation separation systems. Master's thesis, 1996.

[202] S. X. Liu and M. Peng. The simulation of the simple batch distillation of multiple-component mixtures via Rayleigh's equation. *Computer Applications in Engineering Education*, 15(2):198–204, 2007.

[203] R. Mohan, H. Lorenz, and Myerson Allan S. Solubility measurement using differential scanning calorimetry. *Industrial & Engineering Chemistry Research*, 41(19):4854–4862, 2002.

[204] G. Narin, V. F. D. Martins, M. Campo, A. M. Ribeiro, A. Ferreira, J. C. Santos, K. Schumann, and Alirio E. Rodrigues. Light olefins/paraffins separation with 13X zeolite binderless beads. *Separation and Purification Technology*, 133:452–475, 2014.

[205] K. M. Kim, H. T. Oh, S. J. Lim, K. Ho, Y. Park, and Chang-Ha Lee. Adsorption equilibria of water vapor on zeolite 3A, zeolite 13X, and dealuminated Y zeolite. *J. Chem. Eng. Data*, 4(61):1547–1554, 2016.

[206] S. Y. Zhang, O. Talu, and David T. Hayhurst. High-pressure adsorption of methane in zeolites NaX, MgX, CaX, SrX and BaX. *J. Phys. Chem.*, 4(95):1722–1726, 1991.

[207] J. Moise, J. Bellat, and A. Methivier. Adsorption of water vapor on X and Y zeolites exchanged with Barium. *Microporous and Mesoporous Materials*, 43, 2001.